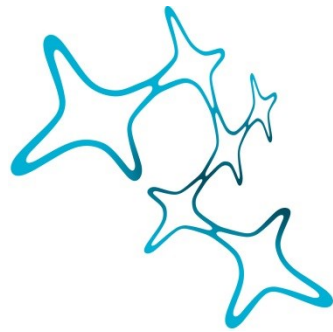

ACTIVATION OF TRANSLOCATOR PROTEIN BY
XBD173 AMELIORATES COGNITIVE DEFICITS
AND NEUROPATHOLOGY IN AN ALZHEIMER'S
MOUSE MODEL

ARPIT KUMAR PRADHAN



Graduate School of
Systemic Neurosciences

LMU Munich



Dissertation der
Graduate School of Systemic Neurosciences der
Ludwig-Maximilians-Universität München

11.07.2023

Supervisor:

Prof. Dr. Gerhard Rammes

Klinik für Anaesthesiologie und Intensivmedizin der Technischen Universität München

Klinikum rechts der Isar

Ismaningerstr. 22

81675 München

First Reviewer: Prof. Dr. Gerhard Rammes

Second Reviewer: Prof. Dr. Osborne Almeida

External Reviewer: Prof. Dr. Gunnar Gouras

Date of Submission: 11.07.2023

Date of Defense: 30.11.2023

Dedicated to my Papa and Mama!

Table of Contents

List of Figures.....	7
List of Tables	10
List of Abbreviations	11
Summary.....	17
1. Introduction.....	19
1.1 Alzheimer’s disease	19
1.1.1 Pathophysiology and Genetics of Alzheimer’s	19
1.1.1.1 Pathological Hallmarks of AD.....	19
1.1.1.2 Glutamatergic and GABAergic Neurotransmission in Alzheimer’s disease.....	23
1.1.1.2.1 Glutamatergic Neurotransmission.....	23
1.1.1.2.1 GABAergic Neurotransmission	24
1.1.1.3 Genetics of AD and risk factors.....	25
1.1.2 Amyloid Cascade Hypothesis.....	26
1.1.3 Amyloid- β peptide and aggregation in AD	28
1.1.4 Arctic mutation mouse model of AD	30
1.2 Depression	32
1.2.1 Depression and Sleep: From a Molecular and Cellular Perspective	32
1.2.2 From Depression to Dementia: In Retrospection	33
1.3 Translocator Protein, Neurosteroids, and GABA_A receptors	36
1.3.1 Structure and function of translocator protein.....	36
1.3.2 Translocator Protein Ligands in Neurodisorders.....	40
1.3.3 XBD173 in neurodisorders.....	42
1.3.4 Benzodiazepines and Neurosteroids.....	43
1.3.4.1 GABA _A Receptors: Structure and Composition	44
1.3.4.2 Benzodiazepines and Neurosteroid's Effects on GABA _A receptors	46
1.3.4.3. Neurosteroids and their Role in neurodisorders.....	50
1.4 Astrocytes and Complement Pathway	50
1.4.1 Role of glial cells in Pruning and Homeostasis.....	50
1.4.2 Astrocytes in Alzheimer’s Disease.....	53
1.4.3 Complement Proteins and their association with Astrocytes	53
1.5 Aim of this study.....	55
2. Materials and Methods.....	56
2.1 Preparation of test substances and acute hippocampal slices	56
2.1.1 Laboratory Animals.....	56
2.1.2 Preparation of oligomeric A β and test compounds	57
2.1.3 Acute slice preparation	58
2.2 Electrophysiology Recording	60

2.2.1 Electrophysiology Setup.....	60
2.2.2 Long-term potentiation recordings	60
2.3 Spine imaging and classification of individual spines	62
2.4 Fluorescence-activated cell sorting (FACS) staining and analysis	65
2.5 Hippocampus-dependent Spatial learning test, plaque quantification, and measurement of soluble Aβ levels	67
2.5.1 Behavioral test: Water Cross Maze	67
2.5.2 Methoxy staining	70
2.5.3 Enzyme-linked immunosorbent assay (ELISA) of soluble A β	71
2.6 Immunofluorescent staining and analyses: Image Acquisition, 3D reconstruction, and quantification	71
2.6.1 Synaptic engulfment measurement.....	71
2.6.2 Plaque Astrocyte and Plaque C1q Interaction	72
2.6.3 Confocal Microscope Setup.....	73
2.6.4 3D reconstruction of astrocytes and synaptic pruning.....	75
2.7 Golgi-Cox staining of the spines from in vivo XBD173 treated mice	82
2.8 Steroid profiling by gas chromatography coupled to tandem mass spectrometry (GC-MS/MS)	82
2.9 Statistical analysis	84
3. Results	85
3.1 XBD173 (emapunil) averts the potential neurotoxic effect of Aβ₁₋₄₂ oligomers on CA1-LTP in the hippocampus	85
3.2 TSPO is necessary for XBD173 to exert its neuroprotective effect against the Aβ₁₋₄₂ oligomer	87
3.3 Preincubation of XBD173 prevents individual dendritic spine loss resulting from Aβ₁₋₄₂ oligomers.....	88
3.4 Acute intraperitoneal administration of XBD173 does not improve the cognitive deficit in the transgenic ArcAβ AD mice model.....	92
3.5 Chronic intraperitoneal treatment of XBD173 improves hippocampus-dependent spatial learning in transgenic ArcAβ AD mice	95
3.6 TSPO is required for the alleviation of cognitive impairment in chronic XBD173 treated ArcAβ mice	100
3.7 Chronic Administration of XBD173 reduces the pathogenic amyloid load and rescues the spine loss in ArcAβ mice model	106
3.8 Chronic Administration of XBD173 increases neurosteroid levels in transgenic AD mice.....	109

3.9 Ex vivo XBD173 treatment does not affect the microglial polarization states which are altered via A β ₁₋₄₂ oligomers	111
3.10 XBD173 chronic treatment primarily affects and reduces abnormal astrocytic phagocytosis and synaptic pruning.....	113
3.11 Treatment with chronic XBD173 leads to a decrease in C1q aggregates in AD mice as well as a reduction in the engulfment of C1q protein by astrocytes.....	116
3.12 Astrocytes surround the methoxy plaques and more astrocytes are found near the periphery of plaques than farther away from it.....	120
3.13 Methoxy plaque clearance in the cortex is not facilitated by astrocytic phagocytosis	121
3.14 XBD173 induces TSPO-mediated neurosteroids synthesis, which affects the activity of delta-subunit containing GABA _A receptor and confers neuroprotection against A β oligomers	123
3.15 XBD173 incubation prevents LTP impairment resulting from A β ₁₋₄₂ arctic mutation oligomer.....	128
4. Discussion.....	130
4.1 Key Objectives and Findings.....	130
4.3 The role of XBD173 in ameliorating the energy imbalance in the AD pathology	138
4.4 Complement Protein C1q Deposits and their Involvement in AD	143
4.5 Clinical relevance of TSPO-dependent XBD173 in AD and peri-operative anesthesia	146
4.6 Limitations of the Study and future perspectives	148
5. References	151

List of Figures

Figure 1. Representative Stainings from AD hippocampal sections.	21
Figure 2. Schematic representation of GABAergic signaling in AD-related mechanism.....	25
Figure 3: Amyloidogenic and non-amyloidogenic pathway of APP processing.	30
Figure 4: Representative schematics showing the location of Swe and Arc mutations in the human APP containing the A β sequence	32
Figure 5: Translocator protein helps in importing cholesterol to inner mitochondrial membrane..	39
Figure 6: Cholesterol binds to the CRAC domain at the C terminal of 18kDa TSPO.	40
Figure 7: Representative schematic of the GABA _A receptor and its associated binding sites	45
Figure 8: Structural representations of epipregnanolone (Epi), allopregnanolone (ALLO), and isopregnanolone (Iso). The position of the hydroxy group at the C3 position alters the stereo confirmation resulting in stereoisomers	47
Figure 9: Structure of the stereoisomers of THDOC (3 α 5 α -THDOC and 3 α 5 β -THDOC)	48
Figure 10. Synaptic and extrasynaptic GABA _A receptors and the neurosteroid-mediated action at these sites.....	49
Figure 11: Comparison of glial cell function in a normal and a diseased brain.....	52
Figure 12: Representative schematic showing the astrocytic phagocytic receptors (MEGF10 and MERTK) participating in direct elimination synapses via C1q “eat-me tag”.....	54
Figure 13: Hippocampal slice showing a representative positioning of electrodes in the Schaffer collateral pathway to obtain CA1-LTP	61
Figure 14: Representative image showing different spine classes.	64
Figure 15: Microglial FACS gating strategy to study the polarization states.	66
Figure 16: Acute and chronic treatment schedule of Water Cross Maze.....	70
Figure 17. Overview of the C1q-GFAP interaction in the hippocampus	75
Figure 18. Volumetric Rendering of astrocytes takes place in four steps	76
Figure 19. Managing the correct threshold level for the volumetric reconstruction of the astrocyte	77
Figure 20. Removal of unwanted background signals from the rendered astrocyte	78
Figure 21. Masking the astrocytic surface.....	79
Figure 22. Analysis of the astrocytic engulfment using colocalization (COLOC) analysis with Imaris	80
Figure 23. Synaptic engulfment and volumetric rendering of the astrocyte	82

Figure 24: Contrary to the effect of XBD173 on Aβ₁₋₄₂ oligomers, there is a partial rescue of the LTP impairments resulting from Aβ₁₋₄₀ oligomers.	86
Figure 25: CA1-LTP in the hippocampus is impaired after the incubation with Aβ₁₋₄₂ and XBD173 prevents these adverse synaptotoxic effects.....	87
Figure 26: TSPO is necessary for XBD173 to rescue the synaptotoxic effect of Aβ₁₋₄₂ oligomers	88
Figure 27: Representative spine reconstruction using IMARIS filament function	90
Figure 28: TSPO-dependent XBD173 inhibits the detrimental synaptotoxic effects of Aβ₁₋₄₂ oligomers on dendritic spines.	91
Figure 29: Cognitive deficits in AD mice are not ameliorated by acute administration of XBD173.	94
Figure 30: XBD173 chronic treatment rescues spatial learning deficits in transgenic AD mice in the training phase.....	97
Figure 31: XBD173 chronic treatment rescues spatial learning deficits in transgenic AD mice in both retests.	98
Figure 32: XBD173 or vehicle treatment affects the individual animals uniformly.	99
Figure 33: Transgenic AD mice have a lower percentage of accurate learners whereas chronic XBD173 treatment improves the percentage of accurate learners.....	100
Figure 34: XBD173 treatment is dependent upon TSPO to confer beneficial effects in spatial learning tests.....	102
Figure 35: TSPO heterozygous expression impacts the effect of XBD173 on the spatial learning of ArcAβ transgenic animals in Retests.....	103
Figure 36: XBD173-mediated cognitive improvement is dependent upon TSPO.....	105
Figure 37: XBD173 chronic treatment reduces the cortex plaque load in the transgenic Arc Aβ mice model of AD.....	107
Figure 38: Golgi Cox-stained apical dendrites show prevention in dendritic spine loss after chronic XBD173 administration in Arc Aβ mice.	109
Figure 39: Chronic XBD173 administration results in an elevation of neurosteroid levels in Arc Aβ mice.	110
Figure 40: In ex vivo slice experiments, XBD173 has no effect on microglial polarization altered by Aβ₁₋₄₂ oligomers.	112
Figure 41: Representative image of astrocytic engulfment of synaptophysin in the cortex and hippocampus of different treatment groups.....	114
Figure 42: The chronic administration of XBD173 reduces synaptic pruning and aberrant astrocytic phagocytosis.....	115
Figure 43: The chronic administration of XBD173 reduces enhanced astrocytic engulfment of C1q complement protein.	118

Figure 44: Representative confocal scope image of astrocyte interaction with C1q complement protein.....	119
Figure 45. The % overlap between plaque and C1q is not affected by XBD173 treatment.....	119
Figure 46: The C1q aggregates load, as well as cortex soluble Aβ₁₋₄₂ levels, are reduced in chronic XBD173 treated AD mice.	120
Figure 47: XBD173 treatment does not increase astrocytosis-mediated plaque clearance.	122
Figure 48: LTP deteriorations induced by Aβ₁₋₄₂ oligomers incubation is not rescued by pregnenolone.	124
Figure 49: Allopregnanolone (Allo) prevents the LTP impairment from Aβ₁₋₄₀ oligomers but doesn't affect the LTP deterioration resulting from Aβ₁₋₄₂ oligomers.	125
Figure 50: 3α5α THDOC prevents LTP impairments resulting from Aβ₁₋₄₂ oligomers.	126
Figure 51: XBD173 stimulates TSPO-regulated production of diverse neurosteroids such as THDOC, which increases delta subunit-containing GABA_A receptor activity.....	127
Figure 52: XBD173 (300 nM) rescues the Arctic Aβ₁₋₄₂ synaptotoxic effect on LTP	129
Figure 53: Schematic showing the possible working mechanism for TSPO-dependent XBD173 in the AD model.	132
Figure 54: Mitochondrial cholesterol loading in AD and the possible effect of XBD173 on it.	137
Figure 55: Synaptic plasticity model in physiological conditions.	141
Figure 56: Synaptic plasticity model in AD-related pathology.....	141
Figure 57: Comparison of side-effect profile of Benzodiazepines and XBD173.....	148

List of Tables

Table 1: List of animal lines used in the study	56
Table 2: Mess Ringer solution (aCSF) solution ingredients.....	59
Table 3: Preparation Ringer solution ingredients.....	59
Table 4: Treatment schematics for the slice incubation with XBD173 and Aβ₁₋₄₂.	62
Table 5: Antibodies used in FACS study	66
Table 6: Antibody staining mix composition	67
Table 7: Antibody staining used in the immunofluorescent study	72

List of Abbreviations

Aβ	Amyloid beta
ACSF	Artificial cerebrospinal fluid
AD	Alzheimer's disease
AICD	APP intracellular domain
AMPA	α -amino-3-hydroxy-5-methyl-4-isoxazolepropionic acid
ANT	Adenine nucleotide transporter
APH-1	Anterior pharynx-defective-1
APOE	Apolipoprotein E
APP	Amyloid Precursor Protein
ATP	Adenosine triphosphate
BIN1	Bridging Integrator 1
BACE1	Beta-secretase 1
BBB	Blood-brain barrier
BDNF	Brain-derived neurotrophic factor
BSA	Bovine Serum Albumin
BZD	Benzodiazepine
CAA	Cerebral amyloid angiopathy
cAMP	Cyclic adenosine monophosphate
CLU	Clusterin
CR3	Complement receptor 3

CRAC	Cholesterol-recognizing amino acid consensus domain
CREB	cAMP-response element binding protein
CRH	Corticotropin-releasing hormone
CRI	Complement receptor 1
CTFβ	Tethered-C-terminal β fragments
DAG	Diacylglycerol
DHDOC	Dihydrodeoxycorticosterone
DHEA	Dehydroepiandrosterone
DHT	Dihydrotestosterone
DMSO	Dimethyl sulfoxide
DOC	Deoxycorticosterone
EAAT2	Excitatory amino acid transporter
EAE	Autoimmune encephalomyelitis
EDTA	Ethylenediaminetetraacetic acid
ELISA	Enzyme-linked immunosorbent assay
EPHA1	Ephrin type-A receptor 1
FACS	Fluorescence-activated cell sorting
FEPS	Field excitatory postsynaptic potentials
GABA	Gamma-aminobutyric acid
GAD	Glutamic acid decarboxylase
GAT	GABA transporters

GC	Gas chromatograph
GLT-1	Glutamate transporter-1
GPCR	G Protein-coupled receptors
GSH	Glutathione
HFBA	Heptafluorobutyric anhydride
HFIP	Hexafluoroisopropanol
HFS	High-frequency stimulation
HHPROG	Hexahydroprogesterone
HPA	Hypothalamus-Pituitary-Adrenal
I.C.V	Intracerebroventricular injections
I.P.	Intraperitoneal
iGluRs	Ionotropic glutamate receptors
IL	Interleukin
IP3	Inositol trisphosphate
IPSC	Inhibitory postsynaptic potentials
LC	Locus coeruleus
LTP	Long-Term Potentiation
MEGF10	Multiple EGF-like-domains 10
MERTK	MER tyrosine kinase
MFI	Mean/median fluorescence intensity
mGluRs	Metabotropic glutamate receptors

mGSH	Mitochondrial GSH
MMP	Mitochondria membrane potential
mPRs	Metabotropic progesterone receptors
MS	Mass spectrometer
MS4A	Membrane-spanning 4-domains subfamily
NCAM2	Neural cell adhesion molecule 2
NGS	Normal goat serum
NMDA	N-Methyl-D-aspartic acid
NRCAM	Neuronal cell adhesion molecule
PAM	Positive allosteric modulators
PAR1	Protease-activated receptor 1
PBS	Phosphate-buffered saline
PBS/T	PBS containing 0.1% tween 20
PEN-2	Presenilin enhancer-2
PFA	Paraformaldehyde
PIP2	Phosphatidylinositol 4,5-bisphosphate
PKA	Protein Kinase A
PLC	Phospholipase C
Preg	Pregnenolone
PSEN1	Presenilin1
PSEN2	Presenilin2

PTSD	Post-traumatic stress disorders
REM	Rapid eye moment
RGC	Retinal ganglion cell
ROI	Region of Interest
ROS	Reactive oxygen species
sAPPβ	Soluble α -APP fragments
SPARC	Secreted protein acidic and rich in cysteine
SSRI	Selective serotonin reuptake inhibitors
T	Testosterone
TGN	Trans-Golgi-network
THDOC	Tetrahydrodeoxycorticosterone
THPROG	Tetrahydroprogesterone
THT	Tetrahydrotestosterone
TNF	Tumor necrosis factor
TREM2	Triggering receptor expressed on myeloid cells 2
TRPA1	Transient receptor potential A1
TSPO	Translocator Protein
VDAC	Voltage-dependent anion channel
VGluT	Vesicular glutamate transporter
WCM	Water Cross Maze
δ-KO	Delta Knock out

20 β -DHP 20 β -dihydroprogesterone

3 α ,5 α -THP Allopregnanolone

Summary

One of the most prevalent forms of dementia among elderly patients, Alzheimer's disease (AD) affects millions of people worldwide and brings a huge burden to the individual as well as the global economy. Accumulation of β -amyloid peptide ($A\beta$) is a major characteristic feature of AD. Previous clinical studies suggest that depression is a common antecedent of AD and may be an early manifestation of dementia, suggesting biological mechanisms that are partly similar in both these disorders. Targeting the molecular mechanism behind these connected disorders can be an excellent therapeutic strategy. The mitochondrial translocator protein (18 kDa) (TSPO) plays an essential role in neurosteroidogenesis and TSPO ligands are neuroprotective in several neurodisorders. We hypothesized that XBD173 since it induces rapid anxiolysis, may have early (neuro) protective effects in AD pathophysiology. Additionally, previous studies concerning XBD173 show a lower side-effect profile compared to benzodiazepines.

Both in-vitro electrophysiological recordings, as well as the cognitive performance of the mice, were accessed to unravel the effect of XBD173 on the pathophysiology of AD. First from the CA1-Long Term Potentiation (CA1-LTP) recordings, we observed that 90 min incubation of $A\beta_{1-42}$ (50 nM) to murine hippocampal slices, prevented the CA1-LTP development after tetanic stimulation of the Schaffer collaterals. Additionally, there was a reduction in the total spine density of CA1 pyramidal neurons. XBD173 (300 nM) restored LTP deficit as well as spine density in the presence of $A\beta_{1-42}$. XBD173 incubation recovered mushroom and thin spines, as well as overall spine density, as reflected by Imaris dendritic spine rendering. Interestingly, the incubation of XBD173 did not restore the LTP deficit resulting from $A\beta_{1-42}$ incubation in a global TSPO knockout (KO) mouse model, suggesting a TSPO-mediated action for XBD173.

Chronic administration of TSPO-dependent XBD173 (1mg/kg every second day for 3 months) improves the cognitive performance in 9 months ArcA β (transgenic AD) mice accessed by the water cross maze. Analyzing the brains of these mice showed that chronic XBD173 treatment reduced plaque load (Methoxy-04 staining) and total $A\beta_{1-42}$ levels (ELISA) in the cortex. Additionally, we found that chronic treatment with XBD173 reduces astrocytic synaptic pruning in the hippocampus and cortex, which in AD mice was exacerbated. Given, the important role of complement proteins in advancing the pathophysiology of AD, we focused on complement protein

C1q which acts as an “eat-me” tag for the neurons to be destroyed. We found that astrocytes in transgenic AD mice contain more C1q engulfment compared to the wild-type. Chronic XBD173 treatment reduces this aberrant astrocytic engulfment of C1q tags. It was interesting to observe that amyloid plaques colocalize with C1q aggregates and these C1q aggregates are reduced in XBD173-treated mice compared to their transgenic counterparts. Additionally, we observed that the activation of TSPO by XBD173 in a chronic-treatment model elevates the levels of the neurosteroids including allopregnanolone, dihydrodeoxycorticosterone (DHDOC), and $3\beta 5\alpha$ THDOC in the cortex and hippocampus.

We further studied whether neurosteroids could potentially be the main players behind the effectiveness of XBD173 treatment in AD. From the CA1-LTP experiment, we found that $3\alpha 5\alpha$ THDOC (100 nM) and $3\beta 5\alpha$ THDOC (100 nM), similar to XBD173 (300 nM), restored the LTP deficit in $A\beta_{1-42}$ treated slices. However, both XBD (300 nM) and $3\alpha 5\alpha$ THDOC (100 nM), could not prevent the CA1-LTP impairments in GABA delta KO mice. These findings highlight a TSPO-mediated increase in neurosteroidogenesis by XBD173, which, upon release, elevates GABA_A receptor activity containing the GABA delta subunit. Allopregnanolone (100 nM) prevents the LTP deficits resulting from $A\beta_{1-40}$ incubation but not $A\beta_{1-42}$ incubation. Taken together, the present study highlights the beneficial effects of XBD173 against A β -derived pathophysiology. Chronic XBD173 treatment improves cognition and appears to have a disease-modifying effect when applied early in the course of AD. This hypothesis is supported by the reduction of soluble A β levels, plaque load, and synaptic pruning by XBD173. In conclusion, our work shows that XBD173, in a TSPO-dependent manner provides neuroprotective benefits in a rodent Alzheimer model evident from both the in vitro as well as in vivo behavioral studies. This study paves the way for further advancements in AD treatments and research and provides a possible effective intervention for AD pathophysiology.

1. Introduction

1.1 Alzheimer's disease

Alzheimer's disease (AD), the most prevalent form of dementia, currently affects more than 55 million individuals worldwide and this is expected to double every 20 years, reaching 78 million in 2020 and 139 million in 2050 [1]. Alzheimer-related fatalities have doubled from 2000 to 2019 [2]. Among elderly patients, 1 in 3 people dies from AD [2]. Globally, each year there are 10 million new cases of dementia which would mean one new case every 3.2 seconds [3]. Alzheimer's disease, therefore, is not only an individual disease but also a huge setback to the nation's economy and resources. The first symptoms and the neuropathological features of Alzheimer's were described and discovered by Dr. Alois Alzheimer in a 51 year-old-patient Auguste Deter, the first impression of which he considered a 'peculiar case of cerebral cortex' [4]. Histopathological examination of the brain revealed abnormal deposits within and around the brain cells [4].

1.1.1 Pathophysiology and Genetics of Alzheimer's

1.1.1.1 Pathological Hallmarks of AD

Detection of AD is based on macroscopic and microscopic features, both of which are essential for its pathologic characterization. Amongst the macroscopic features, the predominant ones include moderate cortical atrophy associated with limbic lobe structures and cortices [5]. Additionally, enlarged sulcal space in temporal and frontal cortices with cortical gyri atrophy is also often observed in AD [6]. Increasing evidence associates atrophy in posterior cortical areas particularly in the posterior cingulate gyrus and precuneus in AD [7,8]. This results in decreased brain weight and an enlargement in the frontal and temporal horns of the lateral ventricles [5]. Another characteristic feature of AD is the medial temporal atrophy affecting the hippocampus and amygdala with enlargement of the temporal horn [6,9,10].

The classic feature of AD which defines the true diagnostic nature is the presence of extracellular amyloid plaques and intercellular neurofibrillary tangles [4,5] (**Figure 1**). The presence of tau-positive neuropil threads, dystrophic neurites, reactive astrogliosis, and activated microglia are additional characteristic features of AD [5]. Senile amyloid plaques result from the extracellular

accumulation of amyloid beta ($A\beta$): $A\beta_{1-42}$ and $A\beta_{1-40}$ peptides [5]. Abnormal processing of amyloid precursor protein by β - and γ -secretases leads to the accumulation of the $A\beta$ peptides [11]. The $A\beta_{1-42}$ peptide is often considered the most aggregated, fibrillar, and predominant component of amyloid plaques [12]. Based on the staining intensity, morphology, and individual components, the amyloid plaques are usually categorized into diffuse plaques and dense-core plaques [5]. The dense-core plaques unlike the diffuse plaques are strongly stained by the thioflavin S and the congo-red derivatives [5,13,14]. Additionally, a subset of these dense-core plaques is known to contain tau-positive or dystrophic neurites-associated neuritic components [14,15]. They are followed by aggravated synapse loss and reactive astrocytes surrounding the plaques [10,16]. Apart from tau-positive neurites, neurofilament proteins are also present in dystrophic neurites [5]. Additional components of dystrophic neurites include lysosomal bodies and vesicles, and degenerating mitochondria [10]. The classical distribution of plaques is suggested by a three-step process. Stage A affects the basal, frontal, and temporal lobes. Stage B includes the extension to neocortices and hippocampus and Stage C finally affects primary cortices, subcortical nuclei, and cerebellum [17].

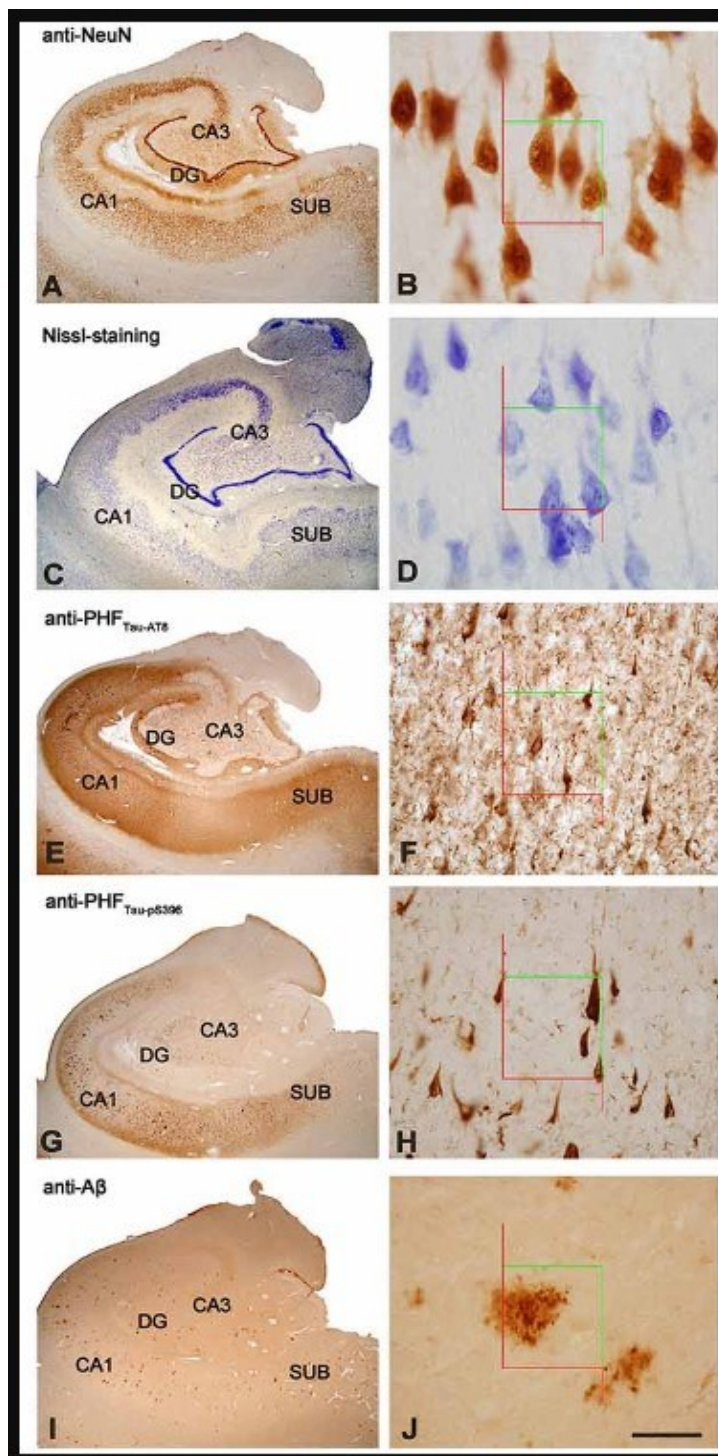


Figure 1. Representative Stainings from AD hippocampal sections (Adapted with permission from [18]).

The left column shows a lower magnification of hippocampal sections stained with A. NeuN-ir, C. Nissl-staining, E. PHF_{Tau-AT8}-ir, G. PHF_{Tau-pS396}-ir I. Aβ-ir. The right column shows higher magnification images of

the hippocampal CA1 region (B, D, F, F, H, J) of respective stainings on the left column images. The green line indicates the inclusion boundary whereas the red line shows the exclusion boundary

The deposition of A β peptides in cerebral blood vessels (cerebral amyloid angiopathy (CAA)) has been observed for around 85-95 % of AD cases [5]. These amyloid deposits in CAA affect small arteries, capillaries of the grey matter of the cerebral cortex, and arterioles [19]. Another characteristic trademark of AD is the neurofibrillary tangles which are often referred to as the “ghost tangles” and are associated with neuronal death and accumulation [20]. The tau filaments in AD (paired helical filaments) have a distinct periodicity as observed in electron microscopy and are thought to be composed of two smaller twisted filaments around 10 nm in diameter [5,21]. Hyperphosphorylation of tau proteins and their abnormal folding are specific to AD [22]. With a higher aggregation and nucleation propensity, the hyperphosphorylated tau plays a key role in the pathophysiological progression of AD and is unable to stabilize the microtubule [22]. Several reports suggest the entorhinal cortex to be the first susceptible brain region in AD from where it progresses to the different areas of the hippocampus [23]. It is interesting to observe from several longitudinal studies of Autosomal Dominant AD patients that the first stages of A β deposition occur in the precuneus and striatum [24,25]. Additionally, compared to Late-Onset AD, individuals with Early Onset AD show severe temporoparietal hypermetabolism [24].

An additional pathological change associated with AD and similar neurodegenerative disorders is granulovacuolar degeneration [5]. This 3 - 5 μ m vacuole considered autophagic granules are lysosomal markers and are distributed frequently in pyramidal neurons cytoplasm in the hippocampus [26,27]. Reactive astrogliosis and activated microglia are among the predominant inflammatory responses associated with AD [5]. Both the glial cells, astrocytes, and microglia, regulate synaptic homeostasis in developing as well as maturing synapses [28], however, in AD, these are activated and surround the senile plaques [29]. A β fibrils are thought to bind the receptors on microglia and initiate the inflammatory response [30]. A shift in the polarization of microglia from M2 (anti-inflammatory) to M1 (pro-inflammatory) has been previously reported in an AD-like state [31,32]. TREM2, a glial receptor involved in microglial phagocytosis is often considered a potential risk factor in AD [33]. Reactive astrocytes constitute a significant part of the chronic neuroinflammation associated with AD [5]. These are discussed further in the subsequent section. Apart from amyloid plaques and neuroinflammation, synaptic loss, and associated cognitive

deficits form the major hallmark feature of AD [5,34]. Loss of neuronal synaptic markers and associated cognitive decline has been well documented in several clinical and imaging experiments [34,35].

1.1.1.2 Glutamatergic and GABAergic Neurotransmission in Alzheimer's disease

1.1.1.2.1 Glutamatergic Neurotransmission

Glutamate produced by the enzyme glutaminase forms the primary excitatory neurotransmitter system in the brain [36]. The glutamatergic neurotransmission which involves both α -amino-3-hydroxy-5-methyl-4-isoxazolepropionic acid (AMPA) and the N-Methyl-D-aspartic acid (NMDA) receptors forms a crucial role in the induction of long-term potentiation, which is crucial for synaptic plasticity and learning and memory formation [37]. Glutamate receptors are categorized into two families based on their mechanism of action: 1. G protein-coupled metabotropic glutamate receptors (mGluRs) and 2. Ligand-gated ionotropic glutamate receptors (iGluRs). Activation of mGluRs by glutamate binding involves the GPCRs which activates phospholipase C (PLC) and decomposes Phosphatidylinositol 4, 5-bisphosphate (PIP₂) into Diacylglycerol (DAG) and Inositol trisphosphate (IP₃) [38]. The IP₃ via the release of Ca²⁺ activates multiple downstream signaling pathways [37]. On the other hand, the iGluRs are composed of three subfamilies: AMPA receptors, kainate receptors, and NMDA receptors [38]. These receptors are ionotropic and are dependent on the membrane potential for activation. Based on their activation kinetics these ionotropic receptors are categorized as either Fast-acting or slow-acting. Both AMPA and kainate receptors are fast-acting receptors [39]. While AMPA receptors are permeable to Na⁺ and Ca²⁺, the kainate receptors are permeable to Na⁺ and K⁺ ions [39]. The NMDA receptors on the other hand have slow activation kinetics and are permeable to Ca²⁺ ions. In a resting state, the NMDA receptors are blocked by Mg²⁺ ions [39]. During synaptic transmission, higher glutamate concentration and strong postsynaptic membrane depolarization release the Mg²⁺ ion block and activate the NMDA receptors [39]. The NMDA receptors then allow the entry of Na⁺, K⁺, and Ca²⁺ ions which form the basis of excitatory postsynaptic current [39]. In AD, glutamatergic dysfunctions of AMPA and NMDA receptors disturb the excitatory to inhibitory neurotransmission balance [40]. Glutamatergic excitotoxicity via the NMDA receptors is a characteristic feature of AD [39]. Previously, it has been reported that chronic synaptotoxic

effects of A β oligomers are mediated particularly via the GluN2B subunit of the NMDA receptors [41]. Memantine, an NMDA receptor antagonist, target this excitotoxicity of the glutamate receptors in AD [42].

1.1.1.2.1 GABAergic Neurotransmission

The inhibitory balance in the mammalian nervous system is maintained by γ -aminobutyric acid (GABA) [43]. GABA is produced from L-glutamate by glutamic acid decarboxylase (GAD) [39]. GAD65 and GAD67 are the two primary GAD isoforms found in the mammalian brain. While GAD65 is located in the presynaptic terminal, GAD67 is distributed widely in the cytosol [39]. Similar to glutamate receptors, the GABA receptors are broadly classified as metabotropic GABA receptors (GABA_B receptors) or ionotropic GABA receptors (GABA_A receptors). GABA transporters (GATs) are responsible for the uptake and recycling of GABA from the synaptic cleft [39]. GABA is catalyzed to succinate in astrocytes by GABA transaminase (GABA-T) and succinate semialdehyde dehydrogenase [39]. The succinate is then used to generate glutamate [39]. The binding of GABA to GABA_A receptors allows the influx of chloride ions which is responsible for membrane hyperpolarization [39]. On the other hand, GABA binding to GABA_B receptors dissociates coupled G protein to G α i and G $\beta\gamma$ leading to the activation of postsynaptic K⁺ efflux channels and inhibition of presynaptic Ca²⁺ influx [44,45]. Since intracellular cyclic AMP (cAMP) signaling modulates the excitatory glutamatergic signaling, the G α i exerts inhibitory tone via the reduction of cAMP level [39]. By promoting the efflux of K⁺ and suppressing Ca²⁺ influx, G $\beta\gamma$ induces hyperpolarization and inhibition [45]. GABAergic remodeling has been associated with the pathophysiology of AD [39,46] (**Figure 2**). Given the glutamatergic excitotoxicity in AD, targeting the GABAergic tone has often been hypothesized as a viable solution for the development of therapeutics in AD. Additionally, around 22% of AD patients experience epileptic seizures [47]. GABAergic dysfunction in AD is often accounted for this epileptic seizure and therefore anti-epileptic drugs are currently in a clinical trial in AD [48]. Apart from glutamatergic and GABAergic dysbalance in AD, monoaminergic and cholinergic neurotransmission is also altered in AD [39].

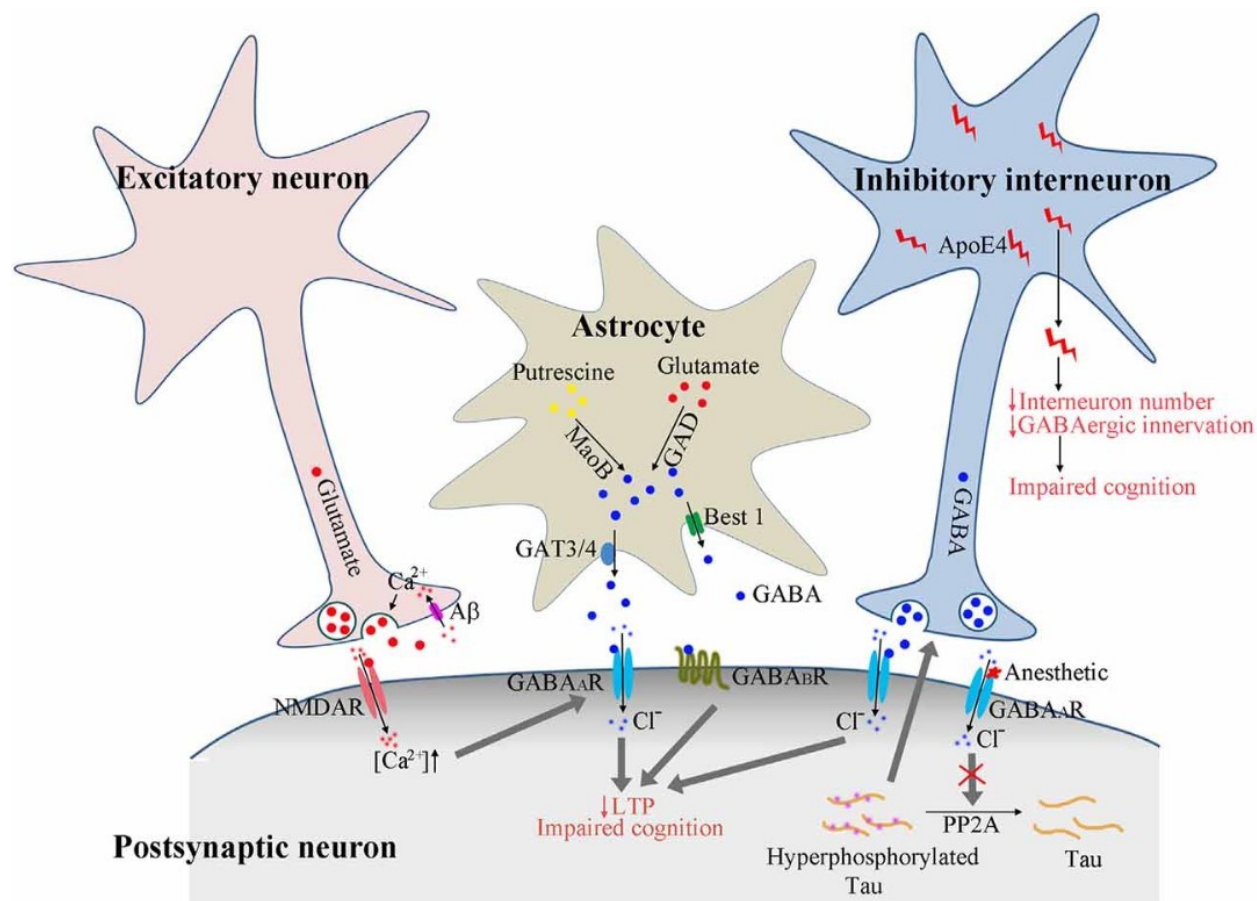


Figure 2. Schematic representation of GABAergic signaling in AD-related mechanism (Adapted with permission from [49]).

Increased Calcium influx from A β mediated pathology activates the release of glutamate from the presynaptic terminal. This further triggers the activation of the postsynaptic terminal. To counter the enhanced excitatory signal NMDA receptors enhance the GABA receptor activation. In AD pathology, possibly an enhanced release of GABA from the astrocyte activates the extrasynaptic GABA receptors which result in impaired LTP.

1.1.1.3 Genetics of AD and risk factors

A larger fraction of AD cases (90%) is sporadic [50]. The gene that is often associated with sporadic load is the apolipoprotein E (*APOE*) gene [51]. Only a small portion of the AD cases appear to be familial and these are largely attributed to the mutations in Amyloid Precursor Protein (*APP*), Presenilin1 (*PSEN1*), or Presenilin2 (*PSEN2*) [52]. *APP* mutations account for 10-15 % of early-onset familial AD [53]. The most common examples of *APP* mutations that lead to an

increase in A β production and pathogenesis of AD include “Swedish” mutations (APPK670N, and M671L) and the “London” mutations (APPLON and APPV717I) [54,55]. Based on these APP mutations several transgenic mouse models including APP23, PDAPP, Tg2576, TgCRND8, and J20 lines have been generated and are studied for the different regiments of molecular details of pathophysiology as well as for the development of therapeutics [56]. Impairments of *PSEN1* and *PSEN2* genes have also been regularly attributed to AD [53]. Both PSEN1 and PSEN2 are essential components of the γ -secretase enzyme, which is responsible for the cleavage and production of A β [57]. Mutations in both *PSEN1* and *PSEN2* genes are associated with an increase in the ratio of A β_{1-42} to A β_{1-40} [53,57]. Additionally, it is important to note that early-onset AD caused by genetic mutations is primarily associated with elevations in A β_{1-42} levels. The location of the mutation in the presenilin gene is reported to differentially affect the production of A β . While *PSEN1*-L166P reduces A β production, *PSEN1*-G384A significantly increases A β_{42} production [53]. Mutations in the *APOE* gene are associated with both sporadic and familial AD. ApoE has a crucial role in the metabolism and distribution of triglycerides and cholesterol in different cell types [53]. Carriers of the *APOE* risk allele ($\epsilon 4$) display higher levels of cholesterol and have higher amyloid pathology and mitochondrial damage compared to the ones carrying other polymorphisms of *APOE* [53]. Recent GWAS studies have added potential genetic players to the current pool of risk genes. These include triggering receptor expressed on myeloid cells 2 (*TREM2*), bridging integrator 1 (*BINI*), *ABCA7*, complement receptor 1 (*CR1*), *CD33*, clusterin (*CLU*), membrane-spanning 4-domains subfamily A (*MS4A*), ephrin type-A receptor 1 (*EPHA1*), and phosphatidylinositol binding clathrin assembly protein (*PICALM*) genes [58]. Age is considered to be a crucial risk factor in AD [59]. Other risk factors in AD include frequent smoking, regular alcohol consumption, and obesity [60]. Previously APP transgenic mice fed with a high-fat diet have been reported to exacerbate the pathophysiology of AD [61,62]. Another, essential and undermined risk factor of AD is depression (discussed in the next section).

1.1.2 Amyloid Cascade Hypothesis

The amyloid cascade hypothesis is one of the most widely accepted explanations for AD pathology which stresses the role of A β deposit in the pathophysiology [63]. Over the years, there have been several discoveries supporting this hypothesis as well as several arguments which counter the amyloid cascade hypothesis. The hypothesis has been modified over the years to accommodate

features and the association of cognitive decline with A β deposit. Soluble forms of oligomeric A β which are intermediate to the monomeric and the fibrillar form of A β are strongly associated with the neurotoxicity of A β peptide [64]. These oligomeric forms of A β are often thought to lead the A β aggregation, formation of paired helical filaments (PHFs) and finally leading to neuronal death [65]. Familial AD is associated with gene mutations that are directly associated with A β production. The association of mutation in *PSEN1* and *PSEN2* of γ -secretase with AD pathology supports the amyloid cascade hypothesis [63,66]. Another interesting correlation that supports the amyloid cascade hypothesis comes from a parallel study of patients with Down's syndrome [67,68]. These patients have an extra copy of the APP gene in chromosome 2, thereby producing excessive APP, and develop A β plaques and dementia by an early age estimate of about 40 [69]. Different types of soluble A β oligomers have been extensively studied and associated with the impairment of long-term potentiation (LTP) in the hippocampus [70–72]. Similarly, soluble A β oligomers are associated with neuronal loss and neuroinflammation including reactive astrogliosis [73]. All these studies posit A β as a critical factor in the pathophysiology of AD.

However, there are several arguments against this hypothesis. Hyperphosphorylated tau protein in neurofibrillary tangles is correlated with a higher degree of cognitive impairment than A β deposits [5]. This however is countered by the involvement of A β in the early phase and the occurrence of tau at a later phase where cognitive deficits are prominent. While the involvement of tau cannot be undermined, it is possible that the synaptotoxic action of A β is mediated and aggravated by the tau protein. This is supported by the human genetics study which shows APP mutations enhance the A β production and alter the downstream modulation of wild-type tau, while tau mutations do not lead to enhanced A β production or associated dementia [74]. The presenilin hypothesis is another alternative to the amyloid cascade hypothesis which suggests impairment of presenilin function leads to progressive neuropathology in AD [75]. This is supported by the presenilin KO study which leads to cognitive impairment and loss of cortical neurons [76]. This, however, doesn't still overrule the possibility of enhanced A β production in the loss of function of presenilin, since A β is upstream of the cascade that leads to the loss of presenilin function. Another crucial argument that counters the amyloid cascade hypothesis is the failure of several anti-amyloid therapies in reducing all the pathophysiological features of AD [77,78]. This could partially be attributed to the low penetration of these substances in the brain. Additionally the recent success with lecanemab and donanemab which shows marked reduction of amyloid and associated slowing

down of cognitive decline [79–81] challenges the argument and strengthens the amyloid cascade hypothesis. Also, AD being multimodal in terms of pathology affects multiple pathways and while A β potentially could be the initiator of this cascade, several other crucial players progress the pathophysiology of AD. Targeting only A β production might not, therefore, be a viable solution. The energy burden resulting from an enhanced energy demand in AD has often been understudied while developing therapeutics. It is crucial therefore to focus on the bigger picture instead of targeting individual pathways. All this taken together, still suggests A β as a primary player to initiate the cascade of AD pathology and supports the amyloid cascade hypothesis.

1.1.3 Amyloid- β peptide and aggregation in AD

The endoplasmic reticulum synthesizes APP, a type I transmembrane glycoprotein with a short cytoplasmic domain and a large luminal domain which is transported to the trans-Golgi-network (TGN) by the Golgi apparatus [82]. In a physiological state, upon reaching the cell surface, the fate of APP is decided either via the α -secretase enzyme which cleaves it to form soluble α -APP fragments (sAPP α) or is re-internalized by recognition of the “YENPTY” motif and recycled back to the cell surface [74,83]. Therefore, the non-amyloidogenic processing of AD by α -secretase leads to the generation of non-toxic fragments [83]. In addition to this, previous studies show that these non-toxic fragments antagonize the generation of A β [83]. On the other hand, APP processing via the amyloidogenic pathway results in A β biogenesis [74,83]. The availability of APP in acidic compartments like that of the endosomes increases the chances of APP processing to occur via the amyloidogenic pathway [84] (**Figure 3**).

Both β -secretase and γ -secretase play a crucial role in A β biogenesis [83]. The first cleavage of APP by β -secretase produces large soluble β -APP (sAPP β) fragments and membrane tethered-C-terminal β fragments (CTF β) [83,85]. These APP-CTFs are cleaved by γ -secretases to form A β and the APP intracellular domain (AICD) [86,87]. Beta-secretase 1 (BACE1), a transmembrane aspartyl protease, forms the major class of β -secretase which is responsible for the generation of the N-terminus of A β [84,87,88]. Previously alterations in BACE1 levels have been shown to affect the processing of APP [84,89]. Importantly the activity of BACE1 is thought to be the rate-limiting step in A β generation [90,91]. Production of mature BACE1 is dependent on glycosylation, phosphorylation, and endoprotease cleavage of precursor pro-BACE1 [92,93].

These properties of BACE1 have led to diverse studies exploring the therapeutic potential of BACE1. Previous reports from BACE1 knockouts show that they have phenotypic advantages in terms of reduced pathophysiology of AD such as rescued cognitive decline, reduced levels of A β , and amelioration of cholinergic dysfunction [93–97]. In addition to BACE1, BACE2, and cathepsin B are among the relevant β -secretases which affect the A β production levels [98]. Also, it is important to mention that overexpression of APP-CTF β which is a product resulting from β -secretase cleaving has a crucial effect on increasing cytotoxicity and associated neuronal cell death [98,99]. Whether APP-CTF β is individually neurotoxic or their processing further by the γ -secretase contributes to cytotoxicity is not established yet and requires further research. γ -secretase is composed of four essential components: Nicastrin, presenilin (PS, PS1, or PS2), anterior pharynx-defective-1 (APH-1), and presenilin enhancer-2 (PEN-2) [100]. It is important to note though that although all these four components form the complete complex of γ -secretase, the core component of the activity of γ -secretase is dependent on presenilin [101,102]. This is evident from the mutations in the presenilin gene which form the majority cluster of familial AD cases [103,104]. The generation of A β via both the secretases forms the starting point of pathophysiological effects in AD.

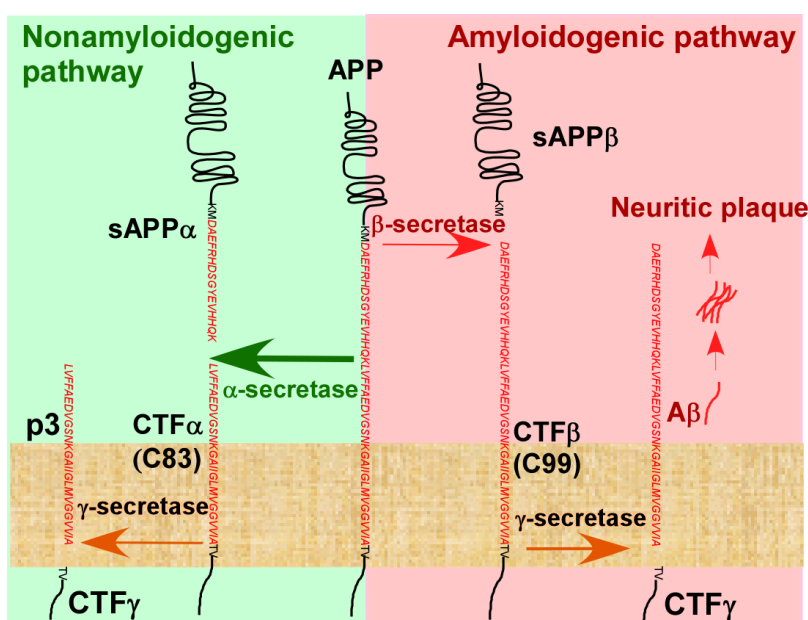


Figure 3: Amyloidogenic and non-amyloidogenic pathways of APP processing (Adapted with permission from [84]).

The fate of APP processing is decided upon either the amyloidogenic (red, right) or the nonamyloidogenic (green, left). Under physiological conditions, APP cleavage within the A β domain is carried out by α -secretase to generate membrane-bound C83 and sAPP α . Further cleavage of C83 by γ -secretase generates an intracellular carboxy-terminal fragment (CTF) γ and an extracellular p3 fragment. On the other hand in the amyloidogenic processing of A β , β -secretase cleaves APP to produce membrane-bound C99 and sAPP β . C99 is further cleaved by γ -secretase to produce A β and intracellular CTF γ .

1.1.4 Arctic mutation mouse model of AD

Transgenic mouse models carrying a mutation in *APP* or *PSEN1* have been explored to study different aspects of AD pathology starting from cholinergic dysfunction to sleep and circadian abnormalities. Given the diverse pathophysiological profile of AD, no single transgenic mice model recapitulates all the features of AD pathology. It is therefore always wise to choose the models based on the questions asked and taking into consideration the pros and cons of each transgenic strain. Overexpression or knock-in models of the human APP gene linked to FAD mutations have resulted in the creation of several transgenic mouse models. Among the most commonly used transgenic mice for AD is the Tg2576 model which overexpresses the human APP gene carrying the Swedish mutation (KM670/671NL) [105]. The Tg2576 mouse line has amyloid plaque formation around 11 to 13 months old and shows reactive gliosis around the plaques [106]. While memory impairment is reported in this line around the age of 10 months, no neuronal loss has been found. J20 model, another transgenic mice line, contains two FAD-linked mutations, the Indiana mutation (V717F) and the Swedish mutation (KM670/671NL), which overexpresses the human APP gene [107]. These mice develop amyloid deposition at 5-7 months old with an increase in hippocampal plaque load. Reactive gliosis at the age of 6-9 months, chronic neuroinflammation, neuronal loss, and cognitive impairment have been reported in this model [108]. PS2APP mouse model on the other hand overexpresses both the human PSEN2 gene with N141I mutation under prion promoter and the human APP gene carrying the Swedish mutation (KM670/671NL) under Thy1.2 promoter [109,110]. The advantage of this model includes the widespread formation of plaques in different brain regions including thalamic and pontine nuclei apart from the hippocampus, neocortex, and amygdala [109]. APP^{swe}/PSEN1^{de9} (APP/PS1) mice are created by two vectors, one which encodes the FAD-linked PSEN1 gene without exon 9 and the other

vector with APP gene carrying the Swedish (KM670/671NL) mutation [111]. These mice lines exhibit early deposition of A β around 6 months and exhibit spatial learning deficits in the Morris water maze [112,113].

The Tg-ArcSwe mice carry both Swedish mutation (KM670/671NL) and Arctic mutation (E693G) under the Thyl promoter and it overexpresses the human APP gene [114]. These mice exhibit early learning impairments around the age of 4 months and have also been reported to have amyloid deposits accompanied by reactive astrogliosis and neuronal loss [115]. Another commonly used AD transgenic mouse model which expresses 5 FAD-linked mutations Florida (I716V), Swedish (KM670/671NL), and London (V717I) mutations in the APP gene, and the L286V and M146L (A > C) mutations in the PSEN1 gene is the 5xFAD mice [116]. The appearance of plaques occurs as early as 2 months old and progresses rapidly with age till 7 months [109,116]. Spatial memory is impaired by 6 months of age. There exists a transgenic model which increases the A β generation without overexpressing the APP gene. The mouse line AppNL-G-F knock-in is one such example where the APP mouse gene is introduced with the Swedish (KM670/671NL), Arctic (E693G), and Iberian (I716F) mutations [117]. While this line does not show any neuronal loss, it shows cortical A β deposition, impaired memory, and reactive gliosis [117]. Apart from these mouse lines which exhibit mutations linked to FAD, there are other tauopathy models which comprise both genetically modified models and tau seed injection models. Some of these widely used mutations in the microtubule-associated protein tau (MAPT) gene are expressed under prion promoter and induce cognitive deficits and neuronal loss [109]. In summary, different transgenic mouse AD lines are created and studied by the researchers to capture different aspects of AD and to answer questions pertaining to the multimodal nature of AD. In addition to these genetic models, there have been attempts to recreate pathology-mimicking models such as the ones where chronic stress enhances the amyloidogenic processing of APP [118]. However, a major disadvantage of this model system includes variable amounts of chronic stress which cannot be directly quantified as well as cannot be correlated with chronic stress in humans.

In the current project, we have used the ArcA β transgenic AD mice model which contains overexpression of human APP695 containing both Swedish and Arctic mutation under the prion promoter gene [119] (**Figure 4**). Previously ArcA β has been associated with cognitive impairment from the age of 6 months. One of the primary reasons for choosing this model for our project was

that the ArcA β model encompasses both the Swedish and Arctic mutation in a single construct which increases the propensity and stability of A β aggregation. Additionally, since we planned to test memory retention via retests which requires a long-time frame, this model was suitable due to the early development of cognitive impairments. Both 6-month-old and 9-month-old mice showed impaired cognitive learning as evident from the Y-maze and the Morris water maze [119]. A reduced percentage of arm alteration in the Y maze also indicated an impaired working memory. Formation of intracellular A β aggregates has been reported at this age with no apparent plaque load [119]. These intracellular A β deposits are therefore thought to correlate with associated cognitive impairments. Formation of plaque load has been reported to start at the age of 9 months old. Importantly, the mouse line consists of dense-core plaques which are usually associated with the Swedish mutation [119]. Another interesting correlate of this model is that the dense core plaque formation coincides with severe CAA [119]. Furthermore, significant locomotor and exploratory hyperactivity have been shown in this model at the age of 3 months. This hyperactivity however becomes normal with age as examined around 6 and 9 months old [119]. We used this model to study further the pathophysiology of AD and examine if TSPO activation via XBD173 could rescue the pathophysiological features of AD in this transgenic model.

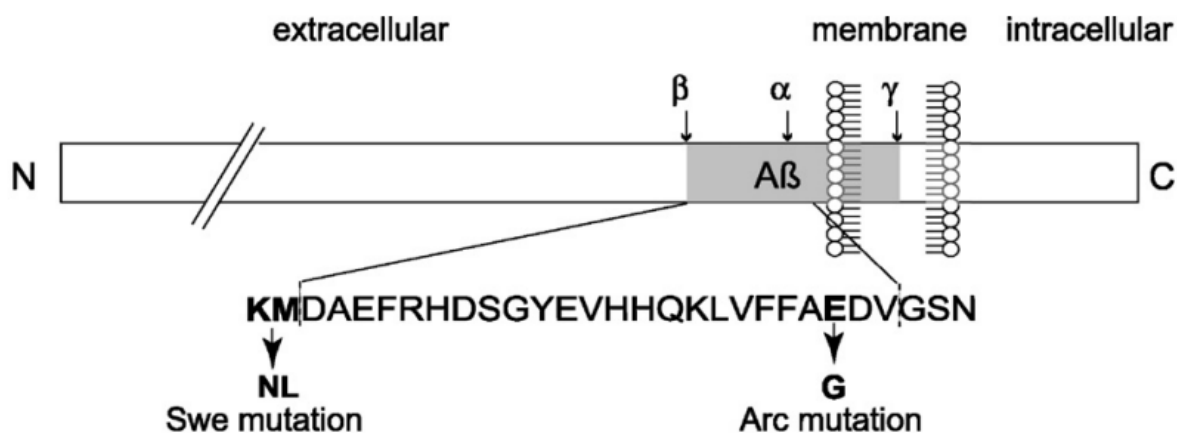


Figure 4: Representative schematics showing the location of Swe and Arc mutations in the human APP containing the A β sequence (Adapted with permission from [119]).

1.2 Depression

1.2.1 Depression and Sleep: From a Molecular and Cellular Perspective

The criteria for defining a major depressive episode is a history of depressed mood or anhedonia (diminished enjoyment of normally pleasurable activities) for at least 2 weeks with at least 3 of the following symptoms: psychomotor agitation or retardation, sleep disorders, frequent thoughts of suicide, significant weight change or change in appetite, feelings of guilt and worthlessness, difficulty concentrating, and impairments [120]. From previous clinical evidence, chronic depression has resonated with stress and the Hypothalamus-Pituitary-Adrenal Axis (HPA axis) [120–122]. For instance, elevated levels of cortisol and hypothalamic corticotropin-releasing hormone (CRH) have been associated with patients of depression [120,123]. The association of depression with sleep impairments is evident from HPA axis dysfunction [124–126]. Among several sleep parameters, the crucial ones affected by depression include reduced slow-wave sleep in the first cycle, increased intermediate awakenings, lower rapid eye moment (REM) latency, and a higher REM sleep density [127]. CRHR1 antagonists, therefore, are known to better the sleep cycle in cases of depression and alleviate depression-like behavior in rodents [128]. An essential aspect of depression is the reduced monoaminergic tone and elevated levels of glucocorticoids are thought to be the major player which affects the levels of monamines [129,130]. This leads to impaired serotonergic signaling and reduced hippocampal neurogenesis [131]. Alteration in the levels of the intracellular secondary messenger cyclic adenosine monophosphate (cAMP) affects the CREB phosphorylation by protein kinase A (PKA), leading to impaired neurogenesis in depression [132–134].

1.2.2 From Depression to Dementia: In Retrospection

Clinical studies over several years have studied the association of depression or depressive symptoms as well as anxiety-disorders to the development of dementia [135–137]. The fundamental question that arises is whether late-life depression or early-life depression constitutes a major risk factor for cognitive impairment in dementia [138–140]. One of the longest longitudinal studies with a 17-year follow-up has highlighted a 70% increase in the risk of developing dementia in depressed patients [137]. While both early- and late-life depression posits certain risks to the development of dementia, multiple cohorts of study have outlined a strong association between late-life depression and dementia [141–145]. Additionally, anxiety-like disorders associated with depressive symptoms posit a higher risk for the development of dementia [146–148].

The cellular and molecular underpinnings of depression and dementia are one of the primary factors which are thought to correlate with both these neurodisorders. As discussed earlier, major depression affects the stress-related HPA axis leading to increased cortisol production and causing hippocampal atrophy [124,126]. Activation of the HPA axis also increases the production of glucocorticoid which affects the glucocorticoid receptors as well as damages the hippocampus causing cognitive decline [126]. This impaired glucocorticoid mechanism has also been strongly documented in dementia [149]. Depressive episodes are correlated with a high degree of stress. Cumulation of this phenomenon over time is thought to progress to dementia.

A β deposits and hyperphosphorylated tau constitute key pathological changes with the progression of AD. Previous studies have demonstrated an enhanced accumulation of plaques and tangles in the hippocampus of AD patients with depression compared to the ones without depression [150,151]. This essentially highlights that in addition to being a prodrome of dementia, the depressive disorder could also potentiate and aggravate the pathophysiology of AD. The stress pathway associated with depression correlates with increased A β production in AD [152,153]. Indirect evidence comes from the study that reports glucocorticoid administration promotes A β production by increasing BACE1 levels [154]. Additionally, depression via an imbalance in the serotonergic system could accelerate the A β accumulation process [152,155]. Amyloid-associated depression, in which depressed patients show elevated levels of plasma A β might therefore represent an intermediate phase between the transitioning from depression to dementia [156]. The impaired monoaminergic system (serotonergic and noradrenergic) involved in both depression and AD provides another link between these disorders [157]. Locus coeruleus (LC) lesions are associated with aggravated pathophysiology including pronounced neuronal damage, increased plaque burden, and chronic inflammation [158,159]. Additionally, serotonin plays an important role in the processing of APP via non-amyloidogenic pathways via 5-hydroxytryptamine (5-HT₄) receptors [160]. A reduction in serotonin levels (in both depression and dementia) could therefore favor the processing of APP via the amyloidogenic pathway.

Chronic neuroinflammation, a key pathophysiological effect in AD is also seen in major depression [161–163]. Increased levels of pro-inflammatory cytokines such as interleukin (IL) - 6

and tumor necrosis factor (TNF) associated with depression could lead to a decrease in anti-inflammatory cytokine as well as affect hippocampal neurogenesis via interference with the 5-HT metabolism [163,164]. In AD, A β deposits are known to affect the glial cells to release more pro-inflammatory cytokine and this has been correlated with increased loss of functional neurons leading to cognitive decline [165]. A reduction in neurotrophic factors such as brain-derived neurotrophic factors is another similarity between depression and dementia [153]. The similarity between these disorders on a cellular level as well as the association from the longitudinal studies strongly suggests that depression increases the risk of developing dementia as well as might aggravate the AD pathology.

Antidepressants have clinically been shown to rescue cellular atrophy and increase neurogenesis by reversing the effects of stress. Commonly used antidepressants such as Fluoxetine rescued and ameliorated the stress-induced hippocampal neurogenesis and impaired brain-derived neurotrophic factor (BDNF) levels in mice [166]. Previously, depressed patients administered chronic antidepressant treatment for a longer duration were associated with a lower risk of AD than those who were prescribed antidepressants for a shorter duration [167]. Long-term treatment with antidepressants, therefore, has been proven to be beneficial in either significantly delaying the progression to AD or decreasing the risk of developing dementia. From a pathophysiological perspective, SSRIs commonly administered to patients suffering from major depressive episodes are shown to reduce plaque burden, ameliorate cognitive deficits as well and shift the balance to non-amyloidogenic processing of APP from amyloidogenic processing of APP [168–170]. Fluoxetine treatment in AD transgenic mice line decreases the A β accumulation [171]. Chronic treatment with antidepressants additionally has been shown to rescue the impaired cAMP-PKA-CREB pathway which leads to betterment in synaptic plasticity [172,173].

The ability of antidepressants to interfere with the A β production as well as a shift from amyloidogenic processing to non-amyloidogenic processing of APP contributes greatly to its neuroprotective effects in the case of AD. The chronic neuroinflammatory response exerted in AD has also previously been shown to be ameliorated to a certain extent by antidepressants [174–176]. This is partly due to the anti-inflammatory properties of these drugs. For instance, SSRIs like fluoxetine limit reactive gliosis and promote a shift from pro-inflammatory cytokines to anti-inflammatory cytokines [177]. All this evidence taken together strongly suggests an association

between depression and AD and also highlights the importance of new therapeutic interventions which should target these overlapping cellular mechanisms.

1.3 Translocator Protein, Neurosteroids, and GABA_A receptors

1.3.1 Structure and function of translocator protein

The translocator protein (169 amino-acid residues), previously known as the peripheral benzodiazepine receptor, is a highly conserved protein with five transmembrane domains and is located on the outer mitochondrial membrane [178,179]. This 18 kDa protein was first identified in 1977 as a benzodiazepine binding site (BZD) in peripheral organs [180]. Since then, TSPO has been explored further in terms of both structural as well as functional profiles. Given the extensive role of mitochondria in energy homeostasis, ion transport, Ca²⁺ balance, inflammation, production of reactive oxygen species (ROS), apoptosis, and metabolite biogenesis [181–183], they are associated with neurological conditions and neurodegenerations such as Parkinson's, Huntington's, and AD [184,185]. Mitochondrial membrane proteins, therefore, are excellent targets for the development of therapeutics against these neurodisorders. TSPO on the outer mitochondrial membrane interacts with neighboring proteins including the voltage-dependent anion channel (VDAC) and adenine nucleotide transporter (ANT) to form a complex [186–188]. The expression of TSPO is higher in steroid-synthesizing organs such as the gonad, adrenal, and brain cells [178,179]. Previously, during inflammation glial cells (microglia and astrocytes) were predominantly thought to express TSPO in the central nervous system [189]. Recent studies show their expression is also affected by neuronal activity which challenges the general assumption of their expression being altered only during inflammatory responses [190].

TSPO, which forms a crucial element of the outer mitochondrial membrane, mediates several mitochondrial functions, the primary ones being the transport of cholesterol, synthesis of steroids (**Figure 5**), programmed cell death, cell proliferation, and mitochondrial respiration [191]. TSPO's role in steroid production, apoptosis, and proliferation has been established using knockout (Homologous recombination), knockdown (TSPO antisense vectors) as well as RNA silencing techniques [192–198]. TSPO plays a crucial role in the transport of cholesterol from the outer to the inner mitochondrial membrane, which is the rate-limiting step in the production of neurosteroids [178,179,191].

Aberrations in the *TSPO* gene in Leydig cells are associated with malfunctions in cholesterol transport and subsequent production of steroids [199]. Recently, however, some studies have challenged the role of TSPO in the synthesis of neurosteroids [200]. This is supported by the animal model studies where knockout of TSPO does not affect the viability or phenotype of the mouse line [201]. However, the upregulation of steroid levels by TSPO ligands counters this argument. Additionally, *in vitro* expression studies, as well as site-directed mutagenesis show a cholesterol-recognizing amino acid consensus domain (CRAC) in the cytosolic C terminus of the TSPO protein [202,203] (**Figure 6**). NMR spectroscopy establishes the binding of TSPO to cholesterol at the CRAC domain [191,204]. All these suggest that the C-terminal side of the TSPO protein which is exposed to the cytosol plays a crucial role in the import of cholesterol.

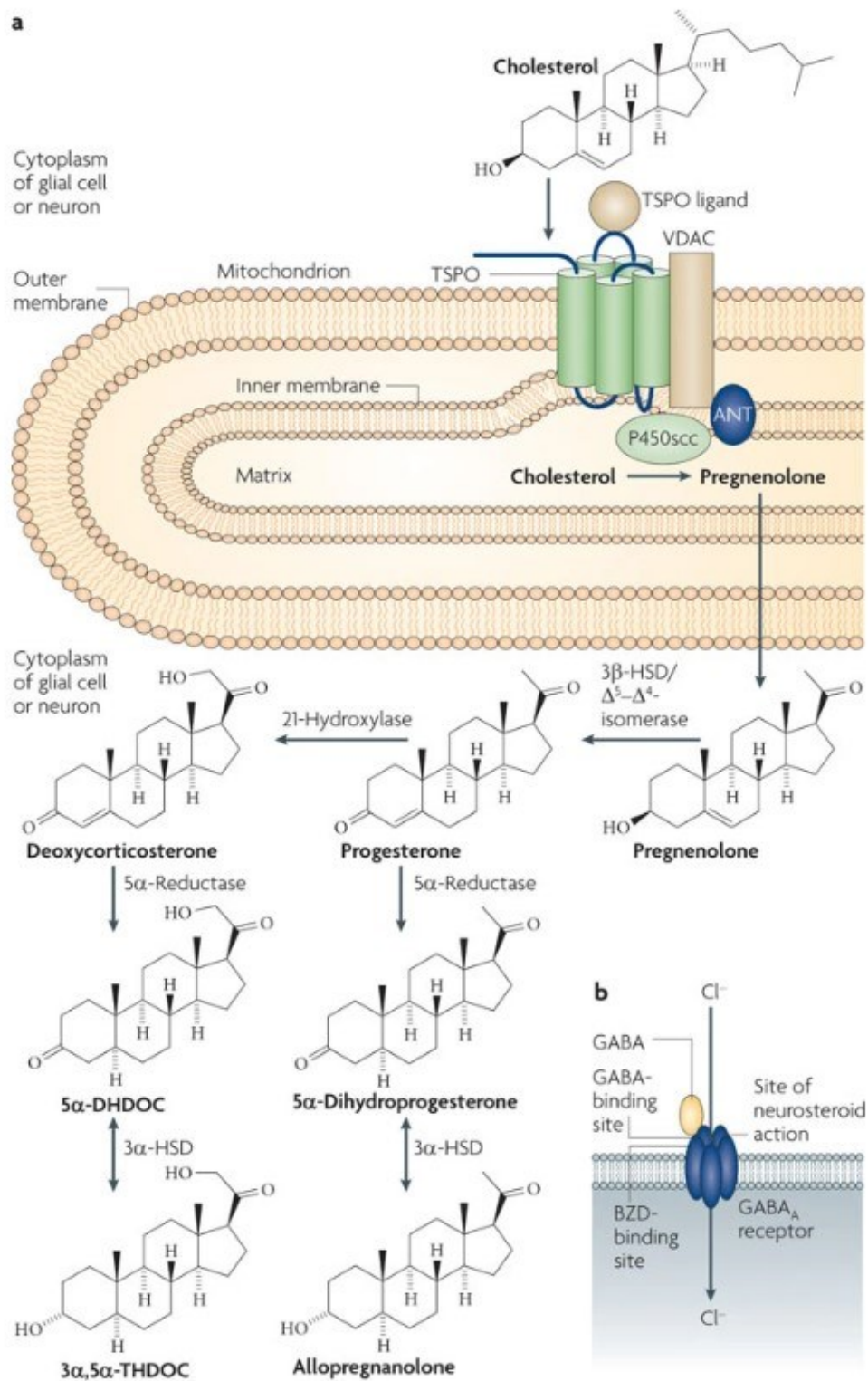


Figure 5: Translocator protein helps in importing cholesterol to the inner mitochondrial membrane (Adapted with permission from [191])

A. Cholesterol upon reaching the inner mitochondrial membrane gets converted to pregnenolone by cholesterol side-chain-cleaving cytochrome P450 enzyme (P450_{scc}). Pregnenolone forms the base for the generation of a diverse range of neurosteroids. B. The 3 α -reduced neurosteroids are potent allosteric modulators of the synaptic and extrasynaptic GABA_A receptors and bind at a site different from the BZD binding site. 3 β -HSD: 3 β -Hydroxysteroid dehydrogenase; 3 α -HSD: 3 α -Hydroxysteroid dehydrogenase; BZD: Benzodiazepine; 3 α , 5 α THDOC: 3 α , 5 α Tetrahydrodeoxycorticosterone; 5 α DHDOC: 5 α Dihydrodeoxycorticosterone; VDAC: voltage-dependent anion channel protein

Neuronal injury or neurodegeneration is known to elevate the expression of TSPO [191]. For instance, TSPO expression in injury is elevated in Schwann cells, neurons, and microglia and the expression of TSPO is proportional to the degree of damage [205–207]. TSPO expression has long been explored as a definitive biomarker in neurodegeneration because of its upregulation at the degenerative sites [191]. Interestingly, a previous study shows the association of differential expression of TSPO in glial cells with neuroprotection [208,209]. The upregulation of TSPO in astrocytic cells was found to be neuroprotective in contrast to those in microglia where upregulation of TSPO was associated with neuronal loss [210]. It is therefore possible that the upregulation of TSPO is the brain's way to counter the degeneration. This is evident from the role of TSPO in regenerative processes. Importantly, however, psychiatric disorders involving anxiety disorders, post-traumatic stress disorders (PTSD), and panic disorders, were associated with a marked reduction of TSPO protein [191].

Among the endogenous ligands of TSPO are cholesterol, endozepines, and porphyrins. Cholesterol and porphyrins have nanomolar and micromolar affinities for TSPO respectively [191]. Benzodiazepines which also bind to TSPO require additional VDAC for optimal binding and other drug ligands primarily bind to a region within the amino terminus [211]. Apart from endogenous ligands, several synthetic ligands of TSPO have been studied to elucidate the role of TSPO in different disorders [191].

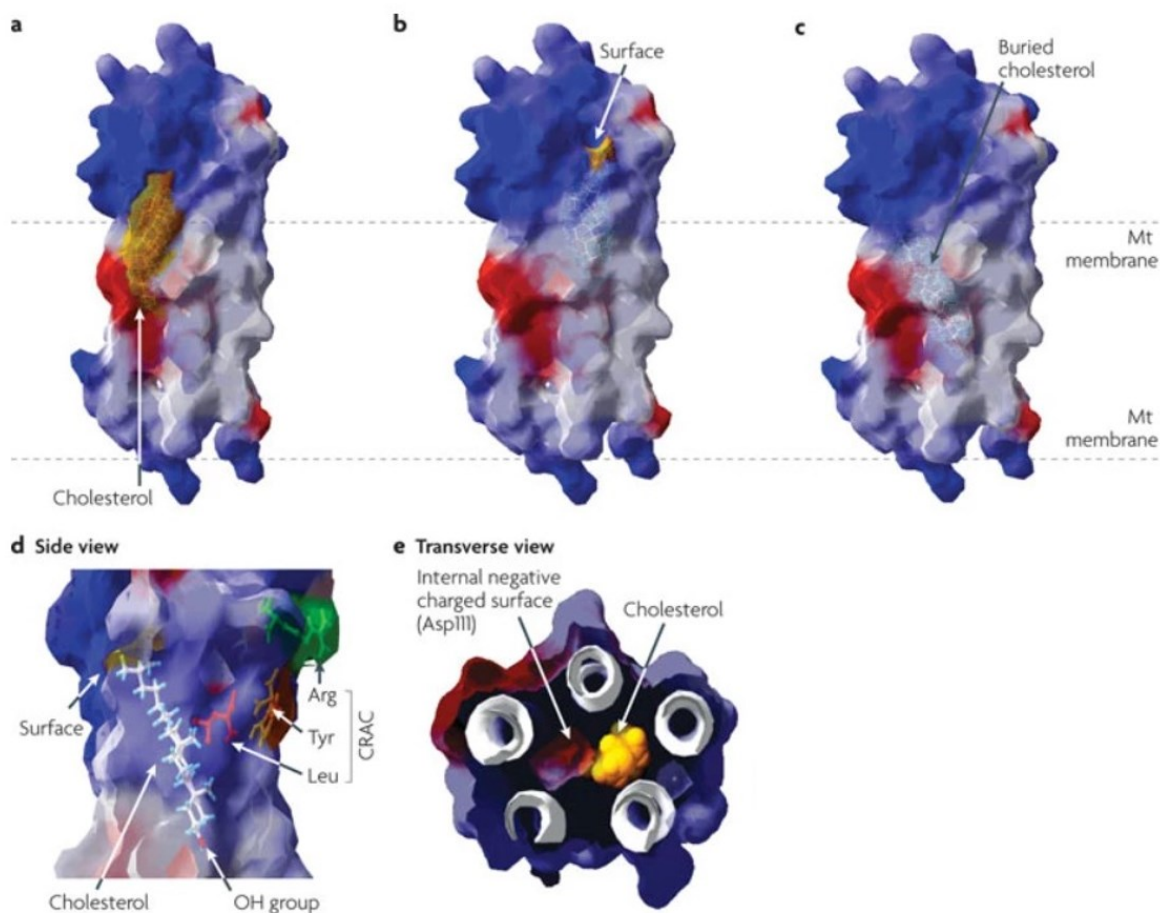


Figure 6: Cholesterol binds to the CRAC domain at the C terminal of 18kDa TSPO (Adapted with permission from [191]).

a. Electrostatic potential map showing cholesterol docked to TSPO b, c 2 different TSPO conformational models giving an insight of cholesterol import from outer to the inner mitochondrial membrane. In the electrostatic potential map, white represents the hydrophobic surface, blue color shows positively charged areas whereas red color shows negatively charged regions. d. The CRAC domain consists of Leu/Tyr/Arg residues with internalized cholesterol. e. Three-dimensional TSPO transverse model showing that negatively charged residue might assist in cholesterol import (Asp111). The white circles represent the transmembrane alpha helices.

1.3.2 Translocator Protein Ligands in Neurodisorders

Given the diverse profile and functional role of the TSPO protein, ligands targeting the translocator protein are now being explored for their therapeutic potential in several neurodisorders. For

instance, TSPO ligand SSRI80575 promotes functional recovery in facial nerve injury [212]. The TSPO ligand olesoxime also protects motor neurons from axotomy-induced cell death and regenerates sciatic nerves following injury [213]. Further studies on olesoxime have shown its neuroprotective potential against chemotherapy-induced peripheral neuropathy [191]. Etifoxine, another TSPO ligand, promotes axonal growth after freeze injury in rats [214]. Classical TSPO benzodiazepine ligand Ro5-4864 prevented kainic acid-mediated excitotoxicity. Brain intracerebroventricular injections (i.c.v) of kainic acid are neurotoxic and result in neuronal loss and hippocampal astrogliosis [215]. TSPO ligands are well known to modulate macrophage activation and affect the production of inflammatory cytokines after nerve injury [191]. For instance, both Ro-4864 and PK11195 in rodent models reduce glial activation as well as the levels of pro-inflammatory cytokines [215,216]. In psychiatric disorders, TSPO ligands have been explored greatly for their potent anxiolytic effects [217–219]. Etifoxine for instance shows a comparable anxiolytic effect as benzodiazepine lorazepam [220]. Similarly, the highly-specific ligand for TSPO XBD173 shows a potent anxiolytic effect without having an adverse side-effect profile compared to the commonly used benzodiazepines in perioperative anesthesia [221].

TSPO ligand Ro5-4864 ameliorated the pathophysiology in a rodent tauopathy model [222]. R05-4864 rescues brain atrophy as well as prevents hippocampal neuronal loss [223]. TSPO ligands compound 2a and 2b prevent overt cytotoxic effects from A β mediated bioenergetics deficits and also reduce oxidative injury under stress conditions [224]. In models of retinal degeneration, targeting TSPO by ligands belonging to the class of N, N-dialkyl-2-arylindol-3-ylglyoxylamides (PIGAs) reduces apoptosis and inflammation [225]. Administration of etifoxine in a mouse experimental model of autoimmune encephalomyelitis (EAE) before the development of clinical signs improves recovery and proves to be neuroprotective by increased oligodendroglial regeneration and less peripheral cell infiltration of the spinal cord [226]. In 3xTgAD transgenic AD mouse models, TSPO ligands Ro5-4864 and PK11195 attenuated the neuropathological developments such as reduction in hippocampal A β accumulation, decreased gliosis, and improved cognition [223]. Administration of Ro5-4864 was correlated with elevated brain testosterone and progesterone levels in 3xTgAD mice [223]. Previously, TSPO overexpression has been associated with providing anxiolytic as well as antidepressant-like effects [227], possibly suggesting that the activation of TSPO affects the underlying mechanism of these neurodisorders and could be a

suitable target for AD. All these pieces of evidence when put together highlights the importance of TSPO ligands in exerting neuroprotective benefits in injury as well as in neurodisorders.

1.3.3 XBD173 in neurodisorders

XBD173, an 8 oxopurine derivative with anxiolytic potential, binds selectively to TSPO with nanomolar affinity [217]. It has little affinity for neurotransmitter receptors, including GABA_A [217]. XBD173/Emapunil as a benzodiazepine alternative has been explored in terms of side-effect profiling. Previously XBD173 has been associated with anxiolytic properties in both animal models as well as in human subjects [228]. XBD173 was additionally shown to potentiate the duration and amplitude of GABA-mediated IPSCs in mouse brain slices via the synthesis of neurosteroids. The inhibition of this effect was achieved with finasteride, a 5 α -reductase inhibitor, suggesting 5 α -reduced neurosteroids mediate the actions of GABA receptors [228]. In the rodents, XBD173 countered the panic attacks without exhibiting benzodiazepine-like sedative effects and the anxiolytic effects were comparable to benzodiazepine alprazolam [228]. Additionally, the withdrawal symptoms that are commonly associated with benzodiazepine use were absent in XBD173 treatment. Activation of TSPO by XBD173 promotes the synthesis of neuroactive steroids which affects the GABA_A receptors thereby exhibiting anxiolytic properties [228]. XBD173's anxiolytic properties during stress tests were prevented by TSPO antagonist PK11195, suggesting a TSPO-dependent role of XBD173 [228]. XBD173 was shown to have comparable anxiolytic potential as that of the benzodiazepine alprazolam. The side-effect profile after XBD173 administration was comparable to the placebo group. On the other hand, benzodiazepine alprazolam showed a more severe side-effect profile including tolerance and withdrawal symptoms. A comparison of the side-effect profile between these drugs therefore gives XBD173 an upperhand [228].

XBD173 in addition to its anxiolytic profile has been explored for its neuroprotective potential in certain neurodisorders. For instance, XBD173 at a dose of 10-20 mg/kg conferred neuroprotection in the mouse model of multiple sclerosis. This was associated with increased levels of allopregnanolone and decreased pro-inflammatory cytokines [229]. In another study concerning retinal ischemia, XBD173 proved to be neuroprotective by modulating the glial response pattern [230]. In a recent study, XBD173 was shown to have beneficial effects in an MPTP rodent model

of Parkinson's by attenuating neuroinflammation, maintaining dopamine metabolism, rescuing the motor phenotype, and inducing the shift from pro-inflammatory cytokines to anti-inflammatory cytokine [231]. XBD173 therefore compared to the present ligands of TSPO is highly selective and has a lower side-effect profile.

1.3.4 Benzodiazepines and Neurosteroids

Benzodiazepines get their name from the structural fusion of a benzene and a diazepine ring having two nitrogen atoms at positions 1 and 4 [232]. The use of benzodiazepines in clinics has been associated primarily with anxiolytics, seizure reductions, muscle relaxants, and sedation [233–235]. Over the years different categories of benzodiazepines have been developed and clinically used to potentiate anxiolysis [234]. At a molecular level, benzodiazepines bind to GABA_A receptors [236]. The binding of benzodiazepines at the benzodiazepine binding site in GABA_A receptors acts as an allosteric modulator to facilitate the GABA binding and opening of the chloride channel to potentiate neuronal inhibition [236]. The sedative-hypnotic properties of benzodiazepines produce limitations in their use as anxiolytics [228,237].

Neurosteroids were originally termed by Baulieu and refer to the steroids that circulate and potentially modulate the actions of the central nervous system and are independent of peripheral organs [238]. The term “Neuroactive steroid” coined by Paul refers to the endogenous or synthetic steroids which modulate the activity of the nervous system [239]. Neurosteroids are considered to be potent modulators of synaptic transmission. They can bind either to the intracellular receptors which regulate gene transcription or can bind to neurotransmitter-dependent receptors. Depending on their binding to these sites, the receptors are termed classical or non-classical receptors [240,241]. The primary biosynthesis of neurosteroids starts with the translocation of cholesterol from the outer to the inner mitochondrial membrane where it is converted to pregnenolone by cytochrome P450 side-chain cleavage [178,242,243]. The translocation of cholesterol forms the rate-limiting step in the synthesis of neurosteroids and TSPO plays a crucial role in this [178,179]. Pregnenolone then forms the precursor molecule for a diverse range of neurosteroids starting from progesterone which undergoes two consecutive sequential A ring reductions to form allopregnanolone [191]. Alternatively, progesterone could convert to deoxycorticosterone (DOC) by cytochrome P450 21-hydroxylase which could further result in the production of

tetrahydrodeoxycorticosterone (THDOC) [242,243]. A diverse range of neurosteroids including dehydroepiandrosterone, pregnenolone sulfate, progesterone, estradiol, THDOC, pregnenolone, testosterone, allopregnanolone, and dehydroepiandrosterone sulfate is produced in the brain which modulates the action of CNS. Additionally, neurosteroids that act via the GABA_A receptors have been studied for their anxiolytic property without exhibiting benzodiazepine-like side effects [228,242,244]. It is important to note that the production and availability of the neurosteroids are region-specific and depend on the availability of the catalyzing enzymes [191]. It would therefore not be uncommon to think that the role of neurosteroids might vary accordingly in different brain areas. Neurosteroids such as pregnenolone, allopregnanolone, and 3 α 5 α THDOC are considered to be potent modulators of GABA_A receptors [245,246].

1.3.4.1 GABA_A Receptors: Structure and Composition

GABA_A receptors play a crucial role in setting up the inhibition tone in the nervous system. These are ligand-gated chloride ion channels and are composed of pentameric subunits [247]. GABA_A receptors can be composed of different subunits to form a diverse range of receptors having sensitivity to different drug targets and therefore a diverse pharmacological profile. In humans alternative splicing results in 19 subunits for GABA_A receptors which include six alpha (α 1 - 6), three beta (β 1 - 3), three gamma (γ 1 - 3), three rho (ρ 1 - 3), and one each of the pi (π), epsilon (ϵ), delta (δ), and theta (θ) subunits [247–250]. In the human genome, the receptor subunits are arranged in 4 clusters consisting of ϵ , α 3, and θ on chromosome X; α 6, β 2, α 1, and γ 2 on chromosome 5; β 1, α 4, α 2, and γ 1 on chromosome 4; and β 3, α 5, and γ 3 on chromosome 15 [251]. The mature GABA_A receptor isoform is composed predominantly of α 1, β 2, and γ 2 subunits and consists of 450 amino acid residues consisting of an N-terminal domain, four hydrophobic transmembrane domain, and hydrophilic extracellular domain [252,253]. The transmembrane 2 domain is thought to form the pore for the entry of the chloride ion. Post-translation modification in the intracellular domain between transmembrane domains 3 and 4 is thought to modulate the activity of the receptor [252,253].

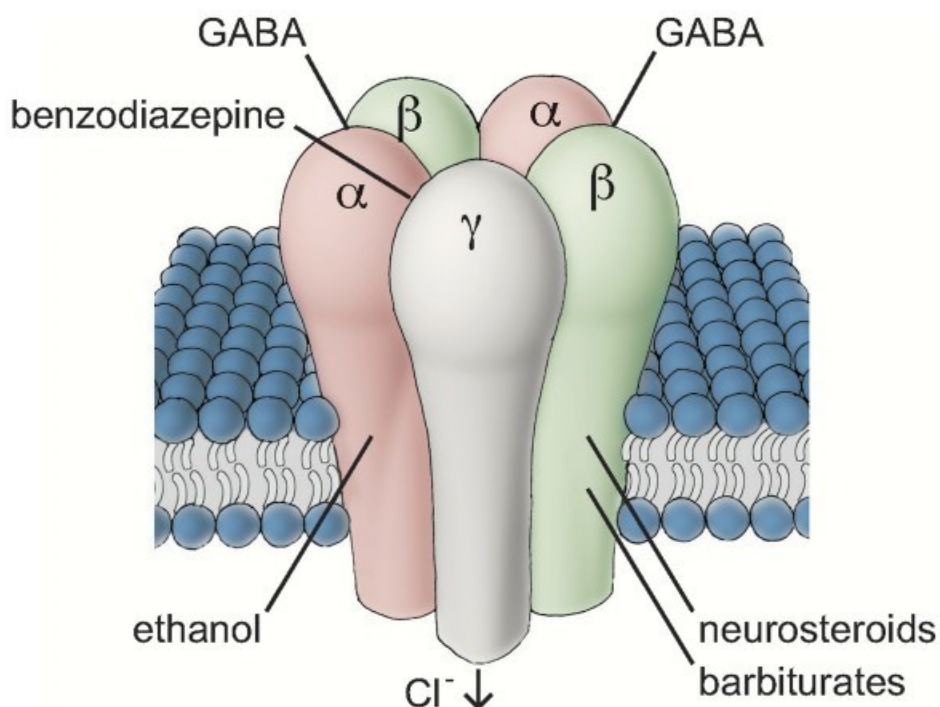


Figure 7: Representative schematic of the GABA_A receptor and its associated binding sites (Adapted with permission from [254]).

The spatial distribution of GABA_A receptors in the brain is different in terms of its subunit composition and region of expression (**Figure 7**). Additionally, while certain subunits have a broad range of expression in the CNS others have a limited/restricted set of expressions [247]. For instance, while the ρ subunit is expressed predominantly in the retina, the $\alpha 6$ has a restricted set of expressions only in the cerebellum [255]. It is possible therefore that this region-specific expression and the subunit composition confer a functional advantage.

The GABA_A receptors produce two broad classes of inhibitory response. First, the phasic inhibition, which comprises transient stimulation of GABA_A receptors (milliseconds). Second, tonic inhibition which is a continuous inhibitory response and plays a crucial role in synaptic plasticity, neurogenesis, or cognitive functions [247]. The GABA_A receptor subunit composition accomplishing the inhibitory effects varies greatly according to phasic or tonic inhibition. The GABA_A receptors localized to postsynaptic sites and conducting phasic inhibition are mainly composed of $\alpha 1-3$, $\beta 1-3$, and $\gamma 2$ subunits, whereas the ones localized to extrasynaptic sites and

carrying out tonic inhibition are primarily composed of $\beta 2/3$, $\alpha 4-6$, and δ subunits [247,256]. The subunit composition carrying out tonic or phasic inhibition varies accordingly to the brain regions [247]. For instance, in the hippocampus, $\alpha 1\beta\delta$ receptors are present whereas the forebrain and cerebellum consist of $\alpha 4\beta\delta$ and $\alpha 6\beta\delta$ receptors respectively [257].

Dysregulation of different subunit expressions has been linked to several neurodisorders including epilepsies, AD, and depression [247,257–261][262]. In AD, misfolded A β accumulation is thought to interfere with the GABAergic activity causing a loss of balance in the excitatory and inhibitory tone which further results in cognitive deficits [259–261]. Transcriptional downregulation of $\alpha 1 - 3, 5; \beta 1 - 3, \delta, \gamma 2/3$, and θ subunits have been associated with post-mortem samples from AD brains [263]. Similarly, GABA neurotransmitter levels are found to be reduced in AD patients [247]. In major depression as well, GABAergic signaling is impaired. Previous studies show decreased GABA and GAD67 levels in depressed patients as well as in stress-related rodent models [247,262,264].

1.3.4.2 Benzodiazepines and Neurosteroid's Effects on GABA_A receptors

The benzodiazepine binding site at the GABA_A receptor comprises α - (1, 2, 3, or 5) and $\gamma 2$ -subunits. The receptors containing α - (4 or 6) subunits are not usually compatible with benzodiazepines. The potent action of benzodiazepines is mediated by the amino acids in the N-terminal domain of the α and γ subunit. The $\gamma 2$ subunit of GABA_A determines the sensitivity of the receptor to benzodiazepines [235]. The α isoforms $\alpha 1$ and $\alpha 2$ mediate the sedative or anxiolytic action of benzodiazepines respectively [265]. The negative effect of benzodiazepines on memory is thought to be mediated by the $\alpha 5$ subunit of GABA_A receptors [266,267]. The $\alpha 5$ subunits are highly expressed in the hippocampus and are thought to play a crucial role in learning and memory [266]. However, very recently it has been found that after the application of midazolam $\alpha 1$ subunits are mainly involved in mediating the detrimental effects on LTP [268]. Benzodiazepines such as diazepam and lorazepam are also clinically known for their use as anesthetics [269]. In one of the previous reports, the benzodiazepine diazepam in the presence of low GABA concentrations was shown to produce a biphasic response. In the nM concentration range, it is dependent on the $\alpha 1\beta 2\gamma 2$ -receptor channel, whereas, in the μ M range, it is independent of the $\gamma 2$ subunit [270]. Benzodiazepines apart from the GABA_A receptors also bind to the TSPO protein [228,271].

Neurosteroids on the other hand bind to GABA receptors at a site different from those of benzodiazepine or GABA, which allows allosteric modulation of the GABA_A receptors and further activation of the chloride channel [246]. The neurosteroid's allosteric action is specifically thought to be at the N-terminus of the middle of the second transmembrane domain [246,272]. Among the first neurosteroids shown to regulate neuronal excitability were allopregnanolone (3 α 5 α -THP), progesterone, 3 α ,5 α tetrahydrodeoxycorticosterone (3 α 5 α -THDOC), and deoxycorticosterone [246]. Neurosteroids also target NMDA, serotonergic, muscarinic, or adrenergic receptors [246]. The δ subunit of the GABA_A receptor plays a major role in tonic inhibition and is essential for the neurosteroid-dependent modulation of the GABA_A receptor [273]. Knockout of the δ subunit of the GABA_A receptor has previously been associated with decreased sensitivity and anxiolytic potential of neurosteroids pregnenolone and alfaxalone [274].

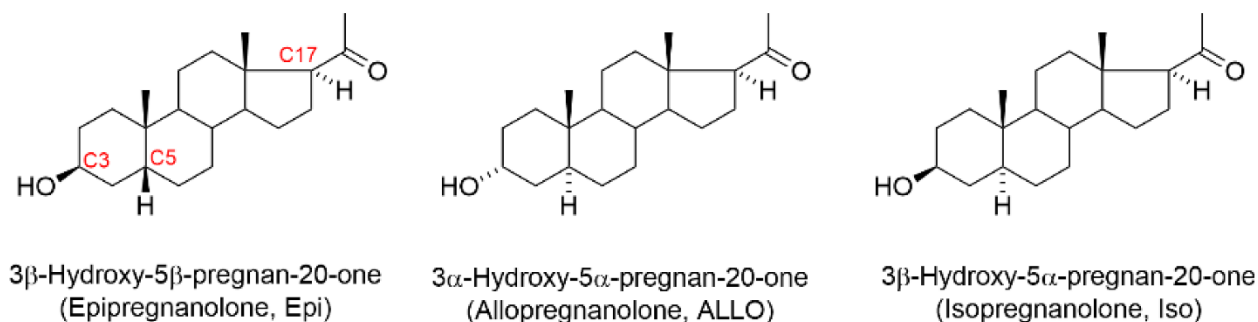


Figure 8: Structural representations of epipregnanolone (Epi), allopregnanolone (ALLO), and isopregnanolone (Iso) (Adapted with permission from [275]). The position of the hydroxy group at the C3 position alters the stereo confirmation resulting in stereoisomers.

Neurosteroids are broadly classified as positive or negative allosteric modulators of the GABA_A receptors. While still in debate, the 3 β -OH neurosteroids such as epi and iso pregnanolone are considered to be negative allosteric modulators of GABA_A receptors (**Figure 8**). In one such study that countered this argument, Epipregnanolone was shown to act as a positive modulator of GABA_A receptors in rat hippocampal and cerebral neurons [275]. The potential of neurosteroid action is also heterogeneous and greatly dependent on the brain region [246]. For instance, the effect of 3 α 5 α -THDOC is more pronounced in the hippocampal CA3 region and subiculum as compared to the CA1 or entorhinal cortex [276]. In addition to the complexity, the different conformation of neurosteroids also affects their potency on the GABA_A receptors. 5 α reduced

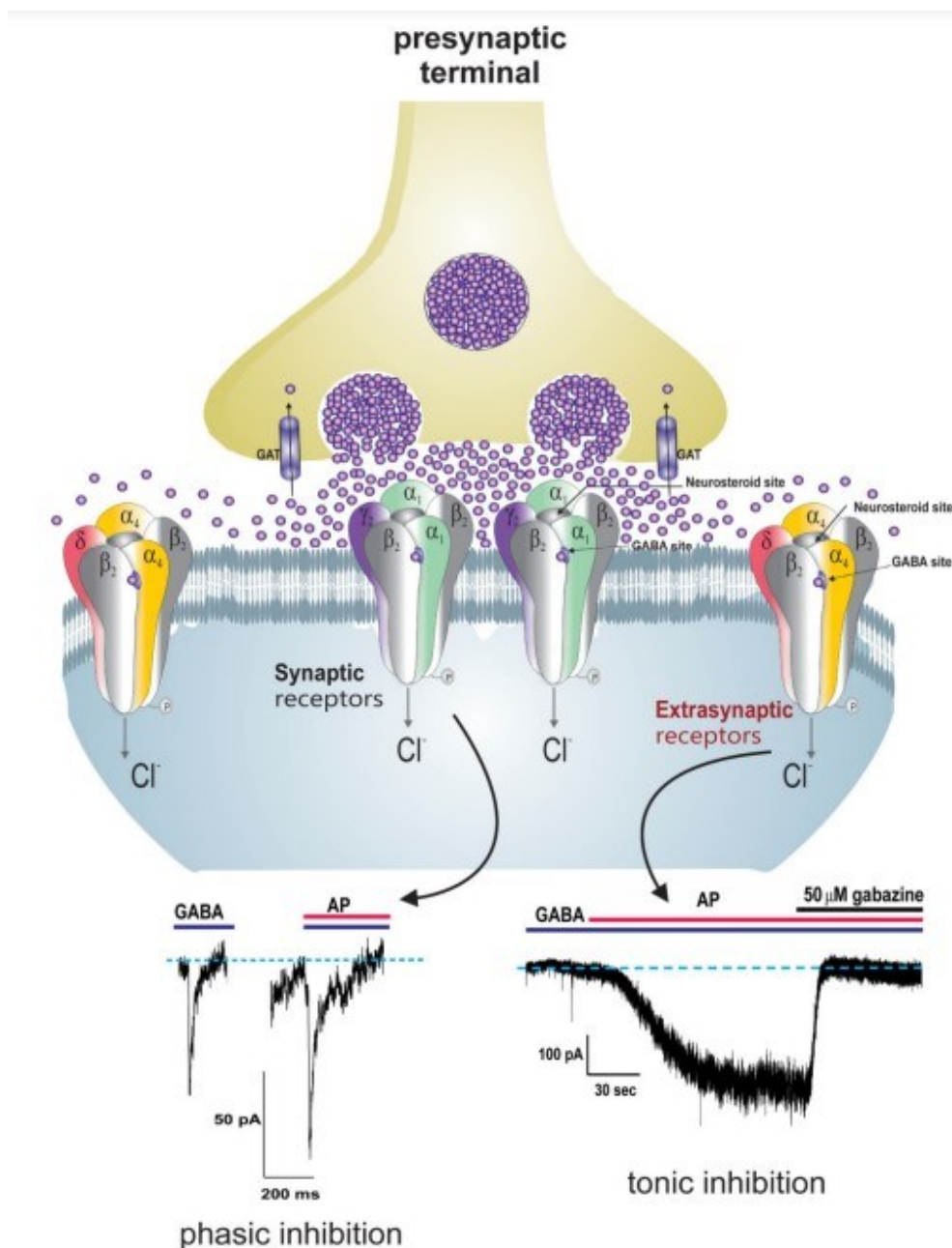


Figure 10. Synaptic and extrasynaptic GABA_A receptors and the neurosteroid-mediated action at these sites (Adapted with permission from [283]).

Neurosteroids and benzodiazepine binding sites are distinct from each other. Based on the location of the receptors, the neurosteroids mediate a differential response. For instance, the synaptic GABA_A receptors are known to mediate phasic inhibition whereas the extrasynaptic ones are primarily thought to mediate tonic inhibition.

1.3.4.3. Neurosteroids and their Role in neurodisorders

The homeostatic balance of neurosteroids is essential in maintaining a healthy synapse and glial function. Previously endogenous neurosteroids in the CNS have been associated with cognitive impairments and learning and memory deficits in anxiety disorders [284]. In chronic stress disorders such as PTSD, allopregnanolone levels were found to be significantly altered [285]. Additionally, their implication in depression and their use as therapeutics to treat depressive episodes make them attractive potential targets [286,287]. In progressive neurodisorders such as Parkinson's, the neuroprotective role of neurosteroids has been elucidated. For instance, the administration of progesterone in male rats was associated with increased dopamine content in the striatum and neuroprotection in the MPTP Parkinson's animal model [288]. Impaired progesterone metabolism has been associated with animals having nigrostriatal lesions that resemble the pathological features of Parkinson's disease [289]. Neurosteroids like $3\alpha,5\alpha$ -THP provide neuroprotective effects by restoring the cells in the nigrostriatal tract and TH-immunoreactive neurons in the MPTP rodent model of Parkinson's [290]. In AD, as well neurosteroid levels are significantly altered. Several compounds, including pregnenolone (PREG) and Dehydroepiandrosterone (DHEA), are altered in AD, including their ester sulfate compounds [291]. The involvement of allopregnanolone in AD has been suggested in multiple clinical as well as non-clinical studies. The use of allopregnanolone as a neuroprotective agent in AD against multiple pathophysiological features has been studied [292,293]. Taken together, neurosteroids play a crucial role in modulating neurotransmission and can be considered essential therapeutic targets in neurodegenerative disorders.

1.4 Astrocytes and Complement Pathway

1.4.1 Role of glial cells in Pruning and Homeostasis

The formation of synapses and their further integration into functional neuronal circuits requires meticulous coordination between neural cells and glial cells. Glial cells, astrocytes, and microglia play a crucial role as "Guiding stars" during the process of synapse formation and circuit assembly. In addition to this, they help remodel, monitor, and instruct the developing synapses and play a major role in forming mature synapses [294–296]. Imbalance in the glial cell population or regulation can therefore be associated with the onset and progression of various neurodegenerative

disorders (**Figure 11**). Microglia maintains neuronal homeostasis and participates actively in synaptic remodeling by promoting the phagocytic clearance of neuronal debris and apoptotic cells [297]. Apoptotic sources are tagged with “eat-me signals” which are recognized by microglia leading to the initiation of phagocytosis by microglia [298]. The microglia-mediated phagocytosis involves complement cascade proteins such as C1q which form an important component of death tags for the neurons to be destroyed [299,300]. The C1q-associated synapse activates the downstream complement cascade and further proceeds the synapse elimination via the complement receptor 3 (CR3) pathway [301]. This process of complement-mediated phagocytosis is influenced by astrocyte-secreted TGF- β [302]. Astrocytes form a diverse population of glial cells in terms of functionality, gene expression profile, and morphology [303,304]. It is elusive however whether these heterogeneities and region-specificity are intrinsic in astrocytes or whether they are influenced by the local microenvironment [305,306]. Astrocytes are crucial regulators of development and a prime reason that strengthens this hypothesis is the coincidence of astrocytic membrane domain expansion with synaptic refinements including motor, sensory, memory, and visual processing [305,307–311]. For instance, in the developing mouse cortex after the first postnatal week, astrocytes extend the fine processes and this coincides with synaptogenesis [312].

The first involvement of astrocytes in the process of synaptogenesis was first described by the lab of Dr. Barres by using a retinal ganglion cell (RGC) culture system [313,314]. Functional synapses are fine-tuned by the interaction of synaptogenic and anti-synaptogenic cues derived from astrocytes. Two crucial signals include Hevin and secreted protein acidic and rich in cysteine (SPARC) which regulate each other in a feedback loop to fine-tune neuronal circuitry [305]. Hevin is produced by astrocytes and localized to excitatory synapses, where it has been demonstrated to be essential for glutamatergic synapse maturation [305,307,315]. SPARC, a Hevin homolog, on the other hand, is a competitive inhibitor against Hevin-induced synaptogenesis. Hevin and SPARC, therefore, act in a loop to exercise the maturation and formation of excitatory synapses [307]. In addition, astrocytes also play an important role in the maturation of inhibitory synapses [305]. The astrocytic neuronal cell adhesion molecule (NRCAM) has been studied extensively in this context which binds to NRCAM-gephyrin complexes to induce the formation of inhibitory GABAergic synapses [316]. Both astrocytes and microglia actively phagocytose synapses via MEGF10 and MERTK phagocytic receptors. While previously, microglia were thought to play an essential role in synapse elimination, recent studies show astrocytes in addition to microglia are

crucial regulators of synaptic elimination [305]. In addition to participation in synaptogenesis astrocytes play a major role in neuronal signaling. The neuronal activity coincides with Ca^{2+} transients in the astrocytes [317–320]. During sensory tasks, mouse whisker stimulation shows synchronicity between neuronal and glial calcium waves [321,322]. Recent studies have illustrated that these Ca^{2+} transients in the astrocytes can lead to the release of ATP, glutamate, and D-serine a calcium and SNARE protein-dependent mechanism [323–326]. Modulation of Ca^{2+} activity by the astrocytes, therefore, plays a crucial role in the maintenance of synaptic homeostasis [305].

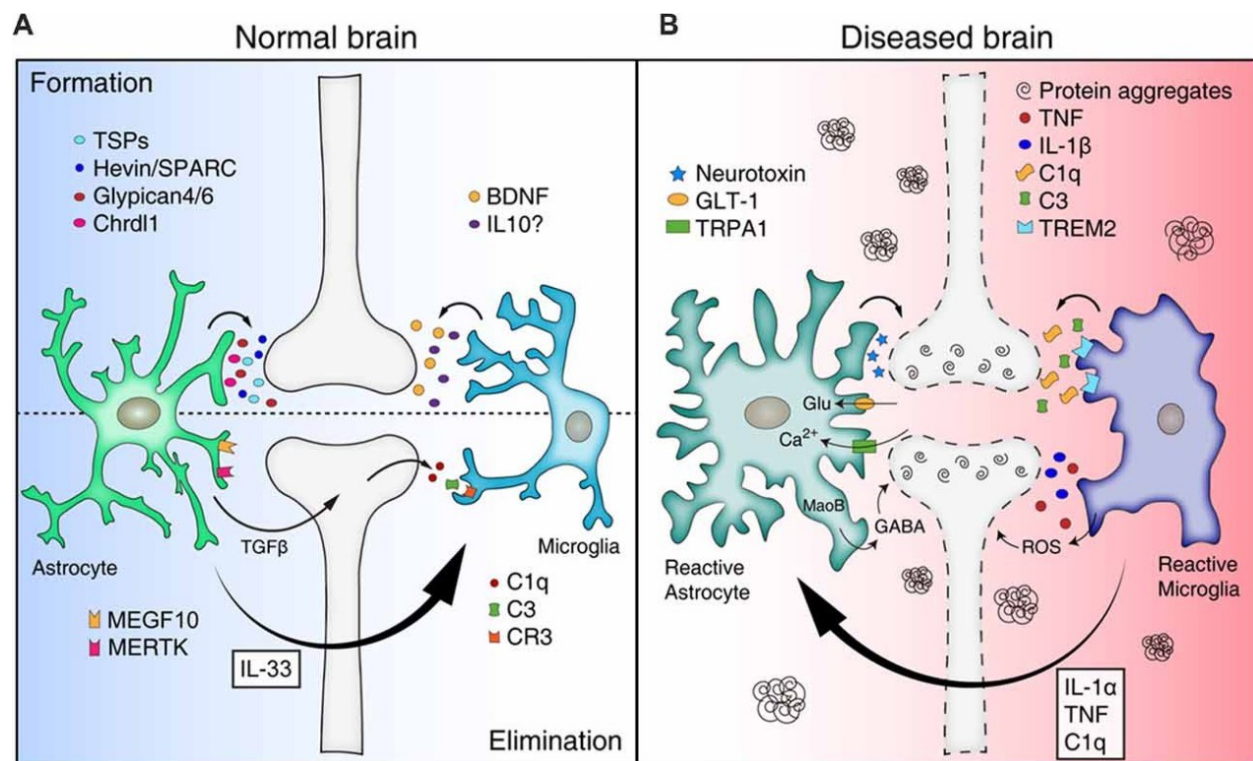


Figure 11: Comparison of glial cell function in a normal and a diseased brain (Adapted with permission from [327]).

(A) In a physiological state, glial cells (microglia and astrocytes) release synaptogenic cues which include BDNF, interleukin10 from microglia and Chrdl1, Hevin, SPARC, and thrombospondins (TSPs) from astrocytes. Phagocytic receptors such as MEGF10 and MERTK on astrocytes help to mediate synaptic pruning. Complement signals (C1q, C3, and complement receptor 3 (CR3)) play a crucial role in mediating synapse elimination during synapse maturation and development. (B) Reactive gliosis is commonly used in neurodegenerative diseases. Aberrant communication between microglia and astrocytes through the complement proteins leads to the loss of functional synapses.

1.4.2 Astrocytes in Alzheimer's Disease

Synapse loss is one of the primary pathophysiological features which is an indication of the disease progression in neurodegenerative diseases. Soluble A β oligomers as discussed earlier act as important players which induce synapse loss, phosphorylation of tau, and reactive astrogliosis. Dysregulation of neural cell adhesion molecule 2 (NCAM2) by A β leads to the loss of functional synapses in the hippocampus [328]. It is often hypothesized that A β plaques sequester toxic A β oligomeric species [329,330]. Reactive astrocytes surround the amyloid plaques and the astrocytic processes have been shown to be associated with A β plaques [331,332]. In recent studies, the astrocytes surrounding the A β plaques have been shown to follow the A1 astrocytic fate and are therefore believed to have less phagocytosing capacity [333]. It is possible therefore that A β plaques interact with the astrocytes and decrease the phagocytosing capacity of the astrocytes [334]. Additionally, reactive astrocytes display abnormal expression of glutamate transporter-1 (GLT-1) and glutamine synthetase which affects synaptic transmission and neuronal excitability [335–337]. This suggests that A β impairs the glutamate reuptake by astrocytes and increases the availability of glutamate in the synaptic cleft which leads to synapse loss [335,336]. Moreover, they can add up the excitatory to inhibitory signal imbalance by the excess production of inhibitory GABA. The impaired excitatory inhibitory signal caused by the reactive astrocyte could therefore lead to the disease progression. The oligomeric A β species enhances calcium activity in the astrocytes via the transient receptor potential A1 (TRPA1) channels [338]. Dysregulation of calcium transients caused by the A β oligomers could therefore directly affect the astrocyte-synapse interaction and initiate the loss of synapses.

1.4.3 Complement Proteins and their association with Astrocytes

The complement system acts as a first-line defense system by executing innate immune functions and forming a first line of defense against foreign bodies [339]. In addition to this, the complement system plays an essential role in regulating age-related synapse loss and cognitive decline [340]. Importantly, astrocytes are a reservoir of complement system proteins, particularly of C3 complement proteins [339]. The interplay of signals between the glial cells and the CNS resident immune cells plays an important role in deciding the fate of the astrocyte. Astrocytes are known to express several complement protein receptors including C3aR, CR3, C5aR1, and C5aR2 [341–344]. Human astrocytes express gC1qR which is a receptor for the C1q globular domain [339,345–

347]. Similarly, astrocytes and other neural populations are known to express CD91/low-density lipoprotein receptor-related proteins which directly interact with C1q for the clearance of C1q-tagged synapses [348,349]. Megf10, expressed on the astrocytic surface is required for the normal clearance of apoptotic cells and neuronal activity-dependent synapse remodeling by astrocytes [350].

Synaptic pruning can take place via both C1q-dependent and independent pathways [351] (**Figure 12**). In the C1q-dependent pathway, astrocytes release tumor growth factor- β (TGF- β) upon sensing unnecessary synapses, which increases the expression of C1q tags. Microglia upon recognizing the tag release inflammatory cytokine to engulf the synapse through phagocytosis. On the other hand in the C1q independent pathway astrocytes via multiple EGF-like-domains 10 (MEGF10) and MER tyrosine kinase (MERTK) receptors destroy the synapse [352]. The complement proteins interact closely with the glial cells to regulate activity-dependent synaptic restructuring.

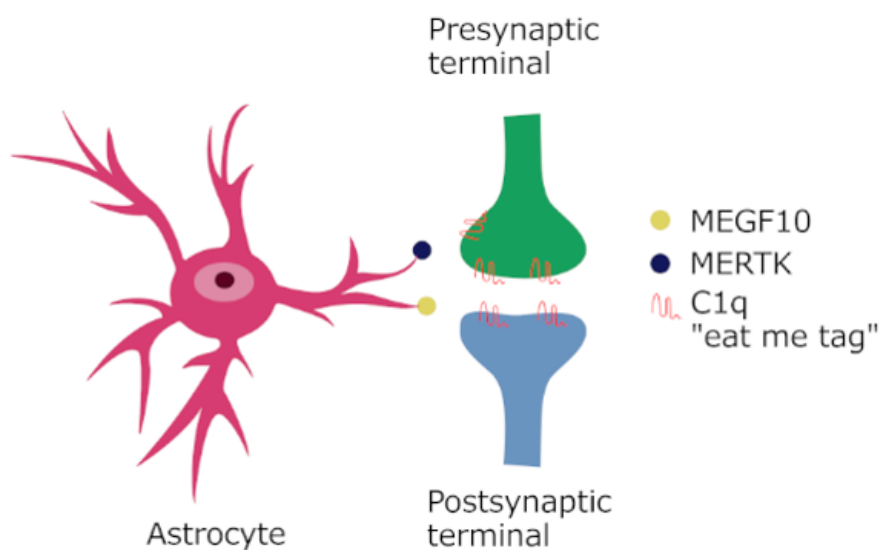


Figure 12: Representative schematic showing the astrocytic phagocytic receptors (MEGF10 and MERTK) participating in direct elimination of synapses via C1q “eat-me tag” (Adapted with permission from [353])

1.5 Aim of this study

The upregulation of glial TSPO expression in AD as well as its well-suited functionality in the outer mitochondrial membrane in importing cholesterol from the outer to inner mitochondrial membrane for the regulated synthesis of neurosteroids makes TSPO an excellent target as a therapeutic option in AD. We, therefore, wanted to see the role of TSPO activation via specific TSPO ligand XBD173 and its impact on the pathophysiology of AD. Specifically, we wanted to address if XBD173, TSPO ligand in addition to providing a symptomatic benefit as an anxiolytic in AD, could act as a stand-alone entity in providing neuroprotective benefits against the multifaceted pathophysiological symptoms of AD. To address this, we asked if XBD173 could rescue the LTP impairment in the CA1 region of the hippocampus resulting from the incubation of A β oligomers and whether this is exclusively dependent on the TSPO. To understand this, we performed in vitro CA1-LTP recordings using different A β oligomers such as A β ₁₋₄₂ and A β ₁₋₄₀ oligomers. To access the role of TSPO in this XBD173-mediated action on the A β oligomers we used hippocampal slices from TSPOKO animals.

Given the cognitive decline paradigm in AD pathogenesis, we designed an acute and a chronic model of XBD173 treatment and asked if in vivo treatment of XBD173 could confer the neuroprotective effect in terms of cognitive and memory impairment and also accessed the role of TSPO protein in XBD173 mediated action. To study the cognitive impairment in the transgenic AD mice we used a water cross maze which accesses hippocampus-dependent spatial learning in rodents. To understand the role of TSPO in XBD173-mediated cognitive action we made use of het TSPOKO X ArcA β mice. To address whether this TSPO-mediated action by XBD173 is carried by neurosteroids we analyzed a broad spectrum of neurosteroids from the different treatment groups.

Additionally, we ventured into the role of glial cells in the TSPO activation by XBD173 in a transgenic AD model. To capture this aspect, we developed a quantification protocol to access the synaptic engulfment of pre- and post-synaptic particles and C1q “eat-me tags” from high-resolution individual astrocytes. The engulfment of synaptic particles by astrocytes was compared among different treatment groups.

2. Materials and Methods

2.1 Preparation of test substances and acute hippocampal slices

2.1.1 Laboratory Animals

All animal study protocols were carried out following German animal experimentation regulations and were authorized first by the animal care committee at Technical University Munich, Munich, Germany. It was taken care that all the animal experiments were in accordance and strictly adherence to the regulatory standards of the institute. All the mice (maximum of 6 mice per cage) irrespective of the start of the experiment were housed in a climate-controlled room (23 ± 0.5 °C) with 12 hours of light and darkness with an *ad libitum* supply of food and water. In the course of this study, we have made use of mice of both genders. For the ex vivo set of experiments, animals used were of age group 8-12 weeks. For the behavioral set of experiments, both male and female mice were used. For chronic experiments, mice were treated with the respective drugs starting from the age group of 8-9 months. Acute treatment started at the age of 11 months just before the initial training phase of the experiment. It is very important to note here that the animals utilized in the behavioral testing were housed in similar settings, with the exception of two weeks before the water cross maze behavioral testing, when mice were housed in a reverse light-dark (12-hour light and darkness) cabinet maintained at a temperature (23 ± 0.5 °C). Animal lines used in this study are listed in **Table 1**.

Table 1: List of animal lines used in the study

Mouse line	Modification	Reference/ Source	Designation
WT	Wild type (No genetic modification)	Charles River (Italy)	C57Bl6/N
GABA δ K O	δ subunit is knocked out. Reduced sensitivity to anxiolytic effects of neurosteroids is shown in these mice	Munich (Germany), Similar to Jackson Laboratory (Jax stock 003725)	B6.129-Gabrdtm1Geh/J

	(https://www.jax.org/strain/003725)		
ArcAβ	Overexpresses human APP695 with the Swedish (K670N/M671L) and Arctic (E693G) mutations	Calco (Italy)	ArcA β
TSPOKO	Global TSPO knock-out model. Detail in Tu <i>et al.</i> , 2014.	https://pubmed.ncbi.nlm.nih.gov/24936060/	TSPOKO
het TSPOKO X ArcAβ	Transgenic ArcA β animals having a heterozygous expression of TSPO	Munich (Germany)	het TSPOKO X ArcA β

Wild-type (C57BL/6, WT) mice were purchased from Charles River (Italy), while ArcA β (APP E693G) mice were procured from CALCO (Italy). In the transgenic mice with an arctic mutation (ArcA β), glycine replaces glutamic acid with a site-directed mutagenesis. Our group in Munich generated the TSPOKO mice, which had a global TSPO deletion. By crossing stable lines of TSPOKO and ArcA β mice, het TSPOKO X ArcA β mice were created in our institute. Our group in Munich developed the GABA δ knock-out (δ -KO) (line B6.129-Gabrdtm1Geh/J) mouse line [274]. The δ -KO mutant line is a knockout of the δ subunit of the GABA_A receptor. The deletion of the δ subunit in these mice's GABA_A receptor results in reduced sensitivity to neurosteroids, as previously described by Mihalek *et al.* [274]. The transgenic lines were confirmed by multiple genotyping analyses as well as western blot protein quantification.

2.1.2 Preparation of oligomeric A β and test compounds

To prepare the A β compounds, A β ₁₋₄₂ (order number H-1368; Bachem, Bubendorf, Switzerland) and A β ₁₋₄₀ (Product Number: 4014442; Bachem, Bubendorf, Switzerland) were dissolved in 100% v/v hexafluoroisopropanol (HFIP, Sigma Aldrich) to bring it up to a concentration of 1 mg/400 μ L HFIP and shaken for 1.5 h at 37 °C. 100 μ g aliquots of both A β ₁₋₄₂ and A β ₁₋₄₀ were prepared per tube. The HFIP was then evaporated with the help of a Speedvac for 30 min. The tubes are labeled and stored at -80 °C after it was completely dry. Before the use of respective A β in the bath solution, they were dissolved in DMSO (Sigma Aldrich) to obtain a concentration of 100 μ M. They were then diluted with Ringer's solution to a concentration of 50 nM of A β ₁₋₄₂ and A β ₁₋₄₀.

DMSO was used to dissolve diazepam and XBD173. In acute slice experiments for LTP electrophysiological recordings, 300 nM concentration of XBD173 was used by dissolving it in aCSF whereas, for other *ex vivo* slice experiments, XBD 173 was dissolved to obtain a 3 μ M concentration. XBD173 and Diazepam at 1mg/kg were diluted using a 0.9% NaCl solution for the chronic and acute behavioral experiments. While the treatment regimen for each chronic and acute experiment are shown in great detail in figures respectively, in brief, acute treatments consist of intraperitoneal (i.p.) injections of XBD173(1 mg/kg), diazepam (1mg/kg), and vehicle (DMSO at similar v/v of other drugs) once 3 days before the starting of the behavioral tests. Chronic treatment on the other hand had i.p. injections of each respective drug every alternate day for 12 weeks. As for the vehicle group, they received only DMSO diluted in NaCl solution at a concentration comparable to what was used in XBD173 [354].

2.1.3 Acute slice preparation

Acute brain hippocampal slices were used in the electrophysiological recording. The preparation of acute hippocampal slices was performed in the S1 safety room. First, mice were deeply anesthetized in an isoflurane chamber with 5% isoflurane concentration and at a flow rate of 2 L/min. Care is taken to ensure that the mice are completely anesthetized. This is done by following the gold standard check that the mice lose their righting reflex. The mouse brain was removed using a guillotine and was immediately placed in an ice-cold Ringer solution consisting (in mM) of 125 NaCl, 2.5 KCl, 25 NaHCO₃, 0.5 CaCl₂, 6 MgCl₂, 25 D-glucose and 1.2 NaH₂PO₄, with a pH of 7.3 and continuously oxygenated with carbogen gas (95% O₂/5% CO₂). From both the brain hemispheres, sagittal hippocampal brain sections of 350 μ m thickness were obtained using a microtome (HM 650 V; Microm International, Germany). Following this, the slices were recovered in a chamber constantly oxygenated with carbogen submerged with artificial cerebrospinal fluid (aCSF) for 30 min at 35 °C. After this, the hippocampal slices were kept at room temperature for 1 hour before starting the experiment or transferring them into the recording chamber. The slices in the recording chamber were held in place with a platinum ring containing two nylon threads while carbonated aCSF was continuously perfused at a flow rate of 5 ml min⁻¹. We conducted all recordings at room temperature (21-23 °C) [354]. The composition of aCSF and preparation ringer solution are listed in **Tables 2 and 3** respectively

Table 2: Mess Ringer solution (aCSF) solution ingredients

Mess Ringer (aCSF)		
Reagents	Final concentration [M]	Amount [g]
NaCl	0.125	7.305
KCl	0.0025	0.186
NaH ₂ PO ₄ -Monohydrate	0.00125	0.172
D-(+) Glucose-Monohydrate	0.025	4.954
NaHCO ₃	0.025	2.100
MgCl ₂ -Hexahydrate	0.001	0.203
CaCl ₂ -Dihydrate	0.002	0.294
Add MgCl ₂ and CaCl ₂ separately. Adjust pH to 7.4 After 10 min of oxygenation with carbogen (95% O ₂ and 5% CO ₂), the actual pH value can be measured, it should be 7.30 (7.20 - 7.40).		

Table 3: Preparation Ringer solution ingredients

Preparation Ringer		
Reagents	Final concentration [M]	Amount [g]
NaCl	0.125	14.610 g
KCl	0.0025	0.373 g
NaH ₂ PO ₄ -Monohydrate	0.00125	0.345 g
D-(+) Glucose-Monohydrate	0.025	9.909 g
NaHCO ₃	0.025	4.201 g
MgCl ₂ -Hexahydrate	0.006	2.440 g
CaCl ₂ -Dihydrate	0.00025	0.074 g

2.2 Electrophysiology Recording

2.2.1 Electrophysiology Setup

We used two different setups for performing the extracellular recording. The first setup consisted of the following components: two stimulating electrodes, one recording electrode, two manual manipulators holding a stimulating electrode each, Wild M3Z Heerbrugg microscope (Wild Heerbrugg, Switzerland), one electronic manipulator (Record-microcontroller, France) for the recording electrode and a light source (Euromex microscopes Holland, The Netherlands) which were kept vibration-cushioned table via pressurized air (Spindler&Hoyer, Germany) and the whole setup was kept inside a well-insulated faraday cage. A PM500-20 Piezomanipulator (Frankenberg, Germany) electric source for controlling the electronic manipulator alongside the Ismatec ISM 852 circulating system was kept outside. The stimulating electrodes were connected to the BA-2S amplifier (npi electronic GmbH, Germany) via two ISO-STIM 01M stimulators (npi electronic GmbH, Germany). The signals were further filtered and recorded in the system. The second system consisted of similar components obtained from the following sources: the two stimulating electrodes (Narishige, Japan and SFB220 MU München, Germany), the manual recording electrode (Narishige, Japan), EA-PS 3032- 10B light source (EA Elektro-Automatik, Germany) and Axiovert 35M microscope (Zeiss, Germany). The stimulating electrodes were connected to the EXT 10-2F amplifier (npi electronic GmbH, Germany), and signals were filtered and channeled to the system via the BNC-2090A interface connection (National Instruments, USA).

2.2.2 Long-term potentiation recordings

We used an already established protocol in our lab for the field excitatory postsynaptic potentials (fEPSP) recording in the sagittal hippocampal slices [355]. The fEPSPs were obtained using aCSF-filled glass micropipettes (1–2 M) in the CA1 region of the hippocampus (**Figure 13**). FEPSPs in the hippocampus CA1 stratum radiatum were measured after stimulation of the Schaffer collaterals-commissural pathway. FEPSPs were induced by alternating test stimulation (50 μ s, 5–20 V) administered via bipolar electrodes (Hugo Sachs Elektronik-Harvard Apparatus, Germany; 50 μ m tip diameter) inserted on both sides of the recording pipette. We were therefore able to stimulate the non-overlapping populations of fibers of the Schaffer collateral-associational commissural pathway. During baseline recording, the stimulation intensity was adjusted to

produce an fEPSP slope of about 25-30% of the maximal response. After at least 20 minutes of stable baseline recordings, a high-frequency stimulation (HFS) train (100 pulses at 100Hz over 1s) was delivered via one of the two stimulating electrodes to induce LTP in the CA1 region of the hippocampus.

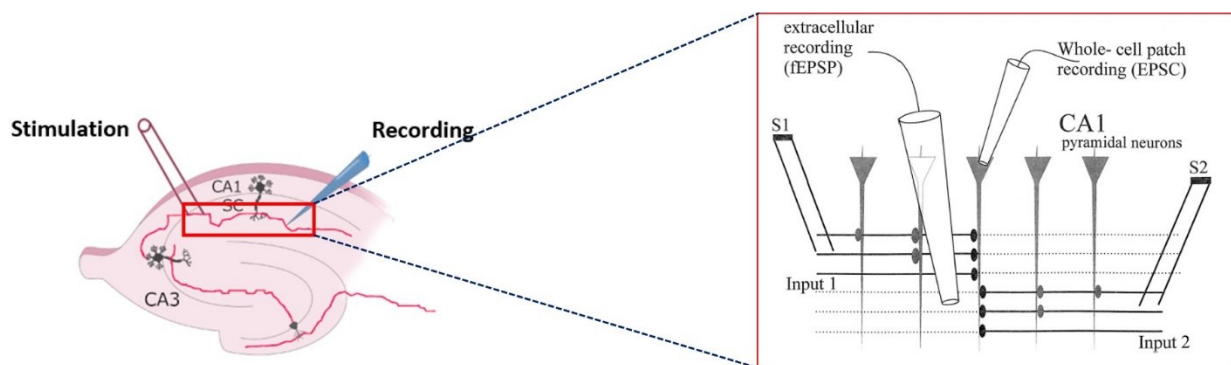


Figure 13: Hippocampal slice showing a representative positioning of electrodes in the Schaffer collateral pathway to obtain CA1-LTP (Adapted with permission from [356]).

The following summarises the different treatment regiments used in the course of this study:

1. For obtaining the fEPSP recording after treatment and comparing it with internal control, independent stimulation with two electrodes was used. After HFS delivery in the absence of any chemical, the potentiation of the fEPSP slope was evaluated for 60 minutes after the tetanic stimulus, while retaining the baseline conditions. In brief, HFS was administered from one of the electrodes in the absence of $A\beta$ ($A\beta_{1-40}$ or $A\beta_{1-42}$), and response activity was observed for at least 60 minutes after tetanic stimulation. Before the second HFS, $A\beta$ ($A\beta_{1-40}$ or $A\beta_{1-42}$) was administered for 90 minutes via the bath solution.
2. For accessing the neurotoxicity of the $A\beta$ oligomers, the slices were first incubated with the respective drugs (XBD173, pregnenolone, allopregnanolone, or THDOC) for 60 minutes before inducing the first HFS train through one stimulating electrode. The response activity was then monitored for another 60 minutes. Then, for 90 minutes, $A\beta$ ($A\beta_{1-40}$ or

A β_{1-42}) was introduced through bath solution before generating LTP in the second input via the HFS train.

We define LTP impairment or blockage when the fEPSP slope in the last 10 minutes after HFS stimulation is not at least 120% higher than the baseline recording. Because stimuli were alternately delivered to each input every 15 seconds, two signals from the same input were averaged to one for analysis and one data point per minute. To analyze the fEPSPs offline WinLTP program was used. fEPSP slopes were measured between 20% and 80% of peak amplitude and then normalized to 20-minute baseline recordings obtained before LTP induction [354].

2.3 Spine imaging and classification of individual spines

Thy1-eGFP mice were used for the dendritic spine analysis of *ex vivo* experiments with A β_{1-42} . The treatment schedule for the spine imaging setup experiments is shown in **Table 4**. The slices were collected after the respective treatment, fixed with 4% paraformaldehyde (PFA) for 2 days, and cryoprotected with 30% sucrose for 3 days. Hippocampal slices of 100 μm thickness (Bremen, Germany) were prepared by using a cryostat (CryoStar NX70, Thermo Fisher Scientific, Bremen, and Germany). After washing with PBS, the slices were placed on slides and coverslipped. We then obtained the images of apical oblique dendritic spines in the CA1 region of the hippocampus with a confocal microscope (Leica SP8, Wetzlar, Germany) with a Z step size of 0.3 μm and a 60X/1.40 N.A. oil-immersion objective. From each slide, we obtained 5-8 dendrites of 20 - 40 μm in length from pyramidal neurons of the stratum radiatum layer in the CA1 region.

Table 4: Treatment schematics for the slice incubation with XBD173 and A β_{1-42} .

Control	30 min at 35°C	210 min at RT		
A β_{1-42}	30 min at 35°C	120 min at RT		A β_{1-42} (50 nM); 90 min
XBD173 and A β_{1-42}	30 min at 35°C	60 min at RT	XBD173 (3 μM); 60 min	A β_{1-42} (50 nM); 90 min

This was then analyzed with the IMARIS 9.7 for Neuroscientists (Oxford Instruments, bitplane). In the first step before categorizing the spines into their subclasses, we reconstructed the dendrites and spines using the filament tool of the IMARIS package. Categorization of dendritic spines into stubby, thin, or mushroom, was done via a MATLAB plugin in the IMARIS software (1) stubby spines—protrusions closely connect to the dendritic shaft and lack a clear neck. (2) thin spines—long and thin protrusions with a bulbous head; (3) mushroom spines—protrusions with a small neck and a large head (**Figure 14**). The following parameters were applied to automatically categorize the spines in the IMARIS: Long Thin Spines: $\text{mean_width (head)} \geq \text{mean_width (neck)}$; Stubby Spines: $\text{length (spine)} < 1$; Long Thin Spines: $\text{mean_width (head)} \geq \text{mean_width (neck)}$ and Mushroom Spines: $\text{length (spine)} < 3$ and $\text{max_width (head)} > \text{mean_width (neck)} * 2$. The spine density was defined as the number of spines per μM of the dendrite [354].

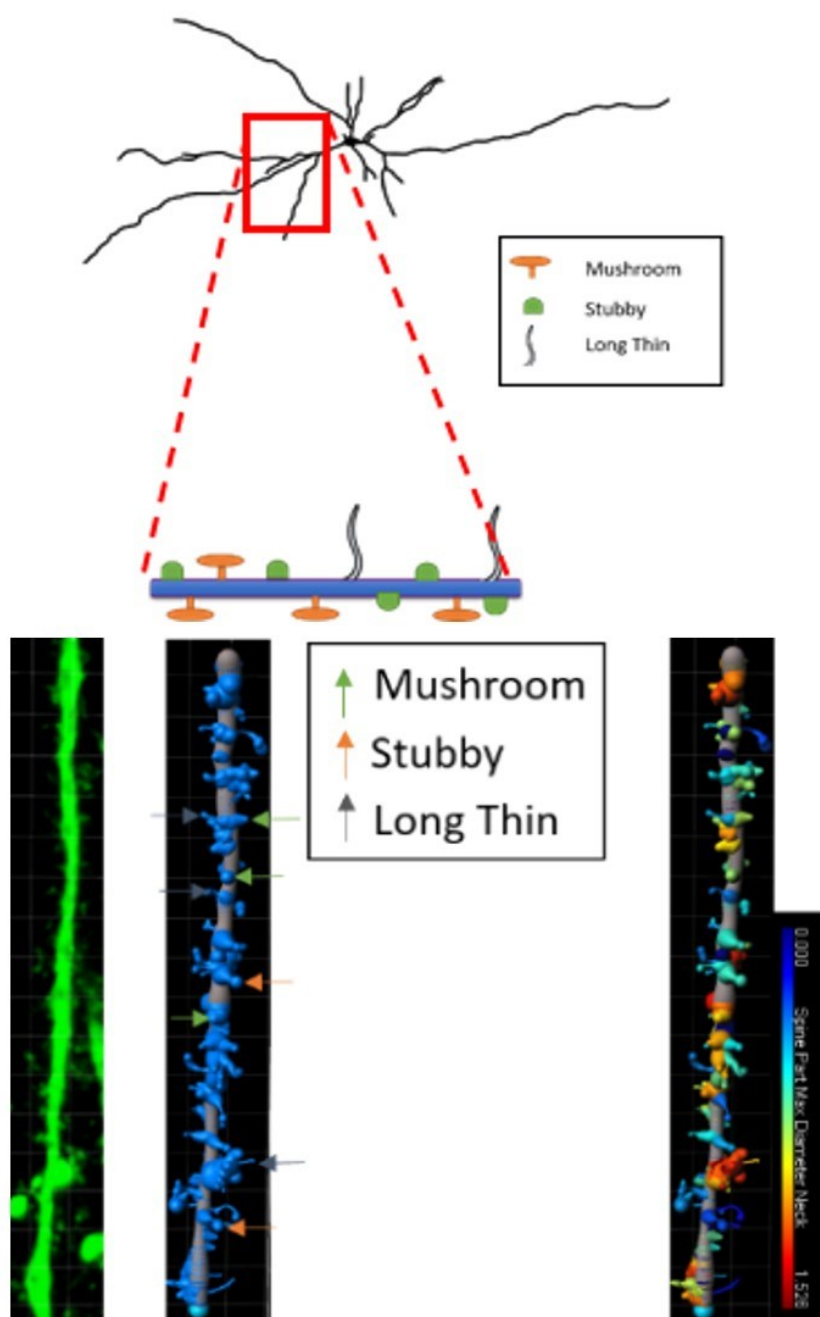


Figure 14: Representative image showing different spine classes.

The lower panel shows reconstructed dendrites and spines using the IMARIS Filament function. [Figure adapted and modified from our manuscript submitted relating to this work (Preprint can be found in [354]). Published version [353]]

2.4 Fluorescence-activated cell sorting (FACS) staining and analysis

The slices after incubation with the respective treatments were channeled for the FACS staining. We separated the hippocampus and the cortex for each of the slices. The slices were digested using 1 ml digestion solution (activated at 37 °C for 5 min) consisting of Ethylenediaminetetraacetic acid (EDTA) (2 mM), L-cysteine (5 mM), and papain (5 units/ml). We performed the enzymatic digestion at 37 °C for 15 minutes. Next, after the slices were dissociated, the suspension was further filtered via a 70 µm cell strainer to obtain a single-cell suspension. Care was taken not to introduce any impurities. The samples were centrifuged for 10 minutes at 600 x g at room temperature after rinsing the cell strainer with 2 ml PBS. We then discarded the supernatant and resuspended the cell pellet in 1 ml Fluorescence-activated cell sorting (FACS) buffer consisting of EDTA (1 mM), Sodium Azide (15 mM), and 1% w/v Bovine Serum Albumin (BSA). It is essential at this step to access the cell count to monitor cell viability. To check for the % cell viability and cell count per sample we made use of a hemocytometer. Blue-stained cells that integrated the trypan blue solution exhibit membrane disruption and are no longer viable.

For the preparation of samples for FACS analysis, they were spun down at 600 x g for 10 minutes at 4 °C before staining with fluorescent antibodies. The antibodies used in the FACS study have been summarised (**Table 5**). We then resuspended the cell pellets in a 50 µl blocking mix (49 µl FACS buffer + 1 µl anti-CD16/32 antibody) per sample and then incubated at 4 °C for 5 minutes. 11.5 µl of the antibody full-staining mix was added per sample and then was incubated (**Table 6**) in the dark at 4 °C for 30 minutes. FACS buffer 100 µl was added and centrifugation of cells was carried out for 5 minutes at 600 x g at 4 °C. Following resuspension of the pellets in 150 µl of FACS fixation buffer and storage at 4 °C, FACS analysis was performed. The BD LSRFortessa™ X-20 using the FACSDiva™ data acquisition was used to perform the FACS analysis. Previously established compensation beads were used to perform compensation of each channel. Samples were measured with a flow rate of around 10.000 events per second. The gating strategy for the single microglial cells is shown in great detail in the figure (**Figure 15**).

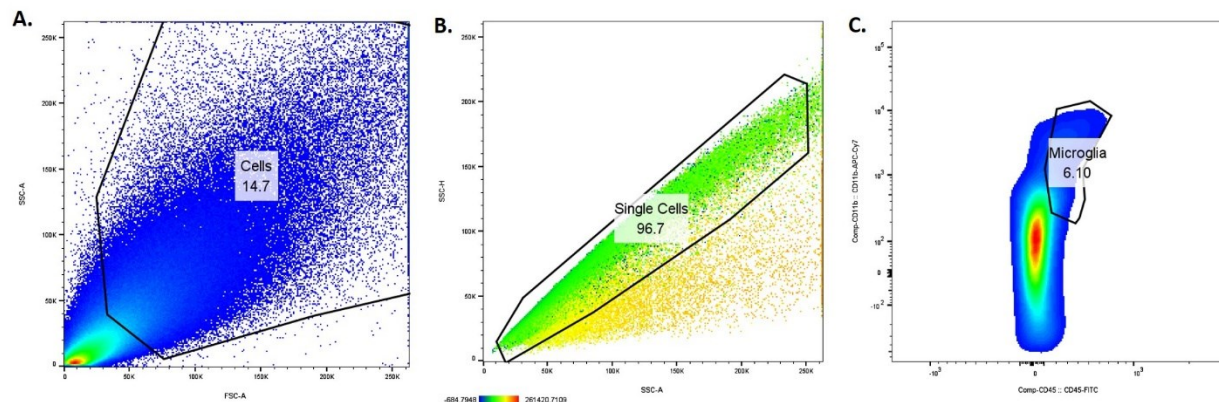


Figure 15: Microglial FACS gating strategy to study the polarization states. [Figure adapted and modified from our manuscript submitted relating to this work (Preprint can be found in [354]). Published version [353]].

A) Cell gating: Front scatter (FCS-A) vs. side scatter (SSC-A) dot plot B) Single-cell gating: SSC-H vs. SSC-A dot plot C) Microglial gating: CD45-FITC vs. CD11b-APC-Cy7 fluorescence intensity dot plot: smoothed, gate for CD45^{low-to-intermediate} and CD11b⁺ cells [Figure adapted and modified from our manuscript submitted relating to this work (Preprint can be found in [354]). Published version [353]].

Table 5: Antibodies used in FACS study

Antibodies	Catalog number	Manufacturer
TruStain FcX™ (anti-mouse CD16/32) Antibody	101320	BioLegend, San Diego (USA)
FITC anti-mouse CD45 Antibody	147709	BioLegend, San Diego (USA)
APC/Cyanine7 anti-mouse/human CD11b Antibody	101225	BioLegend, San Diego (USA)
PE anti-mouse CD163 Antibody	155307	BioLegend, San Diego (USA)
Brilliant Violet 605™ anti-mouse CD80 Antibody	104729	BioLegend, San Diego (USA)
PerCP/Cyanine5.5 anti-mouse F4/80 Antibody	123127	BioLegend, San Diego (USA)
APC anti-P2RY12 Antibody	848005	BioLegend, San Diego (USA)
Brilliant Violet 421™ anti-mouse CX3CR1 Antibody	149023	BioLegend, San Diego (USA)
Tmem119 Monoclonal Antibody (V3RT1GOsz), PE-Cyanine7	25-6119-80	ThermoFisher Invitrogen

Iba1/AIF-1 (E4O4W) XP® Rabbit mAb	17198	Cell Signaling Technology, Frankfurt am Main (GER)
-----------------------------------	-------	---

Table 6: Antibody staining mix composition

Antibody target	Coupled fluorochrome	µl per sample
CD45	FITC	1
CD11b	APC-Cy7	1
F4/80	PerCP-Cy5.5	1.5
TMEM119	PE-Cy7	2
P2RY12	APC	2
CD163	PE	2
CD80	BV605	1
CX3CR1	BV421	1
		11.5

2.5 Hippocampus-dependent Spatial learning test, plaque quantification, and measurement of soluble A β levels

2.5.1 Behavioral test: Water Cross Maze

For behavioral testing, we employed the Water Cross Maze (WCM) which accesses the spatial learning ability of the mice. Mice were trained in Water cross-maze setup modifying a previously well-established protocol from Wotjak *et al.*, [357]. Spatial cues are located in the surroundings and the mice learn to correctly find the right arm containing a hidden platform 1 cm below the surface of the water. In brief, the WCM setup consists of a plus-shaped maze made of clear transparent plexiglass with four identical arms (length and width 50 cm and 10 cm respectively) designated with cardinal directions (N-, S-, E-, and W- arms) (**Figure 16**). The water was changed in the setup every day but not in between the trials each day. The maze was filled with fresh autoclaved water maintained at (22 °C \pm 1 °C) up to a height of 11 cm. The platform height was 10 cm and it stayed 1 cm below the water's surface. This was also made of transparent plexiglass and the surface area (8 cm X 8 cm) was placed in the W arm. The W arm in turn was designated

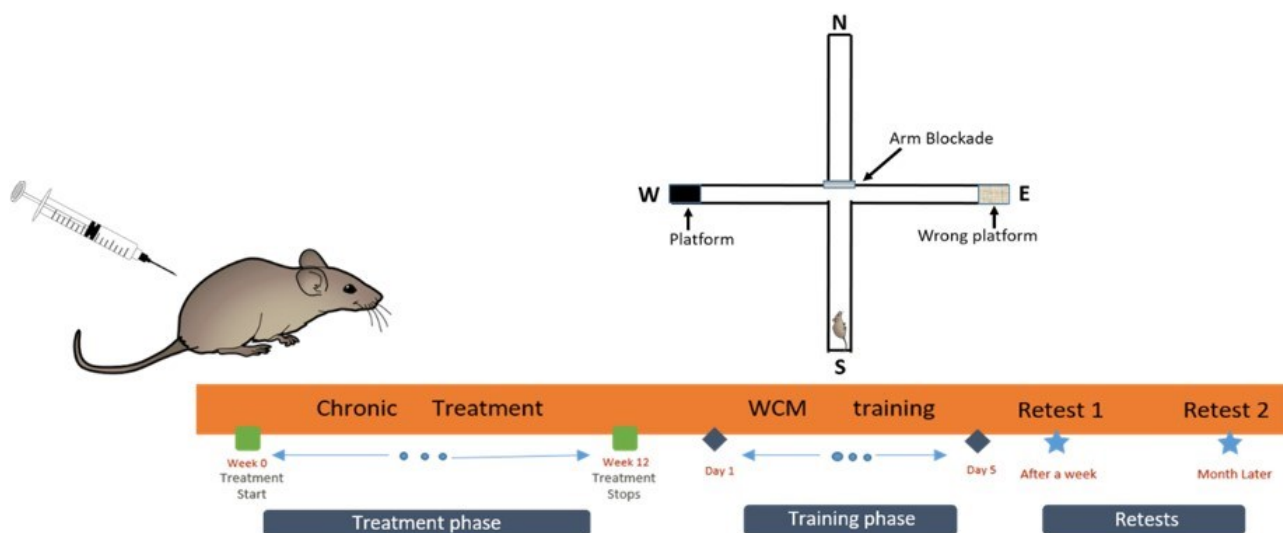
as the right arm whereas the E arm was designated as the wrong arm. The light conditions during the experimental conditions were always < 15 lux (12-13 lux). This was measured and adjusted accordingly every day before the start of the experiment. Care was taken not to change the cage during the training phase. We avoided using direct illumination from the light source as this would act as an additional cue bias. Instead, we used the surgeon's lamp redirected to the wall. The indirect illumination from the wall (12-13 lux) acted as the light source for the behavioral task. Mice were kept in an adjacent cabinet which was maintained at the same temperature and pressure as the room but with an alternate, light-dark cycle to entrain the mice to the reverse dark cycle. Care was taken to keep the mice for at least 14 days in the reverse light-dark cycle before the start of the training period.

The total testing period comprised 3 important phases: a. Training Phase (for a consecutive 5-day period) where the mice acquaint themselves with the spatial cues. b. Retest 1 (performed 7 days after the last day of the training phase) c. Retest 2 (performed after a month from Retest 1). Since AD is a progressive neuro-disorder that worsens with time, the retests were designed to assess the performance with age and to see if the drug's effects are long-lasting. Each day consisted of 6 trials per mouse arranged with pseudo-random order of the starting arm (Day 1: NSSNNS Day 2: SNNSSN continued on a similar pattern) to avoid the start bias and employ a place-dependent learning protocol. A divider was placed to block off the fourth arm, allowing the mice to escape through either E or W arm. The E arm did not consist of any platform and was the false arm. The mice were placed under infrared light after each session and given enough time to relax before the next trial. For each trial, a maximum of 30s was allocated per mouse. In case, where the mice were unable to find the platform it was guided to the platform (in such cases latency of 31 s was noted). The following parameters were used to evaluate spatial learning and memory: 1. Escape Latency: the amount of time it takes to reach the platform from the starting arm (averaged over 6 trials per mouse every day) 2. Accuracy: The number of accurate trials per day in which the mice swam directly to the right arm containing the platform without returning to the beginning or false arm (with no platform) 3. Accurate Learners: The number of mice who correctly completed at least 5 out of 6 trials every day, represented as a percentage of the total number of mice in each group.

Troubleshooting during WCM:

1. Optimization of the WCM is the primary step in accessing spatial learning in AD mice. Care should be taken that the spatial learning task should be on the extremes for mice i.e. should not be too hard or too easy for mice to learn. In our case, the setup was initially too easy for the mice to learn. The cues, therefore, had to be rearranged as well as the positioning of the setup was changed to optimize the setup.
2. Mice need to adapt to the reverse light-dark cycle before they are introduced to the training phase. This adaptation needs at least 10 days. The mice, therefore, were placed in the cabinet with a reverse light-dark cycle at least 10 days before the start of the experiment. Extreme care should be taken not to introduce the cues to the mice before the commencement of the experiment.
3. Since water acts as the only motive force here to find the final platform, it is possible that mice swim in the beginning arm for a longer time instead of reaching for the platform. This is common in the starting days of the training phase. In such cases, a snap at the gloves can be introduced to disrupt the repetitive movement in the starting arm.
4. The resting times in between each trial for the mice should be at least 10 minutes to ensure a complete recovery from the task in the previous trial.

A.



B.

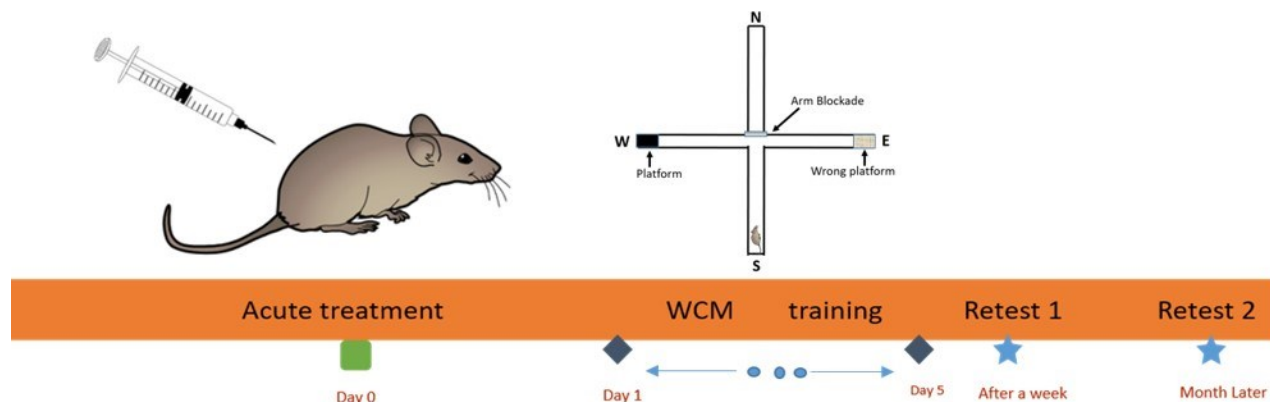


Figure 16: Acute and chronic treatment schedule of Water Cross Maze. [Figure adapted and modified from our manuscript submitted relating to this work (Preprint can be found in [354]). Published version [353]].

A. Chronic treatment schedule, showing the training phase, and retests in the water cross maze. B. Schematic of acute treatment schedule, showing the training phase, and retests in water cross maze [Figure adapted and modified from our manuscript submitted relating to this work (Preprint can be found in [354]). Published version [353]].

2.5.2 Methoxy staining

After the behavioral tests, the mice were anesthetized in an isoflurane chamber, and the brains were decapitated by using a guillotine. To perform biochemical analyses, the brain was snap-frozen in dry ice and stored at -80°C until necessary. Using a cryotome (CryoStar NX70, Thermofisher), one hemisphere of the brain was sliced into $30\ \mu\text{m}$ thick slices in the sagittal plane. The slices were then incubated in the congo-derived methoxy-04 solution ($0.004\ \text{mg/ml}$, Tocris Bioscience, 1:1 Ethanol-PBS solution) for 30 minutes at room temperature. To remove unspecific binding the slices were further washed in 1:1 Ethanol-PBS solution (3X) and with Milli-Q water (2X). Further, using a fluorescent mounting medium (Dako, Germany) the brain slices were mounted on the microscope slides. We then obtained 3D image stacks with an epi-fluorescence microscope (Axio Imager.M2 with ApoTome.2, Jena, Zeiss, Germany). For automatic stitching of the brain slices, we used the tile scan mode. The methoxy staining excitation wavelength was set at $405\ \text{nm}$, and the emitted light was captured between 410 to $585\ \text{nm}$ [354].

After removing the background, the area and amount of plaques were measured using Fiji (ImageJ). In brief, the selection of the specific region of interest, the cortex or hippocampus, was done by the polygonal selection tool. The unselected area was removed and the background was subtracted using sliding paraboloid 5.0px. The color threshold was adjusted and the particles were analyzed [354].

2.5.3 Enzyme-linked immunosorbent assay (ELISA) of soluble A β

We used the second brain hemisphere of the frozen mouse brain for ELISA quantification of soluble A β_{42} . The brain hemisphere was coronally cut and separated from the cortex and hippocampus. In the Eppendorf, the cortex and hippocampus masses were determined and 10 X mass cold 5 M guanidine HCl/50 mM Tris HCl was added to each sample. Using a grinding setup, the samples were thoroughly ground using a pestle, and the homogenate was mixed with a 3D shaker at room temperature for 3 hours. 10 volumes of Ice cold casein buffer consisting of: 0.25 % casein, 5 mmol/l EDTA, 0.05% sodium azide, 10 μ g/ml leupeptin, 20 μ g/ml aprotinin in PBS (pH 8.0) was used to dilute the homogenates which were further centrifuged for 20 minutes at 12,000 X g at 4 °C. We decant the supernatant and stored it at -80 °C until further quantification by the ELISA kit (Human A β Amyloid (42) ELISA kit; Invitrogen KHB 3441). The ELISA methodology was followed exactly as per the manufacturer's instructions. As soon as the stop solution was added, an absorbance reading at 450 nm (Tecan Sunrise; Tecan Trading AG, Switzerland) was taken and the concentration was calculated from the standard curve [354].

2.6 Immunofluorescent staining and analyses: Image Acquisition, 3D reconstruction, and quantification

2.6.1 Synaptic engulfment measurement

Immunofluorescent staining was performed on 30 μ m thick sagittal brain slices. Tissue sections were fixed for 20 minutes in a 1:1 acetone isopropanol solution at room temperature. Permeabilization of the brain sections was performed with 0.3 % triton-X in PBS containing 0.1% tween 20 (PBS/T) followed by a 3X wash with PBS/T. 10% v/v normal goat serum (NGS) was used to block the section at room temperature for 1 hour. After 3X wash with PBS/T, the sections were incubated with primary antibody overnight at 4 °C, and the primary antibody was diluted to

respective concentrations in PBS/T. The primary antibody used in the experiment were Rabbit anti-C1q antibody (1:250; Abcam, ab182451), GFAP (GA5) Mouse mAb (1:600; Cell Signalling Tech, 3670S), and Rabbit anti-Synaptophysin antibody (1:600; Abcam, ab52636). On the subsequent day, the sections were incubated with secondary antibodies Goat Anti-Rabbit IgG Fc (Alexa Fluor® 488) (1:200; Abcam, ab150089) and Goat Anti-Mouse IgG H&L (Alexa Fluor® 647) (1:700; Abcam, ab150115) at room temperature for 2 hours. ProLong™ Glass Antifade Mountant with NucBlue™ Stain (Sigma Aldrich, product no. 57-50-1) was used to stain the nucleus. For the slice where nuclear staining was not necessary DAKO fluorescent mounting media (DAKO, s3023) was used to mount the slides [354].

Table 7: Antibody staining used in the immunofluorescent study

Antibody	Reference/ Source	Identifier	Dilution
Rabbit anti-C1q antibody	Abcam	ab182451	1:250
GFAP (GA5) Mouse mAb	Cell Signalling Tech (CST)	3670S	1:600
Rabbit anti-Synaptophysin antibody	Abcam	ab52636	1:600
Goat Anti-Rabbit IgG Fc (Alexa Fluor® 488)	Abcam	ab150089	1:200
Goat Anti-Mouse IgG H&L (Alexa Fluor® 647)	Abcam	ab150115	1:700
PSD95 (D27E11) XP® Rabbit mAb	Cell Signalling Tech (CST)	3450	1:400
NucBlue™ Stain	Sigma Aldrich	57-50-1	As required

2.6.2 Plaque Astrocyte and Plaque C1q Interaction

For the staining of plaques (Methoxy-04) with astrocytes (GFAP) or with C1q, 30 µm sagittal brain sections were fixed with 4% PFA at room temperature for 15 minutes. As described earlier in synaptic engulfment measurements, the primary and secondary antibodies were permeabilized and incubated similarly. The primary antibody used were Mouse mAb (1:600; Cell Signalling Tech, 3670S), GFAP (GA5), and Rabbit anti-C1q antibody (1:250; Abcam, ab182451). The

secondary antibody used were Donkey anti-Rabbit IgG (H+L) Highly Cross-Adsorbed Secondary antibody Alexa Fluor Plus 647 (Invitrogen, A32795), and Goat Anti-Mouse IgG H&L (Alexa Fluor® 647) (1:700; Abcam, ab150115). The brain sections after secondary antibody incubation were washed with 3X PBS/T followed by 3X 1:1 Ethanol-PBS solution for 5 minutes each. Following this, the slices were stained with Methoxy-04 dye as described earlier. It is important to keep in mind that this entire process is carried out in the dark. The slices after washing with 1:1 Ethanol-PBS solution (3X) and Milli-Q water (2X) were mounted using DAKO fluorescent mounting medium (DAKO, Germany) [354].

2.6.3 Confocal Microscope Setup

We have used the same confocal settings as were optimized in our published paper (*Pradhan et al., 2022*). The following section containing information about the confocal setting, therefore, has been taken from *Pradhan et al., 2022* and modified according to the antibodies used in the current project [358].

Imaging Setup: Leica Confocal SP8.

Lasers: 499 nm (C1q, Synaptophysin Intensity: 5%–10%), 405 nm (NucBlue™, Intensity: 10%), and 653 nm (GFAP, Intensity: 1%–2%), laser power depends on staining efficacy. The power output was fixed at 70% of the maximum output (1.5 mW).

Pinhole: 1 AU.

Gain (Master, analog): 800–1,000 V.

Digital Offset: 0 for 405 channel (PMT), (HyD doesn't require a digital offset).

Frame size: 1024 × 1024 pixels.

Scan Area: Zoom according to the focused astrocyte. On a general note, since we are trying to image individual astrocytes of diverse sizes and shapes, we recommend using the following range of pixel size for the X/Y plane:

X/Y pixel dimension: 0.04–0.08 μm.

Z step size: 0.27–0.30 μm .

Averaging: 2 lines.

Scanning speed: 200 Hz (lines per second).

Z-stack scanning: System optimized (z-step size normally 0.3 μm), scanning from the top to bottom of the focused astrocyte. On average, we collect 30–40 stacks over 6–8 μm (Z axis).

Bit Depth: 8-bit, bidirectional scanning.

Objective: 63 \times oil (Leica Type F Immersion liquid $n_{23} = 1,5180$, $v_e = 46$). NA= 1.40.

Selection of channels: C1q (Alexa 488, Abcam, green, 499 nm laser).

Rabbit anti-Synaptophysin antibody (1:600; Abcam, ab52636)

GFAP (Alexa 647, Cell Signaling Technology, red, 653 nm laser).

NucBlue™ Stain (405 nm laser).

Emission Wavelength: For C1q and Synaptophysin (510 nm–530 nm).

GFAP (663 nm–693 nm).

NucBlue™ Stain (415 nm–457 nm).

Processing: Lightning Function: Adaptive and background subtraction using the IMARIS function.

Refractive Index: 1.44.

The confocal was switched on 30 minutes before imaging and the stage was calibrated. Non-calibration of the stage affects the z-stack and the laser power of the confocal scope should be stabilized before using it. Locating the CA1 area of the hippocampus is a crucial step here. As a principle, we start always from a lower magnification such as (10 \times /0.40 NA) and (20 \times /0.75 NA), and then locate the high-resolution individual astrocyte with a higher magnification. The dentate

gyrus (V shape structure) is easy to locate and the CA1 region can be tracked down using the dentate gyrus as a guide (**Figure 17**). The astrocytes are obtained from the stratum radiatum layer of the CA1 region of the hippocampus. After locating the region of interest higher magnification ($63\times$ (oil)/1.40 NA) is applied to obtain high-resolution individual astrocytes. The images are deconvoluted using the lightning function of the LEICA scope. The images are imported to IMARIS for further processing [358].

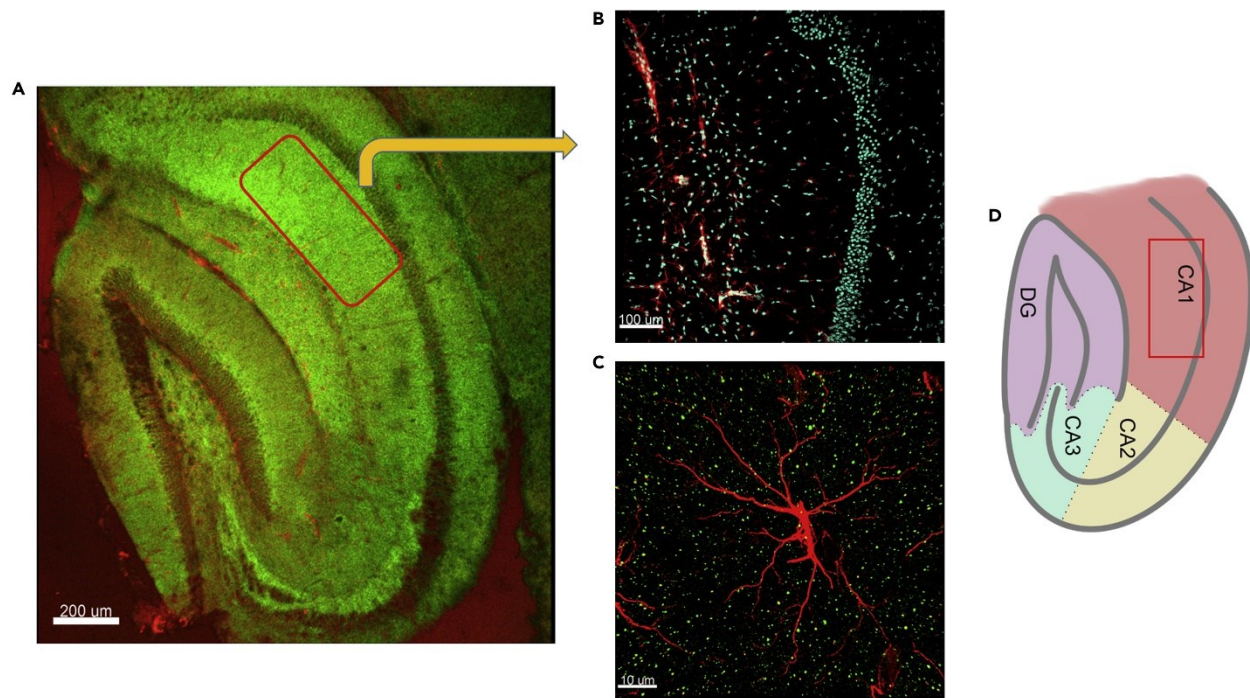


Figure 17. Overview of the C1q-GFAP interaction in the hippocampus (Adapted with permission from [358])

(A) Representative sagittal hippocampal section showing the different regions stained with C1q (green) and GFAP (red) at $10\times/0.40$ magnification. *Scale Bar 200 μm.*

(B) Hippocampal CA1 region stained with NucBlueTM (cyan) and astrocyte (red) at $20\times/0.75$ magnification. *Scale Bar 100 μm.*

(C) High-resolution individual astrocyte (red) stained alongside C1q (green) imaged at $63\times/1.40$ magnification. *Scale Bar 10 μm.*

(D) Representation of the hippocampus and its different regions. The astrocytes are selected from the stratum radiatum layer, shown in magenta, and marked using a red rectangular box.

2.6.4 3D reconstruction of astrocytes and synaptic pruning

We perform the volumetric 3D reconstruction of individual astrocytes and the measurement of synaptic engulfment in the astrocytic volume using IMARIS 9.7 (Oxford Instruments, Bitplane) by our previously optimized and established protocol. Briefly, the surface is created around the astrocytes in four different stages in IMARIS 9.7 (A detailed description is presented with additional details in (Pradhan *et al.*, 2022) [358] (**Figure 18**).

1. Individual astrocytes are segmented using “Segment only a region of Interest” under the “Algorithm Settings” box.
2. The smooth option is unselected as it adds additional bias to the morphology of the astrocytes.
3. In this step, the intensity threshold is set for the red channel. It is essential here not to set the threshold too high or too low and to maintain a balance while setting the threshold (**Figure 19**).
4. In the next step, unwanted disjoint signals which add to the background noise are removed.

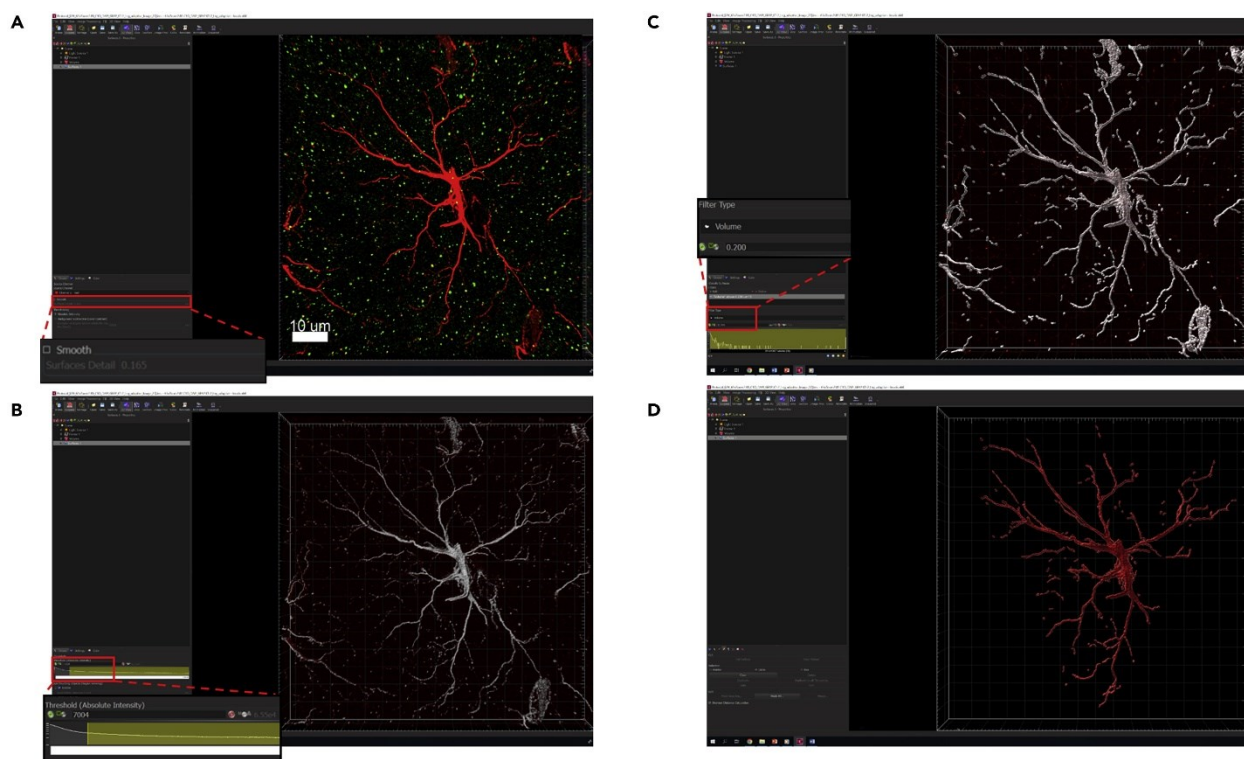


Figure 18. Volumetric Rendering of astrocytes takes place in four steps (Adapted with permission from [358])

(A) The red channel (GFAP) is selected in step 2 and the smoothing option is disabled to avoid the introduction of bias in the rendering process.

(B) The intensity threshold for the red channel is set in step 3. The manual threshold in comparison to the automatic thresholding produces consistent and reliable rendering of the astrocytes.

(C) The unwanted disjoint signals are filtered out in step 4.

(D) Astrocytic surface is rendered. Scale Bar 10 μm .

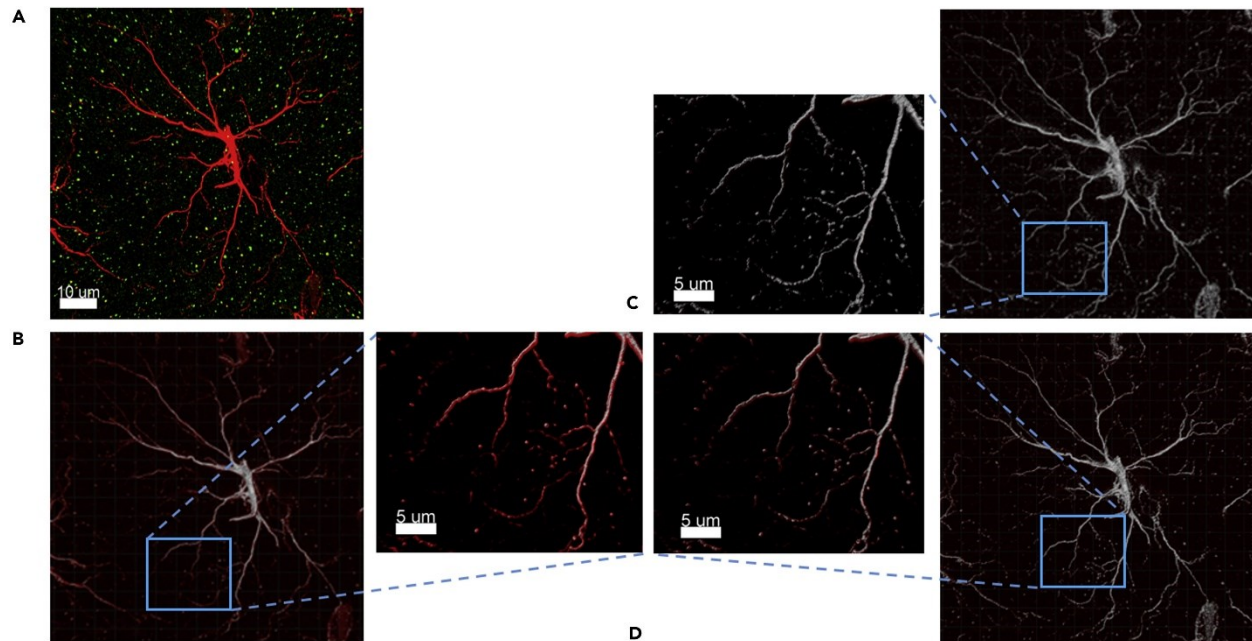


Figure 19. Managing the correct threshold level for the volumetric reconstruction of the astrocyte (Adapted with permission from [358])

(A) Original image of astrocyte-C1q before rendering. Red: Astrocyte and Green: C1q

(B) Insufficient threshold setting resulting in the underrepresentation of astrocytes. In this particular example, not all the processes of the astrocytes are properly rendered.

(C) Overrendering of the astrocytic surface creates bias by introducing unreliable processes.

(D) Example showing a balanced threshold for the unbiased rendering of the astrocytes. *Scale Bar 10 μm . Scale Bar for zoomed-in section (inset) 5 μm .*

The astrocytic surfaces are now rendered. In case of additional background signals, “Circle Selection Mode” can be used to select these signals and eliminate them (**Figure 20**).

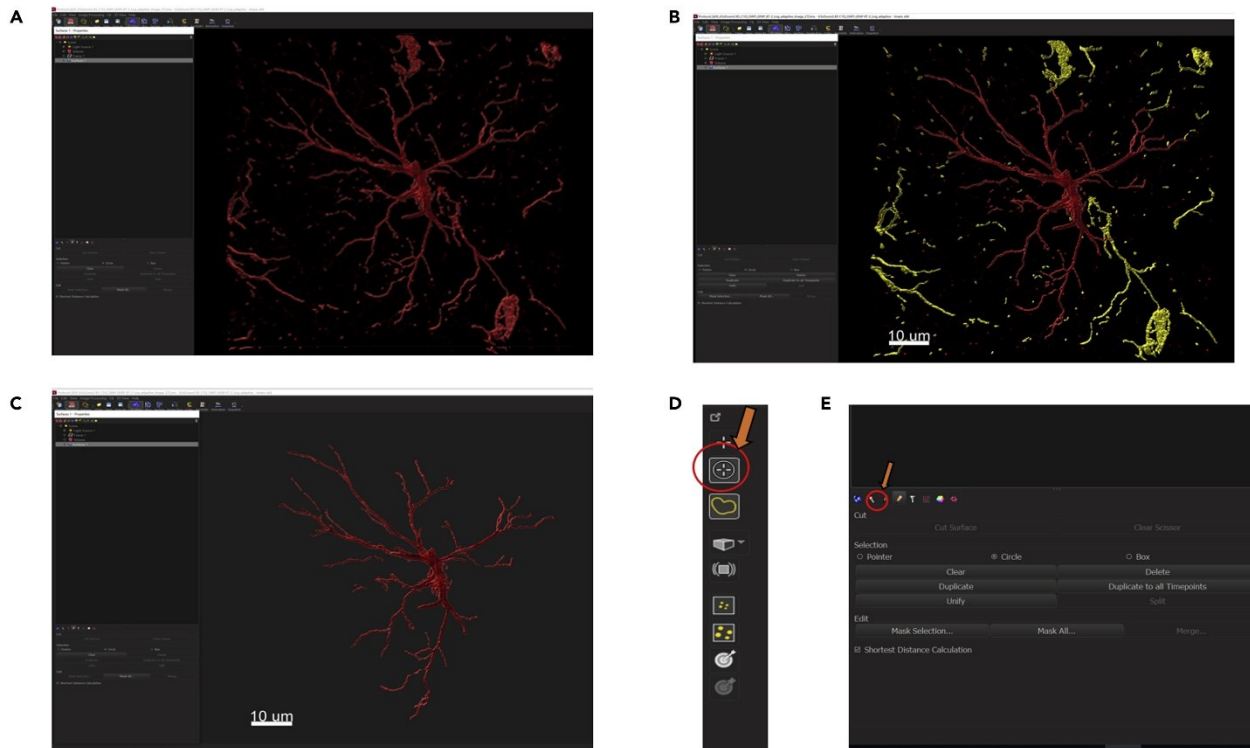


Figure 20. Removal of unwanted background signals from the rendered astrocyte (Adapted with permission from [358]).

(A) After the final step of astrocytic rendering, further processing is required to remove additional background noise in the form of incomplete processes or processes from other astrocytes.

(B) The unnecessary background processes are selected and are shown in yellow.

(C) Processed astrocytes.

(D) The “Circle Selection Mode” shown by an orange arrow is used to select the unwanted disjoint signal.

(E) These are then removed by selecting the delete option in the edit menu. *Scale Bar 10 μ m*.

The next step is to mask the astrocytic surface. This can be achieved by using the “Mask All” option under the “Edit” tab. In the drop-down options of the Mask tab, we select the red channel (GFAP) and set the voxels outside the surface to 0 (**Figure 21**). We reduce additional false positive bias via this method. The *coloc* tab is opened in IMARIS. Imaris provides the option to analyze two specific channels at a particular time point [358]. The automatic threshold option doesn’t

produce reliable results and therefore is discouraged. The channel threshold selection was as follows:

1. For setting the threshold of the green channel manual thresholding method was used. This was done by taking the average of 10 unambiguous puncta.
2. The thresholding setting of the masked red channel was relatively simple. The threshold intensity was set to 1 (**Figure 22**).

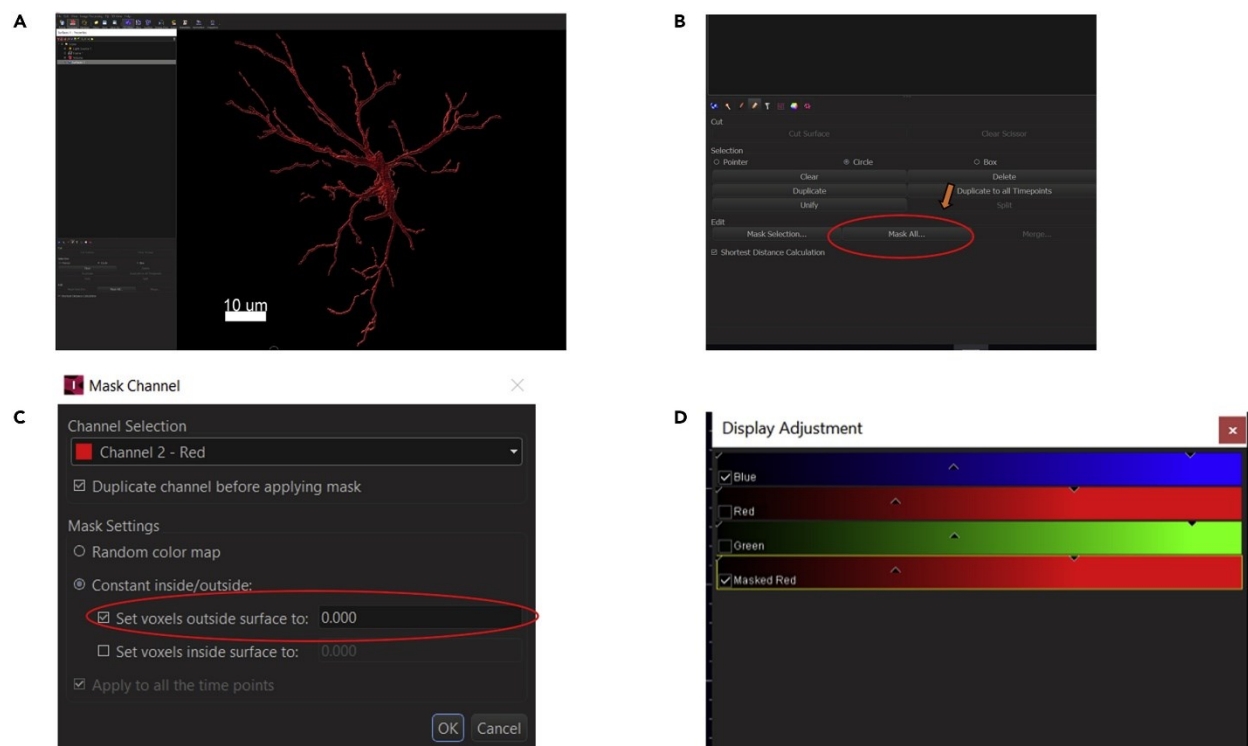


Figure 21. Masking the astrocytic surface (Adapted with permission from [358]).

(A) Rendered and processed astrocyte.

(B) Select the “Mask All” option on the edit menu.

(C) In the drop-down menu select the red channel and set the voxels outside surface to 0.

(D) The masked surface of the astrocyte is now created and shows alongside the other channels in the display channel option. *Scale Bar 10 µm.*

After this, the Region of Interest (ROI) tab in the right corner was set to the masked red GFAP channel, and the threshold was set to 1. The % ROI colocalization measures (proportionally) the

number of synaptic tags engulfed by the astrocytes as a whole (**Figure 23**). By estimating the percentage of colocalization in the masked red channel (which indicates the astrocytic volume), we can determine the percentage of synaptophysin or C1q signals that are inside the astrocytic volume.

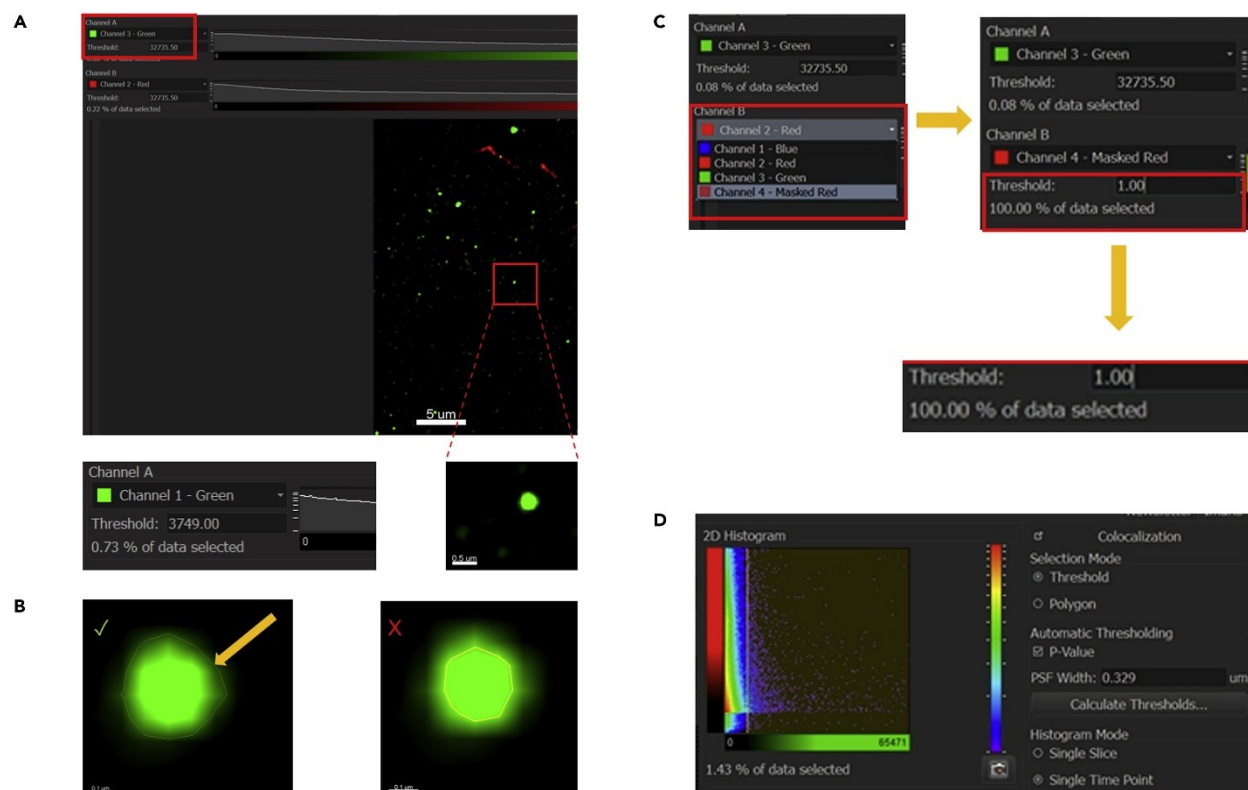


Figure 22. Analysis of the astrocytic engulfment using colocalization (COLOC) analysis with Imaris (Adapted with permission from [358]).

In the “Image Processing” option, select the COLOC tab,

(A) In channel A select green channel and set the threshold by selecting unambiguous punctum as shown in the figure. *Scale Bar for zoomed-in section (inset) 0.5 μ m.*

(B) To obtain the right threshold for the green channel, first right-click on each punctum and create a boundary that encircles the whole of the punctum. The boundary is shown by an arrow. As shown here the yellow boundary should encircle the entire individual green signal. An average of 10 unambiguous puncta is taken to calculate the threshold intensity of the green channel. The left inset shows the right way of encircling whereas the right one shows incorrect threshold measurement. *Scale Bar for zoomed-in section (inset) 0.1 μ m.*

(C) The threshold for channel B (masked red) is set to 1.

(D) While there is an automatic thresholding option provided by imaris, it produces inconsistent results.

The Plaque-astrocyte interaction was measured using a similar method. The neighboring astrocyte was 3D reconstructed and incompletely reconstructed ones were removed. The processes were rendered to an accuracy that entails the whole GFAP volume. The thresholding here for the plaques was done in a way in which the boundary set completely encompasses the plaques (instead of averaging 10 puncta as was done in the case of C1q or synaptophysin). The interaction was measured by the percentage of the entire astrocytic volume that interacts with amyloid plaques. The interaction between C1q and plaque was done using “automatic thresholding” without building any surface or reconstructing any signals. This automatic thresholding produced reproducible colocalization analysis [358].

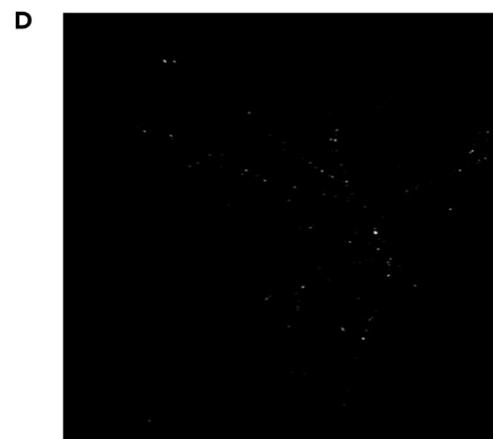
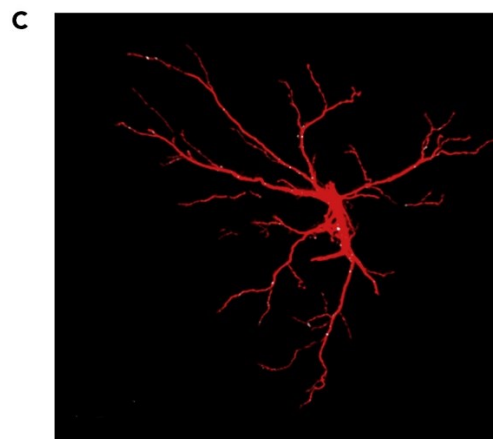
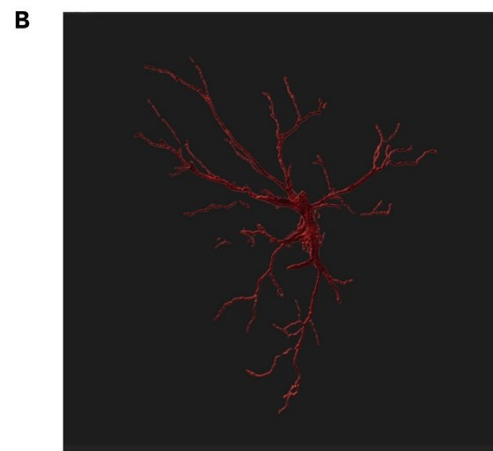
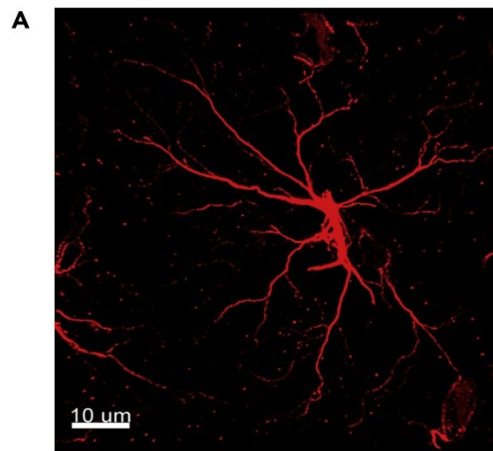


Figure 23. Synaptic engulfment and volumetric rendering of the astrocyte (Adapted with permission from [358]).

- (A) Original processed image of the astrocyte.
- (B) Volumetric 3D rendered image.
- (C) Astrocyte (Red) with colocalization of C1q in white.
- (D) Colocalization shown in white.

2.7 Golgi-Cox staining of the spines from in vivo XBD173 treated mice

After sacrificing the mouse, the brains were sagittally sectioned to 250 μm hippocampal slices in the vibratome. The slices were incubated for 30 minutes at 35°C in an aCSF-filled chamber and left to rest for an additional hour at room temperature. We used the FD Rapid GolgiStain Kit (FD NeuroTechnologies) for the Golgi-Cox staining. The manufacturer's instructions and protocol were followed for staining. Briefly, we incubated the brain slices for 4 days in the impregnation solution. Imaging of apical dendrites was done from pyramidal neurons of layer V using an epifluorescence microscope (Axio Imager.M2 with ApoTome.2, Jena, Zeiss, Germany). The dendritic spines were analyzed in Fiji. Individual dendrites were selected using the rectangle tool. Fiji sharpening tool was used to sharpen the outline of the spines (Process -> Sharpen). The freehand line tool was used to measure the length of the dendrites (Analyze -> Measure). The spines were selected as ROI and were counted [354].

2.8 Steroid profiling by gas chromatography coupled to tandem mass spectrometry (GC-MS/MS)

Quantification and identification of steroids in brain tissues were performed by a GC-MS/MS procedure established and previously validated in terms of reproducibility, accuracy, and linearity in the nervous system [359]. In short, neurosteroids from the cortex and hippocampus were extracted with 10 volumes of MeOH. For steroid quantification following internal controls were included: 10 ng of $^2\text{H}_8$ -corticosterone (B) for B and $5\alpha/b$ -DHB, $5\alpha/b20\alpha$ -THPROG, 2 ng of epietiocholanolone (3β -hydroxy- 5β -androstane-17-one, Steraloids, Newport, Rhode Island) for

5 α /b-dihydrotestosterone (DHT), 2 ng of ¹³C₅-20 (Isosciences) for the analysis of 20 β -dihydroprogesterone (20 α / β -DHP), 2 ng of 19-norPROG for 5 α /b-DHDOC, pregnenolone (PREG), 3 α / β 5 α / β -tetrahydro progesterone (THPROG), 2 ng of ¹³C₅-5 α -DHP (CDN Isotopes, Sainte Foy la Grande, France) for 5 α /b-DHP, 2 ng of ¹³C₃-deoxycorticosterone (DOC) for DOC, 3 α / β 5 α / β 20 α /b-hexahydroprogesterone (HHPROG), 2 ng of ¹³C₃-PROG for PROG, 3 α / β 5 α /b-tetrahydrotestosterone (THT), and 3 α /b5 α /b-tetrahydrodeoxycorticosterone (THDOC), and 1 ng of ¹³C₃-testosterone(T) for T.

The extracts were then purified and fractionated using solid-phase extraction with a C18 cartridge (500 mg, International Sorbent Technology). Next, we filter and fraction the unconjugated steroids-containing fraction by the HPLC system consisting of an LPG-3400SD quaternary pump gradient coupled with an SR-3000 fraction collector (Thermoscientific, USA), WPS-3000SL analytical autosampler, and a Lichrosorb Diol column (25 cm, 4.6 mm, 5 μ m) in a thermostated block at 30 °C. The solvent system of 90% heptane and 10% of a mixture composed of heptane/isopropanol (85/15) was used to equilibrate the column. The flow rate of 1 ml/min was employed to perform the elution, starting with 90% heptane and 10% heptane/isopropanol (85/15) for 15 min, and then with a linear gradient to 100% acetone in 2 min. This mobile phase was kept constant for 13 min.

From the HPLC system, two fractions were collected: In the first HPLC fraction (3-14 min) 5 α / β -DHPROG was eluted and then silylated for 15 minutes at 70 °C with 50 μ l of a mixture of N-methyl-N-trimethylsilyl tri fluoroacetamidemmonium iodide/dithioerythritol (1000:2:5) (vol/wt/wt). All other steroids are present in the second fraction (14-29 min). These were derivatized with 25 μ l heptafluorobutyric anhydride (HFBA) and 25 μ l anhydrous acetone at 80 °C for 1 h. Under a stream of N₂, both fractions were dried and then resuspended in heptane. All1310 autosampler, a Trace 1310 gas chromatograph (GC), and a TSQ8000 mass spectrometer (MS) (Thermoscientific, San Jose, CA) were used to perform the GC-MS/MS analysis of the purified and derivatized extracts. The injection was carried out in splitless mode at 280 °C (1 minute of splitless time), and the temperature of the gas chromatograph oven was first held at 80 °C for 1 minute before ramping between 80 and 200 °C at 20 °C/min, then to 300 °C at 5 °C/min, and lastly to 350 °C at 30 °C/min. A constant flow of 1 ml/min was maintained for the helium carrier gas flow during the analysis. The temperatures in the transfer line and ionization chamber

were 330 °C and 200 °C, respectively. With an ionization energy of 70 eV, electron impact ionization was applied for mass spectrometry. Excalibur®, release 3.0 software (ThermoScientific, USA) was used to analyze GC-MS/MS data on a computer workstation. The identification of steroids was facilitated by their retention duration and two or three transitions. Quantification was carried out in accordance with the change resulting in more abundant production. According to the steroid structure, the detection limit was between 0.5 and 10 pg. Using male mice brains (200 mg) the analytical protocol has been validated.

2.9 Statistical analysis

We use GraphPad Prism 6 (Version 6.01) for all statistical analyses. D'Agostino-Pearson and Shapiro-Wilk tests were used to verify the normality of the data sets. Non-parametric testing was applied when the sample size was smaller and normality detection was not possible. Furthermore, we did not perform any statistical analysis on data sets with fewer than four samples, instead, we used descriptive statistics to describe the differences between them. Except for the escape latency and accuracy curves, which are expressed as mean \pm SD, the data sets are shown with the median and interquartile range. The ROUT method with Q=1% was used to detect the outliers. Using Kruskal–Wallis and Dunn's multiple comparison post hoc tests for data sets that did not have a normal distribution, the significance of differences between experimental groups was determined, and for normally distributed data sets, one-way ANOVA and Bonferroni's post hoc analysis was used. After the multiple comparisons, an adjusted p-value was calculated and is listed in the figure legend. The Mann–Whitney U test is used to analyze differences between two non-normally distributed experimental groups. Each figure legend specifies the statistical test used along with the median and interquartile range for each data set. Statistical significance is indicated in the plots with an asterisk (*) when $p < 0.05$ [354].

3. Results

3.1 XBD173 (emapunil) averts the potential neurotoxic effect of A β ₁₋₄₂ oligomers on CA1-LTP in the hippocampus

CA1-LTP which is generally considered a cellular correlate of learning and memory was first used as an *ex vivo* method to assess the neurotoxic effects of A β oligomers and whether pre-incubation with XBD173 could prevent the LTP impairments. CA1-LTP was induced in the Schaffer Collateral pathway via the stimulating electrodes by delivering electrical stimulation (100 pulses/100 Hz). Previous studies as well as reports from our lab show oligomeric A β application (A β ₁₋₄₂, 3NTyr10-A β , A β ₁₋₄₀, and A β pE3) in sagittal 350 μ m hippocampal slices in a dose-dependent manner impaired and blocked the induction of CA1-LTP [70,355]. In our study, as well, low nanomolar concentrations (50 nM) of both A β ₁₋₄₂ and A β ₁₋₄₀ after 90 minutes of incubation in the bath solution impaired the LTP in the hippocampal slices (**Figures 24 and 25**). The baseline slope (recorded before the induction of HFS) is compared to the last 10 minutes after the induction of high-frequency stimulation. In general, all the recordings were continued even after the usual 60 minutes after the LTP induction, to monitor the fEPSP trajectories. XBD173 was tested at 300 nM to see if it could prevent the neurotoxic action of both A β ₁₋₄₂ and A β ₁₋₄₀ oligomers. It was ensured that XBD173 (300 nM) itself did not block or impair the LTP. Preincubation of hippocampal slices with XBD173 partly improves (not significant) the fEPSP slope impairment resulting from the incubation with A β ₁₋₄₀ oligomers (**Figure 24**). The final fEPSP slope in this case after preincubation with XBD173, however, was still less than 20% higher than the baseline. However, XBD173 (300 nM) completely prevents the LTP impairments resulting from A β ₁₋₄₂ oligomers (**Figure 25**). The differential action of XBD173 on different A β oligomers could be attributed to the different targets of both the A β peptides as well as the differential mechanism of action and kinetics of both peptides.

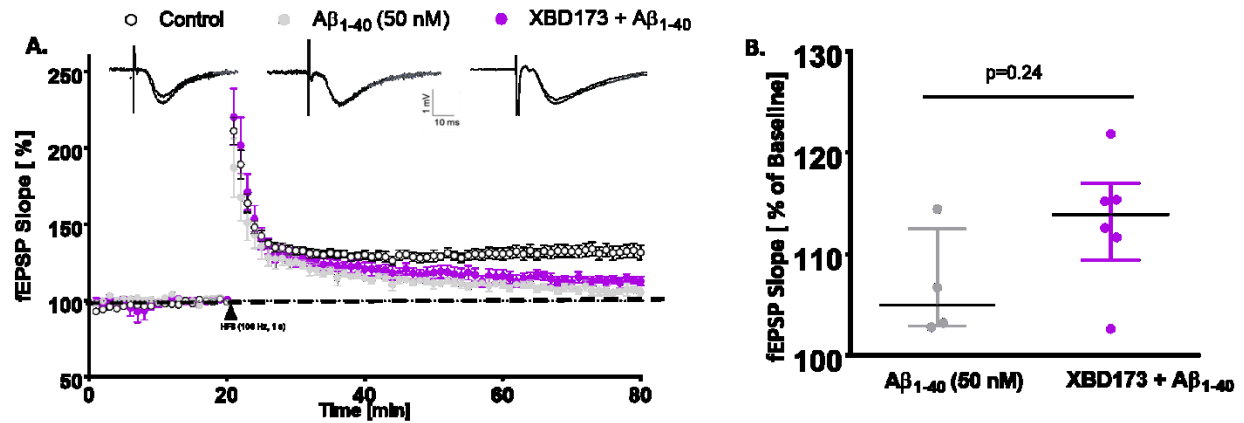


Figure 24: Contrary to the effect of XBD173 on $A\beta_{1-42}$ oligomers, there is a partial rescue of the LTP impairments resulting from $A\beta_{1-40}$ oligomers. [Figure adapted and modified from our manuscript submitted relating to this work (Preprint can be found in [354]). Published version [353]]

A. Normalised fEPSP slope time course following an HFS under control conditions, with 90 min $A\beta_{1-40}$ exposure alone, and the application of XBD173 (300 nM) and $A\beta_{1-40}$ respectively. Representative traces for each treatment group are shown in the insets above. C. For each group, a scatter dot plot summarizing the last 10 minutes (from 50 to 60 minutes) following HFS: Control (n=10), $A\beta_{1-40}$ (n=4), and XBD173 + $A\beta_{1-40}$ (n=6; Mann-Whitney U test; XBD173 + $A\beta_{1-40}$: 113.9 (109.4-117) % of baseline slope vs $A\beta_{1-40}$: 105 (102.9-112.5) % of baseline slope, $p=0.24$). Data are represented as median with their respective interquartile range. * $p < 0.05$. ns: not significant.

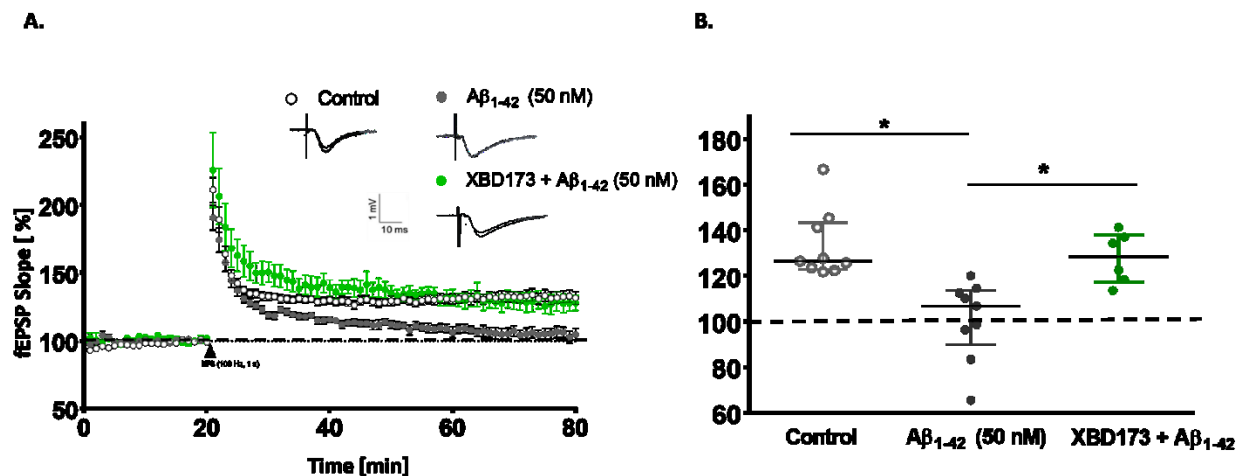


Figure 25: CA1-LTP in the hippocampus is impaired after the incubation with A β ₁₋₄₂ and XBD173 prevents these adverse synaptotoxic effects. [Figure adapted and modified from our manuscript submitted relating to this work (Preprint can be found in [354]). Published version [353]]

A. Normalised fEPSP slope time course following an HFS under control conditions, with A β ₁₋₄₂ exposure alone for 90 min, and the simultaneous application of XBD173 (300 nM) and A β ₁₋₄₂ (50 nM) respectively. Representative traces for each treatment group are shown in the insets above. B. For each group, a scatter dot plot summarizing the last 10 minutes (from 50 to 60 minutes) following HFS: Control (n=10), A β ₁₋₄₂ (n=10), XBD173 + A β ₁₋₄₂ (n=6; Kruskal–Wallis test with a Dunn’s multiple comparisons *post hoc* test; A β ₁₋₄₂: 106.9 (89.93-113.6) % of baseline slope vs Control: 126.5 (123.0-143.3) % of baseline slope, $p=0.0007$; A β ₁₋₄₂ vs XBD173 + A β ₁₋₄₂: 128.5 (117.2-138.1) % of baseline slope, $p=0.0192$). Data are represented as median with their respective interquartile range. * $p < 0.05$. ns: not significant.

3.2 TSPO is necessary for XBD173 to exert its neuroprotective effect against the A β ₁₋₄₂ oligomer

Previously, XBD173 via TSPO protein has been shown to exert an anxiolytic effect in both rodents as well as in humans [228]. In our case, therefore, we tried to assess the importance of the TSPO protein in XBD173’s neuroprotective role against A β ₁₋₄₂ oligomers. We used the sagittal hippocampal slices from TSPOKO animals and monitored the fEPSPs after incubation with XBD173 and A β ₁₋₄₂ oligomers. As expected, the neuroprotective role of XBD173 which was previously observed against A β ₁₋₄₂ oligomer in WT C57Bl6 mice was not seen in TSPOKO hippocampal slices. This highlights the necessity of TSPO for the XBD173-mediated activity in ameliorating LTP impairment. The fEPSPs trajectories clearly show a difference between the XBD173 action in WT slices and TSPOKO hippocampal slices. In the latter case, the preincubation of XBD173 is not able to prevent the neurotoxic effects of the A β ₁₋₄₂ oligomer (**Figure 26**). This suggests two essential factors (neuroprotective action against the A β ₁₋₄₂ oligomers and dependency on TSPO protein) in XBD173’s action in an *ex vivo* setup.

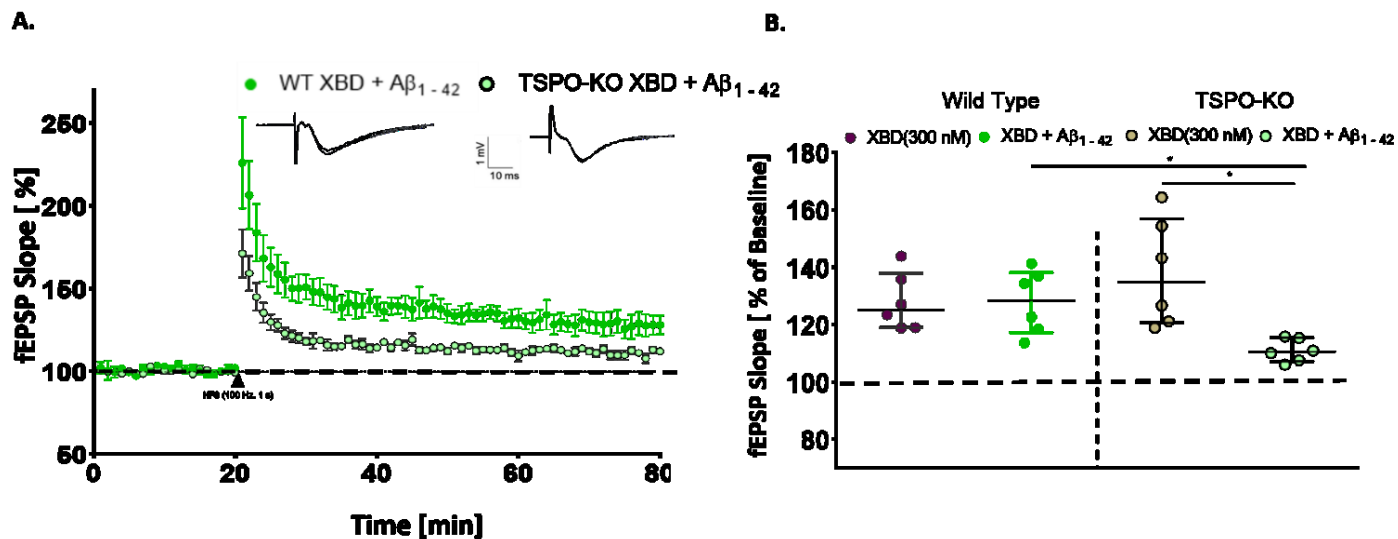


Figure 26: TSPO is necessary for XBD173 to rescue the synaptotoxic effect of $A\beta_{1-42}$ oligomers [Figure adapted and modified from our manuscript submitted relating to this work (Preprint can be found in [354]). Published version [353]]

A. Normalised fEPSP slope time course following an HFS in WT (XBD173 + $A\beta_{1-42}$), and TSPO-KO (XBD173 + $A\beta_{1-42}$). Representative traces for each treatment group are shown in the insets above. B. For each group, a scatter dot plot summarizing the last 10 minutes (from 50 to 60 minutes) following HFS: WT XBD173 (n=6), TSPO-KO XBD173 (n=6), WT XBD173 + $A\beta_{1-42}$ (n=6) and TSPO-KO XBD173 + $A\beta_{1-42}$ (n=6; Mann–Whitney U test: WT XBD173 + $A\beta_{1-42}$:128.5 (117.2-138.1) % of baseline slope vs WT XBD173: 125.2 (118.9-137.8) % of baseline slope, $p=0.7879$; TSPO-KO XBD173 + $A\beta_{1-42}$:110.5 (107.2-115.4) % of baseline slope vs TSPO-KO XBD173: 134.9 (120.6-156.9) % of baseline slope, $p=0.0022$; WT XBD173 + $A\beta_{1-42}$ vs TSPO-KO XBD173 + $A\beta_{1-42}$, $p=0.0087$). Data are represented as median with their respective interquartile range. * $p < 0.05$. ns: not significant.

3.3 Preincubation of XBD173 prevents individual dendritic spine loss resulting from $A\beta_{1-42}$ oligomers

Spines, the small protrusions on the dendritic surface play a critical role in regulating the functionality of neural systems and maintaining the dynamic synaptic system [360]. Synaptic signaling is orchestrated via these small protrusions. LTP attenuation as well as induction have an

associated effect with these dendritic spines [361–363]. Previously, stress-induced spine loss has been associated with the attenuation of hippocampal LTP [364]. Similarly, the stabilization of dendritic spines occurs during the LTP process [365]. These small dynamic protrusions are thought to constitute an important player in learning-related processes and play a crucial role during the process of synaptic transmission [361,364,366]. Because of these features, the dendritic spines act as a platform to receive excitatory inputs to the hippocampus, cortex, and other brain areas. Given this correlation between synaptic transmission and dendritic spines, we speculated that the impairment of LTP caused by the A β ₁₋₄₂ oligomers was associated with changes in the dynamic structure of the dendritic spines. We used hippocampal slices obtained from Thy1-eGFP mice and used the same treatment strategy with XBD173 and A β ₁₋₄₂ oligomers as in the *ex vivo* LTP experiments. Consistent with this line of thought, we observed a clear reduction in the total spine density after the incubation with A β ₁₋₄₂ oligomers (50 nM). This reduction in the total spine density correlates with LTP impairment as was observed from the electrophysiology recording. This falls in line with one of our previous studies in the lab which shows A β oligomers reduce neuronal spines in hippocampal slices, and antagonizing GluN2b receptors reversed this effect [355]. The role of XBD173 in conferring protection against the LTP impairments induced by A β ₁₋₄₂ oligomers made us ask if these changes are also reflected in changes in the dendritic spines. We found that preincubation with XBD173 indeed prevents the loss of dendritic spines occurring from the incubation with A β ₁₋₄₂ oligomers.

Given the morphological differences between the different classes of spines and their associated functionality with memory-related processes, we asked if A β ₁₋₄₂ oligomer incubation affects the different spine subclasses. Based on the head volume, neck length, and total length of the spines, these small protrusions are critically categorized as stubby, mushroom, or long-thin spines. Mushroom spines, given their higher head volume, have often been associated with learning and memory-related processes whereas long-thin spines given their dynamic nature and flexibility are considered “learning spines” and are important in the new memory formation during synaptic transmission. Stubby spines occur early during postnatal development and decrease in adulthood [360,367]. Given these parameters, we analyzed the different subclasses of spines after reconstructing the dendrites in the IMARIS (**Figure 27**). There was a significant increase in mushroom, stubby, and long-thin spine counts after preincubation with XBD173, and the synaptotoxic effect of A β ₁₋₄₂ oligomers on dendritic spine growth was prevented (**Figure 28**). The

morphological specialty of both mushroom and long-thin spines and the rescue of these spines after XBD173 incubation could potentially play a critical factor in the neuroprotective role of XBD173.

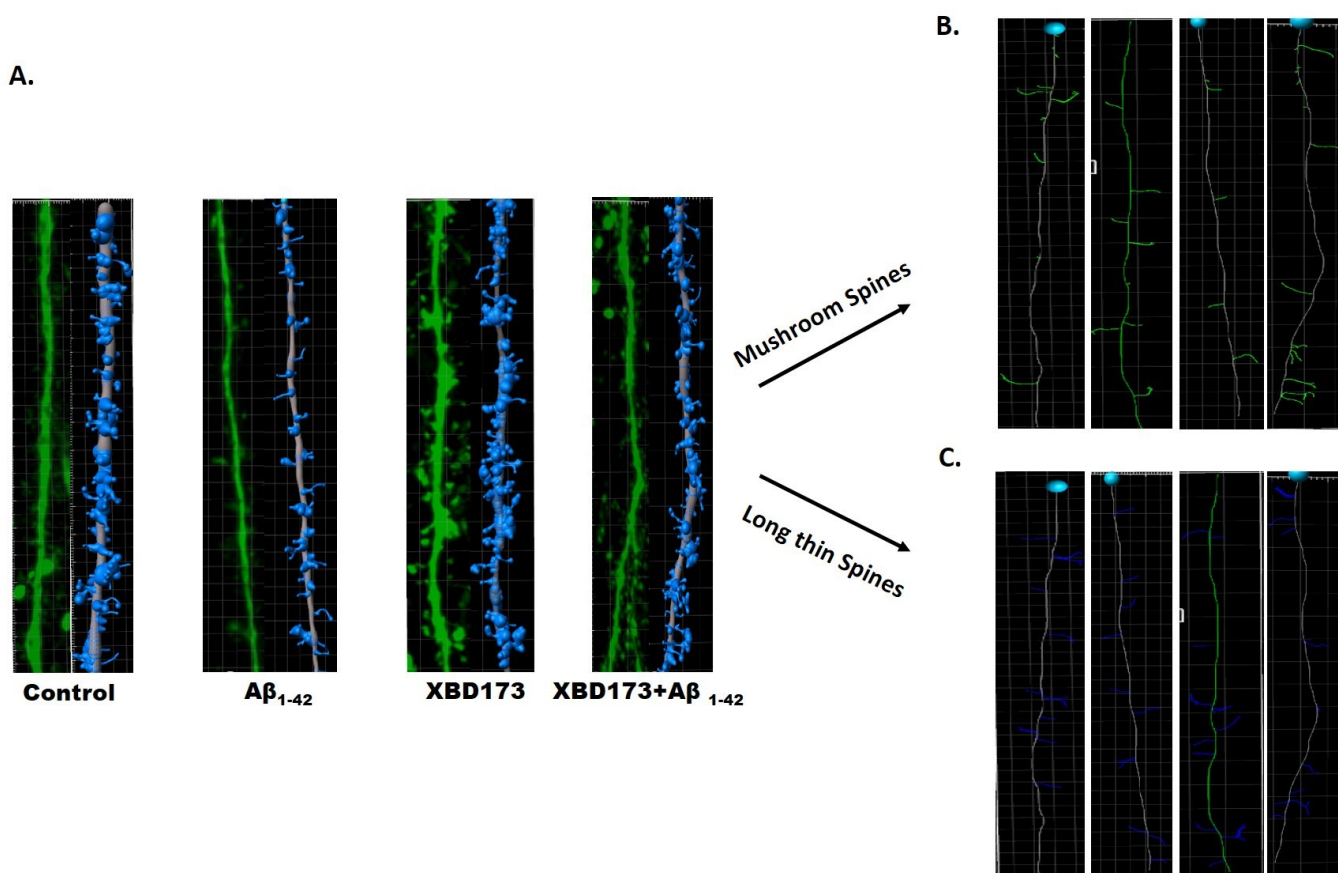


Figure 27: Representative spine reconstruction using IMARIS filament function. [Figure adapted and modified from our manuscript submitted relating to this work (Preprint can be found in [354]).

Published version [353]]

A. Dendritic spine images of each group with its reconstructed spine using IMARIS. Control (n=6), XBD173 (n=4), $A\beta_{1-42}$ (n=5), and XBD173 + $A\beta_{1-42}$ (n=4) B. Classification of dendritic spines to mushroom spines for each treatment group. C. Classification of dendritic spines to long thin spines for each treatment group.

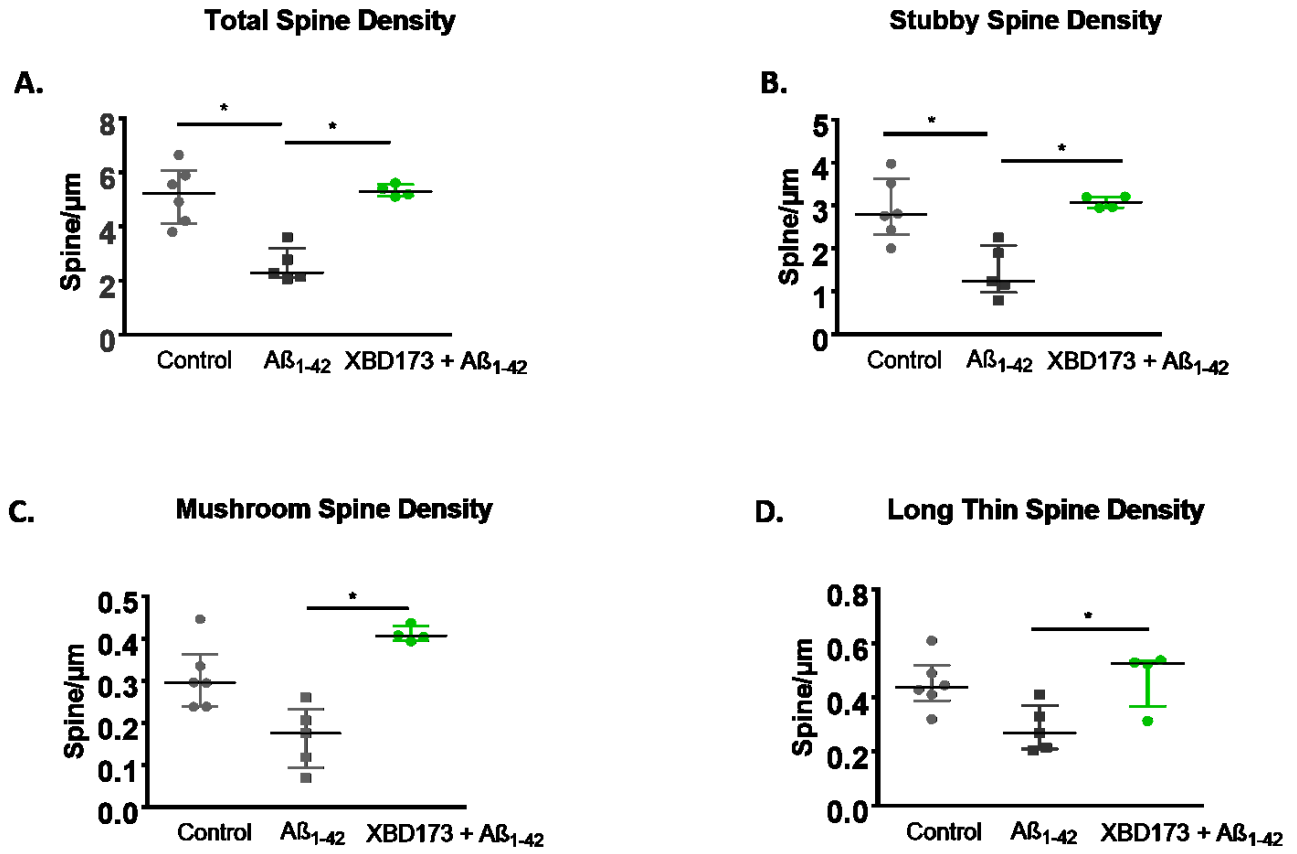


Figure 28: TSPO-dependent XBD173 inhibits the detrimental synaptotoxic effects of Aβ₁₋₄₂ oligomers on dendritic spines. [Figure adapted and modified from our manuscript submitted relating to this work (Preprint can be found in [354]). Published version [353]]

A. Comparison of total spine density in treatment groups: Control (n=6), Aβ₁₋₄₂ (n=5), and XBD173 + Aβ₁₋₄₂ (n=4; Kruskal–Wallis test with a Dunn’s multiple comparisons *post hoc* test; Aβ₁₋₄₂: 2.302 (2.113-3.194) spines/ μm vs Control: 5.236 (4.108-6.080) spines/ μm, $p=0.0136$; Aβ₁₋₄₂ vs XBD173 + Aβ₁₋₄₂: 5.297 (5.134-5.563) spines/ μm, $p=0.0196$) B. Comparison of stubby spine density in treatment groups: Control (n=6), Aβ₁₋₄₂ (n=5), and XBD173 + Aβ₁₋₄₂ (n=4; Kruskal–Wallis test with a Dunn’s multiple comparisons *post hoc* test; Aβ₁₋₄₂: 1.244 (0.979-2.078) spines/ μm vs Control: 2.790 (2.332-3.639) spines/ μm, $p=0.0340$; Aβ₁₋₄₂ vs XBD173 + Aβ₁₋₄₂: 3.086 (2.956-3.210) spines/ μm, $p=0.0114$). C. Comparison of mushroom spine density in different treatment groups: Control (n=6), Aβ₁₋₄₂ (n=5), and XBD173 + Aβ₁₋₄₂ (n=4; Kruskal–Wallis test with a Dunn’s multiple comparisons *post hoc* test; Aβ₁₋₄₂: 0.1756 (0.0942-0.2332) spines/ μm vs Control: 0.2959 (0.2390-0.3629) spines/ μm, $p=0.0897$; Aβ₁₋₄₂ vs XBD173 + Aβ₁₋₄₂: 0.4063 (0.3966-0.4302) spines/ μm, $p=0.0049$). D. Comparison of long-thin spine density in treatment groups: Control

(n=6), A β ₁₋₄₂ (n=5), and XBD173 + A β ₁₋₄₂ (n=4; Kruskal–Wallis test with a Dunn’s multiple comparisons *post hoc* test; A β ₁₋₄₂: 0.2698 (0.2103-0.3712) spines/ μ m vs Control: 0.4378 (0.3889-0.5203) spines/ μ m, $p=0.0846$; A β ₁₋₄₂ vs XBD173 + A β ₁₋₄₂: 0.5272 (0.3662-0.5369) spines/ μ m, $p=0.0490$). Data are represented as median with their respective interquartile range. * $p < 0.05$. ns: not significant.

3.4 Acute intraperitoneal administration of XBD173 does not improve the cognitive deficit in the transgenic ArcA β AD mice model

The *ex vivo* experiments with XBD173 showed that it could confer TSPO-dependent neuroprotective benefits against the A β ₁₋₄₂ oligomer-induced LTP impairment and dendritic spine loss. Since memory impairment and progressive cognitive decline form a major component of AD, we asked whether XBD173 treatment could reverse/rescue the progressive cognitive decline and learning impairments. To address this question, we used the WCM behavioral test which has been established as a sensitive tool to investigate cue-dependent hippocampal spatial learning in rodents. Compared to food rewards, water acts as the only motive force and selective reinforcement paradigm thereby leading to more robust and accurate performance. Additionally, compared to the traditionally used Morris water maze, the water cross maze exerts less stress thereby bringing lower biases to the behavioral testing [357]. All these factors make WCM a suitable platform to test the cognitive impairments in the transgenic AD model and whether XBD173 can rescue the cognitive impairment.

From previous studies conducted in this model, we know ArcA β mice develop cognitive impairments starting from the age of 6-7 months [119]. As discussed in the methods section, we used 2 different treatment paradigms to understand the XBD173 effect on cognitive performance in AD mice: acute and chronic treatment of the respective drugs. In the case of acute treatment, the administration of XBD173 (1 mg/kg) or the respective control drugs began two days before the initiation of the water cross-maze training period. The escape latency trajectory of transgenic ArcA β mice when compared to the wild-type control shows clear impairment during the training phase. Similarly, the accuracy curve of the transgenic mice differs from the wild-type mice. The ArcA β mice treated acutely with XBD173 were at par with their transgenic counterparts. To quantify the learning tasks based on the escape latency and accuracy we used the mean of the performance on the 4th and 5th days. During the training phase, the wild-type mice had lower escape latency and higher accuracy compared to the transgenic mouse indicating better and more

precise performance in WT mice. The XBD173-treated (acute) transgenic AD line did not have any improvement in escape latency and accuracy compared to the transgenic vehicle-treated ArcA β animals (**Figure 29 A, B**). Similarly, Retests 1 and 2 performed after a week and a month later respectively did not show any differences between the vehicle treatment and the XBD173-treated group (**Figure 29 C, D**). This suggests that the acute treatment of XBD173 might not be sufficient to affect the pathophysiology and subsequently the cognitive impairment in AD.

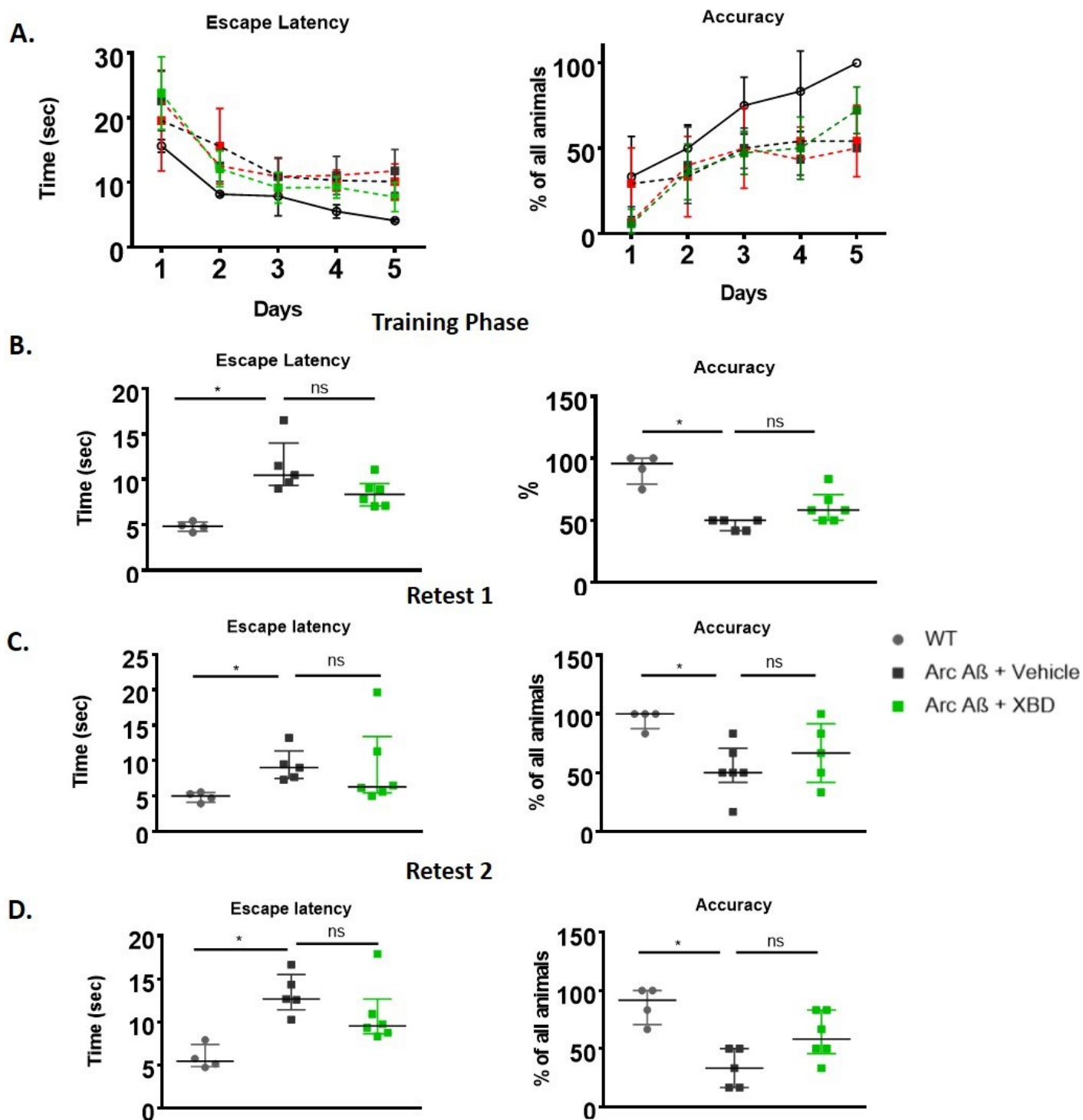


Figure 29: Cognitive deficits in AD mice are not ameliorated by acute administration of XBD173.
 [Figure adapted and modified from our manuscript submitted relating to this work (Preprint can be found in [354]). Published version [353]]

A. Trajectory of Escape latency and accuracy during the 5-day training phase in the WCM. The red-dotted trajectory belongs to untreated transgenic AD mice. B. Escape latency (Kruskal–Wallis test with a Dunn’s multiple comparisons *post hoc* test; Arc A β + XBD: 8.355 (7.095-9.548) s vs Arc A β + vehicle: 10.47 (9.345-14.02) s, $p=0.27$) and accuracy comparison (Kruskal–Wallis test with a Dunn’s multiple comparisons *post hoc* test; Arc A β + vehicle: 50 (41.67-50) % Arc A β + XBD: 58.33 (50-70.84) %, $p=0.17$) groups in the training phase. WT (n=4), Arc A β + vehicle (n=5), and Arc A β + XBD (n=6). Accuracy is expressed as the % of trials correctly performed for each animal, C. Escape latency (Kruskal–Wallis test with a Dunn’s multiple comparisons *post hoc* test; Arc A β + XBD: 6.302 (5.488-13.39) s vs Arc A β + vehicle: 9.01 (7.473-11.36) s, $p=0.69$) and accuracy comparison (Kruskal–Wallis test with a Dunn’s multiple comparisons *post hoc* test; Arc A β + XBD: 66.66 (41.67-91.67) % vs Arc A β + vehicle: 50 (41.67-70.83) %, $p=0.82$) in the Retest 1 phase. D. Escape latency (Kruskal–Wallis test with a Dunn’s multiple comparisons *post hoc* test; Arc A β + XBD: 9.542 (8.643-12.67) s vs Arc A β + vehicle: 12.67 (11.42-15.51) s, $p=0.44$) and accuracy comparison (Kruskal–Wallis test with a Dunn’s multiple comparisons *post hoc* test; Arc A β + XBD: 58.33 (45.83-83.33) % vs Arc A β + vehicle: 33.33 (16.66-50) %, $p=0.19$) in the Retest 2 phase. Data are represented as median with their respective interquartile range. * $p < 0.05$. ns: not significant.

3.5 Chronic intraperitoneal treatment of XBD173 improves hippocampus-dependent spatial learning in transgenic ArcA β AD mice

Chronic treatment of the drugs was administered for a period of 12 weeks when the mice were 8-9 months old. Both male and female mice were administered 1mg/kg of the respective drugs and were followed up with the WCM schedule. Diazepam another clinically used anxiolytic with a potentially higher side-effect profile was used as a reference drug to compare the performance with the transgenic ArcA β mice. Similar to the observations from the acute treatment regiment, the transgenic ArcA β mice had poorer escape latency and accuracy trajectory indicating impairments in spatial learning. Chronic treatment with XBD173 however improves the trajectory of both escape latency and accuracy. Additionally, starting from the training phase itself compared to vehicle-treated transgenic mice, the mice that were treated with XBD173 had significantly improved escape latency (**Figure 30**). Compared to the transgenic group, the XBD173-treated animals had a tendency for higher accuracy in the training phase. Both the parameters of escape latency and accuracy play a major role in deciding the spatial learning deficiency in mice. Retests

1 and 2 were designed to see if the effect induced by XBD173 on cognition is short-lived or long-lived after the termination of the treatment. Interestingly, in both retests 1 and 2, XBD173 improved the spatial learning in both accuracies and escape learning parameters compared to the vehicle-treated transgenic ArcA β mice (**Figure 31 A, B**). This suggests that XBD173 can confer the neuroprotective effect and is able to rescue the cognitive impairments in AD-modelled mice. Additionally, a better performance profile of the animals treated with XBD173 in the retests highlights long-term protection conferred by XBD173 after the termination of the treatment for more than 30 days.

The diazepam treatment schedule was comparable to the XBD173 treatment (1mg/kg every alternate day for 12 weeks). Unlike the XBD173 treatment, the diazepam-treated group did not show any marked improvement in the spatial learning parameters. The escape latency and accuracy of these animals were compared to the transgenic counterparts, indicating no benefits on the cognitive performance of the transgenic ArcA β mice. We also assessed the change in accuracy and escape latency in retests compared to the training phase. Our study suggests that the treatment (XBD173 or vehicle treatment) affects uniformly the performance of individual animals i.e. each animal has a similar performance profile in the retests compared to the training phase (**Figure 32**). Importantly, the XBD173-treated group had a higher percentage of accurate learners at the end of the training phase as well as in both the retests compared to the vehicle-treated and diazepam-treated transgenic mice (**Figure 33**).

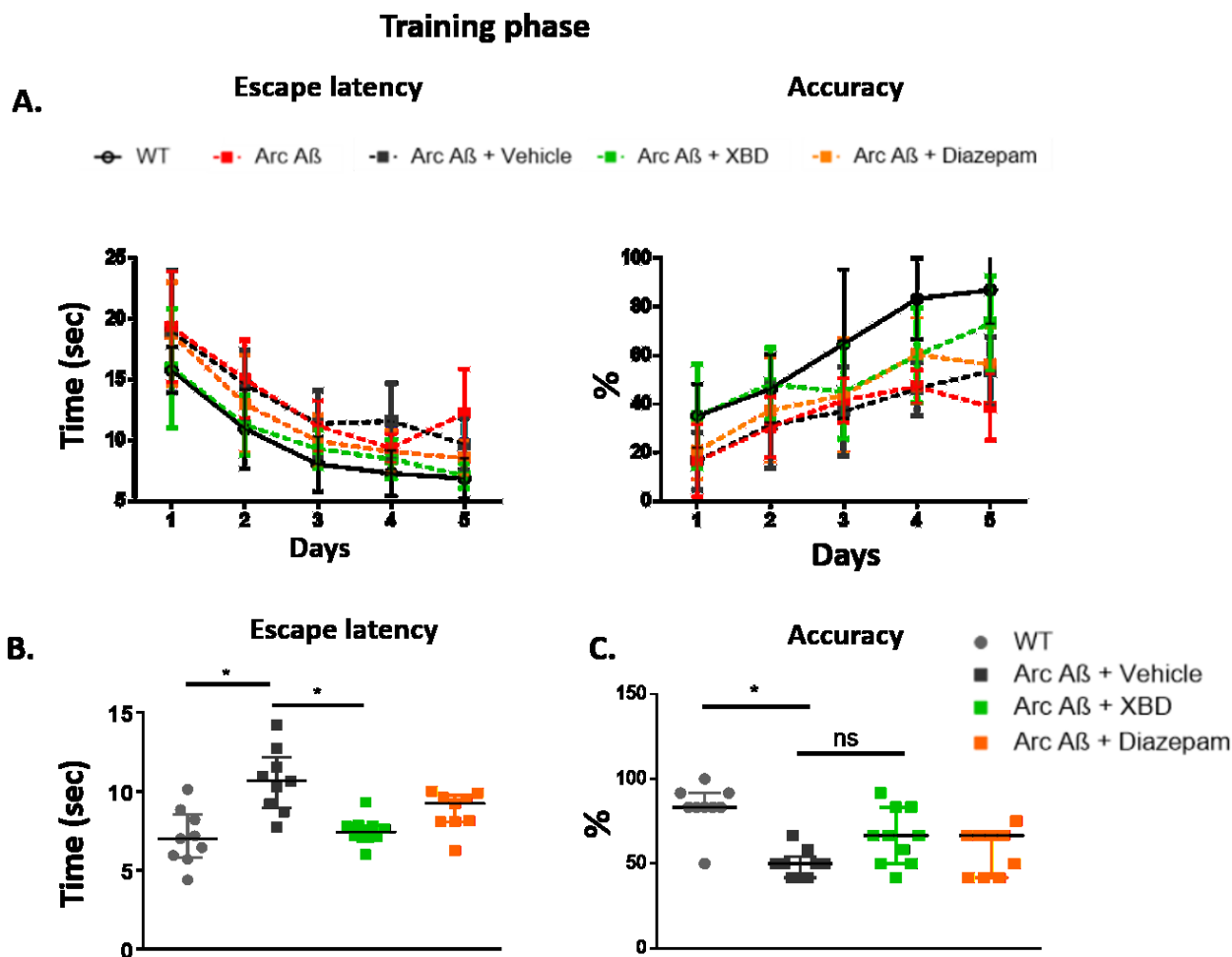


Figure 30: XBD173 chronic treatment rescues spatial learning deficits in transgenic AD mice in the training phase. [Figure adapted and modified from our manuscript submitted relating to this work (Preprint can be found in [354]). Published version [353]]

A. Trajectory of escape latency and accuracy during the 5-day training phase in the WCM. B. Comparison of escape latency and accuracy between the treatment groups in the training phase. WT (n=9), Arc A β + vehicle (n=9), Arc A β + XBD (n=10), and Arc A β + diazepam (n=9; Kruskal–Wallis test with a Dunn’s multiple comparisons *post hoc* test; Arc A β + vehicle: 10.66 (8.948-12.14) s vs WT: 7 (5.825-8.518) s, $p=0.0013$; Arc A β + XBD: 7.420 (7.109-7.816) s vs Arc A β + vehicle, $p=0.0075$; Arc A β + diazepam: 9.320 (8.073-9.758) s). C. Accuracy comparison (Kruskal–Wallis test with a Dunn’s multiple comparisons *post hoc* test; Arc A β + vehicle: 50 (41.67-54.17) % vs WT: 83.33 (83.33-91.67) %, $p=0.0004$; Arc A β + XBD: 66.66 (50-83.33) % vs Arc A β + vehicle, $p=0.1155$; Arc A β + diazepam: 66.66 (41.67-66.67) %). Data are represented as median with their respective interquartile range. * $p < 0.05$. ns: not significant.

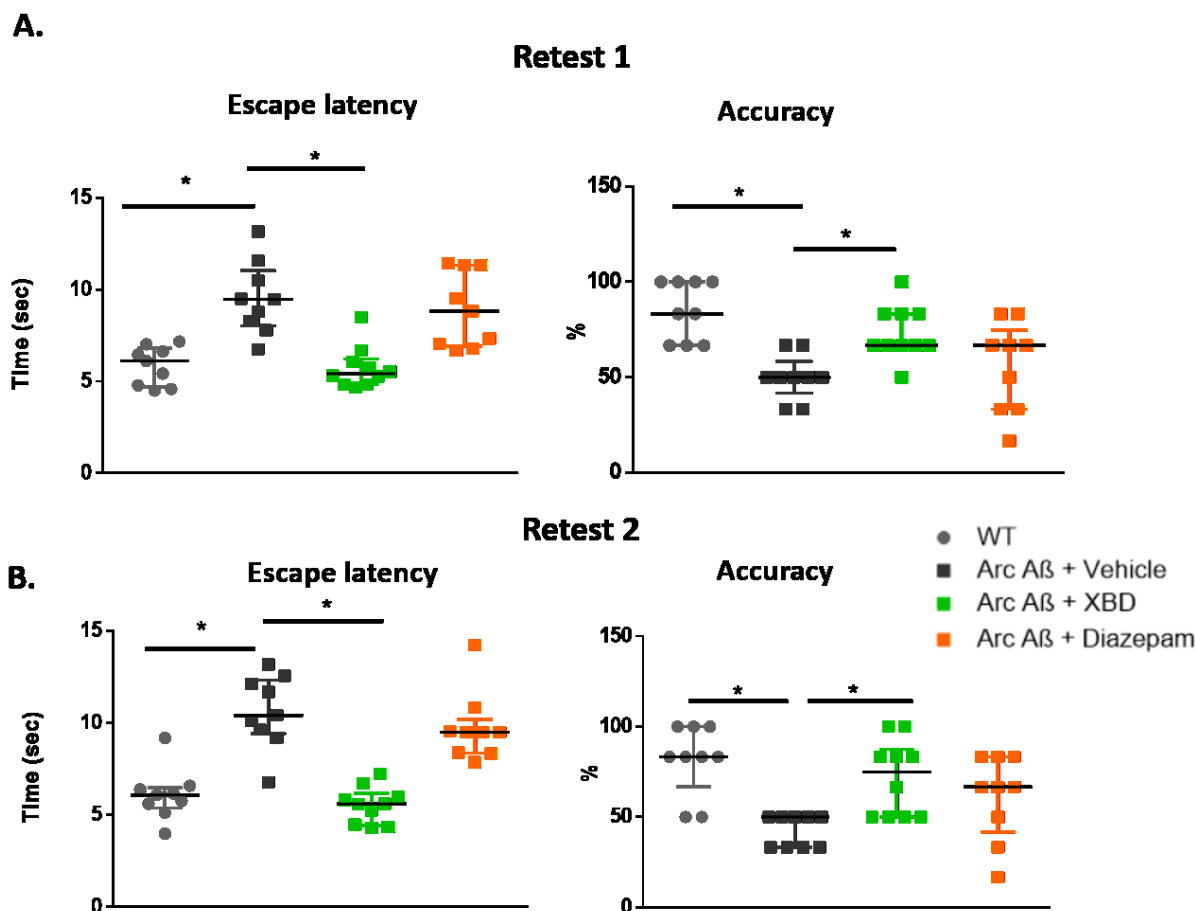


Figure 31: XBD173 chronic treatment rescues spatial learning deficits in transgenic AD mice in both retests. [Figure adapted and modified from our manuscript submitted relating to this work (Preprint can be found in [354]). Published version [353]]

A. Escape latency (Kruskal–Wallis test with a Dunn’s multiple comparisons *post hoc* test; Arc A β + vehicle: 9.477 (8.035-11.05) s vs WT: 6.113 (4.693-6.829) s, $p=0.0018$; Arc A β + diazepam: 8.833 (6.931-11.34) s; Arc A β + vehicle vs Arc A β + XBD: 5.430 (4.844-6.237) s, $p=0.0008$) and accuracy comparison (Arc A β + vehicle: 50 (41.67-58.33) % vs WT: 83.33 (66-100) %, $p=0.0003$; Arc A β + diazepam: 66.66 (33.33-75) %; Arc A β + vehicle vs Arc A β + XBD: 66.66 (50-66.66) %, $p=0.0145$; Kruskal–Wallis test with a Dunn’s multiple comparisons *post hoc* test) between different groups in the Retest 1 phase. WT (n=9), Arc A β + vehicle (n=9), Arc A β + XBD (n=10) and Arc A β + diazepam (n=9). B. Escape latency (Arc A β + vehicle: 10.41 (9.426-12.35) s vs WT: 6.092 (5.375-6.498) s, $p=0.0007$; Arc A β + diazepam: 9.508 (8.363-10.20) s; Arc A β + vehicle vs Arc A β + XBD: 5.608 (4.444-6.166) s, $p<0.0001$; Kruskal–Wallis test with a Dunn’s multiple comparisons *post hoc* test) and accuracy comparison (Arc A β + vehicle: 50 (33.33-50) % vs WT: 83.33 (66.66-100) %, $p=0.0008$; Arc A β + diazepam: 66.66 (41.67-83.33) %; Arc A β + vehicle

vs Arc A β + XBD: 75 (50-87.5) %, $p=0.0102$; Kruskal–Wallis test with a Dunn’s multiple comparisons *post hoc* test) between the different groups in the Retest 2 phase. WT (n=9), Arc A β + vehicle (n=9), Arc A β + XBD (n=10) and Arc A β + diazepam (n=9). Data are represented as median with their respective interquartile range. * $p < 0.05$. ns: not significant.

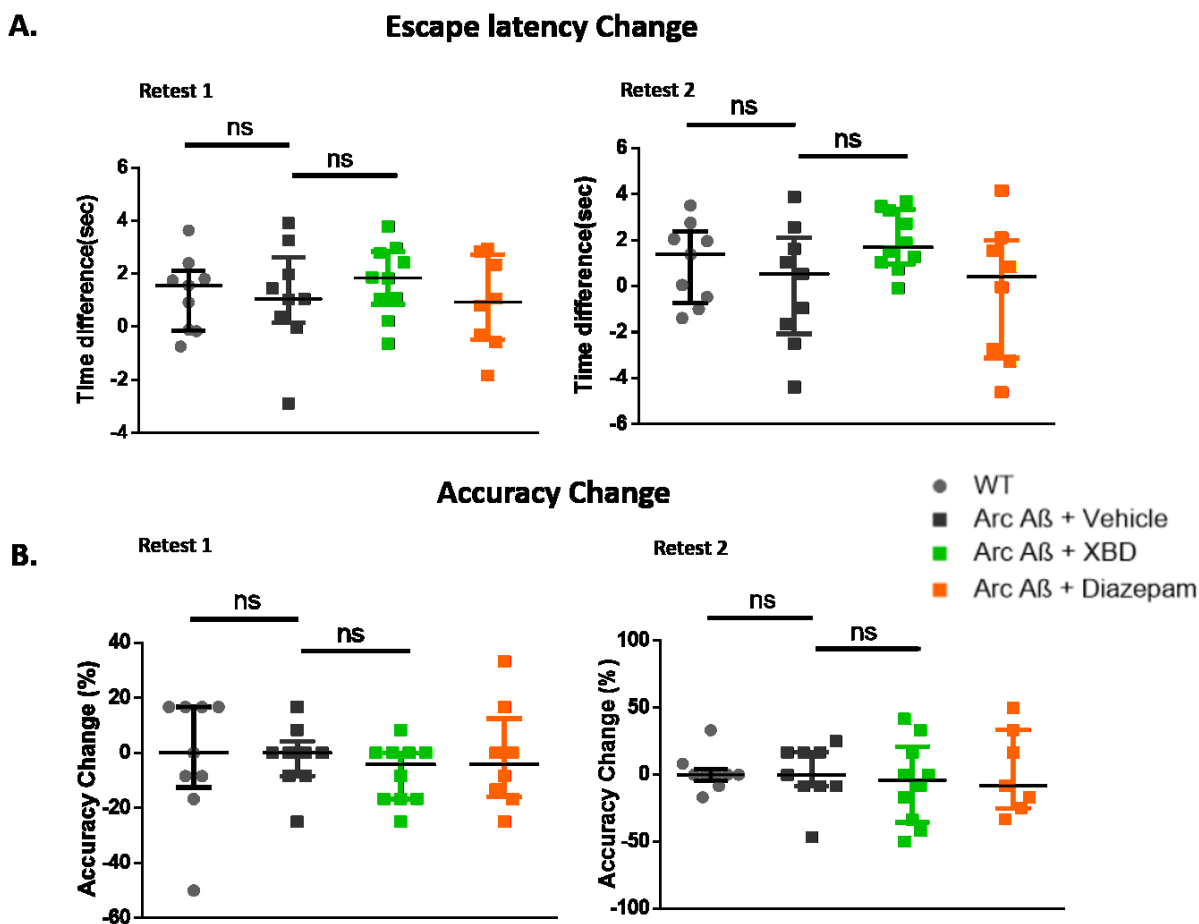


Figure 32: XBD173 or vehicle treatment affects the individual animals uniformly. [Figure adapted and modified from our manuscript submitted relating to this work (Preprint can be found in [354]). Published version [353]]

A. Comparison of escape latency change for the different chronic treatment groups in Retest 1 and 2 from the training phase. WT (n=9), Arc A β + XBD (n=10), Arc A β + Vehicle (n=9), and Arc A β + Diazepam (n=8). B. Comparison of accuracy change for the different chronic treatment groups in Retest 1 and 2 from the training phase.

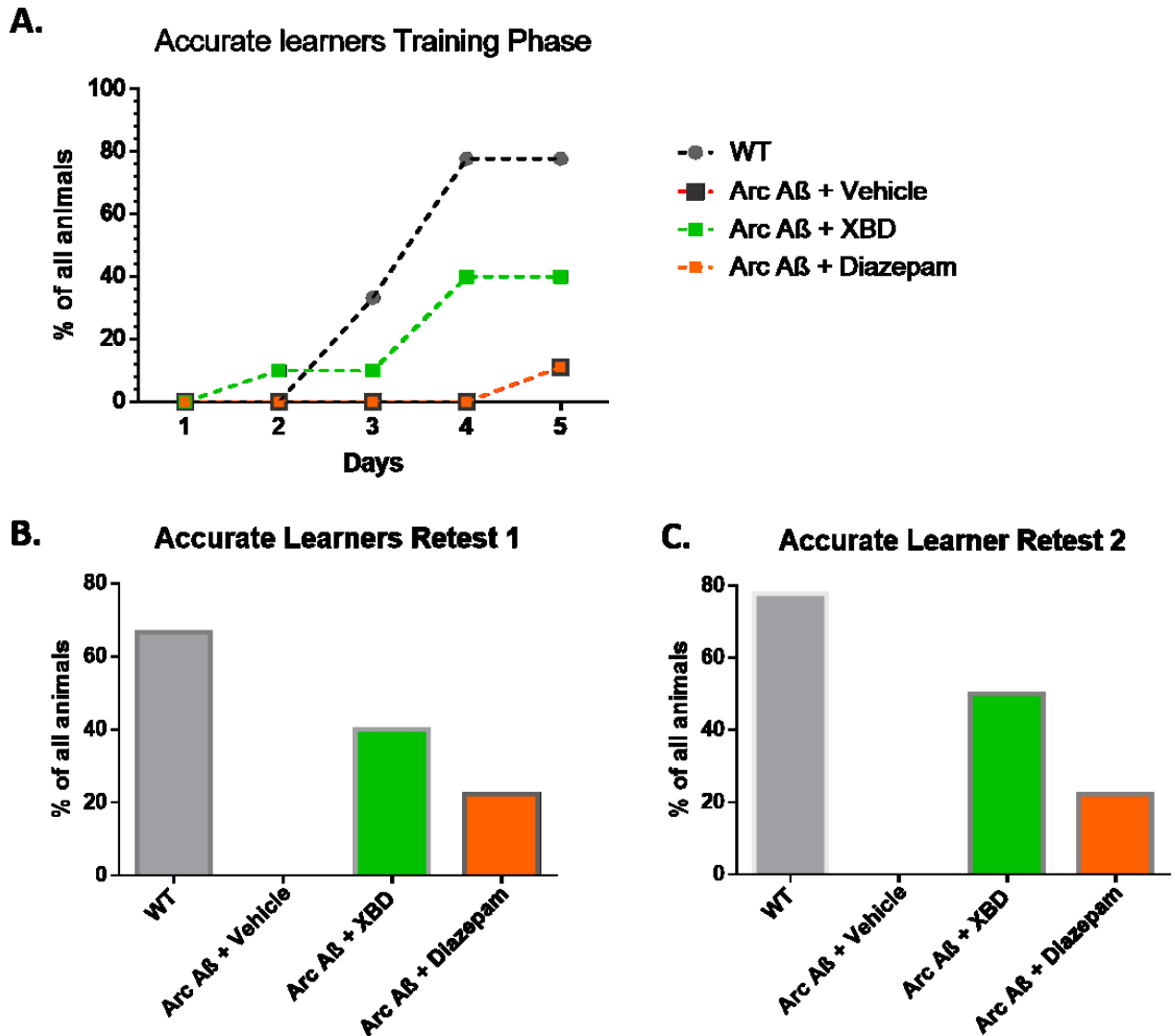


Figure 33: Transgenic AD mice have a lower percentage of accurate learners whereas chronic XBD173 treatment improves the percentage of accurate learners. [Figure adapted and modified from our manuscript submitted relating to this work (Preprint can be found in [354]). Published version [353]]

A. Accurate learner comparison for different treatment groups during the training phase. B. Bar plot showing Accurate learners in Retest 1. C. Bar plot showing Accurate learners in Retest 2

3.6 TSPO is required for the alleviation of cognitive impairment in chronic XBD173 treated ArcA β mice

As discussed previously, in ex vivo setup TSPO is required for the XBD173 mediated rescue of LTP impairment resulting from the A β ₁₋₄₂ oligomers, we asked therefore if the role of chronic XBD173 treatment in preventing spatial learning impairment in transgenic AD mice is also dependent on the mitochondrial TSPO protein. To address this question, we crossbred the ArcA β line with homozygous TSPOKO animals. Unfortunately, however, the homozygous transgenic line of TSPOKO X ArcA β mice showed behavioral deficits in the form of epileptic seizures in one-third of the mice line. The seizure percentage was higher and for a longer duration whenever there was a cage change. This line was therefore not suitable to undergo behavioral testing to avoid additional stress and bias resulting from seizure in cognitive testing. We, therefore, used the heterozygous TSPOKO X ArcA β line (hetTSPOKO X ArcA β) mice line which had no behavioral abnormality. This difference in behavioral saliences could be attributed to the increasing mutational burden of 2 separate transgenic lines.

Training Phase

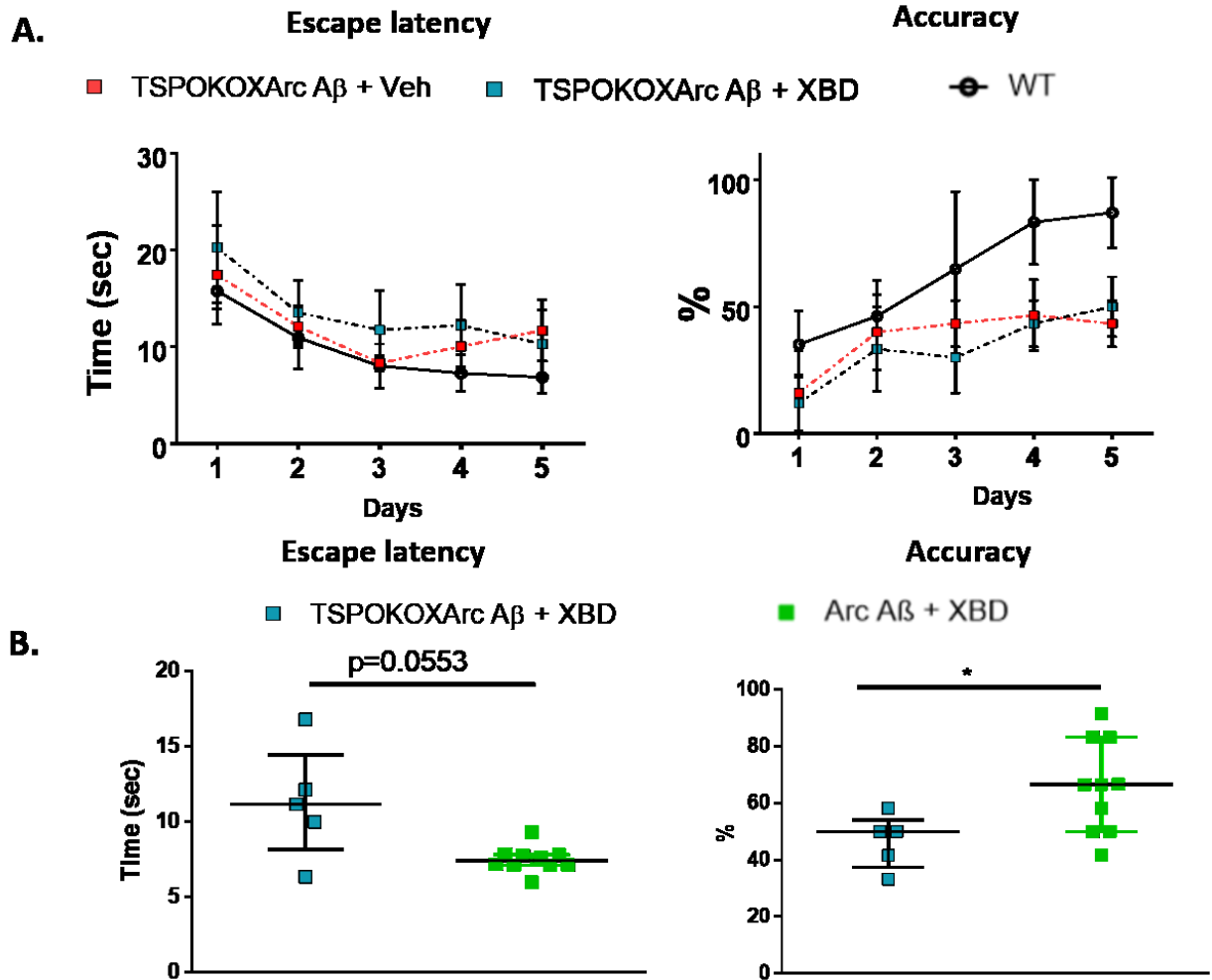


Figure 34: XBD173 treatment is dependent upon TSPO to confer beneficial effects in spatial learning tests. [Figure adapted and modified from our manuscript submitted relating to this work (Preprint can be found in [354]). Published version [353]]

A. Trajectory of escape latency and accuracy during the 5-day training phase in the WCM. hetTSPOKO X Arc A β + XBD (n=5) and hetTSPOKO X Arc A β + Veh (n=5). B. Escape latency (Arc A β + XBD: 7.420 (7.109-7.816) s vs hetTSPOKO X Arc A β + XBD: 11.16 (8.168-14.46) s, $p=0.0553$ Mann-Whitney U test) and accuracy comparison (Arc A β + XBD: 66.66 (50.00-83.33) % vs hetTSPOKO X Arc A β + XBD: 50.00 (37.50-54.17) %; Mann-Whitney U test, $p=0.0296$) between the different treatment groups in the training phase. Arc A β + XBD (n=10), and hetTSPOKO X Arc A β + XBD (n=5) groups. Data are represented as median with their respective interquartile range. * $p < 0.05$. ns: not significant.

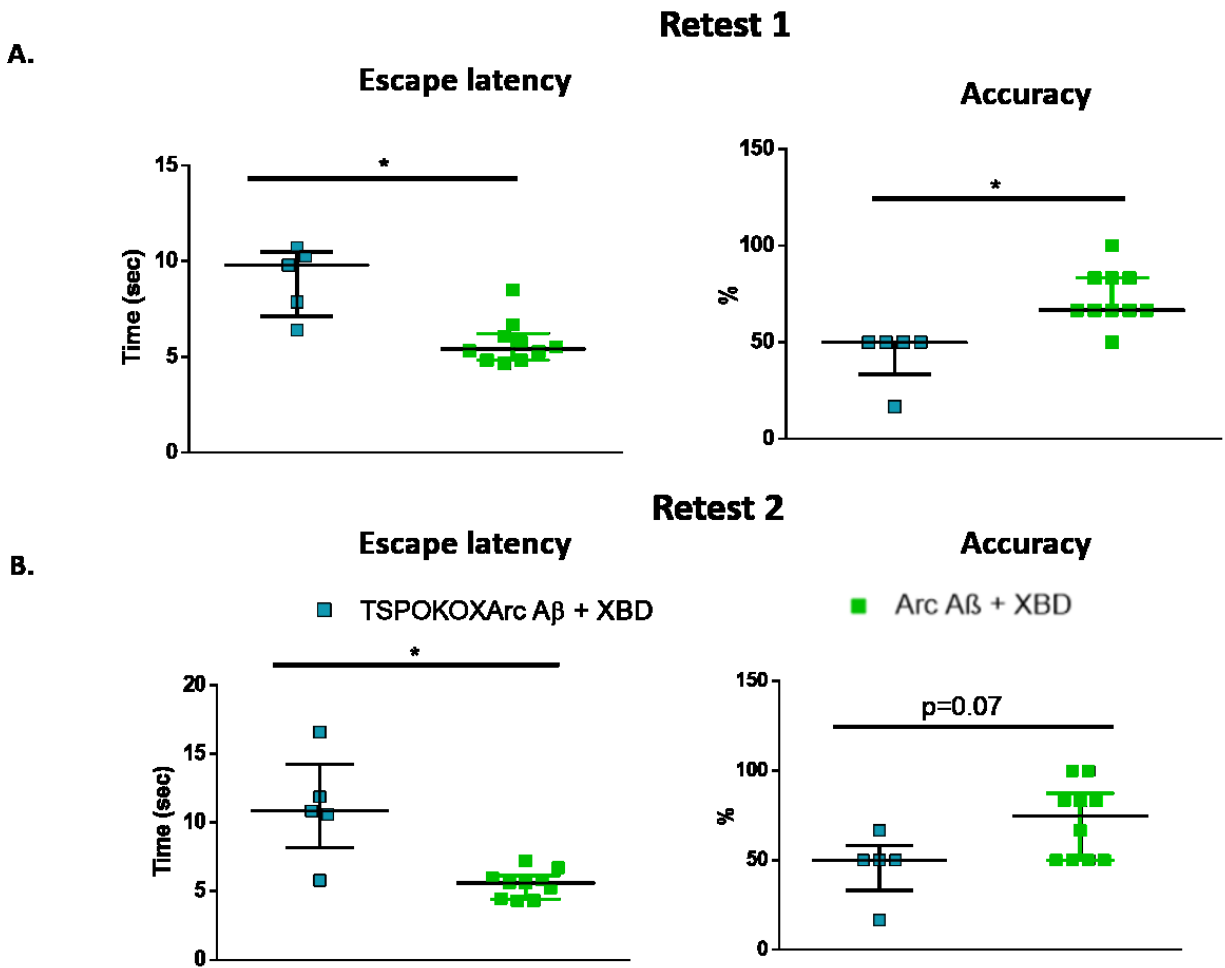


Figure 35: TSPO heterozygous expression impacts the effect of XBD173 on the spatial learning of ArcA β transgenic animals in Retests. [Figure adapted and modified from our manuscript submitted relating to this work (Preprint can be found in [354]). Published version [353]]

A. Escape latency (Arc A β + XBD: 5.430 (4.844-6.237) vs hetTSPOKO X Arc A β + XBD: 9.800 (7.138-10.50) s, $p=0.0047$; Mann–Whitney U test) and accuracy comparison (Arc A β + XBD: 66.66 (50-66.66) % vs hetTSPOKO X Arc A β + XBD: 50.00 (33.33-50) %, $p=0.0033$; Mann–Whitney U test) between the different treatment groups in the Retest 1 phase. B. Escape latency (Arc A β + XBD: 5.608 (4.444-6.166) s vs hetTSPOKO X Arc A β + XBD: 10.86 (8.2-14.24) s, $p=0.008$; Mann–Whitney U test) and accuracy comparison (Arc A β + XBD: 75 (50-87.5) % vs hetTSPOKO X Arc A β + XBD: 50.00 (33.33-58.33) %, $p=0.07$; Mann–Whitney U test) between the different groups in the Retest 2 phase. Data are represented as median with their respective interquartile range. * $p < 0.05$. ns: not significant.

The ArcA β animals treated with XBD173 showed significantly better cognitive results compared to the hetTSPOKO X ArcA β animals treated with either XBD173 or vehicle (**Figure 34, Figure 35**). The hetTSPOKO X ArcA β animals had delayed response times and lower accuracy levels than the WT animals as well as the transgenic ArcA β mice which were chronically treated with XBD173 (**Figure 34, Figure 35**). The XBD173-treated hetTSPOKO X ArcA β animals did not demonstrate any significant improvement in cognitive ability when compared to the vehicle-treated group, as seen by their escape latency and accuracy parameters in both the training phase and retests (**Figure 36**). This data unequivocally shows that XBD173 has a neuroprotective effect in improving spatial learning in the AD mice model, relying on the TSPO protein.

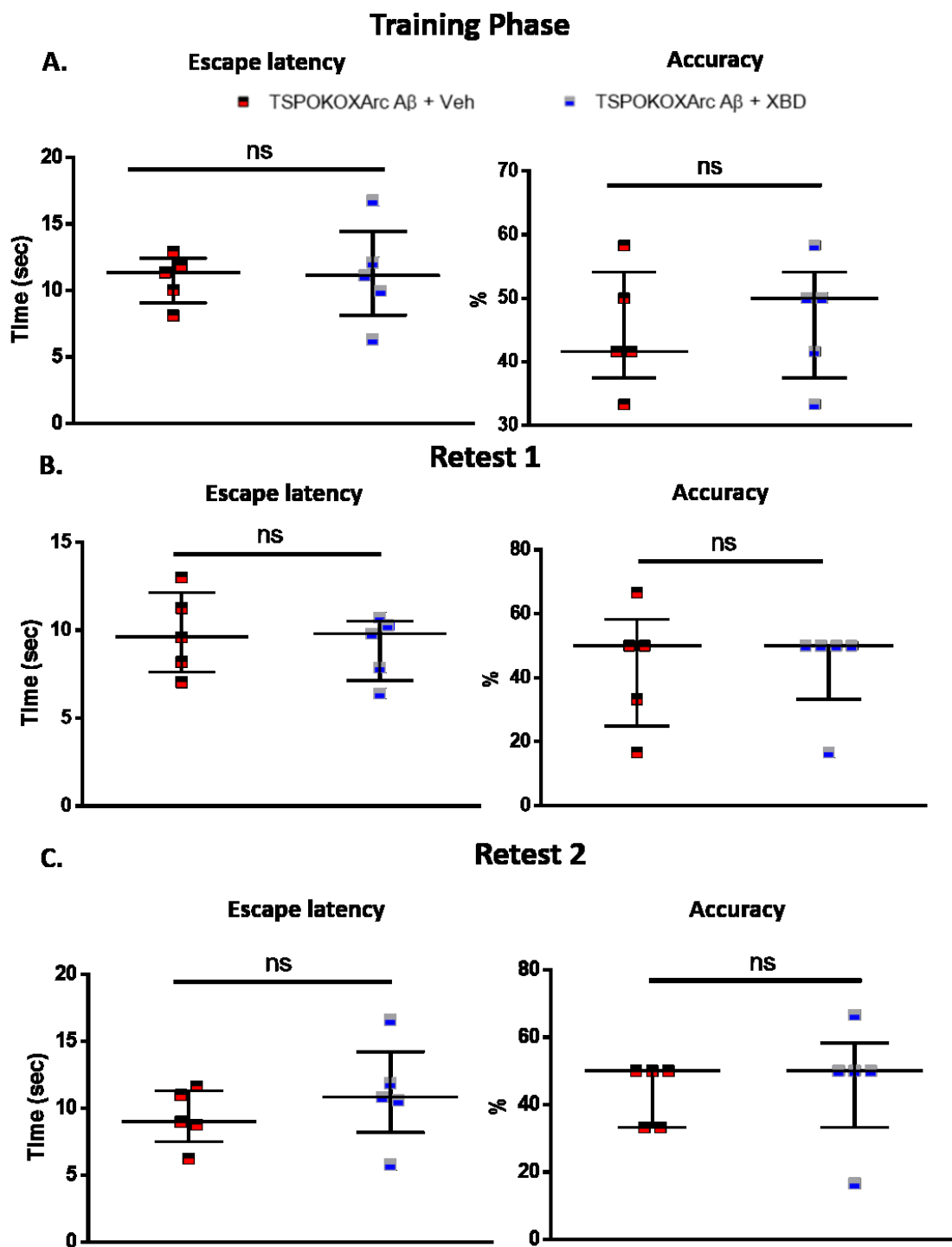


Figure 36: XBD173-mediated cognitive improvement is dependent upon TSPO. [Figure adapted and modified from our manuscript submitted relating to this work (Preprint can be found in [354]). Published version [353]]

A. Escape latency (hetTSPOKO X Arc A β + Veh: 11.40 (9.097-12.43) s vs hetTSPOKO X Arc A β + XBD: 11.16 (8.168-14.46) s, $p=0.944$; Mann–Whitney U test) and accuracy comparison (hetTSPOKO X Arc A β + Veh (n=5): 41.67 (37.50-54.17) % vs hetTSPOKO X Arc A β + XBD: 50.00 (37.50-54.17) %, $p=0.904$; Mann–Whitney U test) between the different treatment groups in the training phase. hetTSPOKO X Arc A β + Veh (n=5), and hetTSPOKO X Arc A β + XBD (n=5) groups. B. Escape latency (hetTSPOKO X Arc A β + Veh: 9.600 (7.62-12.13) s vs hetTSPOKO X Arc A β + XBD: 9.800 (7.138-10.50) s, $p=0.66$; Mann–Whitney U test) and accuracy comparison (hetTSPOKO X Arc A β + Veh: 50.00 (25.00-58.33) % vs hetTSPOKO X Arc A β + XBD: 50.00 (33.33-50) %, $p>0.99$; Mann–Whitney U test) between the different treatment groups in the Retest 1 phase. C. Escape latency (hetTSPOKO X Arc A β + Veh: 9 (7.528-11.33) s vs hetTSPOKO X Arc A β + XBD: 10.86 (8.2-14.24) s, $p=0.53$, Mann–Whitney U test) and accuracy comparison (hetTSPOKO X Arc A β + Veh: 50 (33.33-50) % vs hetTSPOKO X Arc A β + XBD: 50.00 (33.33-58.33) %, $p=0.64$; Mann–Whitney U test) between the different treatment groups in the Retest 2 phase. Data are represented as median with their respective interquartile range. * $p<0.05$. ns: not significant.

3.7 Chronic Administration of XBD173 reduces the pathogenic amyloid load and rescues the spine loss in ArcA β mice model

We looked at the effects of chronic XBD173 treatment on AD pathology by comparing different pathophysiological measures. After staining with congo derivative methoxy-04, we investigated the plaque load in the cortex and hippocampus of the XBD173-treated transgenic mice and compared them to the vehicle-treated counterparts (**Figure 37 A**). The mice treated with XBD173 showed a reduction in plaque load and plaque count in the cortex rather than the hippocampus (**Figure 37 B-E**). While amyloid plaques themselves might not contribute to neurotoxicity, they are known to sequester soluble A β and are also known to affect the functionalities of the glial cells. Reduction in the plaque load in the cortex of XBD173-treated animals could therefore directly correlate with reduced pathogenicity after the treatment. In the hippocampus, however, we observed only a small fragment of the hippocampal area being covered with the amyloid plaques in the transgenic ArcA β mice model. This could be one of the reasons for not having clear differences in the plaque load in the hippocampus of XBD173-treated animals to the vehicle-treated animals.

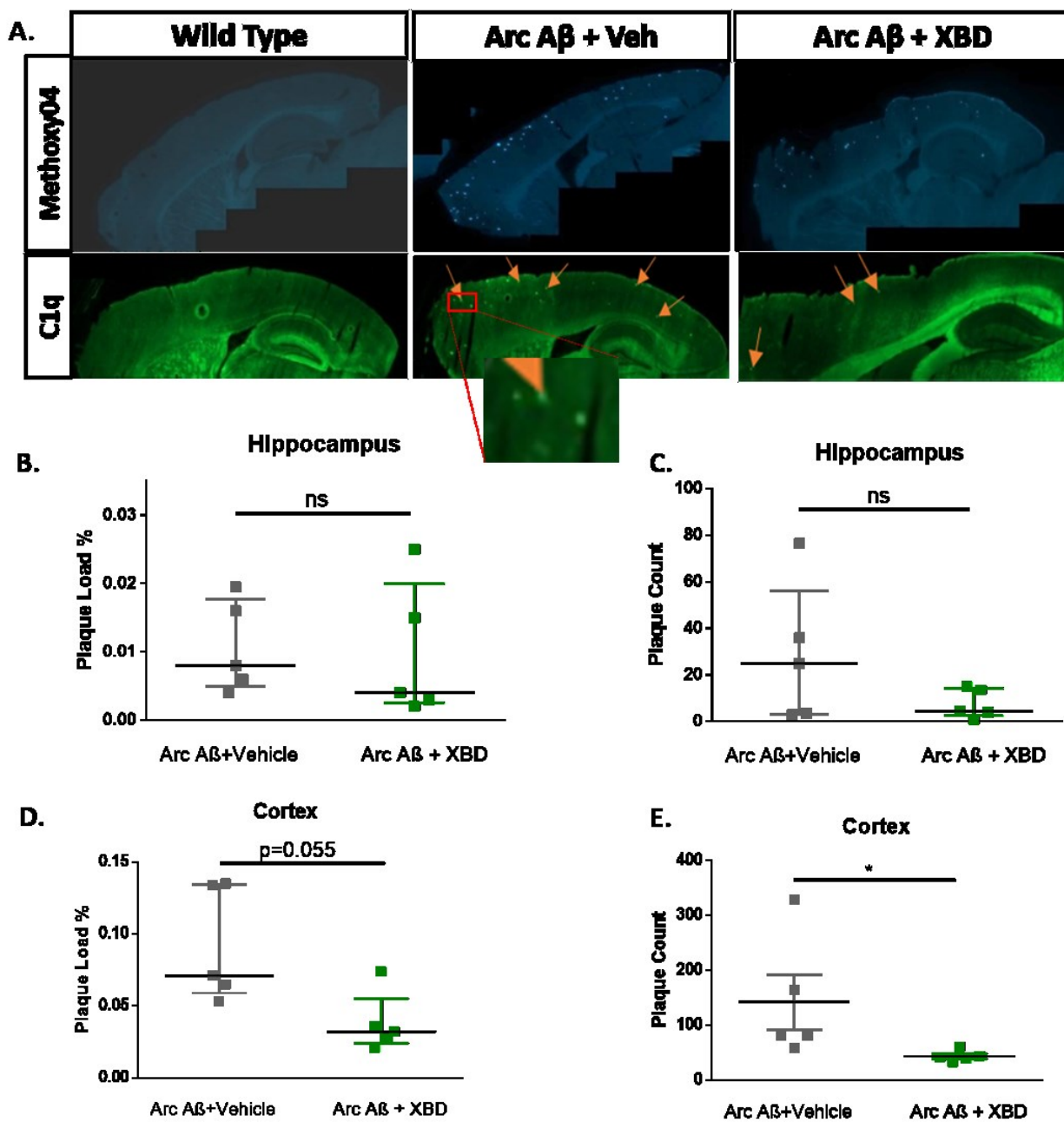


Figure 37: XBD173 chronic treatment reduces the cortex plaque load in the transgenic Arc A β mice model of AD. [Figure adapted and modified from our manuscript submitted relating to this work (Preprint can be found in [354]). Published version [353]]

A. Amyloid plaque staining (First row) and C1q aggregates staining (second row) in WT, Arc A β + vehicle, Arc A β + XBD groups. An enlarged view of C1q aggregates at 63X magnification is shown in Figure 45. B. Comparison of plaque load % between Arc A β + XBD (n=5) and Arc A β + vehicle (n=5) in the hippocampus (Arc A β + XBD: 0.0040 (0.0025-0.0200) % vs Arc A β + vehicle: 0.0080 (0.0050-0.01775) %, $p=0.4524$; Mann–Whitney U test). C. Comparison of plaque count between Arc A β + XBD (n=5) and Arc A β + vehicle (n=5) in the hippocampus (Arc A β + XBD: 4.5 (2.5-14.30) vs Arc A β + vehicle: 25 (3.25-56.25) vs, $p=0.4127$; Mann–Whitney U test). D. Comparison of plaque load between Arc A β + vehicle (n=5) and Arc A β + XBD (n=5) in the cortex (Arc A β + XBD: 0.0320 (0.0240-0.0550) % vs Arc A β + vehicle: 0.0710 (0.0590-0.1345) %, $p=0.055$; Mann–Whitney U test). E. Comparison of plaque count between Arc A β + vehicle (n=5) and Arc A β + XBD (n=5) in the cortex (Arc A β + XBD: 41 (36.15-52.50) vs Arc A β + vehicle: 81.00 (69.50-246.3) vs, $p=0.0159$; Mann–Whitney U test). Data are represented as median with their respective interquartile range. * $p < 0.05$. ns: not significant.

Soluble A β has been considered more neurotoxic compared to amyloid plaques [368,369]. Previously, a reduction in soluble A β levels has been associated with reduced pathophysiology of AD. Owing to the improvement in cognitive behavior of XBD173-treated AD mice, we assessed the soluble A β levels (A β_{1-42}) in the cortex and hippocampus of the mice treated with XBD173. The ArcA β mutation which causes the hemizygous overexpression of APP leads to a substantial increase in the soluble A β levels. Interestingly enough, consistent with the plaque load analysis, only the cortex of the XBD173-treated mice showed a clear reduction of soluble A β levels (**Figure 46 B, C**). Reduction of spines has long been associated with cognitive impairments in AD, both in humans as well as rodent AD models. Our next step, therefore, was to quantify the spine by the Golgi-cox staining method to see if the improvement in spatial learning is related to better structural plasticity and maintenance of the dendritic spines. We were able to show that chronic XBD173 treatment rescues the loss of spines in transgenic AD mice (**Figure 38**). This reduction in plaque load, soluble A β levels as well as improvement in the spine density directly contributes to the significant reduction of pathophysiology in the XBD173 treated ArcA β mice model.

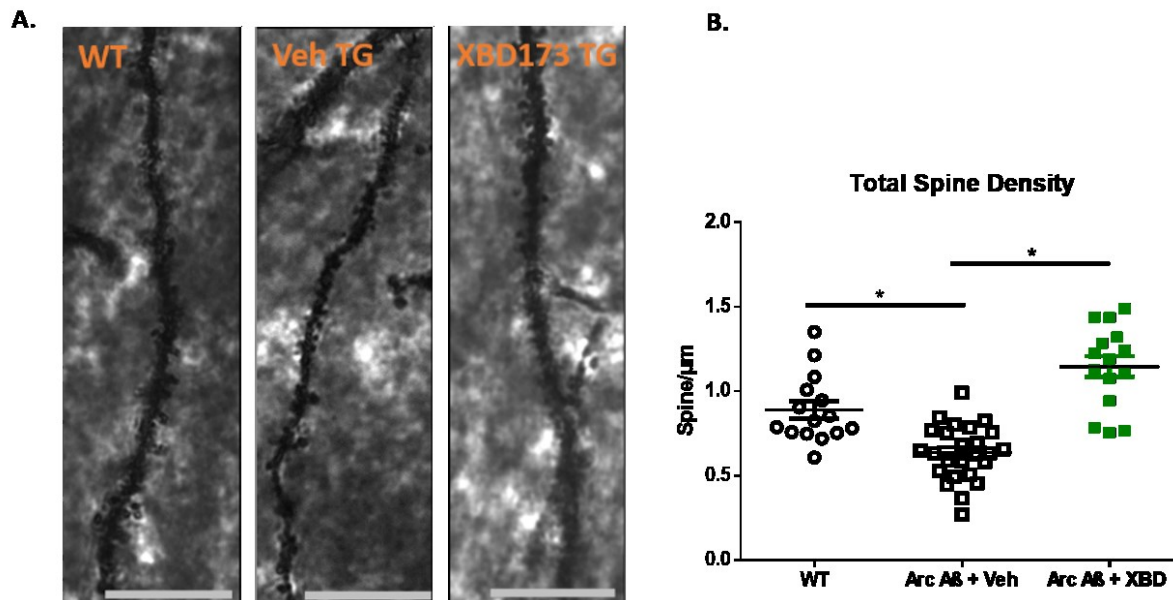


Figure 38: Golgi Cox-stained apical dendrites show prevention in dendritic spine loss after chronic XBD173 administration in Arc A β mice. [Figure adapted and modified from our manuscript submitted relating to this work (Preprint can be found in [354]). Published version [353]]

A. Apical dendrites Golgi-Cox stained for WT, Arc A β + vehicle, and Arc A β + XBD groups respectively.

B. Total spine density quantification from $n=15-25$ dendrites obtained from $n=3-4$ mice per group (Arc A β + vehicle: 0.6329 (0.5177-0.7629) spines/ μm vs WT: 0.8244 (0.7545-1.008) spines/ μm , $p=0.0005$; Arc A β + XBD: 1.190 (0.9424-1.320) spines/ μm vs Arc A β + vehicle, $p<0.0001$; one-way ANOVA with a Bonferroni's multiple comparisons *post hoc* test). Data are represented as median with their respective interquartile range. * $p < 0.05$. ns: not significant.

3.8 Chronic Administration of XBD173 increases neurosteroid levels in transgenic AD mice.

Given the potential role of TSPO in neurosteroidogenesis, the neurosteroid levels in different treatment groups were analyzed. GC-MS/MS analysis of XBD173 treated brains suggested an increase in several neurosteroid levels such as allopregnanolone ($3\alpha,5\alpha$ -THP), $3\beta,5\alpha$ -THDOC, and 5α DHDOC in the cortex and hippocampus (**Figure 39 A-D**). It is possible therefore that XBD173-mediated cognitive betterment is carried out by a reduction in plaque load, soluble A β levels, increased neurosteroidogenesis, and preservation of dendritic spines.

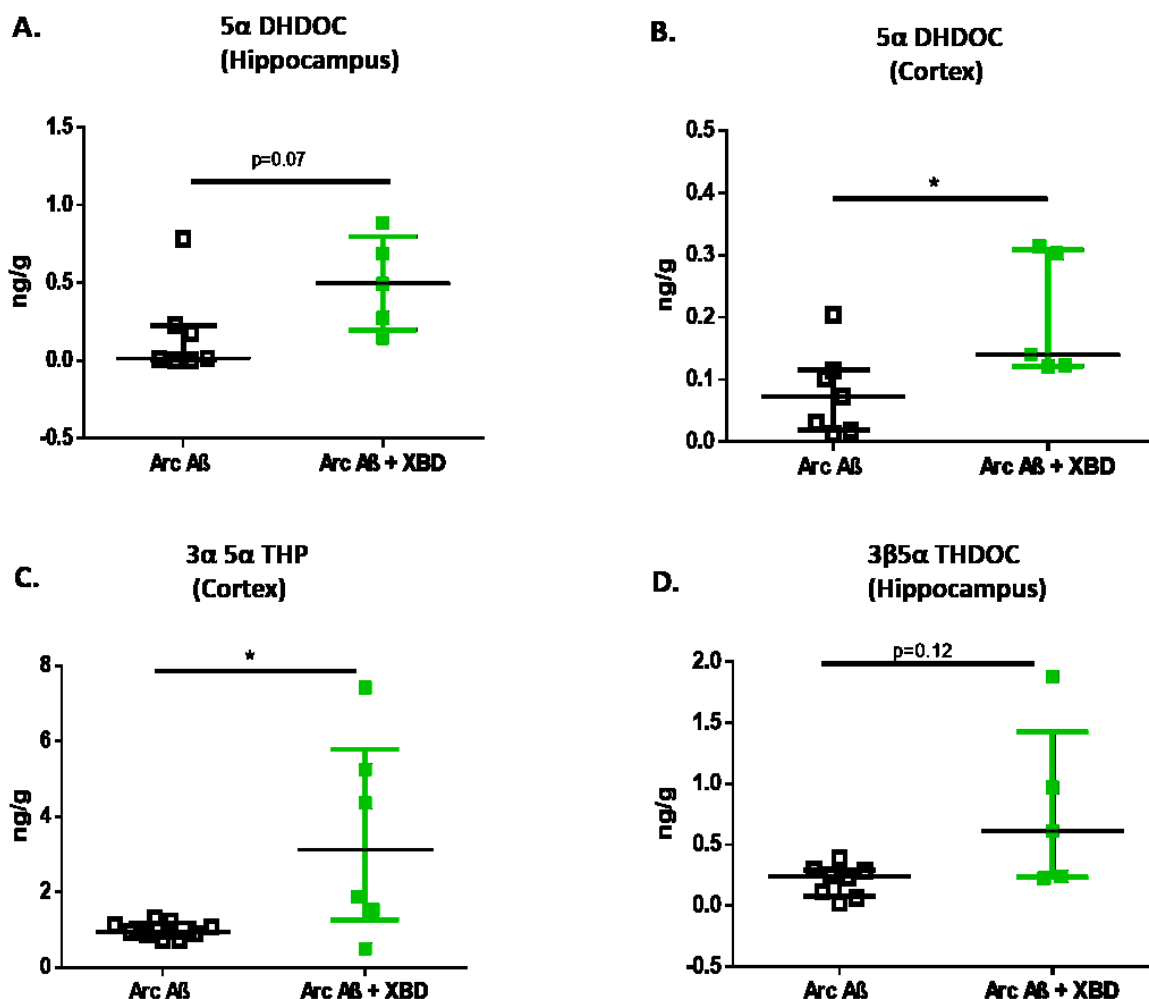


Figure 39: Chronic XBD173 administration results in an elevation of neurosteroid levels in Arc A β mice. [Figure adapted and modified from our manuscript submitted relating to this work (Preprint can be found in [354]). Published version [353]]

A. GC-MS/MS quantification of 5 α DHDOC levels in the hippocampus for Arc A β + vehicle (n=7) and Arc A β + XBD (n=5) (Arc A β + XBD: 0.4940 (0.2115-0.7860) ng/g vs Arc A β + vehicle: 0.0150 (0.0060-0.2270) ng/g, $p=0.07$; Mann–Whitney U test). B. GC-MS/MS quantification of 5 α DHDOC levels in the cortex for Arc A β + vehicle (n=7) and Arc A β + XBD (n=5) (Arc A β + XBD: 0.1400 (0.1220-0.3085) ng/g vs Arc A β + vehicle: 0.0730 (0.0190-0.1150) ng/g, $p=0.0177$; Mann–Whitney U test). C. GC-MS/MS quantification of 3 α ,5 α -THP levels in the cortex for Arc A β + vehicle (n=9) and Arc A β + XBD (n=6) (Arc A β + XBD: 3.127 (1.273-5.791) ng/g vs Arc A β + vehicle: 0.9490 (0.8125-1.188) ng/g, $p=0.036$; Mann–Whitney U test). D. GC-MS/MS quantification of 3 β ,5 α -THDOC levels in the hippocampus for Arc A β + vehicle (n=8) and Arc A β + XBD (n=5) (Arc A β + XBD: 0.6130 (0.2350-1.427) ng/g vs Arc A β + vehicle:

0.2415 (0.076-0.2955) ng/g, $p=0.12$; Mann–Whitney U test). Data are represented as median with their respective interquartile range. * $p < 0.05$. ns: not significant.

3.9 Ex vivo XBD173 treatment does not affect the microglial polarization states which are altered via A β ₁₋₄₂ oligomers

Microglial polarization states as discussed earlier play a crucial role in maintaining the homeostasis of the neural environment in the CNS. The importance of the M2 microglial state in the activation of anti-inflammatory factors has previously been implicated in neuronal repair and neuroprotection [31,32,370]. A shift in the polarization state from M2 to M1 resulting in the subsequent increase of the pro-inflammatory state is seen in several clinical as well as rodent models of AD [31,32]. We asked therefore if this shift in microglial polarization occurs after the *ex vivo* addition of A β ₁₋₄₂ oligomers and if preincubation with XBD173 could reverse the polarisation state from M1 to M2 thereby providing protection *ex vivo*. We observed that in general, there is an inclination for the mean fluorescence intensity (MFI) of various microglial markers (CX3CR1 and TMEM119) to increase after being exposed to A β ₁₋₄₂ oligomers, however, a marked increase in MFI is only detectable in the P2RY12 microglia marker (**Figure 40 C, D, E**). CX3CR1, a chemokine receptor that is expressed on the microglial surface and binds to CX3CL1, is known to regulate microglial recruitment to neuroinflammation sites and has often been seen to have an increased expression in case of AD [371–374]. The P2RY12 receptors are specific purinoreceptors expressed on microglia in the central nervous system [375]. An increase in the microglial marker P2RY12 and CX3CR1 after A β ₁₋₄₂ oligomers incubation indicates an increase in reactive microgliosis. We did not observe any changes after preincubation with XBD173. Using the respective M1 (CD80) and M2 (CD163) markers, we quantified microglial polarization states. The percentage of both M1 and M2 microglial polarization markers increased following subsequent treatment with A β ₁₋₄₂ oligomers (**Figure 40 A, B**). The preincubation with XBD173 does not affect the M1 and M2 levels (**Figure 40 A, B**). Taken together this suggests that *ex vivo* XBD173 treatment does not affect or influence the microglial polarization state after the addition of A β ₁₋₄₂ oligomers.

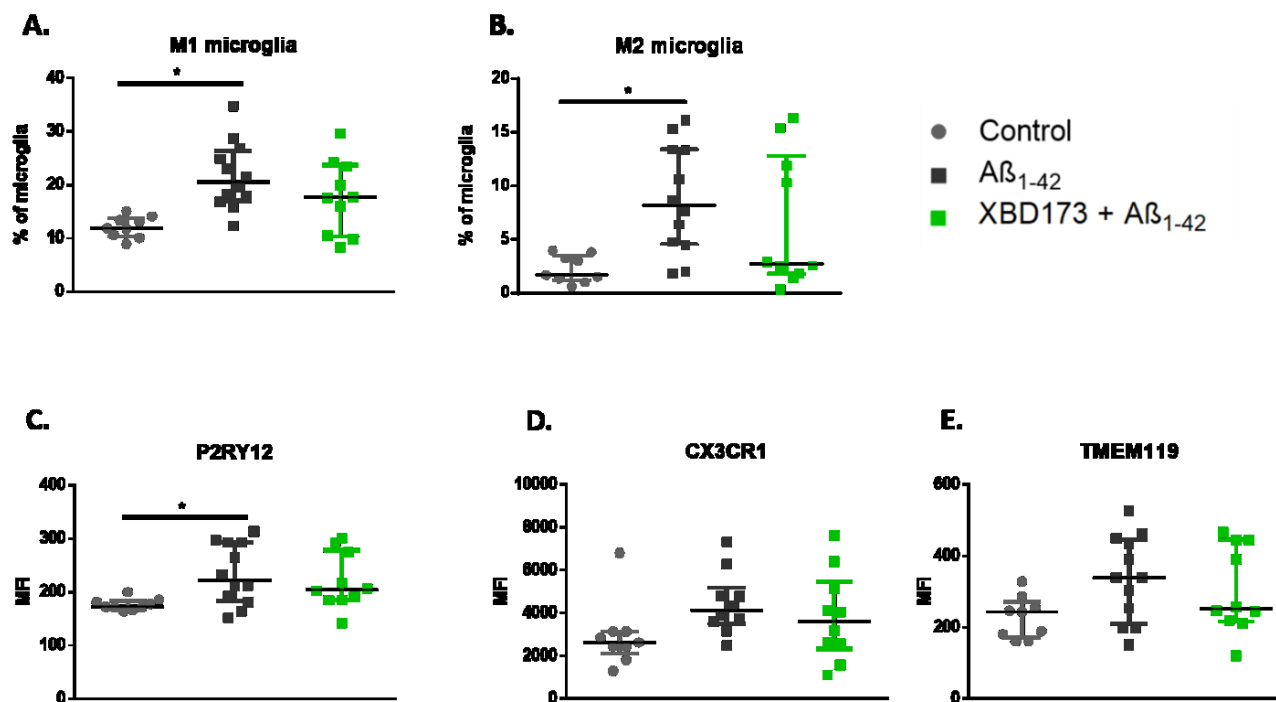


Figure 40: In ex vivo slice experiments, XBD173 has no effect on microglial polarization altered by $A\beta_{1-42}$ oligomers. [Figure adapted and modified from our manuscript submitted relating to this work (Preprint can be found in [354]). Published version [353]]

A. M1 microglia % comparison in the different treatment groups. Control (n=9), $A\beta_{1-42}$ (n=12) and XBD173 + $A\beta_{1-42}$ (n=10) ($A\beta_{1-42}$: 20.55 (17.08-26.4) %, vs Control: 11.9 (10.35-13.75) %, $p=0.0013$; $A\beta_{1-42}$ vs XBD173 + $A\beta_{1-42}$: 17.70 (10.35-23.68) %, $p=0.3081$; Kruskal–Wallis test with a Dunn’s multiple comparisons *post hoc* test). B. M2 microglia % comparison in the different treatment groups. Control (n=9), $A\beta_{1-42}$ (n=12) and XBD173 + $A\beta_{1-42}$ (n=10) ($A\beta_{1-42}$: 8.110 (4.55-13.38) %, $p=0.0068$ vs Control: 1.660 (1.155-3.495) %; $A\beta_{1-42}$ vs XBD173 + $A\beta_{1-42}$: 2.705 (1.740-12.78) %, $p=0.3662$; Kruskal–Wallis test with a Dunn’s multiple comparisons *post hoc* test). Mean fluorescence intensities (MFI) analyzed for P2RY12 ($A\beta_{1-42}$: 222.5 (183.8-293) vs Control: 173 (168.5-183.5), $p=0.0162$; $A\beta_{1-42}$ vs XBD173 + $A\beta_{1-42}$: 204.5 (185-278.8), $p>0.99$; Kruskal–Wallis test with a Dunn’s multiple comparisons *post hoc* test). (C), CX3CR1 (D), and TMEM119 (E) for different treatment groups. Data are represented as median with their respective interquartile range. * $p < 0.05$. ns: not significant.

3.10 XBD173 chronic treatment primarily affects and reduces abnormal astrocytic phagocytosis and synaptic pruning in AD mice

TSPO expression occurs both in glial and neural cells and previous studies have shown that the upregulation of TSPO expression in the astrocytic cells in the hippocampus occurs much before the microglial cells. From a therapeutic point of view, therefore astrocytes can be considered an essential target while focusing on the TSPO-dependent mechanism. Astrocytes participate actively in the process of pruning synapses during the developmental phase. This pruning of synapses however is abnormally increased during the pathogenesis of AD. Previously excessive removal of functional neurons in AD has been thought to be an active contributor to the cognitive decline in AD patients. In line with this hypothesis, we asked if excessive pruning of astrocytes in AD transgenic mice could be an active factor contributing to impaired spatial learning and if chronic XBD173 treatment could reduce this abnormally increased astrocytic pruning. As discussed in detail in the methods section, we analyzed individual high-resolution astrocytes and quantified the percentage of synaptophysin (pre-synaptic marker) inside the volume of these astrocytes (**Figure 41**). It is important to note that the intensity of synaptophysin was comparable in treatment as well as control groups. Compared to the wild-type control we observed the transgenic AD mice had a higher percentage of astrocytic engulfment of synaptic markers. Additionally, we noticed that long-term XBD173 treatment drastically reduces the increased synaptic uptake by astrocytes in both the cortex and hippocampus (**Figure 42**). This suggests that chronic XBD173 treatment reduces the abnormal removal of synapses which could directly improve the cognitive performance of these mice.

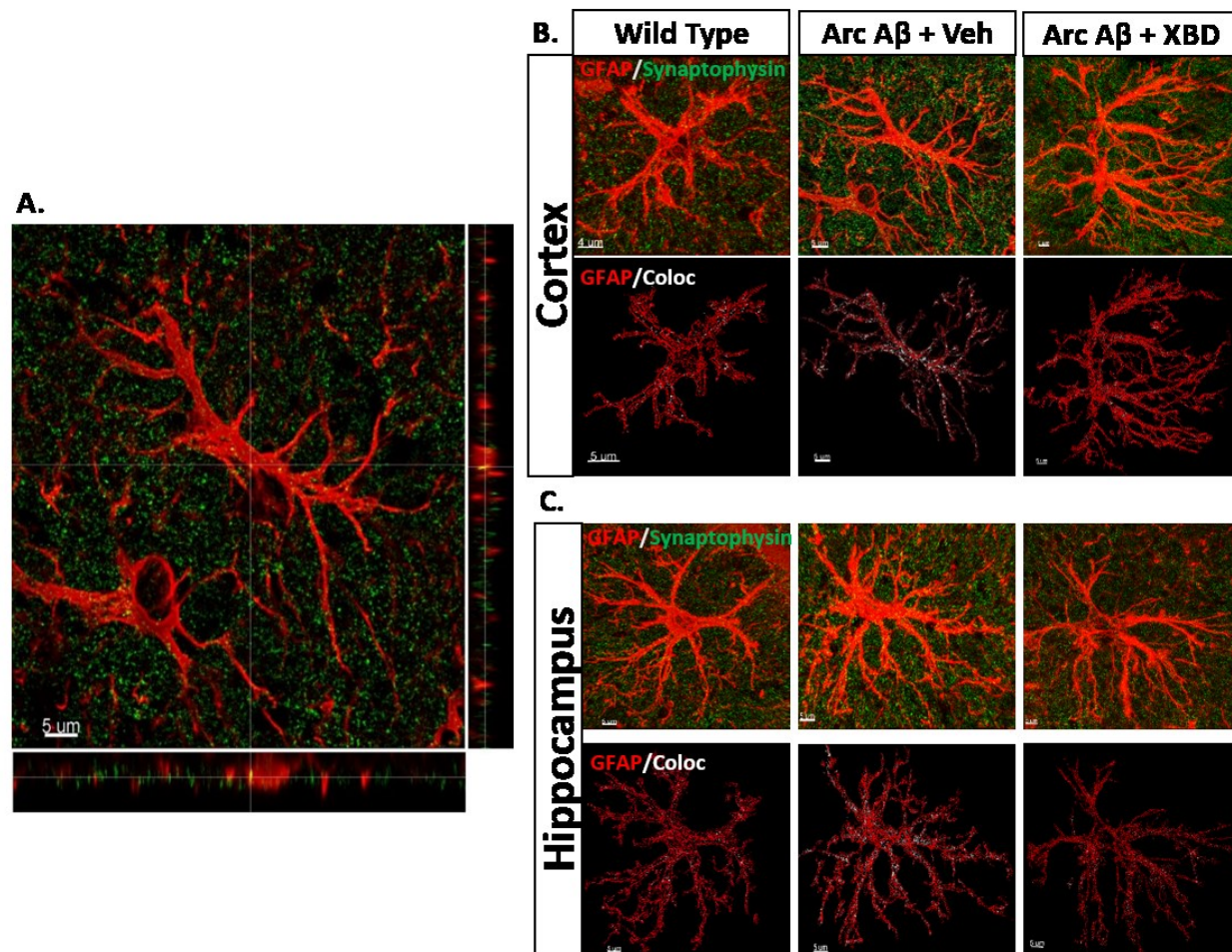


Figure 41: Representative image of astrocytic engulfment of synaptophysin in the cortex and hippocampus of different treatment groups. [Figure adapted and modified from our manuscript submitted relating to this work (Preprint can be found in [354]). Published version [353]]

A. GFAP (red) and synaptophysin (green) interaction are shown in an orthogonal plane. B. Representative images for astrocytic engulfment of synaptophysin (green) by astrocyte (red) in different experimental groups in the cortex. While the first row shows the original image obtained from the confocal scope, the second row shows the reconstructed astrocyte with colocalization point (white) inside it. C. Representative images for astrocytic engulfment of synaptophysin (green) by astrocyte (red) in different experimental groups in the hippocampus. While the first row shows the original image obtained from the confocal scope, the second row shows the reconstructed astrocyte with colocalization point (white) inside it. *Scale bar: 5 μ m.*

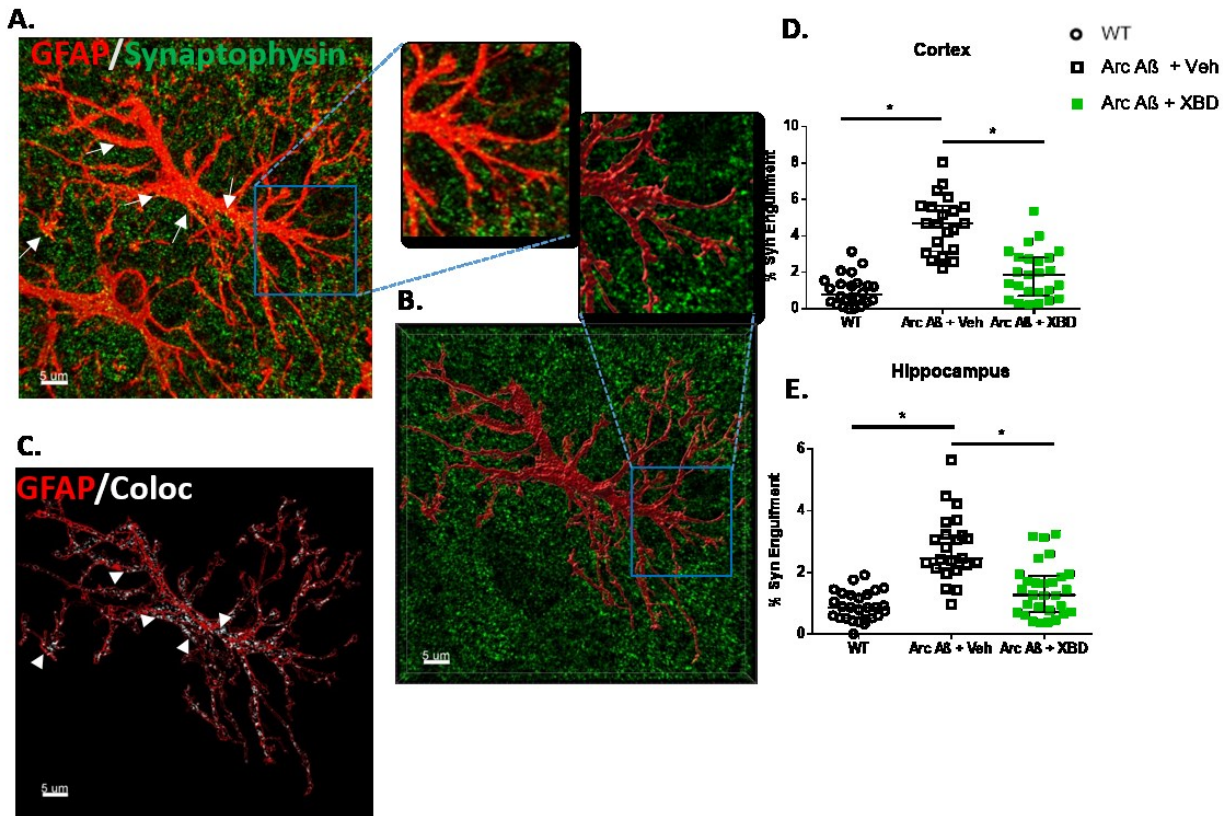


Figure 42: The chronic administration of XBD173 reduces synaptic pruning and aberrant astrocytic phagocytosis. [Figure adapted and modified from our manuscript submitted relating to this work (Preprint can be found in [354]). Published version [353]]

A. Confocal images of high-resolution individual astrocytes (red) and synaptophysin (green). The arrows indicate the colocalization points. B. 3D rendering of astrocytes (red) using IMARIS 9.7. The enlarged view of before and after astrocytic reconstruction is shown in the insets. C. Representative image of rendered outline of astrocyte (red) volume with colocalization point (white, shown by arrowheads). D. Astrocyte engulfment of synaptophysin quantified in different treatment groups in the cortex (Arc A β + vehicle: 4.692 (3.157-5.640) % vs WT: 0.7809 (0.3763-1.411) %, $p < 0.0001$; Arc A β + XBD: 1.866 (0.7195-2.818) spines/ μ m Arc A β + vehicle, $p < 0.0001$; one-way ANOVA with a Bonferroni's multiple comparisons *post hoc* test). E. Astrocyte engulfment of synaptophysin quantified in different treatment groups in the hippocampus (Arc A β + vehicle: 2.468 (2.144-3.232) % vs WT: 0.8785 (0.5336-1.293) %, $p < 0.0001$; Arc A β + vehicle vs Arc A β + XBD: 1.276 (0.7177-1.906) %, $p < 0.0001$; Kruskal–Wallis test with a Dunn's multiple comparisons *post hoc* test; 21-29 astrocytes collected from 4-5 mice per group). Data are represented as median with their respective interquartile range. * $p < 0.05$. ns: not significant.

3.11 Treatment with chronic XBD173 leads to a decrease in C1q aggregates in AD mice as well as a reduction in the engulfment of C1q protein by astrocytes

C1q complement tags are usually considered destruction tags for the synapses to undergo phagocytosis. Under normal physiological conditions, previous studies have reported that astrocytic synaptic pruning is independent of the involvement of C1q. Nonetheless, in pathological states such as AD, astrocytes are strongly implicated in the removal of synapses through C1q-dependent mechanisms [376]. Given the involvement of complement pathway protein particularly the evidence that links the presence of C1q to aggravated pathophysiology of AD, we investigated first if C1q complement proteins are linked to the astrocytic synaptic pruning. The reduction in aberrant synapses by astrocytes by XBD173 treatment led us to hypothesize that individual astrocytes in transgenic mice would engulf more of these signatures of C1q called "eat-me tag" signatures, and XBD173 treatment may affect C1q engulfment by astrocytes. From the volumetric analysis of individually rendered astrocytes, we found significantly increased engulfment of C1q protein in transgenic ArcA β mice. In line with our hypothesis, we did observe a significant reduction of C1q engulfment by the astrocytes both in the cortex as well as in the hippocampus in the transgenic animals treated with XBD173 (**Figure 43 A-D, Figure 44**).

Quite interestingly, we also report the deposition of C1q in the form of aggregates in the transgenic ArcA β mice. To our knowledge, deposition of C1q aggregates has not been shown in any AD mice models previously in the literature. Therefore, whether these aggregates result from the accumulation of dystrophic neurites or are a mere accumulation of complement protein is not known and this needs further investigation. These C1q aggregates highly colocalize with the methoxy-04 stained amyloid plaques. It is, however, essential to note a crucial point, while all the C1q aggregates colocalize with the amyloid plaques, the vice-versa is not true. To understand if there is a change in the overlap percentage of plaque with C1q aggregates, we first asked if XBD173 chronic treatment affects the colocalization percentage. We found that both XBD173 and vehicle-treated groups colocalized the C1q aggregates with plaques in a similar manner (**Figure 45**). However, it was interesting to observe that XBD173 comparatively had a much lower aggregate count compared to the transgenic counterparts (**Figure 46 A**). In retrospect therefore,

given the importance of C1q in aggravating the pathophysiology of AD, a decrease in the C1q aggregates could mean an improvement in the pathophysiology profile.

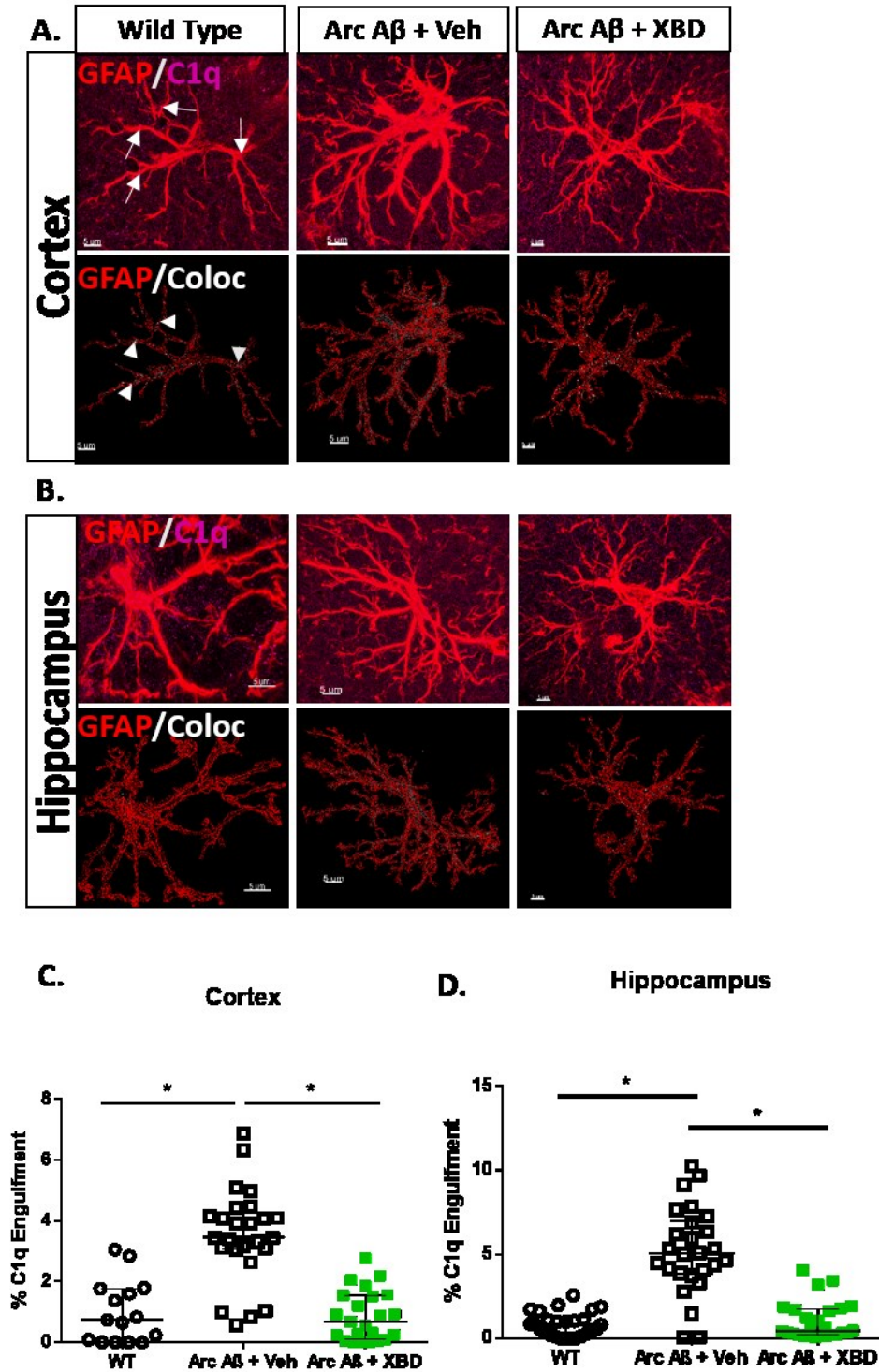


Figure 43: The chronic administration of XBD173 reduces enhanced astrocytic engulfment of C1q complement protein. [Figure adapted and modified from our manuscript submitted relating to this work (Preprint can be found in [354]). Published version [353]]

A. Confocal images of high-resolution individual astrocytes (red) and C1q (magenta) in the cortex. While the first row shows the original image obtained from the confocal scope, the second row shows the reconstructed astrocyte with colocalization point (white) inside it. *Scale bar: 5 μ m*. B. Confocal images of high-resolution individual astrocytes (red) and C1q (magenta) in the hippocampus. While the first row shows the original image obtained from the confocal scope, the second row shows the reconstructed astrocyte with colocalization point (white) inside it. *Scale bar: 5 μ m*. C. Astrocyte engulfment of C1q quantified in different treatment in the cortex (Arc A β + vehicle: 3.448 (3.071-4.300) % vs WT: 0.7465 (0.0033-1.767) %, $p < 0.0001$; Arc A β + XBD: 0.6829 (0.1004-1.543) % vs Arc A β + vehicle, $p < 0.0001$; Kruskal–Wallis test with a Dunn’s multiple comparisons *post hoc* test; 15-23 astrocytes collected from 4-5 mice per group). D Astrocyte engulfment of C1q quantified in different treatments in the hippocampus (Arc A β + vehicle: 5.056 (3.849-6.986) % vs WT: 0.8102 (0.1865-1.250) %, $p < 0.0001$; Arc A β + vehicle vs Arc A β + XBD: 0.4372 (0.1979-1.733) %, $p < 0.0001$; Kruskal–Wallis test with a Dunn’s multiple comparisons *post hoc* test; 26 astrocytes per collected from 5 mice per group). Data are represented as median with their respective interquartile range. * $p < 0.05$. ns: not significant.

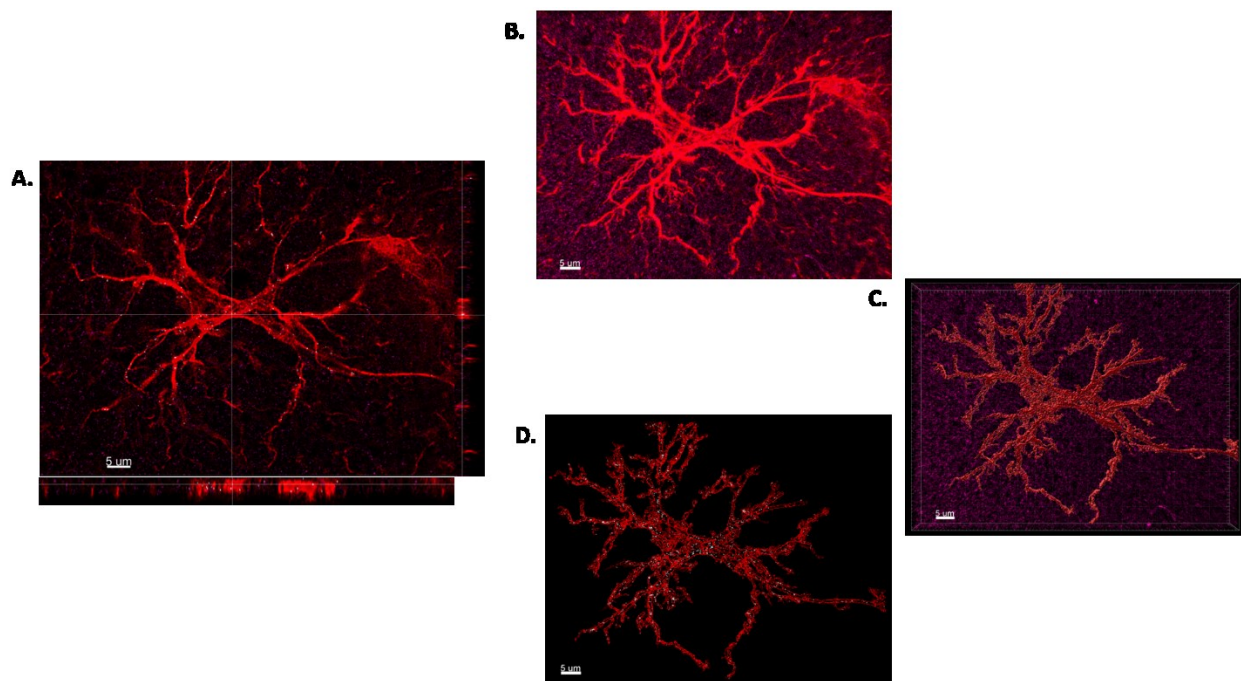


Figure 44: Representative confocal scope image of astrocyte interaction with C1q complement protein. [Figure adapted and modified from our manuscript submitted relating to this work (Preprint can be found in [354]). Published version [353]]

A. Astrocyte (Red) along with colocalization (White) shown in an orthogonal plane. B. Astrocyte (red) and C1q (magenta). C. 3D rendering of astrocytes (Red) using IMARIS 9.7 with C1q (magenta). D. Astrocyte outline (red) with colocalization points (white). *Scale bar: 5 μ m*

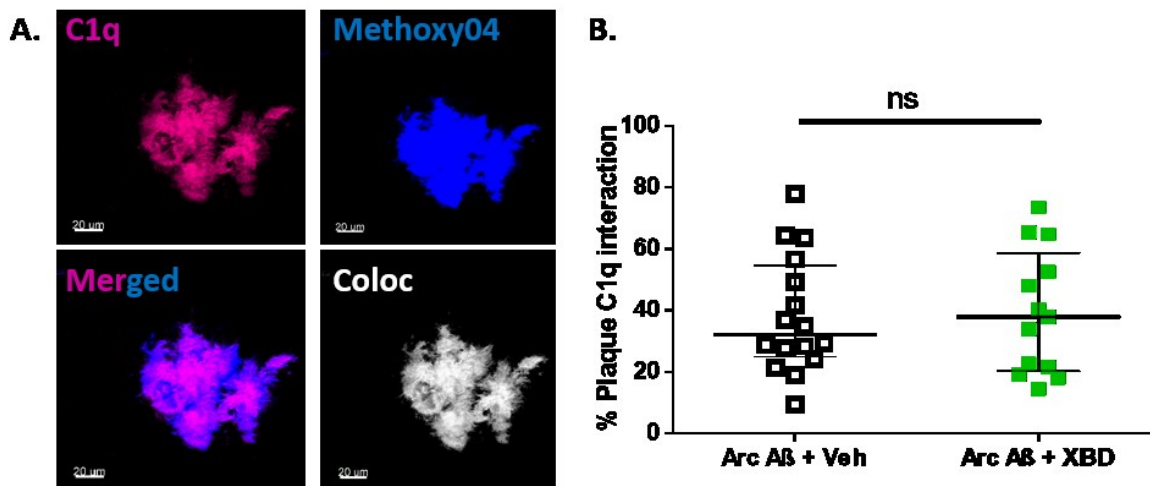


Figure 45. The % overlap between plaque and C1q is not affected by XBD173 treatment. [Figure adapted and modified from our manuscript submitted relating to this work (Preprint can be found in [354]). Published version [353]]

A. Confocal representative 63X images of methoxy-04 plaques (blue), C1q aggregates (magenta), merged, and colocalization (white) in transgenic AD mice. *Scale bar: 20 μ m*. B. % of overlap between plaque C1q in different treatment groups (Arc A β + XBD: 37.99 (20.39-58.68) % vs Arc A β + vehicle: 32.18 (25.07-54.76) %, $p=0.9390$; Mann–Whitney U test; 13-16 astrocytes collected from 4 mice per group). Data are represented as median with their respective interquartile range. * $p < 0.05$. ns: not significant.

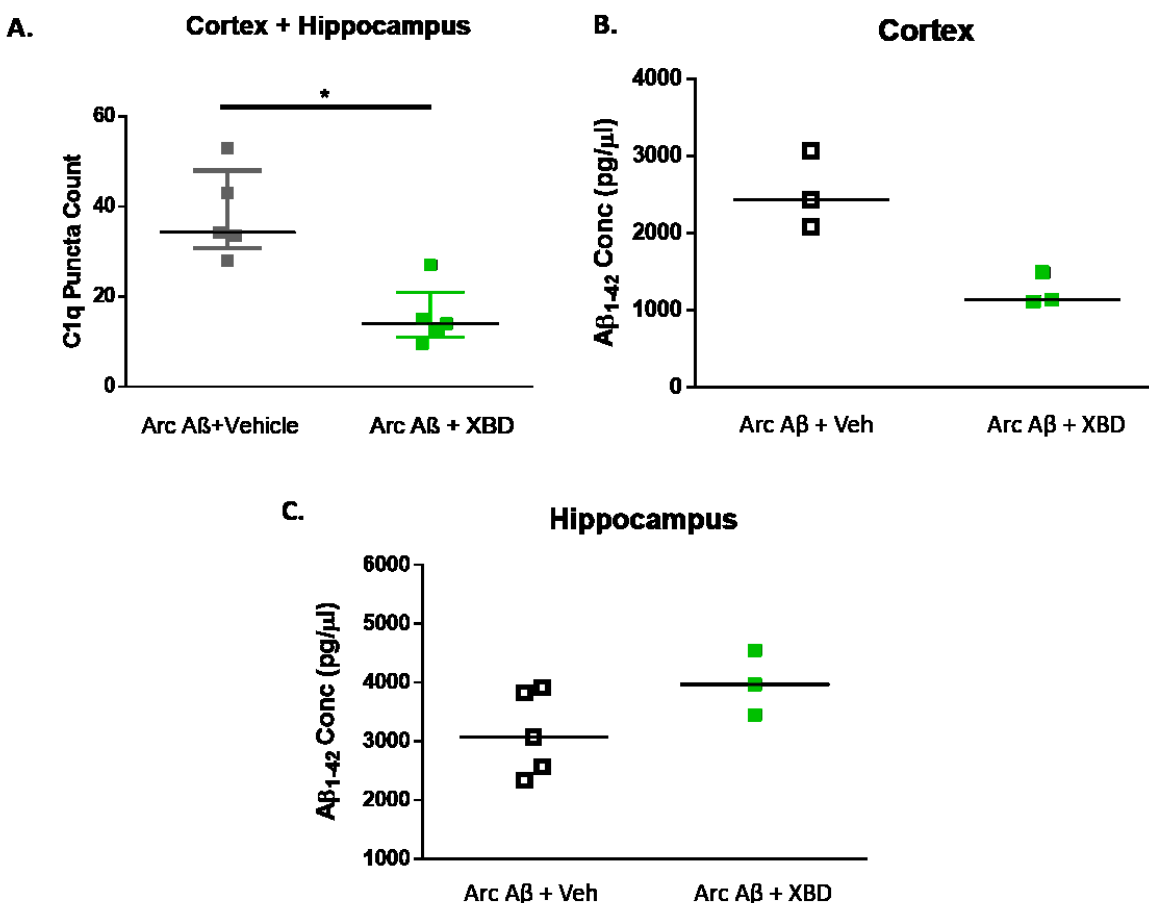


Figure 46: The C1q aggregates load, as well as cortex soluble Aβ₁₋₄₂ levels, are reduced in chronic XBD173 treated AD mice. [Figure adapted and modified from our manuscript submitted relating to this work (Preprint can be found in [354]). Published version [353]]

A. Comparison of C1q aggregates count between Arc Aβ + XBD (n=5) and Arc Aβ + vehicle (n=5) in the cortex and hippocampus (Arc Aβ + XBD: 14 (11-21) vs Arc Aβ + vehicle: 34.33 (30.75-48.00), $p=0.0079$; Mann-Whitney U test). B. ELISA quantification of cortex soluble Aβ₁₋₄₂ levels. WT (n=3), Arc Aβ + vehicle (n=3), and Arc Aβ + XBD (n=3). C. ELISA quantification of hippocampus soluble Aβ₁₋₄₂ levels. WT (n=3), Arc Aβ + vehicle (n=5), and Arc Aβ + XBD (n=3). Data are represented as median with their respective interquartile range. * $p < 0.05$. ns: not significant.

3.12 Astrocytes surround the methoxy plaques and more astrocytes are found near the periphery of plaques than farther away from it

We observed more astrocytes in the periphery of the plaques and a lesser astrocytic count when moving farther away from the plaques. This is in line with previous studies which show a higher glial cell density near the amyloid plaques [377]. Multiple astrocytes come together to form a ball-like structure surrounding the plaque from different sides. If this response is protection machinery that the brain uses to fight back the pathological condition to restore homeostasis is not known.

3.13 Methoxy plaque clearance in the cortex is not facilitated by astrocytic phagocytosis

Previously as discussed, we observed decreased plaque load and count in transgenic animals treated with XBD173. We then asked if astrocytic phagocytosis plays a crucial role in the removal of amyloid plaques specifically in the cortex after the treatment with XBD173. To address this question, we studied the % interaction of the amyloid plaques with their neighboring astrocytes (**Figure 47 A-D**). In both vehicle- and XBD173-treated animals, astrocytic engulfment of plaque was comparable (**Figure 47 E**). This suggests that astrocytic phagocytosis might not be the main contributor to the lower number of plaques in XBD173-treated animals. This hints probably to either a reduction in the plaque production machinery or microglia-dependent phagocytic removal of plaques in XBD173 treated animals.

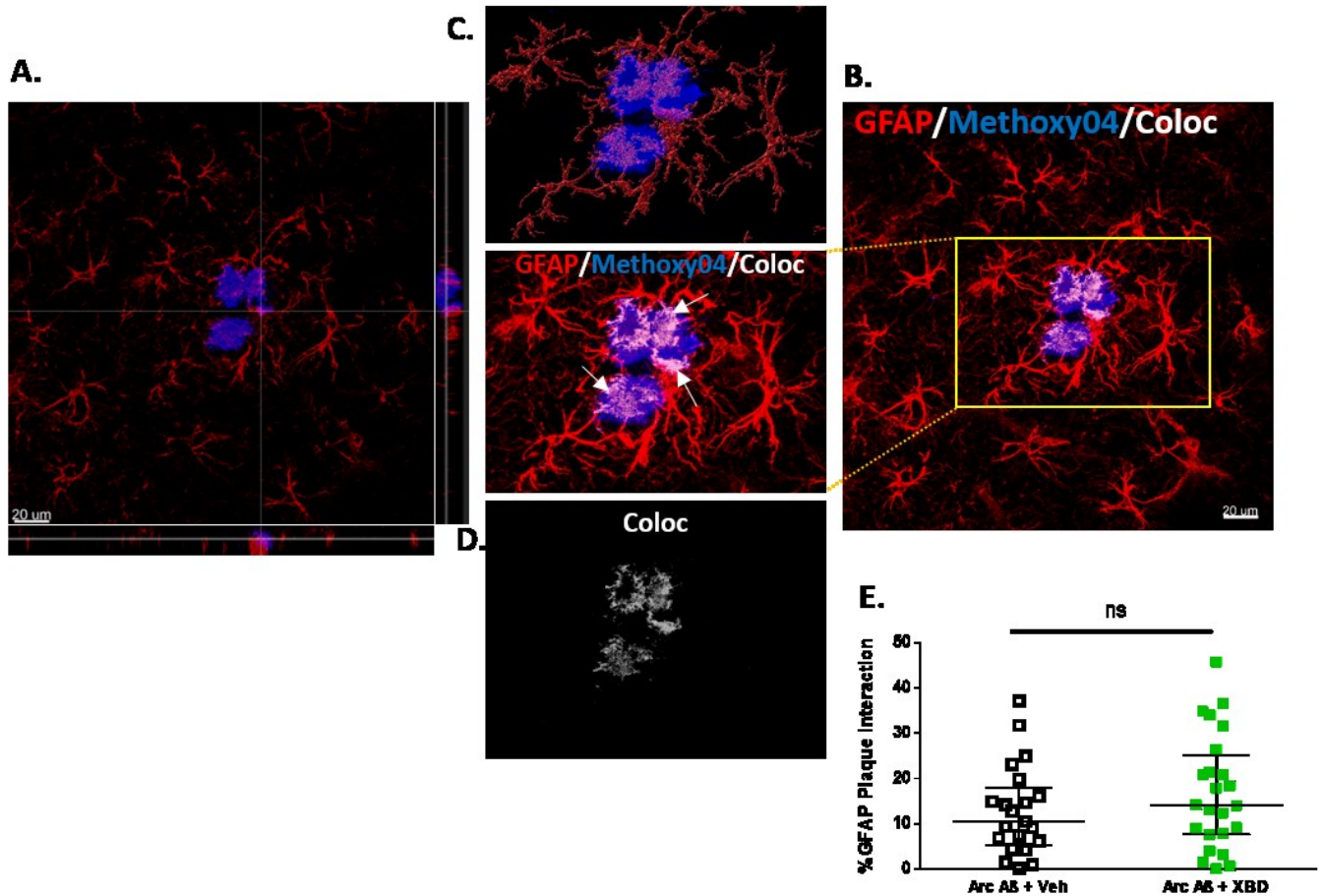


Figure 47: XBD173 treatment does not increase astrocytosis-mediated plaque clearance. [Figure adapted and modified from our manuscript submitted relating to this work (Preprint can be found in [354]). Published version [353]].

A. GFAP (red) and Plaque (blue) interaction are shown in an orthogonal plane. B. Confocal image for GFAP (red) and Plaque (blue). An enlarged view of the interaction marked with white arrows is shown in the inset. C. Rendered astrocytes (red) along with plaques after removal of background signal. D. GFAP and methoxy-04 plaque colocalization points are shown in white. *Scale bar: 20 μm.* E. % interaction of GFAP with plaques in the cortex and hippocampus. Arc Aβ + vehicle and Arc Aβ + XBD (Arc Aβ + XBD: 14.15 (7.715-25.15) % vs Arc Aβ + vehicle: 10.50 (5.305-17.99) %, $p=0.3573$; Mann–Whitney U test; $n=21-24$ plaques obtained from 4 mice per group). Respective groups. *Scale bar: 5 μm.* Data are represented as median with their respective interquartile range. * $p < 0.05$. ns: not significant.

3.14 XBD173 induces TSPO-mediated neurosteroids synthesis, which affects the activity of delta-subunit containing GABA_A receptor and confers neuroprotection against A β oligomers

TSPO protein located on the outer mitochondrial membrane has been implicated in several functions, the primary one being neurosteroidogenesis. As discussed earlier, in the case of neurodegeneration or neuronal injury, TSPO ligands have been shown to elevate the neurosteroid levels thereby ameliorating the pathogenesis. From our observation, XBD173 was TSPO dependent and was providing neuroprotective benefits against the A β ₁₋₄₂ oligomer. We, therefore, investigated the potential involvement of neurosteroids in the TSPO-mediated action of XBD173. Neurosteroids such as allopregnanolone and pregnenolone levels were shown to be previously associated with TSPO-dependent ligands. For instance, XBD173 mediates the anxiolytic effect by affecting allopregnanolone levels [228]. Similarly, XBD173 boosts mitochondrial function by elevating the pregnenolone levels in a TSPO-dependent manner [378].

We tested neurosteroids at different concentrations and asked if they could mimic the neuroprotective role of XBD173 against the A β ₁₋₄₂ oligomer. We first started with the neurosteroids (allopregnanolone and pregnenolone) that had been previously shown to be associated with TSPO-dependent XBD173. Pregnenolone (100 nM), however, was ineffective against the A β ₁₋₄₂ oligomer (**Figure 48 A, B, C**). Similarly, allopregnanolone (10 nM, 30 nM, and 100 nM) could not alleviate protection against A β ₁₋₄₂ oligomer-induced LTP reduction. It is interesting however to note that allopregnanolone (100 nM) rescues the LTP disruption resulting from the A β ₁₋₄₀ peptide (**Figure 49 A - D**).

Additionally, similar to XBD173, 3 α 5 α THDOC (100 nM) also confers neuroprotection against the LTP impairments caused by A β ₁₋₄₂ oligomers (**Figure 50 A, B, C**). Given the importance of the delta subunit in neurosteroid-mediated action, we asked whether 3 α 5 α THDOC was also able to confer neuroprotection in hippocampus slices obtained from GABA- δ KO transgenic animals. In line with our neurosteroid hypothesis, we observed that 3 α 5 α THDOC (100 nM) was not able to rescue the LTP impairment on GABA- δ KO hippocampal slices after incubation with the A β ₁₋₄₂ oligomers (**Figure 51 A, B**). Importantly, XBD173 (300 nM) also fails to prevent the synaptotoxicity of A β ₁₋₄₂ oligomers on LTP impairments in hippocampus slices obtained from

GABA- δ KO transgenic animals (**Figure 51 A, B**). This study shows that the δ subunit-containing GABA_A receptor is crucial for the action of XBD173. The chronic XBD173 treated AD mice also showed an elevation in the 3 β 5 α THDOC levels which is a stereoisomer of 3 α 5 α THDOC. We, therefore, assessed if the 3 β 5 α THDOC could also confer neuroprotection similar to XBD173. We observed that 3 β 5 α THDOC similar to 3 α 5 α THDOC rescues the LTP impairment resulting from A β ₁₋₄₂ oligomers (**Figure 51 C, D**). This evidence highlights the importance of neurosteroids in mediating XBD173's effect on AD pathology.

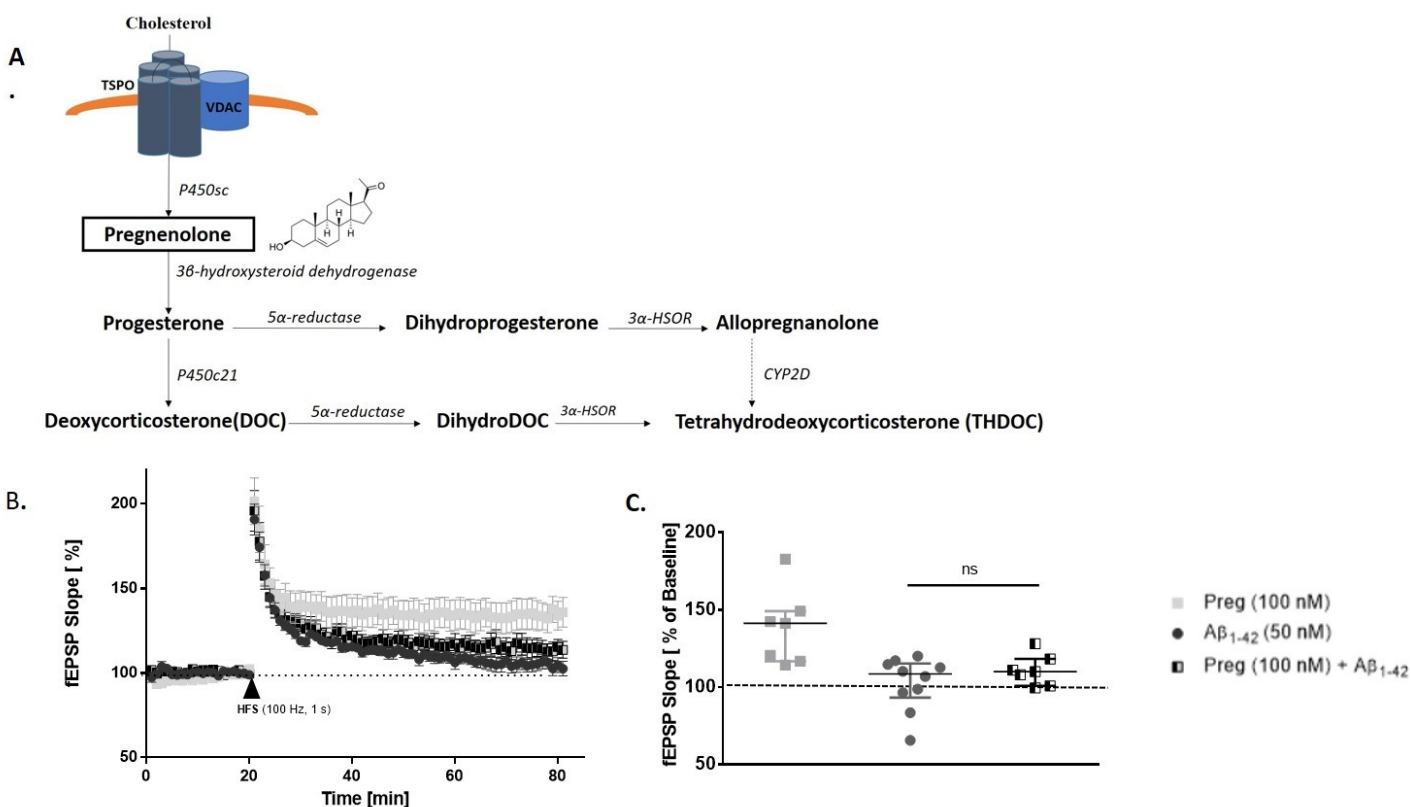


Figure 48: LTP deteriorations induced by A β ₁₋₄₂ oligomers incubation is not rescued by pregnenolone [Figure adapted and modified from our manuscript submitted relating to this work (Preprint can be found in [354]). Published version [353]].

A. Representative Schematic of TSPO-mediated neurosteroid synthesis. B. Normalised fEPSP slope time course following an HFS under pregnenolone (Preg) (100 nM), A β ₁₋₄₂ (50 nM), and Preg+ A β ₁₋₄₂. C. For

each group, a scatter dot plot summarizing the last 10 minutes (from 50 to 60 minutes) following HFS: WT mice: Preg (100 nM) (n=7), A β_{1-42} (50 nM) (n=10) and Preg+ A β_{1-42} (n=7) (Preg (100 nM) + A β_{1-42} : 110 (100.8-118.3) % of baseline slope vs A β_{1-42} : 108.5 (93.18-115.3) % of baseline slope, $p=0.47$; Mann-Whitney U test). Data are represented as median with their respective interquartile range. * $p < 0.05$. ns: not significant.

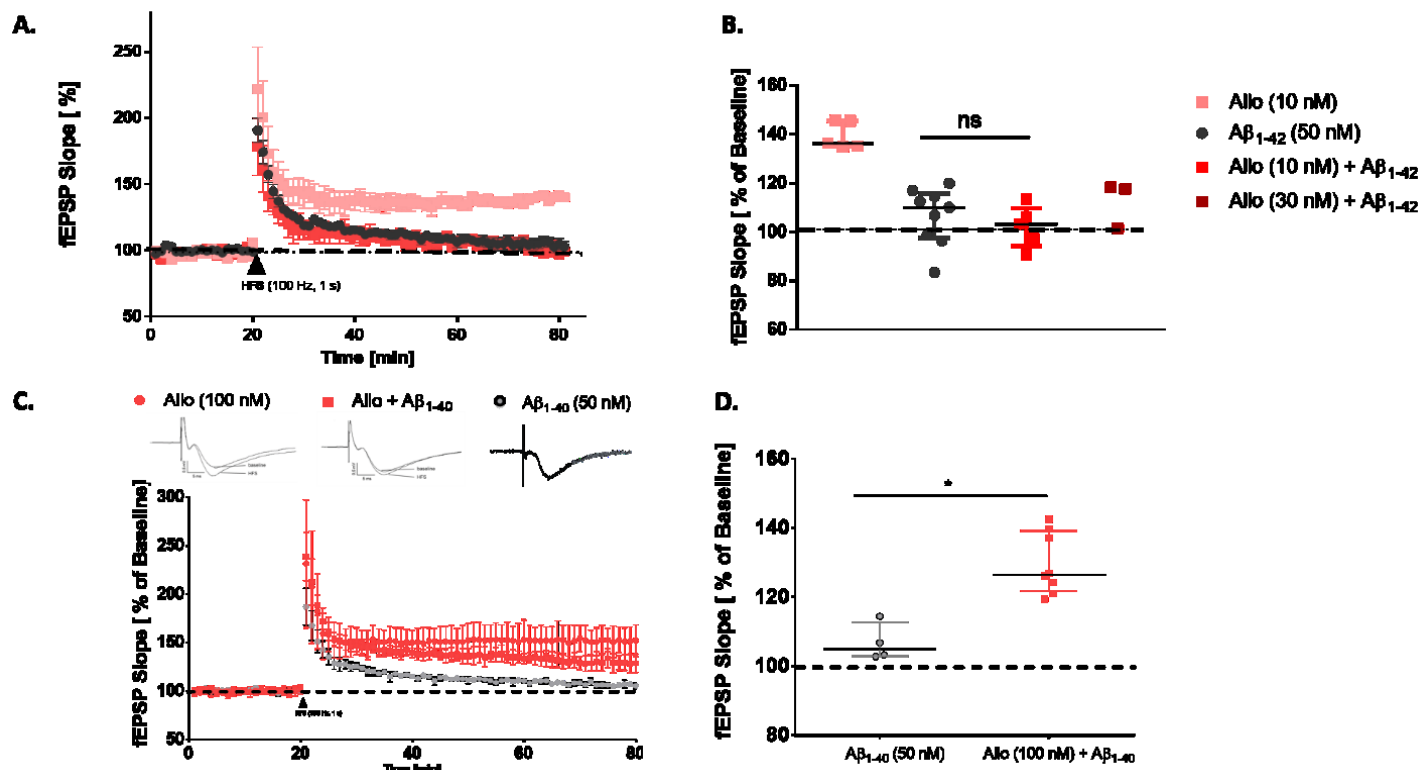


Figure 49: Allopregnanolone (Allo) prevents the LTP impairment from A β_{1-40} oligomers but doesn't affect the LTP deterioration resulting from A β_{1-42} oligomers. [Figure adapted and modified from our manuscript submitted relating to this work (Preprint can be found in [354]). Published version [353]].

A. Normalised fEPSP slope time course following an HFS under Allo (10 nM), A β_{1-42} (50 nM), Allo (10 nM) + A β_{1-42} , and Allo (30 nM) + A β_{1-42} . B. For each group, a scatter dot plot summarizing the last 10 minutes (from 50 to 60 minutes) following HFS in WT C57/Bl6 mice: Allo (10 nM) (n=5), A β_{1-42} (50 nM) (n=9), Allo (10 nM)+ A β_{1-42} (n=5), and Allo (30 nM)+ A β_{1-42} (n=3) (Allo (10 nM) + A β_{1-42} : 103.2 (94.08-109.9) % of baseline slope vs A β_{1-42} : 110.2 (97.55-115.9) % of baseline slope, $p=0.34$; Mann-Whitney U test). C. Normalised fEPSP slope time course following an HFS under Allo (100 nM), A β_{1-40} (50 nM), and Allo + A β_{1-40} . D. For each group, a scatter dot plot summarizing the last 10 minutes (from 50 to 60 minutes) following HFS in WT C57/Bl6 mice: A β_{1-40} (50 nM) (n=4) and Allo (100 nM) + A β_{1-40} (n=8) (Allo

(100 nM) + A β_{1-40} : 126.4 (121.8-139.1) % of baseline slope vs A β_{1-40} : 105 (102.9-112.5) % of baseline slope, $p=0.004$; Mann-Whitney U test). Data are represented as median with their respective interquartile range. * $p < 0.05$. ns: not significant.

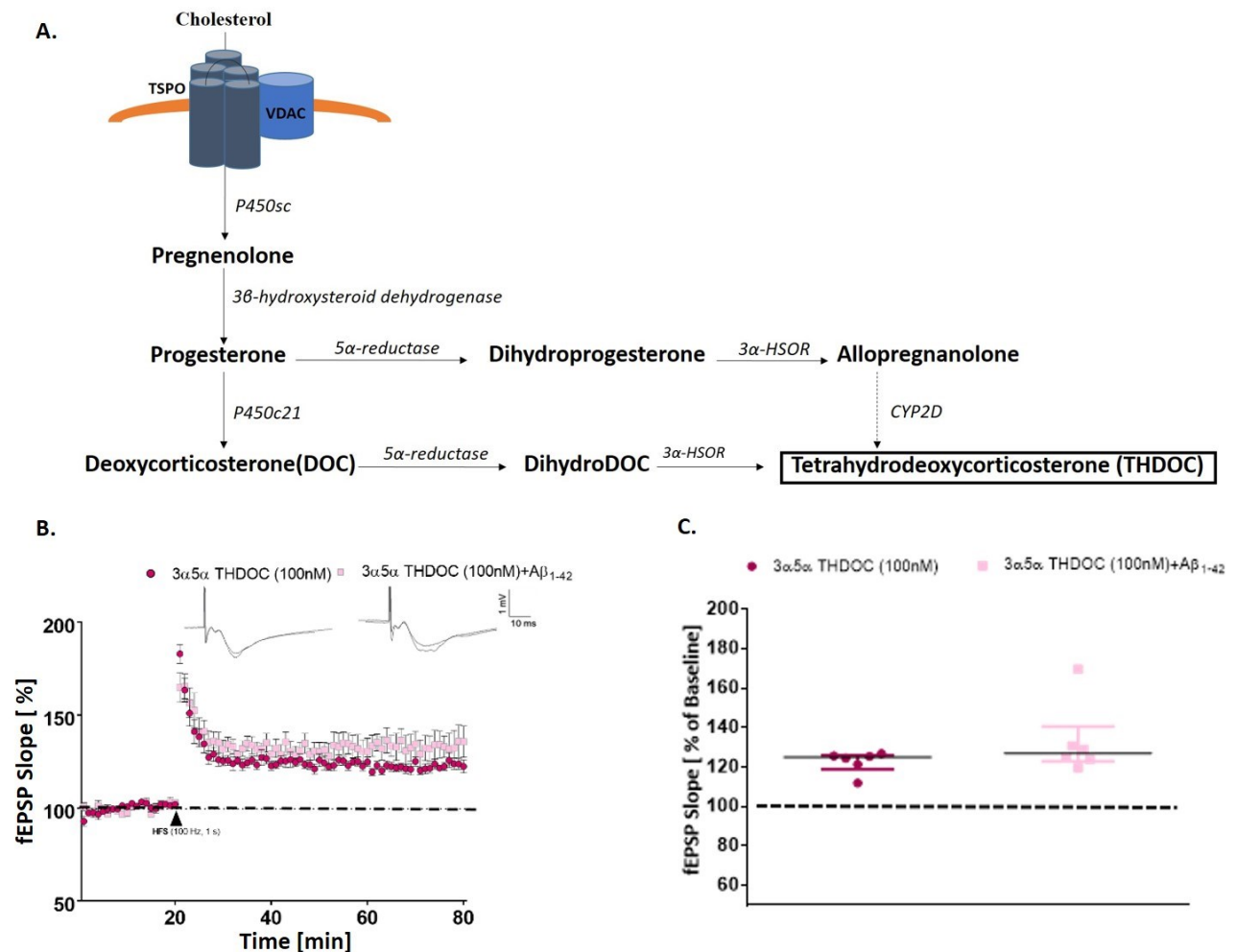


Figure 50: 3 α 5 α THDOC prevents LTP impairments resulting from A β_{1-42} oligomers [Figure adapted and modified from our manuscript submitted relating to this work (Preprint can be found in [354]). Published version [353]].

A. Representative Schematic of TSPO-mediated neurosteroid synthesis. B. Normalised fEPSP slope time course following an HFS under 3 α 5 α THDOC (100 nM) and 3 α 5 α THDOC + A β_{1-42} conditions in WT C57/B16 mice. Representative traces for each treatment group are shown in the insets above. C. For each group, a scatter dot plot summarizing the last 10 minutes (from 50 to 60 minutes) following HFS: 3 α 5 α THDOC (n=6) and 3 α 5 α THDOC + A β_{1-42} (n=6) (WT 3 α 5 α THDOC + A β_{1-42} : 127.1 (122.9-140.5) % of

baseline slope vs WT 3α 5α THDOC: 125.0 (119.0-126.0) % of baseline slope, $p=0.3874$; Mann-Whitney U test). Data are represented as median with their respective interquartile range. $*p < 0.05$. ns: not significant.

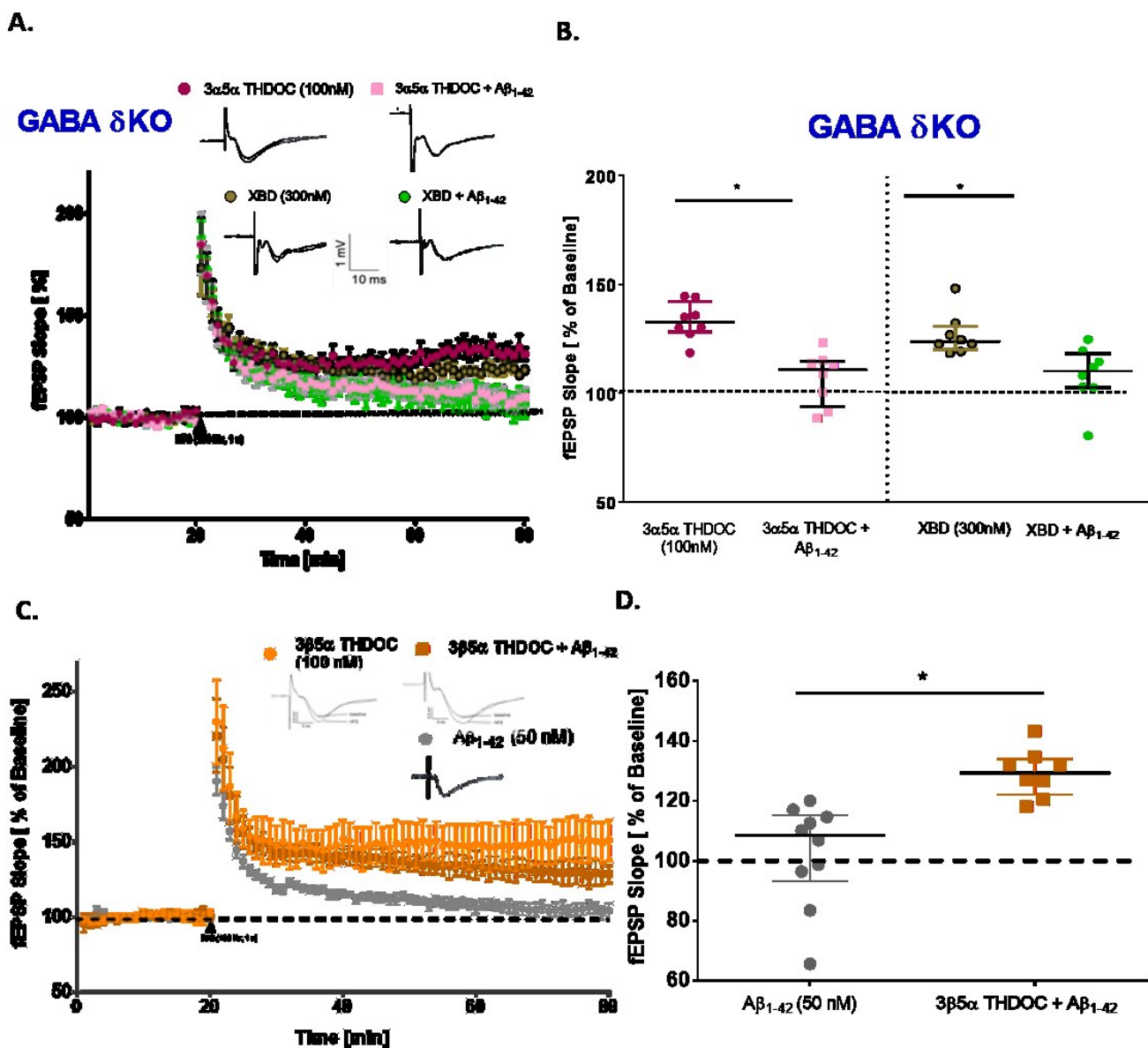


Figure 51: XBD173 stimulates TSPO-regulated production of diverse neurosteroids such as THDOC, which increases delta subunit-containing GABA_A receptor activity [Figure adapted and modified from our manuscript submitted relating to this work (Preprint can be found in [354]). Published version [353]].

A. Normalised fEPSP slope time course following an HFS under 3α 5α THDOC (100 nM), XBD173 (300 nM) and XBD173 + $A\beta_{1-42}$, and 3α 5α THDOC + $A\beta_{1-42}$, conditions in GABA- δ KO transgenic mice. B. For each group, a scatter dot plot summarizing the last 10 minutes (from 50 to 60 minutes) following HFS in GABA- δ KO mice: 3α 5α THDOC (100 nM) (n=7), 3α 5α THDOC + $A\beta_{1-42}$ (n=7), XBD173 (300 nM) (n=6) and XBD173 + $A\beta_{1-42}$ (n=6) (3α 5α THDOC + $A\beta_{1-42}$: 110.8 (93.8-114.7) % of baseline slope vs 3α 5α THDOC: 132.7 (128.1-142.1) % of baseline slope, $p=0.0003$; XBD + $A\beta_{1-42}$: 110.2 (102.7-118.2) % of baseline slope vs XBD: 123.7 (120.1-130.9) % of baseline slope, $p=0.0070$). C. Normalised fEPSP slope time course following an HFS under $3\beta 5\alpha$ THDOC (100 nM), $A\beta_{1-42}$ (50 nM), and $3\beta 5\alpha$ THDOC + $A\beta_{1-42}$. D. For each group, a scatter dot plot summarizing the last 10 minutes (from 50 to 60 minutes) following HFS in C57/Bl6 mice: $A\beta_{1-42}$ (50 nM) (n=10) and $3\beta 5\alpha$ THDOC + $A\beta_{1-42}$ (n=8) ($3\beta 5\alpha$ THDOC + $A\beta_{1-42}$: 129.3 (122.1-134) % of baseline slope vs $A\beta_{1-42}$: 108.5 (93.18-115.3) % of baseline slope vs, $p<0.0001$; Mann-Whitney U test). Data are represented as median with their respective interquartile range. * $p<0.05$. ns: not significant.

3.15 XBD173 incubation prevents LTP impairment resulting from $A\beta_{1-42}$ arctic mutation oligomer

Since transgenic mice containing the arctic mutation impair cognitive performance and XBD173 chronic treatment rescues the cognitive deficits, we asked if this occurs in a cellular process as well. To address this we used the $A\beta_{1-42}$ oligomers containing the mutation of arctic heredity with glycine substituted for glutamic acid at position 22. As expected we found that the $A\beta_{1-42}$ oligomers containing the arctic mutation impaired the hippocampal LTP and incubation with XBD173 prevented this impairment [244] (**Figure 52**). This *ex vivo* finding correlates with the behavioral spatial learning test result and confirms the neuroprotective role of XBD173 both *ex vivo* as well as *in vivo*.

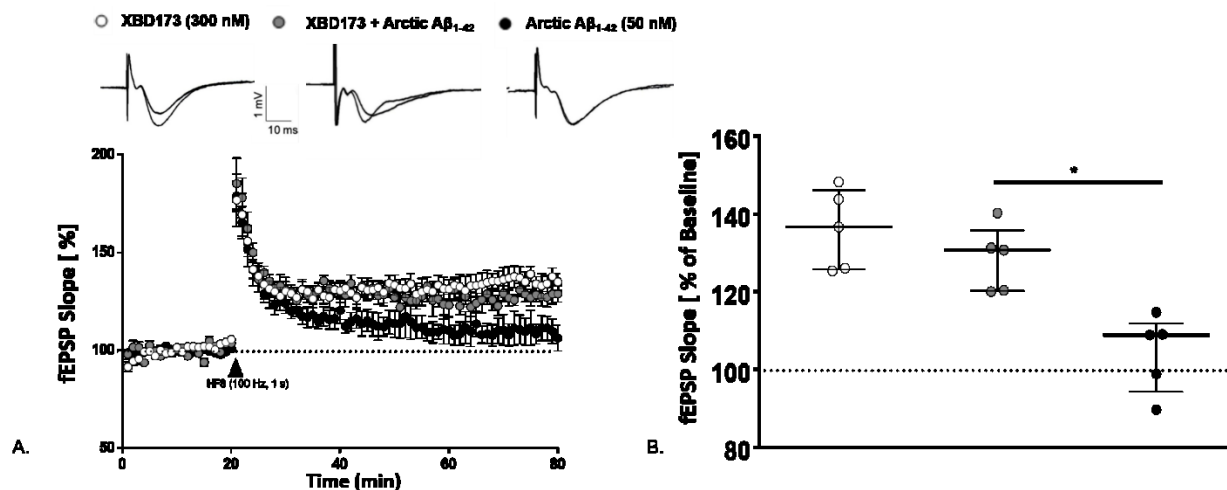


Figure 52: XBD173 (300 nM) rescues the Arctic A β_{1-42} synaptotoxic effect on LTP (Modified with permission from [244]).

(A) Normalized fEPSP slope time course following an HFS under control conditions, with 1.5 h Arctic A β_{1-42} exposure alone and the simultaneous application of XBD173 (300 nM) and Arctic A β_{1-42} (50 nM). (B) For each group, a scatter dot plot summarizing the last 10 minutes (from 50 to 60 minutes) following HFS. (XBD: 136.7 (125.7-146) % of baseline slope n=5; XBD + Arctic A β_{1-42} : 130.8 (120.3-135.8) % of baseline slope n=5; Arctic A β_{1-42} : 108.9 (94.34-111.9) % of baseline slope n=5). Data are represented as median with their respective interquartile range. * $p < 0.05$. ns: not significant. Representative fEPSPs are shown in the inset on the top.

4. Discussion

4.1 Key Objectives and Findings

From the multitude of clinical evidence, depression could be an antecedent of Alzheimer's [135,136,138]. Both these disorders share a commonality in their pathological cellular mechanism. Our interest in targeting both these overlapping cellular mechanisms made us explore in detail TSPO-dependent ligands which confer anxiolytic effects without having benzodiazepines-like side effects. Given the differences in the binding site distribution as well as the sensitivity to the different GABA_A receptor subunits for benzodiazepines and 3 α -reduced neurosteroids (neurosteroids are sensitive to the δ -subunit of GABA_A receptors, whereas benzodiazepines are sensitive to the γ 2-subunit of GABA_A receptors) [244,246,379], we hypothesized that neurosteroid production via the activation of TSPO could provide an improved pharmacological profile than the previously used benzodiazepines. Since AD is a progressive neurodisorder with a complex pathophysiological mechanism, we decided to look at both ex vivo and in vivo models of AD, and the effect of translocator protein activation via selective ligand XBD173. Our first goal was to characterize the beneficial effects of XBD173 on CA1 LTP which is a cellular correlate of memory and learning. The next goal was to see if it could provide protective benefits to cognition in vivo. Next, we wanted to look at all possible pathways that could be intervened by the administration of TSPO-dependent XBD173.

Therefore, we examined whether TSPO-dependent XBD173, which has been reported to exert anxiolytic effects in both rodents and humans, could confer neuroprotective benefits in a murine Alzheimer's model. First, we show that XBD173 could prevent LTP impairment resulting from A β ₁₋₄₂ oligomer and this effect is mediated by the translocator protein (**Figure 25, 26**). Among the individual spine classes, XBD173 prevents the loss of mushroom spines and long thin spines (**Figure 28**). From previous evidence, mushroom spines are considered to be memory spines whereas long thin spines are considered to be learning spines [360,380]. This could explain the prevention of LTP impairment in the presence of XBD173. In an in vivo AD transgenic mouse model (ArcA β) we were able to demonstrate that chronic (1mg/kg every alternate day for 12 weeks) but not acute (1mg/kg single dose before the training phase) administration of XBD173 could reverse cognitive decline and keep a sustained neuroprotective benefit even after 45 days

(Figure 29, 20, 31). In het TSPOKO X Arc A β animals, this neuroprotective effect of XBD173 was not observed, thus highlighting the importance of TSPO in full expression for the complete neuroprotective benefit of XBD173 (Figure 34, 35, 36). This is further supported by a significant reduction of plaques and soluble A β levels in the cortex as well as reduced astrocytic phagocytosis of functional synapses in both the hippocampus and cortex (Figure 37, 42). We also show hyperactive involvement of complement system protein in the AD transgenic mice (Figure 43) and that XBD173 reduces the abnormal hyperactivity and thereby reduces the energy imbalance in AD (Discussed further in the energy section).

The chronic administration of XBD173 elevates the levels of multiple neurosteroids such as 3 α 5 α THP in the cortex, 3 β 5 α THDOC in the hippocampus, and 5 α DHDOC in the cortex and hippocampus and also rescues the spine loss (Figure 39). Among the tested neurosteroids, we report that both the stereoisomers of THDOC (100 nM) (3 α 5 α THDOC and 3 β 5 α THDOC) similar to XBD173, prevent the LTP deficits caused by A β ₁₋₄₂ oligomer (Figure 50, 51). Importantly, both XBD173 and 3 α 5 α THDOC fail to prevent the LTP deficit caused by A β ₁₋₄₂ oligomer in the hippocampal slices obtained from GABA- δ knockout (KO) animals (Figure 51), indicating that the δ -subunit is downstream of TSPO activation by XBD173. Allopregnanolone levels which have previously also been reported to be enhanced on the application of TSPO ligands were increased in our chronic treatment model after the application of XBD173. We tested therefore if allopregnanolone could also rescue the LTP impairments from A β oligomers. To our surprise allopregnanolone was not effective in preventing the LTP disruption resulting from the A β ₁₋₄₂ oligomer but was able to rescue the impairments resulting from the incubation of the A β ₁₋₄₀ oligomer (Figure 49). This indicates that XBD173-mediated TSPO activation orchestrates the formation of a diverse range of neurosteroids that target different progression mechanisms of AD. Additionally, while one might speculate that the difference in the working mechanisms of either XBD173 or allopregnanolone towards A β ₁₋₄₂ or A β ₁₋₄₀ oligomer, could be due to a difference in the aggregation propensity of both the oligomers, the observation that XBD173 could only partially rescue the CA1-LTP impairments resulting from A β ₁₋₄₀ oligomer could be due to an insufficient incubation time with XBD173 *ex vivo* which might not produce sufficient allopregnanolone to induce the beneficial effect. XBD173 prevents spine loss resulting from the A β ₁₋₄₂ oligomer. All of this taken together suggests that XBD173 exerts neuroprotective benefits in AD while having a lower side-effect profile than the previously used anxiolytics (Figure 53).

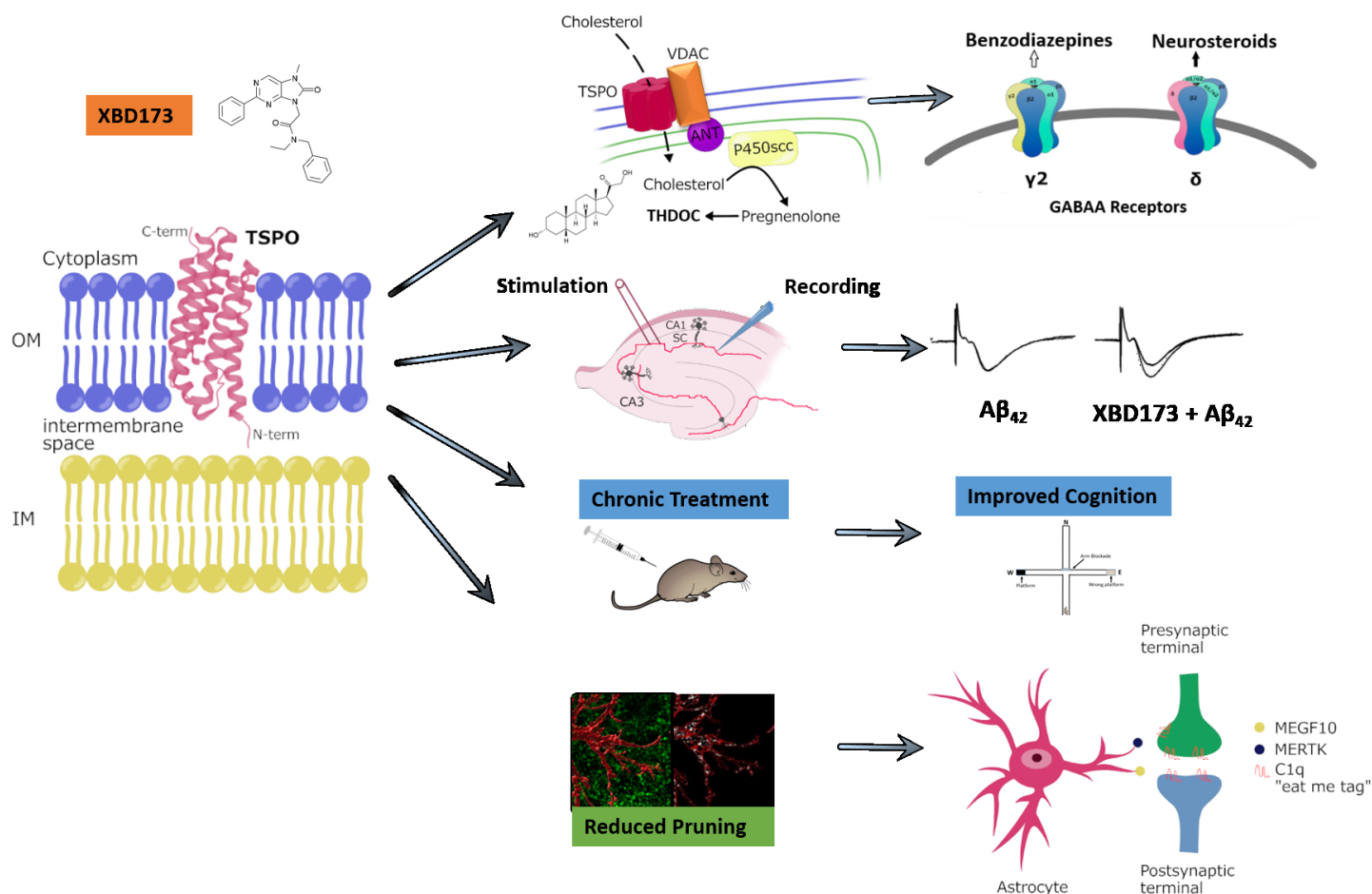


Figure 53: Schematic showing the possible working mechanism for TSPO-dependent XBD173 in the AD model. (Figure adapted and modified from our manuscript submitted relating to this work (Preprint can be found in [354]). Published version [353]).

4.2 TSPO, XBD173, depression, and AD Pathology: From a Cellular and behavioral perspective

Several overlapping studies highlight a clear mechanistic link between clinical depression and AD. For instance, neuronal loss combined with an increase in the pro-inflammatory cytokines and neurotoxins and a decrease in anti-inflammatory cytokines has been associated with both major depression and dementia [161–164]. Dementia risk is more than twice as high in patients with mild cognitive impairment associated with depression as in non-depressed individuals [138]. Activation

of macrophages in the blood and microglia in the brain, which releases pro-inflammatory cytokines, has been thought to contribute to the progression from depression to dementia [161–164]. The presence of A β enhances NMDA receptor-induced neurotoxicity caused by pro-inflammatory cytokines like interleukin-1b (IL-1b) [381,382]. In a reverse scenario, i.c.v injections of A β oligomers increased depression-like behavior in mice and elevated brain levels of IL-1b [383,384]. In addition, clinical studies have shown the positive effects of antidepressants on AD patients. The antidepressants paroxetine and fluoxetine significantly decreased the intracellular concentrations of A β oligomers and increased the concentrations of A β monomers in APP overexpressing N2a neuroblastoma cells [385]. Similarly, in the rodent model of 3xTgAD (transgenic Alzheimer's), chronic treatment with paroxetine decreased the A β ₁₋₄₀ levels in both the hippocampus and cortex [386]. Fluoxetine when applied i.c.v ameliorated A β induced cognitive effect [387,388]. In a recent study, imipramine and escitalopram were shown to rescue the synaptotoxic changes in the pre-synaptic vesicles induced by A β ₁₋₄₂ [389,390]. All of this clinical evidence points towards increased neurotoxicity, neuronal injury, and chronic inflammatory changes as the common characteristic link between major depression and dementia. The use of TSPO-dependent XBD173 which is already known to exert an anxiolytic effect both in humans and rodents can therefore be an excellent choice to study its neuroprotective role in dementia.

TSPO's usefulness as a pharmaceutical target is primarily due to its involvement in the movement of cholesterol from the outer to the inner mitochondrial membrane, which is a rate-limiting step for neurosteroid synthesis. While the role of TSPO in neurosteroid synthesis is still under debate, there is conclusive evidence for the neuroprotective role of TSPO ligands via enhanced neurosteroidogenesis, reduction in apoptosis, less ROS production, and promotion of nerve regeneration [181–183]. Previously in a report TSPO ligands RO5-4864 and PK95111 rescued the pathology in a mouse AD model via enhanced neurosteroidogenesis [223]. It is interesting to note that levels of various neurosteroids are decreased in AD patients [391–393]. Since neurosteroids are potent modulators of synaptic transmission, they could confer neuroprotective benefits to memory and cognitive parameters in AD. XBD173 has been clinically proven for efficacy, safety, and tolerability also in humans [228]. In our study, to understand if in an AD pathological condition, XBD173 still acts via TSPO proteins to exert neuroprotective effects, we designed a similar set of experiments in the global TSPOKO mouse model. XBD173 is orally available and owing to its lipophilic structure it can also cross the blood-brain barrier [394]. Previously XBD173

at 90 mg/d has been tested to be safe without any tolerance effects in healthy volunteers challenged with the panic disorder paradigm. The side-effect profile was comparable to the placebo group [228].

From previous studies, as well as from the ones in our lab different A β species block CA1-LTP in the hippocampus [70,71,355,395]. XBD173 (300 nM) when administered in sagittal hippocampal slices prevented the LTP impairments from the A β ₁₋₄₂ oligomers but only partially rescued the impairments from A β ₁₋₄₀ oligomers. The differential selectivity in this action could be reflected by the differential sensitivity of A β ₁₋₄₂ and A β ₁₋₄₀ oligomers to different targets as well as differences in aggregation kinetics. Some of the possible reasons for the LTP impairment could be because soluble A β can decrease the surface expression of NMDA receptors [42,396]. Previously, synaptic NMDA receptors, not the extrasynaptic ones have been associated with LTP [397]. In another study, however, soluble A β oligomers were shown to facilitate hippocampal long-term depression (LTD) via enhancement of the GluN2B subunit [70,398]. The LTP impairment resulting from A β oligomers therefore could be manifested via the activation of extrasynaptic GluN2B subunit-containing NMDA receptors [399]. A second possible hypothesis, the signal-to-noise hypothesis, and how XBD173 could confer neuroprotective effects in the presence of A β oligomers are described in detail in the energy imbalance section below. Further research needs to address the differences in mechanistic action of different A β oligomers on different receptor subunits and the downstream activation of secondary messenger pathways. In our study, TSPOKO mice were used to further confirm that TSPO protein is involved in this XBD-mediated action. XBD173 was not able to provide neuroprotective benefits in the global TSPOKO model, which confirms the dependency of XBD173 on TSPO protein to mediate the beneficial effects.

Following the results from the CA1-LTP experiment and the role of XBD173 in providing neuroprotective benefits, we asked if these effects were mediated by neurosteroids downstream. We tested several neurosteroids at different concentrations to test their effect in mimicking the action of XBD173 to prevent the LTP impairment caused by the A β oligomers. While pregnenolone and allopregnanolone couldn't rescue the LTP deficits from the A β ₁₋₄₂ oligomers (**Figure 48, 49**), THDOC (100 nM) like XBD173 rescued the LTP impairment caused by A β ₁₋₄₂ oligomers (**Figure 50**). Since the neurosteroids are sensitive to δ -subunits containing the GABA_A receptor, we next investigated the potential involvement of δ -subunits containing the GABA_A

receptor in XBD173-mediated positive effects (**Figure 51**). Both THDOC and XBD173 were not able to exert their previous positive effects in a GABA_A receptor δ -subunits KO model. The results of this study have determined two primary conclusions: (1) XBD173, a TSPO-dependent compound, works through the GABA_A receptor containing the δ -subunit to produce its neuroprotective effects, and (2) The activity of XBD173 may be mediated by a diverse range of neurosteroids such as THDOC, allopregnanolone or DHDOC that acts via the δ -subunit. The different spine classes have specific roles owing to their head size, neck length, and total volume. For instance, mushroom spines, are thought to be associated with long-term memory because they form strong synaptic connections as well have the longest lifetime [360,380]. It is interesting to note that the mushroom spines harbor a greater amount of glutamate receptors on their head surface [400]. This potentially allows them to play a critical role in synaptic plasticity. If we take this further in the context of LTP, A β oligomers reduce the mushroom spines significantly which could be a potential mechanism of LTP impairment. XBD173 pre-incubation however prevents the elimination of mushroom spines by the A β oligomers. While not much study has been done with the long-thin spines, they are usually referred to as the learning spines because of their high adaptability to synaptic input [360,380]. Similar to mushroom spines, TSPO-dependent XBD173 prevents the loss of long-thin spines.

Cognitive deficits and memory impairments are the classical hallmark features of AD which progressively goes bad with time. Given the neuroprotective effects of XBD173 in the ex vivo model, we further investigated if it could also better the cognitive deficits in the transgenic ArcA β mouse model. Water cross maze (WCM) was developed as a highly sensitive platform to assess hippocampal place learning in small animals. A selective reinforcement paradigm with only water as a motive force produces more accurate and robust results than food rewards. Also compared to the traditional Morris water maze, the water cross maze gives less opportunity to cause stress in mice [357]. Therefore, it was ideal to detect deficits in the cognitive performance of the ArcA β mice. Chronic but not acute treatment of XBD173 rescued the cognitive deficits in the ArcA β mice model, suggesting that the acute treatment alone might not be sufficient to show any effect (**Figure 29, 30**). The positive effects on cognition were maintained both in retest 1 and 2 which suggests that the effect of XBD173 is long-lasting even after the termination of the treatment (**Figure 31**). The anxiolytic diazepam used as a reference didn't show any improvement in the cognitive performance of the ArcA β mice (**Figure 30, 31**). To assess if this neuroprotective effect is via the

TSPO protein, we created the double mutant line TSPOKO X ArcA β . There was, however, a high breeding failure rate and homozygous lines showed behavioral saliences (one-third of the mice developed epileptic seizures). Therefore, it was not possible to use these lines in the behavioral experiment involving spatial learning tests. Heterozygous TSPOKO X ArcA β mice were therefore employed as they were healthy and did not exhibit any behavioral abnormalities. Additionally, chronic administration of XBD173 to these mice did not improve the cognitive deficit determined by the water cross maze test. This confirmed the role of TSPO protein in the action of XBD173 against the cognitive deficits in the transgenic AD mice model. Further molecular investigation revealed a lower plaque load and soluble A β levels in the cortex, rescued spine density, and increased neurosteroid levels (**Figure 37, 38, 39**). This gives us a mechanistic insight into how TSPO-dependent XBD173 acts against pathophysiology in AD. Previous reports indicate a shift in the microglial polarisation state from M2 anti-inflammatory microglia to M1 proinflammatory microglia in Alzheimer's [31,32]. In our study, after incubation of hippocampal slices with 50 nM we observed an increase in the proinflammatory cytokine as well as anti-inflammatory cytokines. This, however, is in contrast to the previous studies which show a reduction in antiinflammatory cytokines in AD [31,32]. This could be because of a lower incubation time and the ex vivo setup. XBD173 pretreatment however did not affect these elevated levels of proinflammatory microglial state, which indicates either that 60 min incubation time isn't sufficient for XBD173 to show action on microglial states or XBD173 treatment doesn't alter microglial signaling states (**Figure 40**). It was interesting to note that XBD173 influences a variety of neurosteroids including Allopregnanolone, 3 β 5 α THDOC, and DHDOC. Additionally, XBD173 treatment reduced the aberrant loss of functional synapses by the astrocytes. The central nervous system (CNS) is subject to network disruption when functional synapses are lost due to injury or neurodegeneration as in AD. Taken together, XBD173 provides neuroprotection in a rodent model of AD by interfering with its pathophysiological mechanism.

The functional role and the location of TSPO make it an excellent target in AD. Previously mitochondrial cholesterol has been shown to increase the generation of toxic A β [401–403] by promoting the amyloidogenic processing of APP by β -secretase and γ -secretase [404]. Despite the fact that mitochondria do not synthesize glutathione (GSH), mitochondrial GSH (mGSH) originates from the transport of cytosolic GSH to mitochondria [405]. This pool of mGSH forms an essential antioxidant defense and is therefore crucial in AD pathology, where mitochondria are

susceptible to oxidative stress [406–408]. However, the transport of cytosolic GSH to mitochondria is impaired due to cholesterol-mediated changes in the membrane. This suggests therefore that the mitochondrial cholesterol accumulation in AD forms a crucial point that determines the pathophysiology of AD via the generation of toxic A β as well as increases the susceptibility due to depletion of the mGSH pool [404]. Additionally, increased cholesterol levels have been shown in brain tissue samples obtained from AD [404,409]. Given the role of TSPO in transporting the cholesterol from the outer to the inner mitochondrial membrane, it is possible that TSPO ligand XBD173 increases this transfer of cholesterol to synthesize neurosteroids. This would therefore reduce the excess accumulation of cholesterol and prevent the depletion of the mGSH pool thereby strengthening the antioxidant defense against mitochondrial stress in AD. The increase in neurosteroid levels in XBD173-treated animals indicates more processing of cholesterol (**Figure 54**).

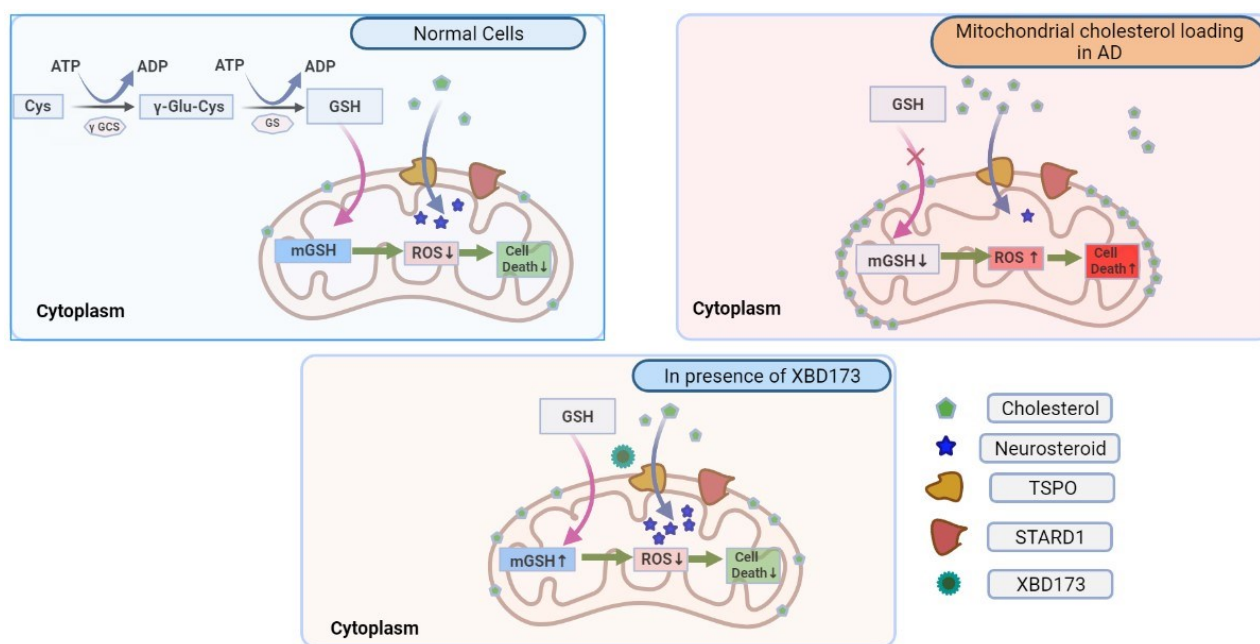


Figure 54: Mitochondrial cholesterol loading in AD and the possible effect of XBD173 on it.

A. Under physiological conditions, cytoplasmic GSH is imported to mitochondria resulting in the formation of mGSH which helps to keep a check on mitochondrial ROS as well as prevents cell death. B. In AD, due to excessive loading of cholesterol, the transport of GSH is halted resulting in increased ROS levels and thereby impacting the mitochondrial health. C. XBD173 as shown in our experiments increased the neurosteroid levels. It is possible that in the AD model, the application of XBD173 reduces the cholesterol

load by converting them into neurosteroids thereby leading to reduced ROS and subsequently improving the mitochondrial health (Created using BioRender.com).

4.3 The role of XBD173 in ameliorating the energy imbalance in the AD pathology

Alzheimer's disease being a multifaceted neurodegenerative disease has different pathophysiological mechanisms that are being targeted by the therapeutics developed around the world. Focusing on the individual mechanisms is essential, but it's also important to look at the big picture of energy homeostasis, which is impaired in Alzheimer's. If we think of our body as a machine, the brain as an individual part uses up more fuel than the rest of the body parts to maintain and regulate the structural and functional balance. We would therefore in detail focus on the disturbances in energy homeostasis in AD and how TSPO-dependent XBD173 could be an effective therapeutic dealing with the energy disturbance in AD. Compared to other neurons, the ones in the hippocampus need relatively higher energy to support and maintain structural and functional integrity [410]. In a physiological state, the blood-brain barrier (BBB) preserves the vascular structure and the glial cells act as the surveillance system by communicating with neurons and smooth vascular muscles [410]. During synaptic transmission, based on glutamate and Na^+/K^+ ion concentration, glial cells regulate the calcium dynamics by sensing neural activity. To maintain functional integrity (synaptic transmission, ion regulation, firing pattern, protein degradation), neurons essentially depend upon oxidative phosphorylation to meet their energy needs [410]. This ensures a smooth homeostatic energy balance and improves the survivability of the neurons. In AD, however, this entire homeostatic regulation is disturbed leading to increased energy demands and therefore leading to the energy crisis. This energy deficit and impairment in AD and the role of TSPO in stabilizing the energy state are discussed below.

The pathological effect of AD on the glutamatergic and GABAergic system homeostasis constitutes one of the primary mediators of the energy crisis. Glutamate neurotransmission disturbance has been long studied and considered a key regulatory step behind the progressive pathology of AD [39]. Chronic excitotoxicity, often associated with AD is the chronic mild activation of the NMDA receptors until ultimate neuronal cell death [42]. Different pathological factors such as soluble $\text{A}\beta$, $\text{A}\beta$ deposition in plaques, neurofibrillary tangles, and mitochondrial

dysfunction have been previously associated with the enhanced sensitivity/response of the glutamate receptors [39]. Glutamate concentrations are in the micromolar range under the physiological state (except for the transient phase during the synaptic transmission where it could reach the mM range) [42]. The uptake of extracellular glutamate is tightly regulated by the glial cells [411,412]. In AD, however, glutamate uptake and recycling are severely impaired. For instance, previous studies have shown a reduction in the glutamate transport capacity, selective loss of vesicular glutamate transporter (VGluT), and protein expression in the frontal/temporal cortex of AD patients [413,414]. Similarly, excitatory amino acid transporter (EAAT2) in perisynaptic astrocytes is reported to have a greater splice variant with reduced functionality in AD [415]. The NMDA receptor owing to its both receptor as well as ligand-gated properties plays a crucial role in synaptic plasticity. The voltage-gated role of the NMDA receptor however becomes its weakness in AD [42,416]. The physiological A β precursor protein (APP) and A β peptide have opposing roles on glutamate uptake as well as the NMDA receptors. While APP has an antagonistic effect on the NMDA receptors and decreases the glutamate from the synaptic cleft, when it is falsely processed to A β , A β has an agonistic effect on the NMDA receptors and also increases the glutamate in the synaptic cleft by impairing the glutamate uptake and recycling [42,416]. The additional evidence of A β oligomers coimmunoprecipitating with the GluN2B and GluN1 subunits indicates a direct effect of the oligomers on the pathological disturbances of NMDA receptors [417].

Both Mg²⁺ ion blockade in NMDA receptors and its high sensitivity to membrane depolarization are of clinical relevance to the energy crisis in AD [418,419]. Under resting conditions at -70 mV, Mg²⁺ ion blockade acts as a filter for the NMDA receptor and guards the unwanted background Ca²⁺ signals that would otherwise pass through the NMDA receptors. However, in AD pathophysiology owing to the voltage change-dependence, Mg²⁺ ion blockade is easily removed due to the moderately prolonged depolarization during chronic excitotoxicity at -50 mV. This, therefore, leads to a prolonged influx of Ca²⁺ ions which adds significantly to the background noise [42,416]. In normal conditions, the synaptic plasticity/learning depends upon the detection of a signal (Transient influx of Ca²⁺ after HFS) from noise (low levels of background signal). This is referred to as the signal-to-noise hypothesis in synaptic plasticity (**Figure 55**). According to the signal-to-noise hypothesis, in AD, the filtering role of Mg²⁺ ions is impaired due to prolonged

overactive glutamatergic activation. The increased background noise from the prolonged influx of Ca^{2+} ions impairs the ability to detect the signal from the presynaptic membrane affecting the plasticity/learning in AD [42,416] (**Figure 56**). Also, the continuous activation of the glutamatergic system increases the energy demand of the system. Apart from this, the prolonged influx of Ca^{2+} ions activates downstream secondary messengers which require energy in the form of ATP [420]. All these additional processes and the downstream channeling combined with the chronic activation of the NMDA receptors enhance the energy demand leading to the energy crisis in AD. Downtuning the noise from the glutamatergic system could therefore provide an effective therapeutic response and enhance the detection of signals from the transient background noise from Ca^{2+} ions. Previously, extrasynaptic GABA_A receptors have been shown to antagonize the over-activation of NMDA receptors on pyramidal cells [421]. The δ subunit-containing GABA_A receptors play a predominant role in exerting this tonic inhibition [422,423]. While neuroactive steroids have long been considered as positive allosteric modulators (PAM) of the GABA_A receptors, a recent study by Parakala *et. al.* shows that apart from acting as the PAM of the GABA_A receptors, neurosteroids such as allopregnanolone can exhibit potential metabotropic effect via the activation of metabotropic progesterone receptors (mPRs) [424]. This metabotropic activation is achieved by promoting the phosphorylation of Ser-408/409 in the $\beta 3$ subunit and this results in strong tonic inhibition [424]. From our study, the XBD173 which exerts a TSPO-dependent neuroprotective effect on LTP requires the δ subunit-containing GABA_A receptors. One possible mechanism by which XBD173 manages the energy crisis in an AD-like state could be via downtuning of the prolonged activation of NMDA receptors during chronic excitotoxicity resulting from $\text{A}\beta_{1-42}$ oligomers via inhibition from δ subunit-containing GABA_A receptors. This would be the primary step to revert the imbalanced energy homeostasis. TSPO ligands have previously been shown to boost mitochondrial function by regulating mitochondrial ROS generation, mitochondria membrane potential (MMP), and adenosine triphosphate (ATP) production. Additionally, they protect against oxidative stress, induce the production of neurosteroids, improve cell bioenergetics, and reduce ROS and $\text{A}\beta$ levels [271,425,426]. All these pieces of evidence from previous reports as well as from our study indicate that TSPO-dependent XBD173 balances the disturbances in energy homeostasis.

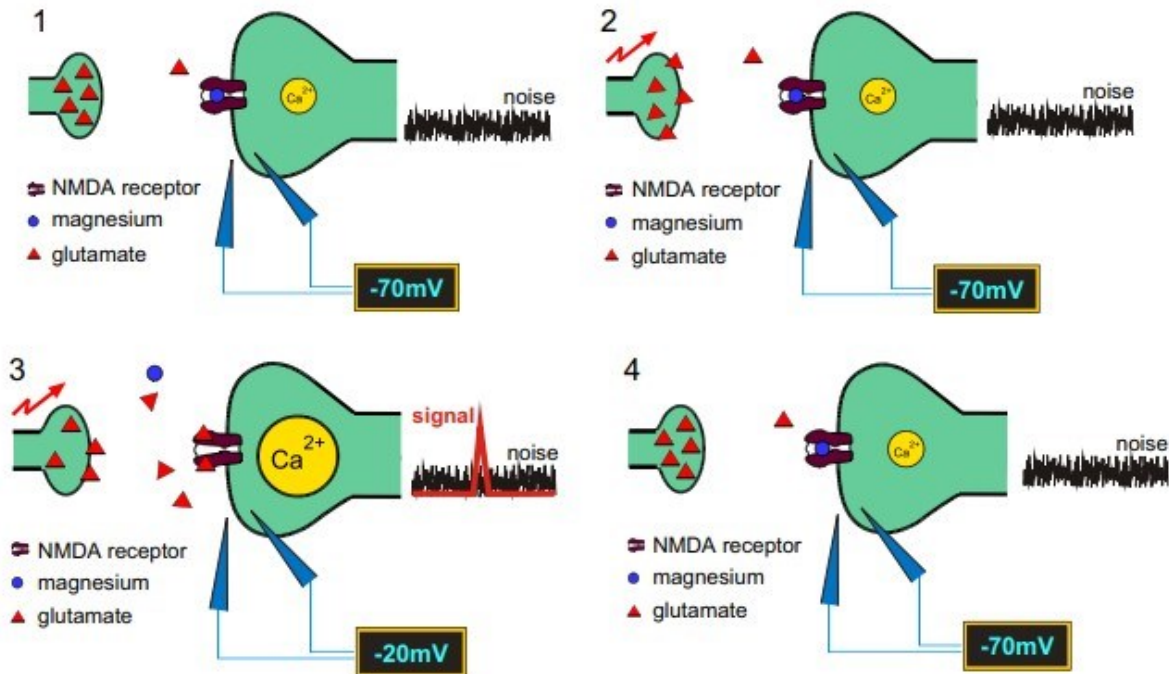


Figure 55: Synaptic plasticity model in physiological conditions (Adapted with permission from [416]).

In the physiological state, learning is dependent upon the filtering of relevant signals from the background noise in the form of intracellular Ca^{2+} levels. The arrival of a presynaptic signal is indicated by a jagged red arrow. Glutamate and Mg^{2+} are shown in red triangles and blue circles, respectively.

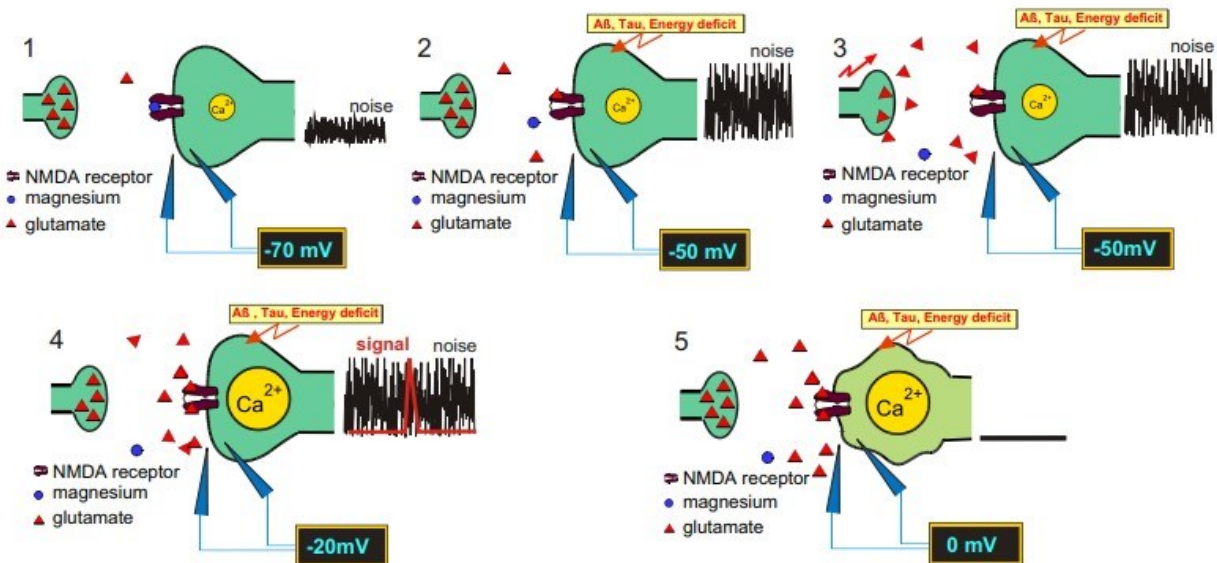


Figure 56: Synaptic plasticity model in AD-related pathology (Adapted with permission from [416]).

In AD due to an overactive glutamatergic system, the Mg^{2+} block is unable to play its filtering role, thereby impairing the detection of relevant signal from the background noise.

The second important energy demand arises due to the process of synaptic pruning. Adult neurons during maturation undergo a series of pruning of unwanted connections to develop functional synapses. From one perspective removal of unwanted synapses removes irrelevant neurons participating in the process of signal transmission, thereby saving energy. However, this process of pruning by the glial cells requires energy. Recent studies have clearly shown that astrocytes mediate synapse elimination in an ATP-dependent manner by activating the purinergic signaling pathway [427]. It is therefore this delicate play between energy balance that in a physiological state orchestrates the process of neuron maturation and development of functional synapses. This balance is also disturbed in a pathological state of AD. The aberrant increase in functional synapse elimination by astrocytes/microglia requires energy and this further adds to the pool of energy crisis in Alzheimer's. As observed from our study, the astrocytic engulfment of synaptic materials highly increases in an AD model of the mouse, and this astrocytic phagocytosis is significantly reduced in the transgenic mice administered with XBD173. As has been previously discussed before, TSPO upregulation in astrocytes precedes much before TSPO upregulation in microglia in the hippocampus [428]. Therefore, the second possible mechanism in which TSPO-dependent XBD173 restores/rescues the energy imbalance is via reduced astrocytic phagocytosis of synaptic material.

The astrocytes, are mostly electrically non-excitabile cells and use Ca^{2+} signals as the language to communicate with the neurons [429]. G Protein-coupled receptors (GPCRs) which activate Inositol phosphate 3 (IP3) via Phospholipase C induce the release of Ca^{2+} from the endoplasmic reticulum into the cytoplasm [430]. Astrocytic factors are known to regulate both inhibitory as well as excitatory transmissions [296]. For instance, during signal transmission enhanced intracellular Ca^{2+} by neuronal synapses, activates glutamate exocytosis by astrocytes as well as the glutamate receptors on the synaptic membrane [431]. This glutamate exocytosis can then activate the presynaptic NMDA receptors to increase Ca^{2+} levels to regulate excitatory synaptic transmission [432]. From previous studies, we know LTP can be induced in CA1, CA3, and the dentate gyrus of the hippocampus [433]. While LTP in the CA3 region is dependent on the

activation of mGlu1 receptors, the LTP in the CA1 region is dependent on mGlu5 receptors [434–436]. These mGlu5 receptors are richly distributed in astrocytes [429]. Interestingly, NMDA receptor activation doesn't only depend upon glutamate but also depends on D-serine which acts as a co-agonist for the activation of NMDA receptors [437]. The D-serine regulation of synaptic plasticity is also dependent upon the Ca^{2+} levels. During signal transmission/high-frequency stimulation, repeated synaptic activity enhances the free Ca^{2+} levels in astrocytes which in turn increases the D-serine production thereby inducing NMDA-dependent LTP [429,438,439]. Additionally, H1 receptors in the hippocampal CA1 region promote NMDA activity and enhance LTP in response to astrocytic activation [440]. Another cluster of receptors, protease-activated receptor 1 (PAR1), present in the astrocytes in the CA1 region of the hippocampus also regulates the Ca^{2+} release via activation of glutamate permeable anion channel Best1 [441]. All these taken together make a clear point of astrocytes regulating the glutamatergic signals and impacting NMDA-regulated LTP in the CA1 hippocampus. Similarly, with regard to the inhibitory transmissions, astrocytes are known to express GAT1 and GAT3 (GABA transporters) and can increase the GABA-mediated currents through Ca^{2+} signaling. This process of synaptic inhibition is potentiated by the GABA_A receptors which involve modulation from the astrocytic GABA_B receptors [429]. As discussed earlier in this section of energy homeostasis, the signal-to-noise ratio assumes a transient prolonged release of Ca^{2+} in AD pathology, which enhances the noise from the NMDA activation thereby impairing the detection of the signal during the plasticity and that TSPO-dependent XBD173 could directly down tune the NMDA mediated noise. One could therefore now speculate that this down tuning/reduction of noise during the plasticity or LTP caused by XBD173 could involve the signaling between the glutamatergic and GABAergic systems via astrocytes.

4.4 Complement Protein C1q Deposits and their Involvement in AD

Complement proteins such as C1q and C3 which in a normal physiological state associate with the glial cells for the pruning of synapses, during the maturation and synapse formation are aberrantly activated in AD. MEGF10 and MERTK are considered to be the essential phagocytic receptors for astrocytes [339,352]. MEGF10 acts as an astrocytic receptor for the eat-me tag C1q proteins on the neurons to be phagocytosed [350]. Previously, it has been shown that inhibition of C1q, C3, or

the microglial receptor CR3 can rescue early synaptic loss in AD [442]. Similarly, the absence of C1q in the knockout models has been associated with fewer pathophysiological effects in AD transgenic mice [443]. Increased colocalization of complement proteins C1q, C3, and C4 with the amyloid plaques has been observed in the postmortem brains obtained from AD patients [444]. Very recently Luchena *et al.* developed an in vitro triple co-culture media of neurons, astrocytes, and microglia and showed cross-communication between the glial cells and how they influence synapse loss via the complement pathway. The reciprocal signaling between the astrocytes and microglia is facilitated by C3. The oligomeric A β when added to this triple coculture system increased microglial CD11b and induced synapse loss [445]. The dysfunction of the complement system therefore could be linked to the severe pathophysiology of AD. This is evident from the study, which suggests C1q could be an essential component that drives the neurotoxic effect of the soluble A β oligomers on the hippocampal LTP [442,446]. A β_{1-42} has also been shown to directly activate the complement pathway by binding to the globular domain of C1q [447].

Reduced or deficient complement protein transgenic animal models have shown faster signs of recovery as well as are associated with fewer pathological symptoms [448]. For instance, C3 gene-deficient mice show fast nerve injury recovery [449]. Similarly, transgenic AD mice (Tg2576 mice) crossed with homozygous C1q KO mice consisted significantly lower amount of activated microglia compared to the transgenic counterparts indicating a lowered glial response in the absence of complement proteins [443]. On a similar note, in the J20 (AD transgenic) mouse brains, C1q immunoreactivity is significantly elevated specifically in the hippocampus and the frontal cortex [442]. In the same study, the administration of compound E (γ secretase inhibitor) reduced the soluble A β levels and also reduced the C1q deposition levels in the J20 mice. Interestingly, oligomeric A β when injected into WT mice increased the association of C1q with a postsynaptic marker indicating an increase in synapse engulfment [442]. All of these studies when combined give us a clear conjugation between complement proteins, C1q and A β . C1q-mediated complement pathway activated by the A β peptide acts in a positive vicious cycle to trigger the pathophysiology in AD. Anti-C1q antibody treatment improves the LTP impairment caused by the oligomeric A β [442]. Also, the deletion of C1q reduces astrocyte-synapse association which causes a decreased astrocytic synaptic engulfment, thereby rescuing the synaptic density [376]. Apart from C1q, other complement proteins are also associated with Alzheimer's pathophysiology. CX3CR and C3 are

among the other studied complement proteins in Alzheimer's disease [450,451]. Results from the current study revealed that astrocyte engulfment of C1q is enhanced in the hippocampus and the cortex of Alzheimer-modelled transgenic ArcA β mice-which likely explains the loss of functional synapses and cognitive impairment as seen from spatial learning text. XBD173 treatment decreases this aberrantly enhanced C1q engulfment in hippocampal astrocytes, thus reducing abnormal synaptic loss. The findings and prior studies suggest that C1q serves as a feasible target for developing drugs to treat AD. As C1q is upstream to C3 and its complex with a cleaved product of C3 serves as a eat me signal for eliminating synapses, targeting it could affect not only the pro-inflammatory state of glial cells but also communication between the glial cell [339,448]. It is also interesting to note the increasing pattern of synaptic engulfment of presynaptic materials (synaptophysin) and C1q in AD transgenic mice in both the cortex and hippocampus. Since C1q are considered as the "eat-me tags" for synapses one could in a retrospective view align the increase in astrocytic phagocytosis of both synapses and C1q. This also aligns with the previous study which shows that preventing the localization of C1q to the synapses was sufficient to prevent synaptic engulfment [339,442,448].

Interestingly, we also report the deposition of C1q in the form of distinct aggregates heavily in the cortex of transgenic Alzheimer's mice (**Figure 45**). There is a high overlap between these C1q aggregates and the amyloid β plaques. Although reports of colocalization of amyloid plaques with C1q of the complement pathway are scarce, Johnson et. al., show colocalization between amyloid β protein and C3 complement protein within substructural domains of drusen [452]. Amyloid plaques and dead cells in the AD brain have also been reported to colocalize with C4 binding protein as well as factor H of the complement pathway [453]. As a result, the formation of the aggregates could be explained retrospectively by dystrophic neurite deposition or neurofibrillary tangles. C1q aggregates do overlap with amyloid plaques, but not all plaques overlap with these C1q aggregates. First of all, this might give us an overview of/the role of complement-mediated inflammation in Alzheimer's disease pathophysiology. Second, it might act as a diagnostic marker for amyloid plaques. In the cortex region of animals treated with XBD173, the number of C1q aggregates is significantly reduced irrespective of the percentage of colocalization between C1q aggregates and amyloid plaques. The results of this study, coupled with what we know about the complement pathway, suggest that C1q plays an important role in the pathogenesis of Alzheimer's

disease. The reason why only a part of the amyloid plaque overlaps with C1q aggregates remains unclear. It needs to be further investigated whether the presence of complement proteins (C1q aggregates) in the plaques influences the severe pathological symptom development of AD. In addition to these results, it is also important to consider an important hypothesis that has been long considered in the field. It is often hypothesized that the amyloid plaque could sequester or buffer the soluble A β to reduce their toxic potentiality [454]. From our study, the deposition of C1q aggregates and their close association with the amyloid plaques suggest the interaction of C1q deposits with the soluble A β . Whether this interaction furthers the pathophysiology or confers the protection as a compensatory mechanism, needs to be studied.

4.5 Clinical relevance of TSPO-dependent XBD173 in AD and peri-operative anesthesia

Benzodiazepines which have been extensively used as anxiolytics in peri-operative anesthesia are associated with several side effects among which are anterograde amnesia, withdrawal symptoms, tolerance effect, impaired coordination, and muscle weakness [234]. While both benzodiazepines and neurosteroids (3 α reduced) are positive allosteric modulators of GABA_A receptors, the binding site of benzodiazepines is characterized by the composition of the α subunits whereas neurosteroids binding mostly occurs at the interfaces of the β subunit [244,455]. Another notable difference between the mechanism of action of benzodiazepines and neurosteroids is that benzodiazepines are sensitive to γ 2 subunit-containing GABA_A receptors whereas neurosteroids are sensitive to the δ subunit-containing GABA_A receptors [235,274]. Both these factors contribute to the significant differences in the pharmacological profile of benzodiazepines and neurosteroids. In our study, we clearly show the association of XBD173 with TSPO protein in mediating the neuroprotective role in AD. The important association of TSPO with the regulation of neurosteroids assigns TSPO ligands a key role as anxiolytics with a different pharmacological profile as compared to benzodiazepines.

In the previous study, selective and high-affinity TSPO ligand XBD173 was shown to exert a rapid anxiolytic effect in animals and humans without the side-effect profile of benzodiazepines [228]. In this study, we show that XBD173 is also neuroprotective in Alzheimer's, which opens up its

usage in dementia as an alternative to benzodiazepines in perioperative anesthesia. Previous reports have also suggested a similar neuroprotective role of TSPO ligands in several neurodegenerative diseases including the MPTP model of Parkinson's, multiple sclerosis, Huntington's, schizophrenia, and an autism spectrum disorder (discussed in the Introduction section). However, our study contradicts one of the recent reports from *Shi et al.*, which suggests that TSPO ligands could alter synaptic plasticity and cause cognitive impairments [456]. The difference in the conditions of both studies could be responsible for this. As mentioned before, in AD cases, the XBD173 can reduce excessive glutamate noise through GABA_A receptors with a delta subunit, allowing for improved plasticity and learning. Conversely, when used physiologically, this could cause an imbalance between glutamate and GABA systems' homeostasis which would ultimately affect plasticity negatively. This is consistent with our findings of lower accuracy in wild-type mice treated with XBD173 than the untreated ones in Retest 2 (though not significant; data not shown). Second, the drug dose and schedule difference between both studies could partially be responsible for this difference. *Shi et al.* used a higher dose concentration of XBD173 (5 mg/kg) whereas in our study we used XBD173 (1 mg/kg) every alternate day [456]. The important message from both these studies, therefore, suggests that both hypo- and hyper-activation of the glutamatergic system can cause neuronal dysfunction and a subtle balance is needed while studying AD. Additionally, *Shi et al.* also observed that XBD173 at 5mg/kg reduces the number of the spine. In our study, we found out that XBD173 applied at 1mg/kg to AD-modeled mice restores spine loss and improves cognitive performance in AD-transgenic mice. Both drug concentration differences as well as the pathological conditions as described above could be responsible for this difference. Keeping in mind the above message, XBD173 at the relevant dose can be a great alternative to benzodiazepines, in perioperative anesthesia (**Figure 57**).

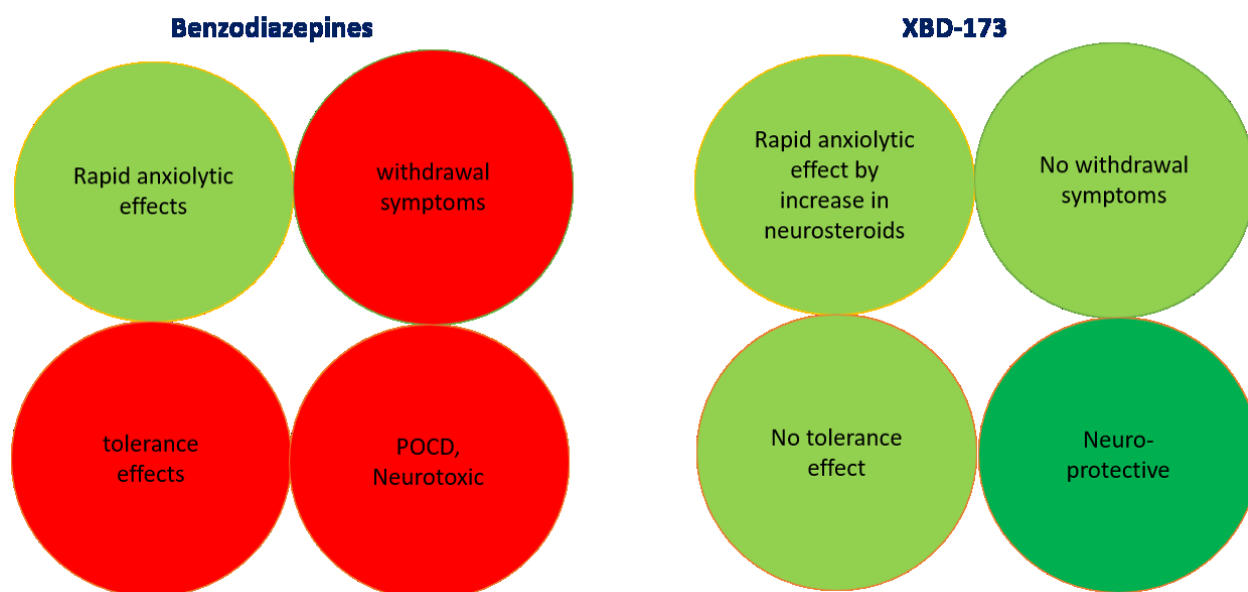


Figure 57: Comparison of side-effect profile of Benzodiazepines and XBD173 [228].

4.6 Limitations of the Study and future perspectives

In this study, we have studied the effect of TSPO protein activation in a pathological Alzheimer's mouse model system. This study while conclusively providing evidence for the neuroprotective role of XBD173 in Alzheimer's disease and also highlighting important mechanisms as to how it provides this protection has certain limitations which need to be discussed before interpreting its results in a clinical setup and as a therapeutics.

1. The ArcA β mice model used in the study while recapitulating some of the major hallmark features of AD such as cognitive impairment, plaque formation, or reactive gliosis lacks another key feature of AD i.e., the presence of neurofibrillary tangles. Therefore, there needs to be further clinical testing in humans.
2. XBD173 as has already been discussed provides anxiolytic effects both in humans and animals. Therefore, one could easily misconceive the anxiolytic effect of XBD173 behind the better behavioral performance of mice that are treated with XBD173 in the water cross maze. While it is not possible to dissect the anxiolytic effect from the betterment of cognitive performance, we have a few arguments to support the latter. First, retests 1 and

- 2 (a week and a month later), were designed to see if the effects of XBD173 on cognition are long-term even after termination of the respective treatment. Since we see these protective benefits even after 45 days of termination of the treatment, it is fair to say that these effects are more neuroprotective. Second, we establish the protective benefits of XBD173 in preventing the A β induced LTP impairment in the CA1 region of the hippocampus. Since LTP is a cellular correlate of learning and memory, we can establish the importance of TSPO-dependent XBD173 in bettering synaptic transmission/plasticity.
3. We faced some major problems while creating the homozygous TSPOKO X ArcA β line. At least one-third of the homozygous transgenic line showed behavioral saliences in the form of epileptic seizures and therefore couldn't be used for the behavioral experiments. We, therefore, had to use the heterozygous TSPOKO X ArcA β mice line. Even with a reduced expression of TSPO, we could see clear differences in the cognitive performances of the animals.

TSPO is a protein that has been long discovered, however, the potentiality of TSPO in neurodegeneration has come to the limelight in recent years. The expression profile of TSPO in neural as well as glial cells makes it an effective target for different pathological interventions. In our study, we show the dependency of XBD173 not only on TSPO but also on the δ subunit-containing GABA $_A$ receptors, which are sensitive to neurosteroids. The positive role of neurosteroids whether in nerve injury or neural disorders has been highlighted in multiple studies. But it is also essential to highlight that activation of TSPO or execution of neuroprotective role by neurosteroids is dependent on different types of neurosteroids. The clinical advantage of using XBD173 is it confers both the anxiolytic effects as well as neuroprotective benefits in dementia, thereby making it an essential therapeutic alternative in perioperative anesthesia in dementia patients. We observed lower plaque load as well as lesser soluble A β , particularly in the cortex and not in the hippocampus. While the region-specific effect could be attributed either to the model system used for AD or differential action of TSPO activation in the different brain regions, we could not find differences in phagocytic removal of plaques by astrocytes between both transgenic groups treated either with XBD173 or with the vehicle. This hints either to lesser production of A β or involvement of microglia in clearing up the plaque load in the XBD173 treated animals. Further research needs to be done to study this. Another important link that needs to be studied further is the difference in the working mechanisms of different A β oligomers i.e. A β ₁₋₄₂ and A β ₁.

⁴⁰, and the effect of different therapeutic interventions on specific A β oligomers. Finally, from our model targeting overlapping mechanisms in AD by a combinatorial approach might provide higher therapeutic success than targeting individual pathological mechanisms.

This research provides potential avenues for future application in the field of TSPO and Alzheimer's disease. Some of these are listed as follows. First, the study provides a direction in exploring the TSPO ligands for their concentration-dependent neuroprotective benefits in other neurodisorders as well as nerve damage/injury. Second, the C1q aggregate composition as well as their potential usage as a biomarker in AD can be studied in association with their role in further aggravating the AD pathology. Third, the impact of TSPO ligands on the amyloidogenic/non-amyloidogenic processing of APP needs further attention to conclusively determine whether there is an impact on A β production machinery. Fourth, given the structural placement and functional role of TSPO, one could explore the role of TSPO ligands on mitochondrial energetics in a pathological scenario. Fifth, given that TSPO ligands affect the excessive aberrant synapse pruning by the astrocytes, one could explore if they potentially affect/impact the astrocytic calcium signaling. Lastly, since phosphorylated tau is another crucial hallmark of AD and is also clinically correlated with cognitive decline, it would be interesting to understand the impact of TSPO ligands on tau-mediated neuronal damage in AD.

5. References

1. World Health Organization . Geneva, S. World Health Organization; 2021. Fact Sheets of Dementia [Internet].
2. The Alzheimer’s Association: <https://www.alz.org/alzheimers-dementia/facts-figures>.
3. Dementia Statistics | Alzheimer’s Disease International (ADI). <https://www.alzint.org/about/dementia-facts-figures/dementia-statistics/>.
4. Alzheimer, A. Uber Eigenartige Erkrankung Der Hirnrinde. *All Z Psychiatr* **1907**, *64*, 146–148.
5. DeTure, M.A.; Dickson, D.W. The Neuropathological Diagnosis of Alzheimer’s Disease. *Mol. Neurodegener.* **2019**, *14*, 1–18.
6. Perl, D.P. Neuropathology of Alzheimer’s Disease. *Mt. Sinai J. Med. A J. Transl. Pers. Med. A J. Transl. Pers. Med.* **2010**, *77*, 32–42.
7. Rami, L.; Sala-Llonch, R.; Solé-Padullés, C.; Fortea, J.; Olives, J.; Lladó, A.; Pena-Gómez, C.; Balasa, M.; Bosch, B.; Antonell, A. Distinct Functional Activity of the Precuneus and Posterior Cingulate Cortex during Encoding in the Preclinical Stage of Alzheimer’s Disease. *J. Alzheimer’s Dis.* **2012**, *31*, 517–526.
8. Zhou, J.; Greicius, M.D.; Gennatas, E.D.; Growdon, M.E.; Jang, J.Y.; Rabinovici, G.D.; Kramer, J.H.; Weiner, M.; Miller, B.L.; Seeley, W.W. Divergent Network Connectivity Changes in Behavioural Variant Frontotemporal Dementia and Alzheimer’s Disease. *Brain* **2010**, *133*, 1352–1367.
9. Apostolova, L.G.; Green, A.E.; Babakchanian, S.; Hwang, K.S.; Chou, Y.-Y.; Toga, A.W.; Thompson, P.M. Hippocampal Atrophy and Ventricular Enlargement in Normal Aging, Mild Cognitive Impairment and Alzheimer’s Disease. *Alzheimer Dis. Assoc. Disord.* **2012**, *26*, 17.
10. Serrano-Pozo, A.; Frosch, M.P.; Masliah, E.; Hyman, B.T. Neuropathological Alterations in Alzheimer Disease. *Cold Spring Harb. Perspect. Med.* **2011**, *1*, a006189.

11. Liu, X.; Liu, Y.; Ji, S. Secretases Related to Amyloid Precursor Protein Processing. *Membranes (Basel)*. **2021**, *11*, 983.
12. Gu, L.; Guo, Z. Alzheimer's A β 42 and A β 40 Peptides Form Interlaced Amyloid Fibrils. *J. Neurochem.* **2013**, *126*, 305–311.
13. Thal, D.R.; Capetillo-Zarate, E.; Del Tredici, K.; Braak, H. The Development of Amyloid β Protein Deposits in the Aged Brain. *Sci. aging Knowl. Environ.* **2006**, *2006*, re1–re1.
14. Yamaguchi, H.; Hirai, S.; Morimatsu, M.; Shoji, M.; Harigaya, Y. Diffuse Type of Senile Plaques in the Brains of Alzheimer-Type Dementia. *Acta Neuropathol.* **1988**, *77*, 113–119.
15. Davies, C.A.; Mann, D.M. Is the "Preamyloid" of Diffuse Plaques in Alzheimer's Disease Really Nonfibrillar? *Am. J. Pathol.* **1993**, *143*, 1594.
16. Yasuhara, O.; Kawamata, T.; Aimi, Y.; McGeer, E.G.; McGeer, P.L. Two Types of Dystrophic Neurites in Senile Plaques of Alzheimer Disease and Elderly Non-Demented Cases. *Neurosci. Lett.* **1994**, *171*, 73–76.
17. Braak, H.; Braak, E. Frequency of Stages of Alzheimer-Related Lesions in Different Age Categories. *Neurobiol. Aging* **1997**, *18*, 351–357.
18. Furcila, D.; Domínguez-Álvaro, M.; DeFelipe, J.; Alonso-Nanclares, L. Subregional Density of Neurons, Neurofibrillary Tangles and Amyloid Plaques in the Hippocampus of Patients with Alzheimer's Disease. *Front. Neuroanat.* **2019**, 99.
19. Biffi, A.; Greenberg, S.M. Cerebral Amyloid Angiopathy: A Systematic Review. *J. Clin. Neurol.* **2011**, *7*, 1–9.
20. Alzheimer, A.; Stelzmann, R.A.; Schnitzlein, H.N.; Murtagh, F.R. An English Translation of Alzheimer's 1907 Paper, "Uber Eine Eigenartige Erkankung Der Hirnrinde". *Clin. Anat. (New York, NY)* **1995**, *8*, 429–431.
21. Kidd, M. Paired Helical Filaments in Electron Microscopy of Alzheimer's Disease. *Nature* **1963**, *197*, 192–193.
22. Alonso, A. del C.; Zaidi, T.; Grundke-Iqbal, I.; Iqbal, K. Role of Abnormally

- Phosphorylated Tau in the Breakdown of Microtubules in Alzheimer Disease. *Proc. Natl. Acad. Sci.* **1994**, *91*, 5562–5566.
23. Grieco, S.F.; Holmes, T.C.; Xu, X. Probing Neural Circuit Mechanisms in Alzheimer's Disease Using Novel Technologies. *Mol. Psychiatry* **2023**, 1–14.
 24. Jagust, W. Imaging the Evolution and Pathophysiology of Alzheimer Disease. *Nat. Rev. Neurosci.* **2018**, *19*, 687–700.
 25. Gordon, B.A.; Blazey, T.M.; Su, Y.; Hari-Raj, A.; Dincer, A.; Flores, S.; Christensen, J.; McDade, E.; Wang, G.; Xiong, C. Spatial Patterns of Neuroimaging Biomarker Change in Individuals from Families with Autosomal Dominant Alzheimer's Disease: A Longitudinal Study. *Lancet Neurol.* **2018**, *17*, 241–250.
 26. Hirano, A.; Dembitzer, H.M.; Kurland, L.T.; Zimmerman, H.M. The Fine Structure of Some Intraganglionic Alterations: Neurofibrillary Tangles, Granulovacuolar Bodies and “Rod-like” Structures as Seen in Guam Amyotrophic Lateral Sclerosis and Parkinsonism-Dementia Complex. *J. Neuropathol. Exp. Neurol.* **1968**, *27*, 167–182.
 27. Funk, K.E.; Mrak, R.E.; Kuret, J. Granulovacuolar Degeneration (GVD) Bodies of Alzheimer's Disease (AD) Resemble Late-stage Autophagic Organelles. *Neuropathol. Appl. Neurobiol.* **2011**, *37*, 295–306.
 28. Vainchtein, I.D.; Molofsky, A. V Astrocytes and Microglia: In Sickness and in Health. *Trends Neurosci.* **2020**, *43*, 144–154.
 29. Di Benedetto, G.; Burgaletto, C.; Bellanca, C.M.; Munafò, A.; Bernardini, R.; Cantarella, G. Role of Microglia and Astrocytes in Alzheimer's Disease: From Neuroinflammation to Ca²⁺ Homeostasis Dysregulation. *Cells* **2022**, *11*, 2728.
 30. Lee, C.Y.D.; Landreth, G.E. The Role of Microglia in Amyloid Clearance from the AD Brain. *J. Neural Transm.* **2010**, *117*, 949–960.
 31. Guo, S.; Wang, H.; Yin, Y. Microglia Polarization from M1 to M2 in Neurodegenerative Diseases. *Front. Aging Neurosci.* **2022**, *14*.

32. Wang, Q.; Yao, H.; Liu, W.; Ya, B.; Cheng, H.; Xing, Z.; Wu, Y. Microglia Polarization in Alzheimer's Disease: Mechanisms and a Potential Therapeutic Target. *Front. Aging Neurosci.* **2021**, *13*.
33. Zheng, H.; Cheng, B.; Li, Y.; Li, X.; Chen, X.; Zhang, Y. TREM2 in Alzheimer's Disease: Microglial Survival and Energy Metabolism. *Front. Aging Neurosci.* **2018**, *10*, 395.
34. Subramanian, J.; Savage, J.C.; Tremblay, M.-È. Synaptic Loss in Alzheimer's Disease: Mechanistic Insights Provided by Two-Photon in Vivo Imaging of Transgenic Mouse Models. *Front. Cell. Neurosci.* **2020**, *14*, 445.
35. Colom-Cadena, M.; Spires-Jones, T.; Zetterberg, H.; Blennow, K.; Caggiano, A.; DeKosky, S.T.; Fillit, H.; Harrison, J.E.; Schneider, L.S.; Scheltens, P. The Clinical Promise of Biomarkers of Synapse Damage or Loss in Alzheimer's Disease. *Alzheimers. Res. Ther.* **2020**, *12*, 1–12.
36. Schousboe, A.; Scafidi, S.; Bak, L.K.; Waagepetersen, H.S.; McKenna, M.C. Glutamate Metabolism in the Brain Focusing on Astrocytes. *Glutamate ATP Interface Metab. Signal. Brain* **2014**, 13–30.
37. Newcomer, J.W.; Farber, N.B.; Olney, J.W. NMDA Receptor Function, Memory, and Brain Aging. *Dialogues Clin. Neurosci.* **2022**.
38. Niswender, C.M.; Conn, P.J. Metabotropic Glutamate Receptors: Physiology, Pharmacology, and Disease. *Annu. Rev. Pharmacol. Toxicol.* **2010**, *50*, 295–322.
39. Ju, Y.; Tam, K.Y. Pathological Mechanisms and Therapeutic Strategies for Alzheimer's Disease. *Neural Regen. Res.* **2022**, *17*, 543.
40. Jacob, C.P.; Koutsilieri, E.; Bartl, J.; Neuen-Jacob, E.; Arzberger, T.; Zander, N.; Ravid, R.; Roggendorf, W.; Riederer, P.; Grünblatt, E. Alterations in Expression of Glutamatergic Transporters and Receptors in Sporadic Alzheimer's Disease. *J. Alzheimer's Dis.* **2007**, *11*, 97–116.
41. Rammes, G.; Mattusch, C.; Wulff, M.; Seeser, F.; Kreuzer, M.; Zhu, K.; Deussing, J.M.; Herms, J.; Parsons, C.G. Involvement of GluN2B Subunit Containing N-Methyl-d-

- Aspartate (NMDA) Receptors in Mediating the Acute and Chronic Synaptotoxic Effects of Oligomeric Amyloid-Beta (A β) in Murine Models of Alzheimer's Disease (AD). *Neuropharmacology* **2017**, *123*, 100–115.
42. Danysz, W.; Parsons, C.G. Alzheimer's Disease, B-amyloid, Glutamate, NMDA Receptors and Memantine—Searching for the Connections. *Br. J. Pharmacol.* **2012**, *167*, 324–352.
 43. Smart, T.G.; Stephenson, F.A. A Half Century of γ -Aminobutyric Acid. *Brain Neurosci. Adv.* **2019**, *3*, 2398212819858249.
 44. Sivilotti, L.; Nistri, A. GABA Receptor Mechanisms in the Central Nervous System. *Prog. Neurobiol.* **1991**, *36*, 35–92.
 45. Terunuma, M. Diversity of Structure and Function of GABAB Receptors: A Complexity of GABAB-Mediated Signaling. *Proc. Japan Acad. Ser. B* **2018**, *94*, 390–411.
 46. Missonnier, P.; Prévot, A.; Herrmann, F.R.; Ventura, J.; Padée, A.; Merlo, M.C.G. Disruption of Gamma–Delta Relationship Related to Working Memory Deficits in First-Episode Psychosis. *J. Neural Transm.* **2020**, *127*, 103–115.
 47. Lam, A.D.; Sarkis, R.A.; Pellerin, K.R.; Jing, J.; Dworetzky, B.A.; Hoch, D.B.; Jacobs, C.S.; Lee, J.W.; Weisholtz, D.S.; Zepeda, R. Association of Epileptiform Abnormalities and Seizures in Alzheimer Disease. *Neurology* **2020**, *95*, e2259–e2270.
 48. Xu, Y.; Zhao, M.; Han, Y.; Zhang, H. GABAergic Inhibitory Interneuron Deficits in Alzheimer's Disease: Implications for Treatment. *Front. Neurosci.* **2020**, *14*, 660.
 49. Li, Y.; Sun, H.; Chen, Z.; Xu, H.; Bu, G.; Zheng, H. Implications of GABAergic Neurotransmission in Alzheimer's Disease. *Front. Aging Neurosci.* **2016**, *8*, 31.
 50. Zhang, Q.; Sidorenko, J.; Couvy-Duchesne, B.; Marioni, R.E.; Wright, M.J.; Goate, A.M.; Marcora, E.; Huang, K.; Porter, T.; Laws, S.M. Risk Prediction of Late-Onset Alzheimer's Disease Implies an Oligogenic Architecture. *Nat. Commun.* **2020**, *11*, 4799.
 51. Kim, J.; Basak, J.M.; Holtzman, D.M. The Role of Apolipoprotein E in Alzheimer's Disease. *Neuron* **2009**, *63*, 287–303.

52. Lanoiselée, H.-M.; Nicolas, G.; Wallon, D.; Rovelet-Lecrux, A.; Lacour, M.; Rousseau, S.; Richard, A.-C.; Pasquier, F.; Rollin-Sillaire, A.; Martinaud, O. APP, PSEN1, and PSEN2 Mutations in Early-Onset Alzheimer Disease: A Genetic Screening Study of Familial and Sporadic Cases. *PLoS Med.* **2017**, *14*, e1002270.
53. Bekris, L.M.; Yu, C.-E.; Bird, T.D.; Tsuang, D.W. Genetics of Alzheimer Disease. *J. Geriatr. Psychiatry Neurol.* **2010**, *23*, 213–227.
54. Goate, A.; Chartier-Harlin, M.-C.; Mullan, M.; Brown, J.; Crawford, F.; Fidani, L.; Giuffra, L.; Haynes, A.; Irving, N.; James, L. Segregation of a Missense Mutation in the Amyloid Precursor Protein Gene with Familial Alzheimer's Disease. *Nature* **1991**, *349*, 704–706.
55. Mullan, M. Familial Alzheimer's Disease: Second Gene Locus Located. *BMJ Br. Med. J.* **1992**, *305*, 1108.
56. Higgins, G.A.; Jacobsen, H. Transgenic Mouse Models of Alzheimer's Disease: Phenotype and Application. *Behav. Pharmacol.* **2003**, *14*, 419–438.
57. Barber, R.C. The Genetics of Alzheimer's Disease. *Scientifica (Cairo)*. **2012**, 2012.
58. Misra, A.; Chakrabarti, S.S.; Gambhir, I.S. New Genetic Players in Late-Onset Alzheimer's Disease: Findings of Genome-Wide Association Studies. *Indian J. Med. Res.* **2018**, *148*, 135.
59. Guerreiro, R.; Bras, J. The Age Factor in Alzheimer's Disease. *Genome Med.* **2015**, *7*, 1–3.
60. Vals, K.; Kiivet, R.-A.; Leinsalu, M. Alcohol Consumption, Smoking and Overweight as a Burden for Health Care Services Utilization: A Cross-Sectional Study in Estonia. *BMC Public Health* **2013**, *13*, 1–9.
61. Mazzei, G.; Ikegami, R.; Abolhassani, N.; Haruyama, N.; Sakumi, K.; Saito, T.; Saido, T.C.; Nakabeppu, Y. A High-fat Diet Exacerbates the Alzheimer's Disease Pathology in the Hippocampus of the App NL⁻ F/NL⁻ F Knock-in Mouse Model. *Aging Cell* **2021**, *20*, e13429.
62. Bracko, O.; Vinarcsik, L.K.; Cruz Hernández, J.C.; Ruiz-Urbe, N.E.; Haft-Javaherian, M.;

- Falkenhain, K.; Ramanauskaite, E.M.; Ali, M.; Mohapatra, A.; Swallow, M.A. High Fat Diet Worsens Alzheimer's Disease-Related Behavioral Abnormalities and Neuropathology in APP/PS1 Mice, but Not by Synergistically Decreasing Cerebral Blood Flow. *Sci. Rep.* **2020**, *10*, 1–16.
63. Reitz, C. Alzheimer's Disease and the Amyloid Cascade Hypothesis: A Critical Review. *Int. J. Alzheimer's Dis.* **2012**, *2012*.
64. Murpy, M.; LeVine III, H. Alzheimer's Disease and the β -Amyloid Peptide. *J. Alzheimers Dis* **2010**, *19*, 311–323.
65. Šimić, G.; Babić Leko, M.; Wray, S.; Harrington, C.; Delalle, I.; Jovanov-Milošević, N.; Bažadona, D.; Buée, L.; De Silva, R.; Di Giovanni, G. Tau Protein Hyperphosphorylation and Aggregation in Alzheimer's Disease and Other Tauopathies, and Possible Neuroprotective Strategies. *Biomolecules* **2016**, *6*, 6.
66. Castellani, R.J.; Plascencia-Villa, G.; Perry, G. The Amyloid Cascade and Alzheimer's Disease Therapeutics: Theory versus Observation. *Lab. Investig.* **2019**, *99*, 958–970.
67. Uddin, M.S.; Kabir, M.T.; Rahman, M.S.; Behl, T.; Jeandet, P.; Ashraf, G.M.; Najda, A.; Bin-Jumah, M.N.; El-Seedi, H.R.; Abdel-Daim, M.M. Revisiting the Amyloid Cascade Hypothesis: From Anti-A β Therapeutics to Auspicious New Ways for Alzheimer's Disease. *Int. J. Mol. Sci.* **2020**, *21*, 5858.
68. Davidson, Y.S.; Robinson, A.; Prasher, V.P.; Mann, D.M.A. The Age of Onset and Evolution of Braak Tangle Stage and Thal Amyloid Pathology of Alzheimer's Disease in Individuals with Down Syndrome. *Acta Neuropathol. Commun.* **2018**, *6*, 1–11.
69. Wiseman, F.K.; Pulford, L.J.; Barkus, C.; Liao, F.; Portelius, E.; Webb, R.; Chávez-Gutiérrez, L.; Cleverley, K.; Noy, S.; Sheppard, O. Trisomy of Human Chromosome 21 Enhances Amyloid- β Deposition Independently of an Extra Copy of APP. *Brain* **2018**, *141*, 2457–2474.
70. Li, S.; Jin, M.; Koeglsperger, T.; Shepardson, N.E.; Shankar, G.M.; Selkoe, D.J. Soluble A β Oligomers Inhibit Long-Term Potentiation through a Mechanism Involving Excessive

- Activation of Extrasynaptic NR2B-Containing NMDA Receptors. *J. Neurosci.* **2011**, *31*, 6627–6638.
71. Lei, M.; Xu, H.; Li, Z.; Wang, Z.; O'Malley, T.T.; Zhang, D.; Walsh, D.M.; Xu, P.; Selkoe, D.J.; Li, S. Soluble A β Oligomers Impair Hippocampal LTP by Disrupting Glutamatergic/GABAergic Balance. *Neurobiol. Dis.* **2016**, *85*, 111–121.
 72. Rammes, G.; Hasenjäger, A.; Sroka-Saidi, K.; Deussing, J.M.; Parsons, C.G. Therapeutic Significance of NR2B-Containing NMDA Receptors and mGluR5 Metabotropic Glutamate Receptors in Mediating the Synaptotoxic Effects of β -Amyloid Oligomers on Long-Term Potentiation (LTP) in Murine Hippocampal Slices. *Neuropharmacology* **2011**, *60*, 982–990.
 73. Selkoe, D.J. Soluble Oligomers of the Amyloid β -Protein Impair Synaptic Plasticity and Behavior. *Behav. Brain Res.* **2008**, *192*, 106–113.
 74. O'Brien, R.J.; Wong, P.C. Amyloid Precursor Protein Processing and Alzheimer's Disease. *Annu. Rev. Neurosci.* **2011**, *34*, 185–204.
 75. Pimplikar, S.W. Reassessing the Amyloid Cascade Hypothesis of Alzheimer's Disease. *Int. J. Biochem. Cell Biol.* **2009**, *41*, 1261–1268.
 76. Soto-Faguás, C.M.; Sanchez-Molina, P.; Saura, C.A. Loss of Presenilin Function Enhances Tau Phosphorylation and Aggregation in Mice. *Acta Neuropathol. Commun.* **2021**, *9*, 1–20.
 77. Cummings, J.L. Challenges to Demonstrating Disease-Modifying Effects in Alzheimer's Disease Clinical Trials. *Alzheimer's Dement.* **2006**, *2*, 263–271.
 78. Lippa, C.F.; Morris, J.C. Alzheimer Neuropathology in Nondemented Aging: Keeping Mind over Matter. *Neurology* **2006**, *66*, 1801–1802.
 79. Mintun, M.A.; Lo, A.C.; Duggan Evans, C.; Wessels, A.M.; Ardayfio, P.A.; Andersen, S.W.; Shcherbinin, S.; Sparks, J.; Sims, J.R.; Brys, M. Donanemab in Early Alzheimer's Disease. *N. Engl. J. Med.* **2021**, *384*, 1691–1704.
 80. Swanson, C.J.; Zhang, Y.; Dhadda, S.; Wang, J.; Kaplow, J.; Lai, R.Y.K.; Lannfelt, L.; Bradley, H.; Rabe, M.; Koyama, A. A Randomized, Double-Blind, Phase 2b Proof-of-

- Concept Clinical Trial in Early Alzheimer's Disease with Lecanemab, an Anti-A β Protofibril Antibody. *Alzheimers. Res. Ther.* **2021**, *13*, 1–14.
81. Van Dyck, C.H.; Swanson, C.J.; Aisen, P.; Bateman, R.J.; Chen, C.; Gee, M.; Kanekiyo, M.; Li, D.; Reyderman, L.; Cohen, S. Lecanemab in Early Alzheimer's Disease. *N. Engl. J. Med.* **2023**, *388*, 9–21.
 82. Tan, J.Z.A.; Gleeson, P.A. The Trans-Golgi Network Is a Major Site for α -Secretase Processing of Amyloid Precursor Protein in Primary Neurons. *J. Biol. Chem.* **2019**, *294*, 1618–1631.
 83. Chow, V.W.; Mattson, M.P.; Wong, P.C.; Gleichmann, M. An Overview of APP Processing Enzymes and Products. *Neuromolecular Med.* **2010**, *12*, 1–12.
 84. Zhang, X.; Song, W. The Role of APP and BACE1 Trafficking in APP Processing and Amyloid- β Generation. *Alzheimers. Res. Ther.* **2013**, *5*, 1–8.
 85. Sun, X.; Chen, W.-D.; Wang, Y.-D. β -Amyloid: The Key Peptide in the Pathogenesis of Alzheimer's Disease. *Front. Pharmacol.* **2015**, *6*, 221.
 86. Nhan, H.S.; Chiang, K.; Koo, E.H. The Multifaceted Nature of Amyloid Precursor Protein and Its Proteolytic Fragments: Friends and Foes. *Acta Neuropathol.* **2015**, *129*, 1–19.
 87. Haass, C.; Kaether, C.; Thinakaran, G.; Sisodia, S. Trafficking and Proteolytic Processing of APP. *Cold Spring Harb. Perspect. Med.* **2012**, *2*, a006270.
 88. Venugopal, C.; Demos, C.M.; Jagannatha Rao, K.S.; Pappolla, M.A.; Sambamurti, K. Beta-Secretase: Structure, Function, and Evolution. *CNS Neurol. Disord. Targets (Formerly Curr. Drug Targets-CNS Neurol. Disord.)* **2008**, *7*, 278–294.
 89. Kurkinen, K.M.A.; Marttinen, M.; Turner, L.; Natunen, T.; Mäkinen, P.; Haapalinna, F.; Sarajärvi, T.; Gabbouj, S.; Kurki, M.; Paananen, J. SEPT8 Modulates β -Amyloidogenic Processing of APP by Affecting the Sorting and Accumulation of BACE1. *J. Cell Sci.* **2016**, *129*, 2224–2238.
 90. Ahmed, R.R.; Holler, C.J.; Webb, R.L.; Li, F.; Beckett, T.L.; Murphy, M.P. BACE1 and

- BACE2 Enzymatic Activities in Alzheimer's Disease. *J. Neurochem.* **2010**, *112*, 1045–1053.
91. Chen, Y.; Huang, X.; Zhang, Y.; Rockenstein, E.; Bu, G.; Golde, T.E.; Masliah, E.; Xu, H. Alzheimer's β -Secretase (BACE1) Regulates the CAMP/PKA/CREB Pathway Independently of β -Amyloid. *J. Neurosci.* **2012**, *32*, 11390–11395.
 92. Creemers, J.W.M.; Dominguez, D.I.; Plets, E.; Serneels, L.; Taylor, N.A.; Multhaup, G.; Craessaerts, K.; Annaert, W.; De Strooper, B. Processing of β -Secretase by Furin and Other Members of the Proprotein Convertase Family. *J. Biol. Chem.* **2001**, *276*, 4211–4217.
 93. Bennett, B.D.; Denis, P.; Haniu, M.; Teplow, D.B.; Kahn, S.; Louis, J.-C.; Citron, M.; Vassar, R. A Furin-like Convertase Mediates Propeptide Cleavage of BACE, the Alzheimer's β -Secretase. *J. Biol. Chem.* **2000**, *275*, 37712–37717.
 94. Citron, M. Emerging Alzheimer's Disease Therapies: Inhibition of β -Secretase. *Neurobiol. Aging* **2002**, *23*, 1017–1022.
 95. Hampel, H.; Vassar, R.; De Strooper, B.; Hardy, J.; Willem, M.; Singh, N.; Zhou, J.; Yan, R.; Vanmechelen, E.; De Vos, A. The β -Secretase BACE1 in Alzheimer's Disease. *Biol. Psychiatry* **2021**, *89*, 745–756.
 96. Ohno, M.; Sametsky, E.A.; Younkin, L.H.; Oakley, H.; Younkin, S.G.; Citron, M.; Vassar, R.; Disterhoft, J.F. BACE1 Deficiency Rescues Memory Deficits and Cholinergic Dysfunction in a Mouse Model of Alzheimer's Disease. *Neuron* **2004**, *41*, 27–33.
 97. Ohno, M. Alzheimer's Therapy Targeting the β -Secretase Enzyme BACE1: Benefits and Potential Limitations from the Perspective of Animal Model Studies. *Brain Res. Bull.* **2016**, *126*, 183–198.
 98. Zhang, Y.; Thompson, R.; Zhang, H.; Xu, H. APP Processing in Alzheimer's Disease. *Mol. Brain* **2011**, *4*, 1–13.
 99. Paris, D.; Bachmeier, C.; Patel, N.; Quadros, A.; Volmar, C.-H.; Laporte, V.; Ganey, J.; Beaulieu-Abdelahad, D.; Ait-Ghezala, G.; Crawford, F. Selective Antihypertensive Dihydropyridines Lower A β Accumulation by Targeting Both the Production and the

- Clearance of A β across the Blood-Brain Barrier. *Mol. Med.* **2011**, *17*, 149–162.
100. Zhang, Y.; Luo, W.; Wang, H.; Lin, P.; Vetrivel, K.S.; Liao, F.; Li, F.; Wong, P.C.; Farquhar, M.G.; Thinakaran, G. Nicastrin Is Critical for Stability and Trafficking but Not Association of Other Presenilin/ γ -Secretase Components. *J. Biol. Chem.* **2005**, *280*, 17020–17026.
 101. McCarthy, J. V.; Twomey, C.; Wujek, P. Presenilin-Dependent Regulated Intramembrane Proteolysis and γ -Secretase Activity. *Cell. Mol. life Sci.* **2009**, *66*, 1534–1555.
 102. Herreman, A.; Van Gassen, G.; Bentahir, M.; Nyabi, O.; Craessaerts, K.; Mueller, U.; Annaert, W.; De Strooper, B. γ -Secretase Activity Requires the Presenilin-Dependent Trafficking of Nicastrin through the Golgi Apparatus but Not Its Complex Glycosylation. *J. Cell Sci.* **2003**, *116*, 1127–1136.
 103. Lleó, A.; Blesa, R.; Queralt, R.; Ezquerra, M.; Molinuevo, J.L.; Pena-Casanova, J.; Rojo, A.; Oliva, R. Frequency of Mutations in the Presenilin and Amyloid Precursor Protein Genes in Early-Onset Alzheimer Disease in Spain. *Arch. Neurol.* **2002**, *59*, 1759–1763.
 104. Tedde, A.; Nacmias, B.; Ciantelli, M.; Forleo, P.; Cellini, E.; Bagnoli, S.; Piccini, C.; Caffarra, P.; Ghidoni, E.; Paganini, M. Identification of New Presenilin Gene Mutations in Early-Onset Familial Alzheimer Disease. *Arch. Neurol.* **2003**, *60*, 1541–1544.
 105. Hsiao, K.; Chapman, P.; Nilsen, S.; Eckman, C.; Harigaya, Y.; Younkin, S.; Yang, F.; Cole, G. Correlative Memory Deficits, A β Elevation, and Amyloid Plaques in Transgenic Mice. *Science (80-)*. **1996**, *274*, 99–103.
 106. Frautschy, S.A.; Yang, F.; Irrizarry, M.; Hyman, B.; Saido, T.C.; Hsiao, K.; Cole, G.M. Microglial Response to Amyloid Plaques in APP^{sw} Transgenic Mice. *Am. J. Pathol.* **1998**, *152*, 307.
 107. Mucke, L.; Masliah, E.; Yu, G.-Q.; Mallory, M.; Rockenstein, E.M.; Tatsuno, G.; Hu, K.; Kholodenko, D.; Johnson-Wood, K.; McConlogue, L. High-Level Neuronal Expression of A β _{1–42} in Wild-Type Human Amyloid Protein Precursor Transgenic Mice: Synaptotoxicity without Plaque Formation. *J. Neurosci.* **2000**, *20*, 4050–4058.

108. Wright, A.L.; Zinn, R.; Hohensinn, B.; Konen, L.M.; Beynon, S.B.; Tan, R.P.; Clark, I.A.; Abdipranoto, A.; Vissel, B. Neuroinflammation and Neuronal Loss Precede A β Plaque Deposition in the HAPP-J20 Mouse Model of Alzheimer's Disease. *PLoS One* **2013**, *8*, e59586.
109. Yokoyama, M.; Kobayashi, H.; Tatsumi, L.; Tomita, T. Mouse Models of Alzheimer's Disease. *Front. Mol. Neurosci.* **2022**, *15*.
110. Richards, J.G.; Higgins, G.A.; Ouagazzal, A.-M.; Ozmen, L.; Kew, J.N.C.; Bohrmann, B.; Malherbe, P.; Brockhaus, M.; Loetscher, H.; Czech, C. PS2APP Transgenic Mice, Coexpressing HPS2mut and HAPPswe, Show Age-Related Cognitive Deficits Associated with Discrete Brain Amyloid Deposition and Inflammation. *J. Neurosci.* **2003**, *23*, 8989–9003.
111. Jankowsky, J.L.; Fadale, D.J.; Anderson, J.; Xu, G.M.; Gonzales, V.; Jenkins, N.A.; Copeland, N.G.; Lee, M.K.; Younkin, L.H.; Wagner, S.L. Mutant Presenilins Specifically Elevate the Levels of the 42 Residue β -Amyloid Peptide in Vivo: Evidence for Augmentation of a 42-Specific γ Secretase. *Hum. Mol. Genet.* **2004**, *13*, 159–170.
112. Lalonde, R.; Kim, H.D.; Maxwell, J.A.; Fukuchi, K. Exploratory Activity and Spatial Learning in 12-Month-Old APP695SWE/Co+ PS1/ Δ E9 Mice with Amyloid Plaques. *Neurosci. Lett.* **2005**, *390*, 87–92.
113. Kamphuis, W.; Mamber, C.; Moeton, M.; Kooijman, L.; Sluijs, J.A.; Jansen, A.H.P.; Verveer, M.; De Groot, L.R.; Smith, V.D.; Rangarajan, S. GFAP Isoforms in Adult Mouse Brain with a Focus on Neurogenic Astrocytes and Reactive Astrogliosis in Mouse Models of Alzheimer Disease. **2012**.
114. Lord, A.; Kalimo, H.; Eckman, C.; Zhang, X.-Q.; Lannfelt, L.; Nilsson, L.N.G. The Arctic Alzheimer Mutation Facilitates Early Intraneuronal A β Aggregation and Senile Plaque Formation in Transgenic Mice. *Neurobiol. Aging* **2006**, *27*, 67–77.
115. Lord, A.; Gumucio, A.; Englund, H.; Sehlin, D.; Sundquist, V.S.; Söderberg, L.; Möller, C.; Gellerfors, P.; Lannfelt, L.; Pettersson, F.E. An Amyloid- β Protofibril-Selective Antibody Prevents Amyloid Formation in a Mouse Model of Alzheimer's Disease. *Neurobiol. Dis.*

- 2009**, *36*, 425–434.
116. Oakley, H.; Cole, S.L.; Logan, S.; Maus, E.; Shao, P.; Craft, J.; Guillozet-Bongaarts, A.; Ohno, M.; Disterhoft, J.; Van Eldik, L. Intraneuronal β -Amyloid Aggregates, Neurodegeneration, and Neuron Loss in Transgenic Mice with Five Familial Alzheimer's Disease Mutations: Potential Factors in Amyloid Plaque Formation. *J. Neurosci.* **2006**, *26*, 10129–10140.
 117. Saito, T.; Matsuba, Y.; Mihira, N.; Takano, J.; Nilsson, P.; Itohara, S.; Iwata, N.; Saido, T.C. Single App Knock-in Mouse Models of Alzheimer's Disease. *Nat. Neurosci.* **2014**, *17*, 661–663.
 118. Catania, C.; Sotiropoulos, I.; Silva, R.; Onofri, C.; Breen, K.C.; Sousa, N.; Almeida, O.F.X. The Amyloidogenic Potential and Behavioral Correlates of Stress. *Mol. Psychiatry* **2009**, *14*, 95–105.
 119. Knobloch, M.; Konietzko, U.; Krebs, D.C.; Nitsch, R.M. Intracellular A β and Cognitive Deficits Precede β -Amyloid Deposition in Transgenic ArcA β Mice. *Neurobiol. Aging* **2007**, *28*, 1297–1306.
 120. Murphy, M.J.; Peterson, M.J. Sleep Disturbances in Depression. *Sleep Med. Clin.* **2015**, *10*, 17–23.
 121. Kernberg, O.F. An Integrated Theory of Depression. *Neuropsychoanalysis* **2009**, *11*, 76–80.
 122. Cacha, L.A.; Poznanski, R.R.; Latif, A.Z.A.; Ariff, T.M. Psychophysiology of Chronic Stress: An Example of Mind-Body Interaction. *NeuroQuantology* **2019**, *17*, 53–63.
 123. Kasckow, J.W.; Baker, D.; Geraciotti Jr, T.D. Corticotropin-Releasing Hormone in Depression and Post-Traumatic Stress Disorder. *Peptides* **2001**, *22*, 845–851.
 124. Buckley, T.M.; Schatzberg, A.F. On the Interactions of the Hypothalamic-Pituitary-Adrenal (HPA) Axis and Sleep: Normal HPA Axis Activity and Circadian Rhythm, Exemplary Sleep Disorders. *J. Clin. Endocrinol. Metab.* **2005**, *90*, 3106–3114.

125. Antonijevic, I.A. Depressive Disorders—Is It Time to Endorse Different Pathophysiologies? *Psychoneuroendocrinology* **2006**, *31*, 1–15.
126. Watson, S.; Mackin, P. HPA Axis Function in Mood Disorders. *Psychiatry* **2006**, *5*, 166–170.
127. Nutt, D.; Wilson, S.; Paterson, L. Sleep Disorders as Core Symptoms of Depression. *Dialogues Clin. Neurosci.* **2022**.
128. Held, K.; Künzel, H.; Ising, M.; Schmid, D.A.; Zobel, A.; Murck, H.; Holsboer, F.; Steiger, A. Treatment with the CRH1-Receptor-Antagonist R121919 Improves Sleep-EEG in Patients with Depression. *J. Psychiatr. Res.* **2004**, *38*, 129–136.
129. Hamon, M.; Blier, P. Monoamine Neurocircuitry in Depression and Strategies for New Treatments. *Prog. Neuro-Psychopharmacology Biol. Psychiatry* **2013**, *45*, 54–63.
130. Blackburn-Munro, G.; Blackburn-Munro, R.E. Chronic Pain, Chronic Stress and Depression: Coincidence or Consequence? *J. Neuroendocrinol.* **2001**, *13*, 1009–1023.
131. Mahar, I.; Bambico, F.R.; Mechawar, N.; Nobrega, J.N. Stress, Serotonin, and Hippocampal Neurogenesis in Relation to Depression and Antidepressant Effects. *Neurosci. Biobehav. Rev.* **2014**, *38*, 173–192.
132. Alhaider, I.A.; Aleisa, A.M.; Tran, T.T.; Alkadhi, K.A. Sleep Deprivation Prevents Stimulation-Induced Increases of Levels of P-CREB and BDNF: Protection by Caffeine. *Mol. Cell. Neurosci.* **2011**, *46*, 742–751.
133. Hagewoud, R.; Bultsma, L.J.; Barf, R.P.; Koolhaas, J.M.; Meerlo, P. Sleep Deprivation Impairs Contextual Fear Conditioning and Attenuates Subsequent Behavioural, Endocrine and Neuronal Responses. *J. Sleep Res.* **2011**, *20*, 259–266.
134. Vecsey, C.G.; Baillie, G.S.; Jaganath, D.; Havekes, R.; Daniels, A.; Wimmer, M.; Huang, T.; Brown, K.M.; Li, X.-Y.; Descalzi, G. Sleep Deprivation Impairs cAMP Signalling in the Hippocampus. *Nature* **2009**, *461*, 1122–1125.
135. Lenoir, H.; Dufouil, C.; Auriacombe, S.; Lacombe, J.-M.; Dartigues, J.-F.; Ritchie, K.;

- Tzourio, C. Depression History, Depressive Symptoms, and Incident Dementia: The 3C Study. *J. Alzheimer's Dis.* **2011**, *26*, 27–38.
136. Hesper, K.; Tebarth, F.; Wiese, B.; Eisele, M.; Bickel, H.; Köhler, M.; Mösch, E.; Weyerer, S.; Werle, J.; König, H.-H. Age of Major Depression Onset, Depressive Symptoms, and Risk for Subsequent Dementia: Results of the German Study on Ageing, Cognition, and Dementia in Primary Care Patients (AgeCoDe). *Psychol. Med.* **2013**, *43*, 1597–1610.
137. Saczynski, J.S.; Beiser, A.; Seshadri, S.; Auerbach, S.; Wolf, P.A.; Au, R. Depressive Symptoms and Risk of Dementia: The Framingham Heart Study. *Neurology* **2010**, *75*, 35–41.
138. Byers, A.L.; Yaffe, K. Depression and Risk of Developing Dementia. *Nat. Rev. Neurol.* **2011**, *7*, 323–331.
139. Almeida, O.P.; Hankey, G.J.; Yeap, B.B.; Golledge, J.; Flicker, L. Depression as a Risk Factor for Cognitive Impairment in Later Life: The Health In Men Cohort Study. *Int. J. Geriatr. Psychiatry* **2016**, *31*, 412–420.
140. Aziz, R.; Steffens, D. Overlay of Late-Life Depression and Cognitive Impairment. *Focus (Madison)*. **2017**, *15*, 35–41.
141. Hébert, R.; Lindsay, J.; Verreault, R.; Rockwood, K.; Hill, G.; Dubois, M.-F. Vascular Dementia: Incidence and Risk Factors in the Canadian Study of Health and Aging. *Stroke* **2000**, *31*, 1487–1493.
142. Chen, R.; Hu, Z.; Wei, L.; Qin, X.; McCracken, C.; Copeland, J.R. Severity of Depression and Risk for Subsequent Dementia: Cohort Studies in China and the UK. *Br. J. Psychiatry* **2008**, *193*, 373–377.
143. Byers, A.L.; Covinsky, K.E.; Barnes, D.E.; Yaffe, K. Dysthymia and Depression Increase Risk of Dementia and Mortality among Older Veterans. *Am. J. Geriatr. Psychiatry* **2012**, *20*, 664–672.
144. Gatz, J.L.; Tyas, S.L.; St. John, P.; Montgomery, P. Do Depressive Symptoms Predict Alzheimer's Disease and Dementia? *Journals Gerontol. Ser. A Biol. Sci. Med. Sci.* **2005**,

- 60, 744–747.
145. Andersen, K.; Lolk, A.; Kragh-Sørensen, P.; Petersen, N.E.; Green, A. Depression and the Risk of Alzheimer Disease. *Epidemiology* **2005**, 233–238.
 146. Mendez, M.F. The Relationship between Anxiety and Alzheimer’s Disease. *J. Alzheimer’s Dis. reports* **2021**, 5, 171–177.
 147. Becker, E.; Rios, C.L.O.; Lahmann, C.; Ruecker, G.; Bauer, J.; Boeker, M. Anxiety as a Risk Factor of Alzheimer’s Disease and Vascular Dementia. *Br. J. Psychiatry* **2018**, 213, 654–660.
 148. Rasmussen, H.; Rosness, T.A.; Bosnes, O.; Salvesen, Ø.; Knutli, M.; Stordal, E. Anxiety and Depression as Risk Factors in Frontotemporal Dementia and Alzheimer’s Disease: The HUNT Study. *Dement. Geriatr. Cogn. Dis. Extra* **2019**, 8, 414–425.
 149. Rothman, S.M.; Mattson, M.P. Adverse Stress, Hippocampal Networks, and Alzheimer’s Disease. *Neuromolecular Med.* **2010**, 12, 56–70.
 150. Rapp, M.A.; Schnaider-Beeri, M.; Grossman, H.T.; Sano, M.; Perl, D.P.; Purohit, D.P.; Gorman, J.M.; Haroutunian, V. Increased Hippocampal Plaques and Tangles in Patients with Alzheimer Disease with a Lifetime History of Major Depression. *Arch. Gen. Psychiatry* **2006**, 63, 161–167.
 151. Rapp, M.A.; Schnaider-Beeri, M.; Purohit, D.P.; Perl, D.P.; Haroutunian, V.; Sano, M. Increased Neurofibrillary Tangles in Patients with Alzheimer Disease with Comorbid Depression. *Am. J. Geriatr. Psychiatry* **2008**, 16, 168–174.
 152. Sierksma, A.S.R.; van den Hove, D.L.A.; Steinbusch, H.W.M.; Prickaerts, J. Major Depression, Cognitive Dysfunction and Alzheimer’s Disease: Is There a Link? *Eur. J. Pharmacol.* **2010**, 626, 72–82.
 153. Caraci, F.; Copani, A.; Nicoletti, F.; Drago, F. Depression and Alzheimer’s Disease: Neurobiological Links and Common Pharmacological Targets. *Eur. J. Pharmacol.* **2010**, 626, 64–71.

154. Green, K.N.; Billings, L.M.; Roozendaal, B.; McGaugh, J.L.; LaFerla, F.M. Glucocorticoids Increase Amyloid- β and Tau Pathology in a Mouse Model of Alzheimer's Disease. *J. Neurosci.* **2006**, *26*, 9047–9056.
155. Cho, S.; Hu, Y. Activation of 5-HT₄ Receptors Inhibits Secretion of β -Amyloid Peptides and Increases Neuronal Survival. *Exp. Neurol.* **2007**, *203*, 274–278.
156. Sun, X.; Steffens, D.C.; Au, R.; Folstein, M.; Summergrad, P.; Yee, J.; Rosenberg, I.; Mwamburi, D.M.; Qiu, W.Q. Amyloid-Associated Depression: A Prodromal Depression of Alzheimer Disease? *Arch. Gen. Psychiatry* **2008**, *65*, 542–550.
157. Wuwongse, S.; Chang, R.C.-C.; Law, A.C.K. The Putative Neurodegenerative Links between Depression and Alzheimer's Disease. *Prog. Neurobiol.* **2010**, *91*, 362–375.
158. Heneka, M.T.; Ramanathan, M.; Jacobs, A.H.; Dumitrescu-Ozimek, L.; Bilkei-Gorzo, A.; Debeir, T.; Sastre, M.; Galldiks, N.; Zimmer, A.; Hoehn, M. Locus Ceruleus Degeneration Promotes Alzheimer Pathogenesis in Amyloid Precursor Protein 23 Transgenic Mice. *J. Neurosci.* **2006**, *26*, 1343–1354.
159. Heneka, M.T.; Nadrigny, F.; Regen, T.; Martinez-Hernandez, A.; Dumitrescu-Ozimek, L.; Terwel, D.; Jardanhazi-Kurutz, D.; Walter, J.; Kirchhoff, F.; Hanisch, U.-K. Locus Ceruleus Controls Alzheimer's Disease Pathology by Modulating Microglial Functions through Norepinephrine. *Proc. Natl. Acad. Sci.* **2010**, *107*, 6058–6063.
160. Lezoualc'h, F.; Robert, S.J. The Serotonin 5-HT₄ Receptor and the Amyloid Precursor Protein Processing. *Exp. Gerontol.* **2003**, *38*, 159–166.
161. Leonard, B.E. Inflammation, Depression and Dementia: Are They Connected? *Neurochem. Res.* **2007**, *32*, 1749–1756.
162. Rojo, L.E.; Fernández, J.A.; Maccioni, A.A.; Jimenez, J.M.; Maccioni, R.B. Neuroinflammation: Implications for the Pathogenesis and Molecular Diagnosis of Alzheimer's Disease. *Arch. Med. Res.* **2008**, *39*, 1–16.
163. Maes, M.; Yirmiya, R.; Noraberg, J.; Brene, S.; Hibbeln, J.; Perini, G.; Kubera, M.; Bob, P.; Lerer, B.; Maj, M. The Inflammatory & Neurodegenerative (I&ND) Hypothesis of

- Depression: Leads for Future Research and New Drug Developments in Depression. *Metab. Brain Dis.* **2009**, *24*, 27–53.
164. Sorrells, S.F.; Sapolsky, R.M. An Inflammatory Review of Glucocorticoid Actions in the CNS. *Brain. Behav. Immun.* **2007**, *21*, 259–272.
165. Farfara, D.; Lifshitz, V.; Frenkel, D. Neuroprotective and Neurotoxic Properties of Glial Cells in the Pathogenesis of Alzheimer’s Disease. *J. Cell. Mol. Med.* **2008**, *12*, 762–780.
166. Dwivedi, Y.; Rizavi, H.S.; Pandey, G.N. Antidepressants Reverse Corticosterone-Mediated Decrease in Brain-Derived Neurotrophic Factor Expression: Differential Regulation of Specific Exons by Antidepressants and Corticosterone. *Neuroscience* **2006**, *139*, 1017–1029.
167. Dafsari, F.S.; Jessen, F. Depression—an Underrecognized Target for Prevention of Dementia in Alzheimer’s Disease. *Transl. Psychiatry* **2020**, *10*, 160.
168. Cirrito, J.R.; Wallace, C.E.; Yan, P.; Davis, T.A.; Gardiner, W.D.; Doherty, B.M.; King, D.; Yuede, C.M.; Lee, J.-M.; Sheline, Y.I. Effect of Escitalopram on A β Levels and Plaque Load in an Alzheimer Mouse Model. *Neurology* **2020**, *95*, e2666–e2674.
169. Sheline, Y.I.; West, T.; Yarasheski, K.; Swarm, R.; Jasielec, M.S.; Fisher, J.R.; Ficker, W.D.; Yan, P.; Xiong, C.; Frederiksen, C. An Antidepressant Decreases CSF A β Production in Healthy Individuals and in Transgenic AD Mice. *Sci. Transl. Med.* **2014**, *6*, 236re4–236re4.
170. Cirrito, J.R.; Disabato, B.M.; Restivo, J.L.; Verges, D.K.; Goebel, W.D.; Sathyan, A.; Hayreh, D.; D’Angelo, G.; Benzinger, T.; Yoon, H. Serotonin Signaling Is Associated with Lower Amyloid- β Levels and Plaques in Transgenic Mice and Humans. *Proc. Natl. Acad. Sci.* **2011**, *108*, 14968–14973.
171. Wang, J.; Zhang, Y.; Xu, H.; Zhu, S.; Wang, H.; He, J.; Zhang, H.; Guo, H.; Kong, J.; Huang, Q. Fluoxetine Improves Behavioral Performance by Suppressing the Production of Soluble β -Amyloid in APP/PS1 Mice. *Curr. Alzheimer Res.* **2014**, *11*, 672–680.
172. Huang, P.; Wei, S.; Luo, M.; Tang, Z.; Lin, Q.; Wang, X.; Luo, M.; He, Y.; Wang, C.; Wei,

- D. MiR-139-5p Has an Antidepressant-like Effect by Targeting Phosphodiesterase 4D to Activate the CAMP/PKA/CREB Signaling Pathway. *Ann. Transl. Med.* **2021**, *9*.
173. Liu, X.; Guo, H.; Sayed, M.D.S.O.M.; Lu, Y.; Yang, T.; Zhou, D.; Chen, Z.; Wang, H.; Wang, C.; Xu, J. CAMP/PKA/CREB/GLT1 Signaling Involved in the Antidepressant-like Effects of Phosphodiesterase 4D Inhibitor (GEBR-7b) in Rats. *Neuropsychiatr. Dis. Treat.* **2016**, *219–227*.
174. Jia, M.; Li, C.; Zheng, Y.; Ding, X.; Chen, M.; Ding, J.; Du, R.; Lu, M.; Hu, G. Leonurine Exerts Antidepressant-like Effects in the Chronic Mild Stress-Induced Depression Model in Mice by Inhibiting Neuroinflammation. *Int. J. Neuropsychopharmacol.* **2017**, *20*, 886–895.
175. Choi, J.H.; Lee, M.J.; Jang, M.; Kim, H.-J.; Lee, S.; Lee, S.W.; Kim, Y.O.; Cho, I.-H. Panax Ginseng Exerts Antidepressant-like Effects by Suppressing Neuroinflammatory Response and Upregulating Nuclear Factor Erythroid 2 Related Factor 2 Signaling in the Amygdala. *J. Ginseng Res.* **2018**, *42*, 107–115.
176. Guo, Y.; Xie, J.; Zhang, L.; Yang, L.; Ma, J.; Bai, Y.; Ma, W.; Wang, L.; Yu, H.; Zeng, Y. Ginsenoside Rb1 Exerts Antidepressant-like Effects via Suppression Inflammation and Activation of AKT Pathway. *Neurosci. Lett.* **2021**, *744*, 135561.
177. Liu, D.; Wang, Z.; Liu, S.; Wang, F.; Zhao, S.; Hao, A. Anti-Inflammatory Effects of Fluoxetine in Lipopolysaccharide (LPS)-Stimulated Microglial Cells. *Neuropharmacology* **2011**, *61*, 592–599.
178. Papadopoulos, V.; Baraldi, M.; Guilarte, T.R.; Knudsen, T.B.; Lacapère, J.-J.; Lindemann, P.; Norenberg, M.D.; Nutt, D.; Weizman, A.; Zhang, M.-R. Translocator Protein (18 KDa): New Nomenclature for the Peripheral-Type Benzodiazepine Receptor Based on Its Structure and Molecular Function. *Trends Pharmacol. Sci.* **2006**, *27*, 402–409.
179. Papadopoulos, V.; Liu, J.; Culty, M. Is There a Mitochondrial Signaling Complex Facilitating Cholesterol Import? *Mol. Cell. Endocrinol.* **2007**, *265*, 59–64.
180. Braestrup, C.; Albrechtsen, R.; Squires, R.F. High Densities of Benzodiazepine Receptors

- in Human Cortical Areas. *Nature* **1977**, *269*, 702–704.
181. Papadopoulos, V. Structure and Function of the Peripheral-Type Benzodiazepine Receptor in Steroidogenic Cells. *Proc. Soc. Exp. Biol. Med.* **1998**, *217*, 130–142.
 182. Azarashvili, T.; Krestinina, O.; Yurkov, I.; Evtodienko, Y. link rid=" q1"; Reiser, G. High-affinity Peripheral Benzodiazepine Receptor Ligand, PK11195, Regulates Protein Phosphorylation in Rat Brain Mitochondria under Control of Ca²⁺. *J. Neurochem.* **2005**, *94*, 1054–1062.
 183. Hirsch, J.D.; Beyer, C.F.; Malkowitz, L.; Beer, B.; Blume, A.J. Mitochondrial Benzodiazepine Receptors Mediate Inhibition of Mitochondrial Respiratory Control. *Mol. Pharmacol.* **1989**, *35*, 157–163.
 184. Dupont, A.-C.; Largeau, B.; Santiago Ribeiro, M.J.; Guilloteau, D.; Tronel, C.; Arlicot, N. Translocator Protein-18 KDa (TSPO) Positron Emission Tomography (PET) Imaging and Its Clinical Impact in Neurodegenerative Diseases. *Int. J. Mol. Sci.* **2017**, *18*, 785.
 185. Varley, J.; Brooks, D.J.; Edison, P. Imaging Neuroinflammation in Alzheimer's Disease and Other Dementias: Recent Advances and Future Directions. *Alzheimer's Dement.* **2015**, *11*, 1110–1120.
 186. McEnery, M.W.; Snowman, A.M.; Trifiletti, R.R.; Snyder, S.H. Isolation of the Mitochondrial Benzodiazepine Receptor: Association with the Voltage-Dependent Anion Channel and the Adenine Nucleotide Carrier. *Proc. Natl. Acad. Sci.* **1992**, *89*, 3170–3174.
 187. Garnier, M.; Dimchev, A.B.; Boujrad, N.; Price, J.M.; Musto, N.A.; Papadopoulos, V. In Vitro Reconstitution of a Functional Peripheral-Type Benzodiazepine Receptor from Mouse Leydig Tumor Cells. *Mol. Pharmacol.* **1994**, *45*, 201–211.
 188. Veenman, L.; Shandalov, Y.; Gavish, M. VDAC Activation by the 18 KDa Translocator Protein (TSPO), Implications for Apoptosis. *J. Bioenerg. Biomembr.* **2008**, *40*, 199–205.
 189. Lee, Y.; Park, Y.; Nam, H.; Lee, J.-W.; Yu, S.-W. Translocator Protein (TSPO): The New Story of the Old Protein in Neuroinflammation. *BMB Rep.* **2020**, *53*, 20.

190. Notter, T.; Schalbetter, S.M.; Clifton, N.E.; Mattei, D.; Richetto, J.; Thomas, K.; Meyer, U.; Hall, J. Neuronal Activity Increases Translocator Protein (TSPO) Levels. *Mol. Psychiatry* **2021**, *26*, 2025–2037.
191. Rupprecht, R.; Papadopoulos, V.; Rammes, G.; Baghai, T.C.; Fan, J.; Akula, N.; Groyer, G.; Adams, D.; Schumacher, M. Translocator Protein (18 KDa)(TSPO) as a Therapeutic Target for Neurological and Psychiatric Disorders. *Nat. Rev. Drug Discov.* **2010**, *9*, 971–988.
192. Zeno, S.; Zaaroor, M.; Leschiner, S.; Veenman, L.; Gavish, M. CoCl₂ Induces Apoptosis via the 18 KDa Translocator Protein in U118MG Human Glioblastoma Cells. *Biochemistry* **2009**, *48*, 4652–4661.
193. Li, W.; Hardwick, M.J.; Rosenthal, D.; Culty, M.; Papadopoulos, V. Peripheral-Type Benzodiazepine Receptor Overexpression and Knockdown in Human Breast Cancer Cells Indicate Its Prominent Role in Tumor Cell Proliferation. *Biochem. Pharmacol.* **2007**, *73*, 491–503.
194. Kletsas, D.; Li, W.; Han, Z.; Papadopoulos, V. Peripheral-Type Benzodiazepine Receptor (PBR) and PBR Drug Ligands in Fibroblast and Fibrosarcoma Cell Proliferation: Role of ERK, c-Jun and Ligand-Activated PBR-Independent Pathways. *Biochem. Pharmacol.* **2004**, *67*, 1927–1932.
195. Hauet, T.; Yao, Z.-X.; Bose, H.S.; Wall, C.T.; Han, Z.; Li, W.; Hales, D.B.; Miller, W.L.; Culty, M.; Papadopoulos, V. Peripheral-Type Benzodiazepine Receptor-Mediated Action of Steroidogenic Acute Regulatory Protein on Cholesterol Entry into Leydig Cell Mitochondria. *Mol. Endocrinol.* **2005**, *19*, 540–554.
196. Levin, E.; Premkumar, A.; Veenman, L.; Kugler, W.; Leschiner, S.; Spanier, I.; Weisinger, G.; Lakomek, M.; Weizman, A.; Snyder, S.H. The Peripheral-Type Benzodiazepine Receptor and Tumorigenicity: Isoquinoline Binding Protein (IBP) Antisense Knockdown in the C6 Glioma Cell Line. *Biochemistry* **2005**, *44*, 9924–9935.
197. Kelly-Herskovitz, E.; Weizman, R.; Spanier, I.; Leschiner, S.; Lahav, M.; Weisinger, G.; Gavish, M. Effects of Peripheral-Type Benzodiazepine Receptor Antisense Knockout on

- MA-10 Leydig Cell Proliferation and Steroidogenesis. *J. Biol. Chem.* **1998**, *273*, 5478–5483.
198. Garnier, M.; Boujrad, N.; Ogwuegbu, S.O.; Hudson Jr, J.R.; Papadopoulos, V. The Polypeptide Diazepam-Binding Inhibitor and a Higher Affinity Mitochondrial Peripheral-Type Benzodiazepine Receptor Sustain Constitutive Steroidogenesis in the R2C Leydig Tumor Cell Line. *J. Biol. Chem.* **1994**, *269*, 22105–22112.
199. Lacapere, J.-J.; Papadopoulos, V. Peripheral-Type Benzodiazepine Receptor: Structure and Function of a Cholesterol-Binding Protein in Steroid and Bile Acid Biosynthesis. *Steroids* **2003**, *68*, 569–585.
200. Selvaraj, V.; Tu, L.N. Current Status and Future Perspectives: TSPO in Steroid Neuroendocrinology. *J Endocrinol* **2016**, *231*, R1–R30.
201. Wang, H.; Zhai, K.; Xue, Y.; Yang, J.; Yang, Q.; Fu, Y.; Hu, Y.; Liu, F.; Wang, W.; Cui, L. Global Deletion of TSPO Does Not Affect the Viability and Gene Expression Profile. *PLoS One* **2016**, *11*, e0167307.
202. Li, H.; Papadopoulos, V. Peripheral-Type Benzodiazepine Receptor Function in Cholesterol Transport. Identification of a Putative Cholesterol Recognition/Interaction Amino Acid Sequence and Consensus Pattern. *Endocrinology* **1998**, *139*, 4991–4997.
203. Li, H.; Yao, Z.; Degenhardt, B.; Teper, G.; Papadopoulos, V. Cholesterol Binding at the Cholesterol Recognition/Interaction Amino Acid Consensus (CRAC) of the Peripheral-Type Benzodiazepine Receptor and Inhibition of Steroidogenesis by an HIV TAT-CRAC Peptide. *Proc. Natl. Acad. Sci.* **2001**, *98*, 1267–1272.
204. Lacapère, J.-J.; Delavoie, F.; Li, H.; Péranski, G.; Maccario, J.; Papadopoulos, V.; Vidic, B. Structural and Functional Study of Reconstituted Peripheral Benzodiazepine Receptor. *Biochem. Biophys. Res. Commun.* **2001**, *284*, 536–541.
205. Mills, C.D.; Bitler, J.L.; Woolf, C.J. Role of the Peripheral Benzodiazepine Receptor in Sensory Neuron Regeneration. *Mol. Cell. Neurosci.* **2005**, *30*, 228–237.
206. Lacor, P.; Gandolfo, P.; Tonon, M.-C.; Brault, E.; Dalibert, I.; Schumacher, M.; Benavides,

- J.; Ferzaz, B. Regulation of the Expression of Peripheral Benzodiazepine Receptors and Their Endogenous Ligands during Rat Sciatic Nerve Degeneration and Regeneration: A Role for PBR in Neurosteroidogenesis. *Brain Res.* **1999**, *815*, 70–80.
207. Karchewski, L.A.; Bloechlinger, S.; Woolf, C.J. Axonal Injury-dependent Induction of the Peripheral Benzodiazepine Receptor in Small-diameter Adult Rat Primary Sensory Neurons. *Eur. J. Neurosci.* **2004**, *20*, 671–683.
208. Gerhard, A.; Schwarz, J.; Myers, R.; Wise, R.; Banati, R.B. Evolution of Microglial Activation in Patients after Ischemic Stroke: A [¹¹C](R)-PK11195 PET Study. *Neuroimage* **2005**, *24*, 591–595.
209. Chen, M.-K.; Guilarte, T.R. Translocator Protein 18 KDa (TSPO): Molecular Sensor of Brain Injury and Repair. *Pharmacol. Ther.* **2008**, *118*, 1–17.
210. Ji, B.; Maeda, J.; Sawada, M.; Ono, M.; Okauchi, T.; Inaji, M.; Zhang, M.-R.; Suzuki, K.; Ando, K.; Staufenbiel, M. Imaging of Peripheral Benzodiazepine Receptor Expression as Biomarkers of Detrimental versus Beneficial Glial Responses in Mouse Models of Alzheimer's and Other CNS Pathologies. *J. Neurosci.* **2008**, *28*, 12255–12267.
211. Hiser, C.; Montgomery, B.L.; Ferguson-Miller, S. TSPO Protein Binding Partners in Bacteria, Animals, and Plants. *J. Bioenerg. Biomembr.* **2021**, *53*, 463–487.
212. Ferzaz, B.; Brault, E.; Bourliaud, G.; Robert, J.-P.; Poughon, G.; Claustre, Y.; Marguet, F.; Liere, P.; Schumacher, M.; Nowicki, J.-P. SSR180575 (7-Chloro-N, N, 5-Trimethyl-4-Oxo-3-Phenyl-3, 5-Dihydro-4H-Pyridazino [4, 5-b] Indole-1-Acetamide), a Peripheral Benzodiazepine Receptor Ligand, Promotes Neuronal Survival and Repair. *J. Pharmacol. Exp. Ther.* **2002**, *301*, 1067–1078.
213. Bordet, T.; Buisson, B.; Michaud, M.; Drouot, C.; Galea, P.; Delaage, P.; Akentieva, N.P.; Evers, A.S.; Covey, D.F.; Ostuni, M.A. Identification and Characterization of Cholest-4-En-3-One, Oxime (TRO19622), a Novel Drug Candidate for Amyotrophic Lateral Sclerosis. *J. Pharmacol. Exp. Ther.* **2007**, *322*, 709–720.
214. Girard, C.; Liu, S.; Cadepond, F.; Adams, D.; Lacroix, C.; Verleye, M.; Gillardin, J.-M.;

- Baulieu, E.-E.; Schumacher, M.; Schweizer-Groyer, G. Etifoxine Improves Peripheral Nerve Regeneration and Functional Recovery. *Proc. Natl. Acad. Sci.* **2008**, *105*, 20505–20510.
215. Veiga, S.; Azcoitia, I.; Garcia-Segura, L.M. Ro5-4864, a Peripheral Benzodiazepine Receptor Ligand, Reduces Reactive Gliosis and Protects Hippocampal Hilar Neurons from Kainic Acid Excitotoxicity. *J. Neurosci. Res.* **2005**, *80*, 129–137.
216. Ryu, J.K.; Choi, H.B.; McLarnon, J.G. Peripheral Benzodiazepine Receptor Ligand PK11195 Reduces Microglial Activation and Neuronal Death in Quinolinic Acid-Injected Rat Striatum. *Neurobiol. Dis.* **2005**, *20*, 550–561.
217. Kita, A.; Kohayakawa, H.; Kinoshita, T.; Ochi, Y.; Nakamichi, K.; Kurumiya, S.; Furukawa, K.; Oka, M. Antianxiety and Antidepressant-like Effects of AC-5216, a Novel Mitochondrial Benzodiazepine Receptor Ligand. *Br. J. Pharmacol.* **2004**, *142*, 1059–1072.
218. Okuyama, S.; Chaki, S.; Yoshikawa, R.; Ogawa, S.; Suzuki, Y.; Okubo, T.; Nakazato, A.; Nagamine, M.; Tomisawa, K. Neuropharmacological Profile of Peripheral Benzodiazepine Receptor Agonists, DAA1097 and DAA1106. *Life Sci.* **1999**, *64*, 1455–1464.
219. Serra, M.; Madau, P.; Chessa, M.F.; Caddeo, M.; Sanna, E.; Trapani, G.; Franco, M.; Liso, G.; Purdy, R.H.; Barbaccia, M.L. 2-Phenyl-imidazo [1, 2-a] Pyridine Derivatives as Ligands for Peripheral Benzodiazepine Receptors: Stimulation of Neurosteroid Synthesis and Anticonflict Action in Rats. *Br. J. Pharmacol.* **1999**, *127*, 177–187.
220. Nguyen, N.; Fakra, E.; Pradel, V.; Jouve, E.; Alquier, C.; Le Guern, M.; Micallef, J.; Blin, O. Efficacy of Etifoxine Compared to Lorazepam Monotherapy in the Treatment of Patients with Adjustment Disorders with Anxiety: A Double-blind Controlled Study in General Practice. *Hum. Psychopharmacol. Clin. Exp.* **2006**, *21*, 139–149.
221. Nothdurfter, C.; Rammes, G.; Baghai, T.C.; Schüle, C.; Schumacher, M.; Papadopoulos, V.; Rupprecht, R. Translocator Protein (18 KDa) as a Target for Novel Anxiolytics with a Favourable Side-effect Profile. *J. Neuroendocrinol.* **2012**, *24*, 82–92.
222. Barron, A.M.; Ji, B.; Sahara, N.; Zhang, M.; Suhara, T.; Higuchi, M. [P3–050]: ANTI-

- INFLAMMATORY EFFECT OF TSPO LIGAND IN MOUSE MODEL OF TAUOPATHY. *Alzheimer's Dement.* **2017**, *13*, P949–P949.
223. Barron, A.M.; Garcia-Segura, L.M.; Caruso, D.; Jayaraman, A.; Lee, J.-W.; Melcangi, R.C.; Pike, C.J. Ligand for Translocator Protein Reverses Pathology in a Mouse Model of Alzheimer's Disease. *J. Neurosci.* **2013**, *33*, 8891–8897.
224. Grimm, A.; Lejri, I.; Hallé, F.; Schmitt, M.; Götz, J.; Bihel, F.; Eckert, A. Mitochondria Modulatory Effects of New TSPO Ligands in a Cellular Model of Tauopathies. *J. Neuroendocrinol.* **2020**, *32*, e12796.
225. Corsi, F.; Baglini, E.; Barresi, E.; Salerno, S.; Cerri, C.; Martini, C.; Da Settimo Passetti, F.; Taliani, S.; Gargini, C.; Piano, I. Targeting TSPO Reduces Inflammation and Apoptosis in an In Vitro Photoreceptor-Like Model of Retinal Degeneration. *ACS Chem. Neurosci.* **2022**, *13*, 3188–3197.
226. Daugherty, D.J.; Selvaraj, V.; Chechneva, O. V; Liu, X.; Pleasure, D.E.; Deng, W. A TSPO Ligand Is Protective in a Mouse Model of Multiple Sclerosis. *EMBO Mol. Med.* **2013**, *5*, 891–903.
227. Li, L.; Wang, W.; Zhang, L.-M.; Jiang, X.-Y.; Sun, S.-Z.; Sun, L.-J.; Guo, Y.; Gong, J.; Zhang, Y.-Z.; Wang, H.-L. Overexpression of the 18 KDa Translocator Protein (TSPO) in the Hippocampal Dentate Gyrus Produced Anxiolytic and Antidepressant-like Behavioural Effects. *Neuropharmacology* **2017**, *125*, 117–128.
228. Rupprecht, R.; Rammes, G.; Eser, D.; Baghai, T.C.; Schüle, C.; Nothdurfter, C.; Troxler, T.; Gentsch, C.; Kalkman, H.O.; Chaperon, F. Translocator Protein (18 KD) as Target for Anxiolytics without Benzodiazepine-like Side Effects. *Science (80-.)*. **2009**, *325*, 490–493.
229. Leva, G.; Klein, C.; Benyounes, J.; Hallé, F.; Bihel, F.; Collongues, N.; De Seze, J.; Mensah-Nyagan, A.-G.; Patte-Mensah, C. The Translocator Protein Ligand XBD173 Improves Clinical Symptoms and Neuropathological Markers in the SJL/J Mouse Model of Multiple Sclerosis. *Biochim. Biophys. Acta (BBA)-Molecular Basis Dis.* **2017**, *1863*, 3016–3027.

230. Mages, K.; Grassmann, F.; Jäggle, H.; Rupprecht, R.; Weber, B.H.F.; Hauck, S.M.; Grosche, A. The Agonistic TSPO Ligand XBD173 Attenuates the Glial Response Thereby Protecting Inner Retinal Neurons in a Murine Model of Retinal Ischemia. *J. Neuroinflammation* **2019**, *16*, 1–16.
231. Gong, J.; Szego, É.M.; Leonov, A.; Benito, E.; Becker, S.; Fischer, A.; Zweckstetter, M.; Outeiro, T.; Schneider, A. Translocator Protein Ligand Protects against Neurodegeneration in the MPTP Mouse Model of Parkinsonism. *J. Neurosci.* **2019**, *39*, 3752–3769.
232. Rudolph, U. Benzodiazepines BT - Encyclopedia of Molecular Pharmacology. In; Offermanns, S., Rosenthal, W., Eds.; Springer Berlin Heidelberg: Berlin, Heidelberg, 2008; pp. 251–254 ISBN 978-3-540-38918-7.
233. Harvey, R.C. Chapter 164 - Benzodiazepines. In; Silverstein, D.C., Hopper, K.B.T.-S.A.C.C.M. (Second E., Eds.; W.B. Saunders: St. Louis, 2015; pp. 864–866 ISBN 978-1-4557-0306-7.
234. Griffin, C.E.; Kaye, A.M.; Bueno, F.R.; Kaye, A.D. Benzodiazepine Pharmacology and Central Nervous System–Mediated Effects. *Ochsner J.* **2013**, *13*, 214–223.
235. Rudolph, U.; Knoflach, F. Beyond Classical Benzodiazepines: Novel Therapeutic Potential of GABAA Receptor Subtypes. *Nat. Rev. Drug Discov.* **2011**, *10*, 685–697, doi:10.1038/nrd3502.
236. Sigel, E.; Buhr, A. The Benzodiazepine Binding Site of GABAA Receptors. *Trends Pharmacol. Sci.* **1997**, *18*, 425–429.
237. Greenblatt, D.J. Pharmacology of Benzodiazepine Hypnotics. *J. Clin. Psychiatry* **1992**.
238. Baulieu, E.-E.; Robel, P. Neurosteroids: A New Brain Function? *J. Steroid Biochem. Mol. Biol.* **1990**, *37*, 395–403.
239. Paul, S.M.; Purdy, R.H. Neuroactive Steroids. *FASEB J.* **1992**, *6*, 2311–2322.
240. Slater, E.P.; Hesse, H.; Beato, M. Regulation of Transcription by Steroid Hormones A. *Ann. N. Y. Acad. Sci.* **1994**, *733*, 103–112.

241. Colciago, A.; Bonalume, V.; Melfi, V.; Magnaghi, V. Genomic and Non-Genomic Action of Neurosteroids in the Peripheral Nervous System. *Front. Neurosci.* **2020**, *14*, 796.
242. Rupprecht, R.; Holsboer, F. Neuroactive Steroids: Mechanisms of Action and Neuropsychopharmacological Perspectives. *Trends Neurosci.* **1999**, *22*, 410–416.
243. Rupprecht, R. Neuroactive Steroids: Mechanisms of Action and Neuropsychopharmacological Properties. *Psychoneuroendocrinology* **2003**, *28*, 139–168.
244. Rainer Rupprecht, Arpit Kumar Pradhan, Marco Kufner, Lisa Marie Brunner, Caroline Nothdurfter, Simon Wein, Jens Schwarzbach, Xenia Puig, Christian Rupprecht, G.R. Neurosteroids, Translocator Protein 18 KDa (TSPO) in Depression: Implications for Synaptic Plasticity, Cognition, and Treatment Options. *Eur. Arch. Psychiatry Clin. Neurosci.* **2022**, *In press*.
245. Reddy, D.S. Pharmacology of Endogenous Neuroactive Steroids. *Crit. Rev. Neurobiol.* **2003**, *15*.
246. Wang, M. Neurosteroids and GABA-A Receptor Function. *Front. Endocrinol. (Lausanne)*. **2011**, *2*, 44.
247. Ghit, A.; Assal, D.; Al-Shami, A.S.; Hussein, D.E.E. GABAA Receptors: Structure, Function, Pharmacology, and Related Disorders. *J. Genet. Eng. Biotechnol.* **2021**, *19*, 1–15.
248. Sieghart, W.; Fuchs, K.; Tretter, V.; Ebert, V.; Jechlinger, M.; Höger, H.; Adamiker, D. Structure and Subunit Composition of GABAA Receptors. *Neurochem. Int.* **1999**, *34*, 379–385.
249. Backus, K.H.; Arigoni, M.; Drescher, U.; Scheurer, L.; Malherbe, P.; Möhler, H.; Benson, J.A. Stoichiometry of a Recombinant GABAA Receptor Deduced from Mutation-Induced Rectification. *Neuroreport* **1993**, *5*, 285–288.
250. Daniel, C.; Öhman, M. RNA Editing and Its Impact on GABAA Receptor Function 2009.
251. Darlison, M.G.; Pahal, I.; Thode, C. Consequences of the Evolution of the GABA A Receptor Gene Family. *Cell. Mol. Neurobiol.* **2005**, *25*, 607–624.

252. Jacob, T.C.; Moss, S.J.; Jurd, R. GABAA Receptor Trafficking and Its Role in the Dynamic Modulation of Neuronal Inhibition. *Nat. Rev. Neurosci.* **2008**, *9*, 331–343.
253. Chen, Z.; Olsen, R.W. GABAA Receptor Associated Proteins: A Key Factor Regulating GABAA Receptor Function. *J. Neurochem.* **2007**, *100*, 279–294.
254. Uusi-Oukari, M.; Korpi, E.R. Regulation of GABAA Receptor Subunit Expression by Pharmacological Agents. *Pharmacol. Rev.* **2010**, *62*, 97–135.
255. Sieghart, W.; Sperk, G. Subunit Composition, Distribution and Function of GABA-A Receptor Subtypes. *Curr. Top. Med. Chem.* **2002**, *2*, 795–816.
256. Maguire, J.L.; Stell, B.M.; Rafizadeh, M.; Mody, I. Ovarian Cycle-Linked Changes in GABAA Receptors Mediating Tonic Inhibition Alter Seizure Susceptibility and Anxiety. *Nat. Neurosci.* **2005**, *8*, 797–804.
257. Luscher, B.; Fuchs, T.; Kilpatrick, C.L. GABAA Receptor Trafficking-Mediated Plasticity of Inhibitory Synapses. *Neuron* **2011**, *70*, 385–409.
258. Ben-Ari, Y.; Gaiarsa, J.-L.; Tyzio, R.; Khazipov, R. GABA: A Pioneer Transmitter That Excites Immature Neurons and Generates Primitive Oscillations. *Physiol. Rev.* **2007**, *87*, 1215–1284.
259. Verret, L.; Mann, E.O.; Hang, G.B.; Barth, A.M.I.; Cobos, I.; Ho, K.; Devidze, N.; Masliah, E.; Kreitzer, A.C.; Mody, I. Inhibitory Interneuron Deficit Links Altered Network Activity and Cognitive Dysfunction in Alzheimer Model. *Cell* **2012**, *149*, 708–721.
260. Craddock, N.; Jones, L.; Jones, I.R.; Kirov, G.; Green, E.K.; Grozeva, D.; Moskvina, V.; Nikolov, I.; Hamshere, M.L.; Vukcevic, D. Strong Genetic Evidence for a Selective Influence of GABAA Receptors on a Component of the Bipolar Disorder Phenotype. *Mol. Psychiatry* **2010**, *15*, 146–153.
261. Frere, S.; Slutsky, I. Alzheimer's Disease: From Firing Instability to Homeostasis Network Collapse. *Neuron* **2018**, *97*, 32–58.
262. Fogaça, M. V.; Duman, R.S. Cortical GABAergic Dysfunction in Stress and Depression:

- New Insights for Therapeutic Interventions. *Front. Cell. Neurosci.* **2019**, *87*.
263. Govindpani, K.; Turner, C.; Waldvogel, H.J.; Faull, R.L.M.; Kwakowsky, A. Impaired Expression of GABA Signaling Components in the Alzheimer's Disease Middle Temporal Gyrus. *Int. J. Mol. Sci.* **2020**, *21*, 8704.
264. Bareggi, S.R.; Franceschi, M.; Bonini, L.; Zecca, L.; Smirne, S. Decreased CSF Concentrations of Homovanillic Acid and γ -Aminobutyric Acid in Alzheimer's Disease: Age-or Disease-Related Modifications? *Arch. Neurol.* **1982**, *39*, 709–712.
265. Rudolf, U.; Crestani, F.; Benke, J.; Brünig, I.; Benson, J.A.; Fritschy, J.M.; Martin, J.R.; Bluethmann, H.; Mohler, H. Benzodiazepine Actions Mediated by Specific M-Aminobutyric AcidA Receptor Suptypes. *Nature* **1999**, *401*, 796–800.
266. Collinson, N.; Kuenzi, F.M.; Jarolimek, W.; Maubach, K.A.; Cothliff, R.; Sur, C.; Smith, A.; Otu, F.M.; Howell, O.; Atack, J.R. Enhanced Learning and Memory and Altered GABAergic Synaptic Transmission in Mice Lacking the A5 Subunit of the GABAAR Receptor. *J. Neurosci.* **2002**, *22*, 5572–5580.
267. Crestani, F.; Keist, R.; Fritschy, J.-M.; Benke, D.; Vogt, K.; Prut, L.; Blüthmann, H.; Möhler, H.; Rudolph, U. Trace Fear Conditioning Involves Hippocampal A5 GABAAR Receptors. *Proc. Natl. Acad. Sci.* **2002**, *99*, 8980–8985.
268. Puig-Bosch, X.; Bielecki, S.; Zeilhofer, H.U.; Rudolph, U.; Antkowiak, B.; Rammes, G. Midazolam at Low Nanomolar Concentrations Affects Long-Term Potentiation and Synaptic Transmission Predominantly via the A1- γ -Aminobutyric Acid Type A Receptor Subunit in Mice. *Anesthesiology* **2022**, *136*, 954–969.
269. Olkkola, K.T.; Ahonen, J. Midazolam and Other Benzodiazepines. *Mod. Anesth.* **2008**, 335–360.
270. Walters, R.J.; Hadley, S.H.; Morris, K.D.W.; Amin, J. Benzodiazepines Act on GABAAR Receptors via Two Distinct and Separable Mechanisms. *Nat. Neurosci.* **2000**, *3*, 1274–1281.
271. Rupprecht, R.; Wetzel, C.H.; Dorostkar, M.; Herms, J.; Albert, N.L.; Schwarzbach, J.; Schumacher, M.; Neumann, I.D. Translocator Protein (18kDa) TSPO: A New Diagnostic

- or Therapeutic Target for Stress-Related Disorders? *Mol. Psychiatry* **2022**, 1–9.
272. Mizota, K.; Ueda, H. N-Terminus of MAP2C as a Neurosteroid-Binding Site. *Neuroreport* **2008**, *19*, 1529–1533.
273. Stell, B.M.; Brickley, S.G.; Tang, C.Y.; Farrant, M.; Mody*, I. Neuroactive Steroids Reduce Neuronal Excitability by Selectively Enhancing Tonic Inhibition Mediated by δ Subunit-Containing GABAA Receptors. *Proc. Natl. Acad. Sci.* **2003**, *100*, 14439–14444.
274. Mihalek, R.M.; Banerjee, P.K.; Korpi, E.R.; Quinlan, J.J.; Firestone, L.L.; Mi, Z.-P.; Lagenaur, C.; Tretter, V.; Sieghart, W.; Anagnostaras, S.G. Attenuated Sensitivity to Neuroactive Steroids in γ -Aminobutyrate Type A Receptor Delta Subunit Knockout Mice. *Proc. Natl. Acad. Sci.* **1999**, *96*, 12905–12910.
275. Bukanova, J.; Solntseva, E.; Kondratenko, R.; Kudova, E. Epipregnanolone as a Positive Modulator of Gabaa Receptor in Rat Cerebellar and Hippocampus Neurons. *Biomolecules* **2021**, *11*, 791.
276. Nguyen, Q.; Sapp, D.W.; Van Ness, P.C.; Olsen, R.W. Modulation of GABAA Receptor Binding in Human Brain by Neuroactive Steroids: Species and Brain Regional Differences. *Synapse* **1995**, *19*, 77–87.
277. Gee, K.W.; Lan, N.C. Gamma-Aminobutyric AcidA Receptor Complexes in Rat Frontal Cortex and Spinal Cord Show Differential Responses to Steroid Modulation. *Mol. Pharmacol.* **1991**, *40*, 995–999.
278. Mennerick, S.; He, Y.; Jiang, X.; Manion, B.D.; Wang, M.; Shute, A.; Benz, A.; Evers, A.S.; Covey, D.F.; Zorumski, C.F. Selective Antagonism of 5α -Reduced Neurosteroid Effects at GABAA Receptors. *Mol. Pharmacol.* **2004**, *65*, 1191–1197.
279. Sperk, G.; Schwarzer, C.; Tsunashima, K.; Fuchs, K.; Sieghart, W. GABAA Receptor Subunits in the Rat Hippocampus I: Immunocytochemical Distribution of 13 Subunits. *Neuroscience* **1997**, *80*, 987–1000.
280. Caraiscos, V.B.; Elliott, E.M.; You-Ten, K.E.; Cheng, V.Y.; Belelli, D.; Newell, J.G.; Jackson, M.F.; Lambert, J.J.; Rosahl, T.W.; Wafford, K.A. Tonic Inhibition in Mouse

- Hippocampal CA1 Pyramidal Neurons Is Mediated by A5 Subunit-Containing γ -Aminobutyric Acid Type A Receptors. *Proc. Natl. Acad. Sci.* **2004**, *101*, 3662–3667.
281. Glykys, J.; Mody, I. Hippocampal Network Hyperactivity after Selective Reduction of Tonic Inhibition in GABAA Receptor A5 Subunit–Deficient Mice. *J. Neurophysiol.* **2006**, *95*, 2796–2807.
282. Jayakar, S.S.; Chiara, D.C.; Zhou, X.; Wu, B.; Bruzik, K.S.; Miller, K.W.; Cohen, J.B. Photoaffinity Labeling Identifies an Intersubunit Steroid-Binding Site in Heteromeric GABA Type A (GABAA) Receptors. *J. Biol. Chem.* **2020**, *295*, 11495–11512.
283. Reddy, D.S.; Estes, W.A. Clinical Potential of Neurosteroids for CNS Disorders. *Trends Pharmacol. Sci.* **2016**, *37*, 543–561.
284. Reddy, D.S. Neurosteroids: Endogenous Role in the Human Brain and Therapeutic Potentials. *Prog. Brain Res.* **2010**, *186*, 113–137.
285. Almeida, F.B.; Pinna, G.; Barros, H.M.T. The Role of HPA Axis and Allopregnanolone on the Neurobiology of Major Depressive Disorders and PTSD. *Int. J. Mol. Sci.* **2021**, *22*, 5495.
286. Uzunova, V.; Sampson, L.; Uzunov, D.P. Relevance of Endogenous 3α -Reduced Neurosteroids to Depression and Antidepressant Action. *Psychopharmacology (Berl.)* **2006**, *186*, 351–361.
287. Longone, P.; Rupprecht, R.; Manieri, G.A.; Bernardi, G.; Romeo, E.; Pasini, A. The Complex Roles of Neurosteroids in Depression and Anxiety Disorders. *Neurochem. Int.* **2008**, *52*, 596–601.
288. Litim, N.; Morissette, M.; Di Paolo, T. Effects of Progesterone Administered after MPTP on Dopaminergic Neurons of Male Mice. *Neuropharmacology* **2017**, *117*, 209–218.
289. Melcangi, R.C.; Caruso, D.; Levandis, G.; Abbiati, F.; Armentero, M.-T.; Blandini, F. Modifications of Neuroactive Steroid Levels in an Experimental Model of Nigrostriatal Degeneration: Potential Relevance to the Pathophysiology of Parkinson’s Disease. *J. Mol. Neurosci.* **2012**, *46*, 177–183.

290. Adeosun, S.O.; Hou, X.; Jiao, Y.; Zheng, B.; Henry, S.; Hill, R.; He, Z.; Pani, A.; Kyle, P.; Ou, X. Allopregnanolone Reinstates Tyrosine Hydroxylase Immunoreactive Neurons and Motor Performance in an MPTP-Lesioned Mouse Model of Parkinson's Disease. *PLoS One* **2012**, *7*, e50040.
291. Caruso, D.; Barron, A.M.; Brown, M.A.; Abbiati, F.; Carrero, P.; Pike, C.J.; Garcia-Segura, L.M.; Melcangi, R.C. Age-Related Changes in Neuroactive Steroid Levels in 3xTg-AD Mice. *Neurobiol. Aging* **2013**, *34*, 1080–1089, doi:<https://doi.org/10.1016/j.neurobiolaging.2012.10.007>.
292. Irwin, R.W.; Brinton, R.D. Allopregnanolone as Regenerative Therapeutic for Alzheimer's Disease: Translational Development and Clinical Promise. *Prog. Neurobiol.* **2014**, *113*, 40–55, doi:<https://doi.org/10.1016/j.pneurobio.2013.08.004>.
293. Wang, J.M.; Singh, C.; Liu, L.; Irwin, R.W.; Chen, S.; Chung, E.J.; Thompson, R.F.; Brinton, R.D. Allopregnanolone Reverses Neurogenic and Cognitive Deficits in Mouse Model of Alzheimer's Disease. *Proc. Natl. Acad. Sci.* **2010**, *107*, 6498–6503.
294. Chung, W.-S.; Barres, B.A. The Role of Glial Cells in Synapse Elimination. *Curr. Opin. Neurobiol.* **2012**, *22*, 438–445.
295. Pfriefer, F.W. Roles of Glial Cells in Synapse Development. *Cell. Mol. life Sci.* **2009**, *66*, 2037–2047.
296. Um, J.W. Roles of Glial Cells in Sculpting Inhibitory Synapses and Neural Circuits. *Front. Mol. Neurosci.* **2017**, *10*, 381.
297. Wang, X.-L.; Li, L. Microglia Regulate Neuronal Circuits in Homeostatic and High-Fat Diet-Induced Inflammatory Conditions. *Front. Cell. Neurosci.* **2021**, *15*, 722028.
298. Arcuri, C.; Mecca, C.; Bianchi, R.; Giambanco, I.; Donato, R. The Pathophysiological Role of Microglia in Dynamic Surveillance, Phagocytosis and Structural Remodeling of the Developing CNS. *Front. Mol. Neurosci.* **2017**, *10*, 191.
299. Stevens, B.; Allen, N.J.; Vazquez, L.E.; Howell, G.R.; Christopherson, K.S.; Nouri, N.; Micheva, K.D.; Mehalow, A.K.; Huberman, A.D.; Stafford, B. The Classical Complement

- Cascade Mediates CNS Synapse Elimination. *Cell* **2007**, *131*, 1164–1178.
300. Stephan, A.H.; Madison, D. V; Mateos, J.M.; Fraser, D.A.; Lovelett, E.A.; Coutellier, L.; Kim, L.; Tsai, H.-H.; Huang, E.J.; Rowitch, D.H. A Dramatic Increase of C1q Protein in the CNS during Normal Aging. *J. Neurosci.* **2013**, *33*, 13460–13474.
 301. Schafer, D.P.; Lehrman, E.K.; Kautzman, A.G.; Koyama, R.; Mardinly, A.R.; Yamasaki, R.; Ransohoff, R.M.; Greenberg, M.E.; Barres, B.A.; Stevens, B. Microglia Sculpt Postnatal Neural Circuits in an Activity and Complement-Dependent Manner. *Neuron* **2012**, *74*, 691–705.
 302. Bialas, A.R.; Stevens, B. Retracted Article: TGF- β Signaling Regulates Neuronal C1q Expression and Developmental Synaptic Refinement. *Nat. Neurosci.* **2013**, *16*, 1773–1782.
 303. Chaboub, L.S.; Deneen, B. Developmental Origins of Astrocyte Heterogeneity: The Final Frontier of CNS Development. *Dev. Neurosci.* **2013**, *34*, 379–388.
 304. Tsai, H.-H.; Li, H.; Fuentealba, L.C.; Molofsky, A. V; Taveira-Marques, R.; Zhuang, H.; Tenney, A.; Murnen, A.T.; Fancy, S.P.J.; Merkle, F. Regional Astrocyte Allocation Regulates CNS Synaptogenesis and Repair. *Science (80-)*. **2012**, *337*, 358–362.
 305. Perez-Catalan, N.A.; Doe, C.Q.; Ackerman, S.D. The Role of Astrocyte-mediated Plasticity in Neural Circuit Development and Function. *Neural Dev.* **2021**, *16*, 1–14.
 306. Freeman, M.R.; Rowitch, D.H. Evolving Concepts of Gliogenesis: A Look Way Back and Ahead to the next 25 Years. *Neuron* **2013**, *80*, 613–623.
 307. Kucukdereli, H.; Allen, N.J.; Lee, A.T.; Feng, A.; Ozlu, M.I.; Conatser, L.M.; Chakraborty, C.; Workman, G.; Weaver, M.; Sage, E.H. Control of Excitatory CNS Synaptogenesis by Astrocyte-Secreted Proteins Hevin and SPARC. *Proc. Natl. Acad. Sci.* **2011**, *108*, E440–E449.
 308. Christopherson, K.S.; Ullian, E.M.; Stokes, C.C.A.; Mallowney, C.E.; Hell, J.W.; Agah, A.; Lawler, J.; Mosher, D.F.; Bornstein, P.; Barres, B.A. Thrombospondins Are Astrocyte-Secreted Proteins That Promote CNS Synaptogenesis. *Cell* **2005**, *120*, 421–433.

309. Buosi, A.S.; Matias, I.; Araujo, A.P.B.; Batista, C.; Gomes, F.C.A. Heterogeneity in Synaptogenic Profile of Astrocytes from Different Brain Regions. *Mol. Neurobiol.* **2018**, *55*, 751–762.
310. Barker, A.J.; Koch, S.M.; Reed, J.; Barres, B.A.; Ullian, E.M. Developmental Control of Synaptic Receptivity. *J. Neurosci.* **2008**, *28*, 8150–8160.
311. Allen, N.J.; Bennett, M.L.; Foo, L.C.; Wang, G.X.; Chakraborty, C.; Smith, S.J.; Barres, B.A. Astrocyte Glypicans 4 and 6 Promote Formation of Excitatory Synapses via GluA1 AMPA Receptors. *Nature* **2012**, *486*, 410–414.
312. Bayraktar, O.A.; Fuentealba, L.C.; Alvarez-Buylla, A.; Rowitch, D.H. Astrocyte Development and Heterogeneity. *Cold Spring Harb. Perspect. Biol.* **2015**, *7*, a020362.
313. Meyer-Franke, A.; Kaplan, M.R.; Pfieger, F.W.; Barres, B.A. Characterization of the Signaling Interactions That Promote the Survival and Growth of Developing Retinal Ganglion Cells in Culture. *Neuron* **1995**, *15*, 805–819.
314. Pfrieger, F.W.; Barres, B.A. Synaptic Efficacy Enhanced by Glial Cells in Vitro. *Science (80-.)*. **1997**, *277*, 1684–1687.
315. Singh, S.K.; Stogsdill, J.A.; Pulimood, N.S.; Dingsdale, H.; Kim, Y.H.; Pilaz, L.-J.; Kim, I.H.; Manhaes, A.C.; Rodrigues, W.S.; Pamukcu, A. Astrocytes Assemble Thalamocortical Synapses by Bridging NRX1 α and NL1 via Hevin. *Cell* **2016**, *164*, 183–196.
316. Takano, T.; Wallace, J.T.; Baldwin, K.T.; Purkey, A.M.; Uezu, A.; Courtland, J.L.; Soderblom, E.J.; Shimogori, T.; Maness, P.F.; Eroglu, C. Chemico-Genetic Discovery of Astrocytic Control of Inhibition in Vivo. *Nature* **2020**, *588*, 296–302.
317. Cornell-Bell, A.H.; Finkbeiner, S.M.; Cooper, M.S.; Smith, S.J. Glutamate Induces Calcium Waves in Cultured Astrocytes: Long-Range Glial Signaling. *Science (80-.)*. **1990**, *247*, 470–473.
318. Dani, J.W.; Chernjavsky, A.; Smith, S.J. Neuronal Activity Triggers Calcium Waves in Hippocampal Astrocyte Networks. *Neuron* **1992**, *8*, 429–440.

319. Newman, E.A.; Zahs, K.R. Calcium Waves in Retinal Glial Cells. *Science* (80-.). **1997**, *275*, 844–847.
320. Nimmerjahn, A.; Kirchhoff, F.; Kerr, J.N.D.; Helmchen, F. Sulforhodamine 101 as a Specific Marker of Astroglia in the Neocortex in Vivo. *Nat. Methods* **2004**, *1*, 31–37.
321. Wang, X.; Takano, T.; Nedergaard, M. Astrocytic Calcium Signaling: Mechanism and Implications for Functional Brain Imaging. *Dyn. brain imaging multi-modal methods vivo Appl.* **2009**, 93–109.
322. Stobart, J.L.; Ferrari, K.D.; Barrett, M.J.P.; Glück, C.; Stobart, M.J.; Zuend, M.; Weber, B. Cortical Circuit Activity Evokes Rapid Astrocyte Calcium Signals on a Similar Timescale to Neurons. *Neuron* **2018**, *98*, 726–735.
323. Covelo, A.; Araque, A. Neuronal Activity Determines Distinct Gliotransmitter Release from a Single Astrocyte. *Elife* **2018**, *7*, e32237.
324. Bezzi, P.; Volterra, A. A Neuron–Glia Signalling Network in the Active Brain. *Curr. Opin. Neurobiol.* **2001**, *11*, 387–394.
325. Guthrie, P.B.; Knappenberger, J.; Segal, M.; Bennett, M.V.L.; Charles, A.C.; Kater, S.B. ATP Released from Astrocytes Mediates Glial Calcium Waves. *J. Neurosci.* **1999**, *19*, 520–528.
326. Hassinger, T.D.; Guthrie, P.B.; Atkinson, P.B.; Bennett, M.V.L.; Kater, S. An Extracellular Signaling Component in Propagation of Astrocytic Calcium Waves. *Proc. Natl. Acad. Sci.* **1996**, *93*, 13268–13273.
327. Lee, E.; Chung, W.-S. Glial Control of Synapse Number in Healthy and Diseased Brain. *Front. Cell. Neurosci.* **2019**, *13*, 42.
328. Leshchyns' ka, I.; Liew, H.T.; Shepherd, C.; Halliday, G.M.; Stevens, C.H.; Ke, Y.D.; Ittner, L.M.; Sytnyk, V. A β -Dependent Reduction of NCAM2-Mediated Synaptic Adhesion Contributes to Synapse Loss in Alzheimer's Disease. *Nat. Commun.* **2015**, *6*, 8836.
329. Koffie, R.M.; Meyer-Luehmann, M.; Hashimoto, T.; Adams, K.W.; Mielke, M.L.; Garcia-

- Alloza, M.; Micheva, K.D.; Smith, S.J.; Kim, M.L.; Lee, V.M. Oligomeric Amyloid β Associates with Postsynaptic Densities and Correlates with Excitatory Synapse Loss near Senile Plaques. *Proc. Natl. Acad. Sci.* **2009**, *106*, 4012–4017.
330. Karisetty, B.C.; Bhatnagar, A.; Armour, E.M.; Beaver, M.; Zhang, H.; Elefant, F. Amyloid- β Peptide Impact on Synaptic Function and Neuroepigenetic Gene Control Reveal New Therapeutic Strategies for Alzheimer's Disease. *Front. Mol. Neurosci.* **2020**, *13*, 577622.
331. Gomez-Arboledas, A.; Davila, J.C.; Sanchez-Mejias, E.; Navarro, V.; Nuñez-Diaz, C.; Sanchez-Varo, R.; Sanchez-Mico, M.V.; Trujillo-Estrada, L.; Fernandez-Valenzuela, J.J.; Vizuite, M. Phagocytic Clearance of Presynaptic Dystrophies by Reactive Astrocytes in Alzheimer's Disease. *Glia* **2018**, *66*, 637–653.
332. Smit, T.; Deshayes, N.A.C.; Borchelt, D.R.; Kamphuis, W.; Middeldorp, J.; Hol, E.M. Reactive Astrocytes as Treatment Targets in Alzheimer's Disease—Systematic Review of Studies Using the APPswePS1dE9 Mouse Model. *Glia* **2021**, *69*, 1852–1881.
333. Sakakibara, Y.; Sekiya, M.; Saito, T.; Saido, T.C.; Iijima, K.M. Amyloid- β Plaque Formation and Reactive Gliosis Are Required for Induction of Cognitive Deficits in App Knock-in Mouse Models of Alzheimer's Disease. *Bmc Neurosci.* **2019**, *20*, 1–14.
334. Sanchez-Mico, M. V; Jimenez, S.; Gomez-Arboledas, A.; Muñoz-Castro, C.; Romero-Molina, C.; Navarro, V.; Sanchez-Mejias, E.; Nuñez-Diaz, C.; Sanchez-Varo, R.; Galea, E. Amyloid- β Impairs the Phagocytosis of Dystrophic Synapses by Astrocytes in Alzheimer's Disease. *Glia* **2021**, *69*, 997–1011.
335. Hynd, M.R.; Scott, H.L.; Dodd, P.R. Glutamate-Mediated Excitotoxicity and Neurodegeneration in Alzheimer's Disease. *Neurochem. Int.* **2004**, *45*, 583–595.
336. Talantova, M.; Sanz-Blasco, S.; Zhang, X.; Xia, P.; Akhtar, M.W.; Okamoto, S.; Dziewczapolski, G.; Nakamura, T.; Cao, G.; Pratt, A.E. A β Induces Astrocytic Glutamate Release, Extrasynaptic NMDA Receptor Activation, and Synaptic Loss. *Proc. Natl. Acad. Sci.* **2013**, *110*, E2518–E2527.
337. Assefa, B.T.; Gebre, A.K.; Altaye, B.M. Reactive Astrocytes as Drug Target in Alzheimer's

- Disease. *Biomed Res. Int.* **2018**, 2018.
338. Bosson, A.; Paumier, A.; Boisseau, S.; Jacquier-Sarlin, M.; Buisson, A.; Albrieux, M. TRPA1 Channels Promote Astrocytic Ca²⁺ Hyperactivity and Synaptic Dysfunction Mediated by Oligomeric Forms of Amyloid- β Peptide. *Mol. Neurodegener.* **2017**, *12*, 1–19.
339. Pekna, M.; Pekny, M. The Complement System: A Powerful Modulator and Effector of Astrocyte Function in the Healthy and Diseased Central Nervous System. *Cells* **2021**, *10*, 1812.
340. Shi, Q.; Colodner, K.J.; Matousek, S.B.; Merry, K.; Hong, S.; Kenison, J.E.; Frost, J.L.; Le, K.X.; Li, S.; Dodart, J.-C. Complement C3-Deficient Mice Fail to Display Age-Related Hippocampal Decline. *J. Neurosci.* **2015**, *35*, 13029–13042.
341. Gasque, P.; Chan, P.; Fontaine, M.; Ischenko, A.; Lamacz, M.; Götze, O.; Morgan, B.P. Identification and Characterization of the Complement C5a Anaphylatoxin Receptor on Human Astrocytes. *J. Immunol. (Baltimore, Md. 1950)* **1995**, *155*, 4882–4889.
342. Sayah, S.; Ischenko, A.M.; Zhakhov, A.; Bonnard, A.; Fontaine, M. Expression of Cytokines by Human Astrocytomas Following Stimulation by C3a and C5a Anaphylatoxins: Specific Increase in Interleukin-6 mRNA Expression. *J. Neurochem.* **1999**, *72*, 2426–2436.
343. Gavriilyuk, V.; Kalinin, S.; Hilbush, B.S.; Middlecamp, A.; McGuire, S.; Pelligrino, D.; Weinberg, G.; Feinstein, D.L. Identification of Complement 5a-like Receptor (C5L2) from Astrocytes: Characterization of Anti-inflammatory Properties. *J. Neurochem.* **2005**, *92*, 1140–1149.
344. Zhang, Y.; Chen, K.; Sloan, S.A.; Bennett, M.L.; Scholze, A.R.; O’Keefe, S.; Phatnani, H.P.; Guarnieri, P.; Caneda, C.; Ruderisch, N. An RNA-Sequencing Transcriptome and Splicing Database of Glia, Neurons, and Vascular Cells of the Cerebral Cortex. *J. Neurosci.* **2014**, *34*, 11929–11947.
345. Ghebrehiwet, B.; Peerschke, E.I.B. CC1q-R (Calreticulin) and GC1q-R/P33: Ubiquitously Expressed Multi-Ligand Binding Cellular Proteins Involved in Inflammation and Infection.

- Mol. Immunol.* **2004**, *41*, 173–183.
346. Fernando, L.P.; Natesan, S.; Joseph, K.; Kaplan, A.P. High Molecular Weight Kininogen and Factor XII Binding to Endothelial Cells and Astrocytes. *Thromb. Haemost.* **2003**, *90*, 787–795.
347. Crossin, K.L.; Tai, M.-H.; Krushel, L.A.; Mauro, V.P.; Edelman, G.M. Glucocorticoid Receptor Pathways Are Involved in the Inhibition of Astrocyte Proliferation. *Proc. Natl. Acad. Sci.* **1997**, *94*, 2687–2692.
348. Duus, K.; Hansen, E.W.; Tacnet, P.; Frachet, P.; Arlaud, G.J.; Thielens, N.M.; Houen, G. Direct Interaction between CD91 and C1q. *FEBS J.* **2010**, *277*, 3526–3537.
349. Xing, P.; Liao, Z.; Ren, Z.; Zhao, J.; Song, F.; Wang, G.; Chen, K.; Yang, J. Roles of Low-Density Lipoprotein Receptor-Related Protein 1 in Tumors. *Chin. J. Cancer* **2016**, *35*, 1–8.
350. Iram, T.; Ramirez-Ortiz, Z.; Byrne, M.H.; Coleman, U.A.; Kingery, N.D.; Means, T.K.; Frenkel, D.; El Khoury, J. Megf10 Is a Receptor for C1Q That Mediates Clearance of Apoptotic Cells by Astrocytes. *J. Neurosci.* **2016**, *36*, 5185–5192.
351. Györfy, B.A.; Kun, J.; Török, G.; Bulyáki, É.; Borhegyi, Z.; Gulyácssy, P.; Kis, V.; Szocsics, P.; Micsonai, A.; Matkó, J. Local Apoptotic-like Mechanisms Underlie Complement-Mediated Synaptic Pruning. *Proc. Natl. Acad. Sci.* **2018**, *115*, 6303–6308.
352. Clarke, L.E.; Barres, B.A. Emerging Roles of Astrocytes in Neural Circuit Development. *Nat. Rev. Neurosci.* **2013**, *14*, 311–321.
353. Pradhan AK, Neumüller T, Klug C, Fuchs S, Schlegel M, Ballmann M, Tartler KJ, Pianos A, Garcia MS, Liere P, Schumacher M, Kreuzer M, Rupprecht R, R.G. Chronic Administration of XBD173 Ameliorates Cognitive Deficits and Neuropathology via 18 KDa Translocator Protein (TSPO) in a Mouse Model of Alzheimer’s Disease. *Transl Psychiatry* **2023**, *13*, 332.
354. Pradhan, A.K.; Neumüller, T.; Klug, C.; Fuchs, S.; Schlegel, M.; Ballmann, M.; Tartler, K.J.; Pianos, A.; Garcia-Sanchez, M.; Liere, P.; et al. Chronic Administration of XBD173 Ameliorates Cognitive Deficits and Neuropathology via 18 KDa Translocator Protein

- (TSPO) in a Mouse Model of Alzheimer's Disease. *bioRxiv* **2023**, 2023.02.23.529740, doi:10.1101/2023.02.23.529740.
355. Rammes, G.; Seeser, F.; Mattusch, K.; Zhu, K.; Haas, L.; Kummer, M.; Heneka, M.; Herms, J.; Parsons, C.G. The NMDA Receptor Antagonist Radiprodil Reverses the Synaptotoxic Effects of Different Amyloid-Beta (A β) Species on Long-Term Potentiation (LTP). *Neuropharmacology* **2018**, *140*, 184–192.
356. Simon, W.; Hapfelmeier, G.; Kochs, E.; Zieglgänsberger, W.; Rammes, G. Isoflurane Blocks Synaptic Plasticity in the Mouse Hippocampus. *J. Am. Soc. Anesthesiol.* **2001**, *94*, 1058–1065.
357. Kleinknecht, K.R.; Bedenk, B.T.; Kaltwasser, S.F.; Grünecker, B.; Yen, Y.-C.; Czisch, M.; Wotjak, C.T. Hippocampus-Dependent Place Learning Enables Spatial Flexibility in C57BL6/N Mice. *Front. Behav. Neurosci.* **2012**, *6*, 87.
358. Pradhan, A.K.; Shi, Q.; Tartler, K.J.; Rammes, G. Quantification of Astrocytic Synaptic Pruning in Mouse Hippocampal Slices in Response to Ex Vivo A β Treatment via Colocalization Analysis with C1q. *STAR Protoc.* **2022**, *3*, 101687.
359. Zhu, X.; Fréchet, M.; Liere, P.; Zhang, S.; Pianos, A.; Fernandez, N.; Denier, C.; Mattern, C.; Schumacher, M.; Guennoun, R. A Role of Endogenous Progesterone in Stroke Cerebroprotection Revealed by the Neural-Specific Deletion of Its Intracellular Receptors. *J. Neurosci.* **2017**, *37*, 10998–11020.
360. Kasai, H.; Matsuzaki, M.; Noguchi, J.; Yasumatsu, N.; Nakahara, H. Structure–Stability–Function Relationships of Dendritic Spines. *Trends Neurosci.* **2003**, *26*, 360–368.
361. Yuste, R.; Bonhoeffer, T. Morphological Changes in Dendritic Spines Associated with Long-Term Synaptic Plasticity. *Annu. Rev. Neurosci.* **2001**, *24*, 1071–1089.
362. Fukazawa, Y.; Saitoh, Y.; Ozawa, F.; Ohta, Y.; Mizuno, K.; Inokuchi, K. Hippocampal LTP Is Accompanied by Enhanced F-Actin Content within the Dendritic Spine That Is Essential for Late LTP Maintenance in Vivo. *Neuron* **2003**, *38*, 447–460.
363. Collin, C.; Miyaguchi, K.; Segal, M. Dendritic Spine Density and LTP Induction in Cultured

- Hippocampal Slices. *J. Neurophysiol.* **1997**, *77*, 1614–1623.
364. Chen, Y.; Rex, C.S.; Rice, C.J.; Dubé, C.M.; Gall, C.M.; Lynch, G.; Baram, T.Z. Correlated Memory Defects and Hippocampal Dendritic Spine Loss after Acute Stress Involve Corticotropin-Releasing Hormone Signaling. *Proc. Natl. Acad. Sci.* **2010**, *107*, 13123–13128.
365. De Roo, M.; Klauser, P.; Muller, D. LTP Promotes a Selective Long-Term Stabilization and Clustering of Dendritic Spines. *PLoS Biol.* **2008**, *6*, e219.
366. Malenka, R.C.; Bear, M.F. LTP and LTD: An Embarrassment of Riches. *Neuron* **2004**, *44*, 5–21.
367. Chidambaram, S.B.; Rathipriya, A.G.; Bolla, S.R.; Bhat, A.; Ray, B.; Mahalakshmi, A.M.; Manivasagam, T.; Thenmozhi, A.J.; Essa, M.M.; Guillemin, G.J. Dendritic Spines: Revisiting the Physiological Role. *Prog. Neuro-Psychopharmacology Biol. Psychiatry* **2019**, *92*, 161–193.
368. Lublin, A.L.; Gandy, S. Amyloid- β Oligomers: Possible Roles as Key Neurotoxins in Alzheimer's Disease. *Mt. Sinai J. Med. A J. Transl. Pers. Med. A J. Transl. Pers. Med.* **2010**, *77*, 43–49.
369. Tolar, M.; Hey, J.; Power, A.; Abushakra, S. Neurotoxic Soluble Amyloid Oligomers Drive Alzheimer's Pathogenesis and Represent a Clinically Validated Target for Slowing Disease Progression. *Int. J. Mol. Sci.* **2021**, *22*, 6355.
370. Xie, Q.; Wu, G.-Z.; Yang, N.; Shen, Y.-H.; Tang, J.; Zhang, W.-D. Delavatine A, an Unusual Isoquinoline Alkaloid Exerts Anti-Inflammation on LPS-Induced Proinflammatory Cytokines Production by Suppressing NF-KB Activation in BV-2 Microglia. *Biochem. Biophys. Res. Commun.* **2018**, *502*, 202–208.
371. Merino, J.J.; Muñetón-Gómez, V.; Álvarez, M.-I.; Toledano-Díaz, A. Effects of Cx3cr1 and Fractalkine Chemokines in Amyloid Beta Clearance and P-Tau Accumulation in Alzheimer, s Disease (Ad) Rodent Models: Is Fractalkine a Systemic Biomarker for Ad? *Curr. Alzheimer Res.* **2016**, *13*, 403–412.

372. González-Prieto, M.; Gutiérrez, I.L.; García-Bueno, B.; Caso, J.R.; Leza, J.C.; Ortega-Hernández, A.; Gómez-Garre, D.; Madrigal, J.L.M. Microglial CX3CR1 Production Increases in Alzheimer's Disease and Is Regulated by Noradrenaline. *Glia* **2021**, *69*, 73–90.
373. Harrison, J.K.; Jiang, Y.; Chen, S.; Xia, Y.; Maciejewski, D.; McNamara, R.K.; Streit, W.J.; Salafranca, M.N.; Adhikari, S.; Thompson, D.A. Role for Neuronally Derived Fractalkine in Mediating Interactions between Neurons and CX3CR1-Expressing Microglia. *Proc. Natl. Acad. Sci.* **1998**, *95*, 10896–10901.
374. Chidambaram, H.; Das, R.; Chinnathambi, S. Interaction of Tau with the Chemokine Receptor, CX3CR1 and Its Effect on Microglial Activation, Migration and Proliferation. *Cell Biosci.* **2020**, *10*, 1–9.
375. Haynes, S.E.; Hollopeter, G.; Yang, G.; Kurpius, D.; Dailey, M.E.; Gan, W.-B.; Julius, D. The P2Y₁₂ Receptor Regulates Microglial Activation by Extracellular Nucleotides. *Nat. Neurosci.* **2006**, *9*, 1512–1519.
376. Dejanovic, B.; Wu, T.; Tsai, M.-C.; Graykowski, D.; Gandham, V.D.; Rose, C.M.; Bakalarski, C.E.; Ngu, H.; Wang, Y.; Pandey, S. Complement C1q-Dependent Excitatory and Inhibitory Synapse Elimination by Astrocytes and Microglia in Alzheimer's Disease Mouse Models. *Nat. Aging* **2022**, *2*, 837–850.
377. Serrano-Pozo, A.; Muzikansky, A.; Gómez-Isla, T.; Growdon, J.H.; Betensky, R.A.; Frosch, M.P.; Hyman, B.T. Differential Relationships of Reactive Astrocytes and Microglia to Fibrillar Amyloid Deposits in Alzheimer Disease. *J. Neuropathol. Exp. Neurol.* **2013**, *72*, 462–471.
378. Bader, S.; Wolf, L.; Milenkovic, V.M.; Gruber, M.; Nothdurfter, C.; Rupprecht, R.; Wetzel, C.H. Differential Effects of TSPO Ligands on Mitochondrial Function in Mouse Microglia Cells. *Psychoneuroendocrinology* **2019**, *106*, 65–76.
379. Smith, S.S.; Shen, H.; Gong, Q.H.; Zhou, X. Neurosteroid Regulation of GABA_A Receptors: Focus on the $\alpha 4$ and δ Subunits. *Pharmacol. Ther.* **2007**, *116*, 58–76.

380. Pchitskaya, E.; Bezprozvanny, I. Dendritic Spines Shape Analysis—Classification or Clusterization? Perspective. *Front. Synaptic Neurosci.* **2020**, *12*, 31.
381. Terrill-Usery, S.E.; Mohan, M.J.; Nichols, M.R. Amyloid- β (1-42) Protofibrils Stimulate a Quantum of Secreted IL-1 β despite Significant Intracellular IL-1 β Accumulation in Microglia. *Biochim. Biophys. Acta (BBA)-Molecular Basis Dis.* **2014**, *1842*, 2276–2285.
382. Tong, L.; Balazs, R.; Soiampornkul, R.; Thangnipon, W.; Cotman, C.W. Interleukin-1 β Impairs Brain Derived Neurotrophic Factor-Induced Signal Transduction. *Neurobiol. Aging* **2008**, *29*, 1380–1393.
383. Wang, W.; Wei, C.; Quan, M.; Li, T.; Jia, J. Sulforaphane Reverses the Amyloid- β Oligomers Induced Depressive-like Behavior. *J. Alzheimer's Dis.* **2020**, *78*, 127–137.
384. Ledo, J.H.; Azevedo, E.P.; Beckman, D.; Ribeiro, F.C.; Santos, L.E.; Razolli, D.S.; Kincheski, G.C.; Melo, H.M.; Bellio, M.; Teixeira, A.L. Cross Talk between Brain Innate Immunity and Serotonin Signaling Underlies Depressive-like Behavior Induced by Alzheimer's Amyloid- β Oligomers in Mice. *J. Neurosci.* **2016**, *36*, 12106–12116.
385. Aboukhatwa, M.; Luo, Y. Antidepressants Modulate Intracellular Amyloid Peptide Species in N2a Neuroblastoma Cells. *J. Alzheimer's Dis.* **2011**, *24*, 221–234.
386. Nelson, R.L.; Guo, Z.; Halagappa, V.M.; Pearson, M.; Gray, A.J.; Matsuoka, Y.; Brown, M.; Martin, B.; Iyun, T.; Maudsley, S. Prophylactic Treatment with Paroxetine Ameliorates Behavioral Deficits and Retards the Development of Amyloid and Tau Pathologies in 3xTgAD Mice. *Exp. Neurol.* **2007**, *205*, 166–176.
387. Torrisi, S.A.; Geraci, F.; Tropea, M.R.; Grasso, M.; Caruso, G.; Fidilio, A.; Musso, N.; Sanfilippo, G.; Tascetta, F.; Palmeri, A. Fluoxetine and Vortioxetine Reverse Depressive-like Phenotype and Memory Deficits Induced by A β 1-42 Oligomers in Mice: A Key Role of Transforming Growth Factor-B1. *Front. Pharmacol.* **2019**, *10*, 693.
388. Caruso, G.; Grasso, M.; Fidilio, A.; Torrisi, S.A.; Musso, N.; Geraci, F.; Tropea, M.R.; Privitera, A.; Tascetta, F.; Puzzo, D. Antioxidant Activity of Fluoxetine and Vortioxetine in a Non-Transgenic Animal Model of Alzheimer's Disease. *Front. Pharmacol.* **2021**, *12*,

- 809541.
389. Wang, Y.-J.; Ren, Q.-G.; Gong, W.-G.; Wu, D.; Tang, X.; Li, X.-L.; Wu, F.-F.; Bai, F.; Xu, L.; Zhang, Z.-J. Escitalopram Attenuates β -Amyloid-Induced Tau Hyperphosphorylation in Primary Hippocampal Neurons through the 5-HT_{1A} Receptor Mediated Akt/GSK-3 β Pathway. *Oncotarget* **2016**, *7*, 13328.
390. Wuwongse, S.; Cheng, S.S.-Y.; Wong, G.T.-H.; Hung, C.H.-L.; Zhang, N.Q.; Ho, Y.-S.; Law, A.C.-K.; Chang, R.C.-C. Effects of Corticosterone and Amyloid-Beta on Proteins Essential for Synaptic Function: Implications for Depression and Alzheimer's Disease. *Biochim. Biophys. Acta (BBA)-Molecular Basis Dis.* **2013**, *1832*, 2245–2256.
391. Marx, C.E.; Trost, W.T.; Shampine, L.J.; Stevens, R.D.; Hulette, C.M.; Steffens, D.C.; Ervin, J.F.; Butterfield, M.I.; Blazer, D.G.; Massing, M.W. The Neurosteroid Allopregnanolone Is Reduced in Prefrontal Cortex in Alzheimer's Disease. *Biol. Psychiatry* **2006**, *60*, 1287–1294.
392. Charalampopoulos, I.; Remboutsika, E.; Margioris, A.N.; Gravanis, A. Neurosteroids as Modulators of Neurogenesis and Neuronal Survival. *Trends Endocrinol. Metab.* **2008**, *19*, 300–307.
393. Wojtal, K.; Trojnar, M.K.; Czuczwar, S.J. Endogenous Neuroprotective Factors: Neurosteroids. *Pharmacol. Reports* **2006**, *58*, 335.
394. Owen, D.R.; Guo, Q.; Kalk, N.J.; Colasanti, A.; Kalogiannopoulou, D.; Dimber, R.; Lewis, Y.L.; Libri, V.; Barletta, J.; Ramada-Magalhaes, J. Determination of [¹¹C] PBR28 Binding Potential in Vivo: A First Human TSPO Blocking Study. *J. Cereb. Blood Flow Metab.* **2014**, *34*, 989–994.
395. Shipton, O.A.; Tang, C.S.; Paulsen, O.; Vargas-Caballero, M. Differential Vulnerability of Hippocampal CA3-CA1 Synapses to A β . *Acta Neuropathol. Commun.* **2022**, *10*, 45.
396. Roselli, F.; Tirard, M.; Lu, J.; Hutzler, P.; Lamberti, P.; Livrea, P.; Morabito, M.; Almeida, O.F.X. Soluble β -Amyloid₁₋₄₀ Induces NMDA-Dependent Degradation of Postsynaptic Density-95 at Glutamatergic Synapses. *J. Neurosci.* **2005**, *25*, 11061–11070.

397. Kimura, R.; Matsuki, N. Protein Kinase CK2 Modulates Synaptic Plasticity by Modification of Synaptic NMDA Receptors in the Hippocampus. *J. Physiol.* **2008**, *586*, 3195–3206.
398. Liu, J.; Chang, L.; Song, Y.; Li, H.; Wu, Y. The Role of NMDA Receptors in Alzheimer's Disease. *Front. Neurosci.* **2019**, *13*, 43.
399. Li, S.; Hong, S.; Shepardson, N.E.; Walsh, D.M.; Shankar, G.M.; Selkoe, D. Soluble Oligomers of Amyloid β Protein Facilitate Hippocampal Long-Term Depression by Disrupting Neuronal Glutamate Uptake. *Neuron* **2009**, *62*, 788–801.
400. Matsuzaki, M.; Ellis-Davies, G.C.R.; Nemoto, T.; Miyashita, Y.; Iino, M.; Kasai, H. Dendritic Spine Geometry Is Critical for AMPA Receptor Expression in Hippocampal CA1 Pyramidal Neurons. *Nat. Neurosci.* **2001**, *4*, 1086–1092.
401. Fassbender, K.; Simons, M.; Bergmann, C.; Stroick, M.; Lütjohann, D.; Keller, P.; Runz, H.; Köhl, S.; Bertsch, T.; Von Bergmann, K. Simvastatin Strongly Reduces Levels of Alzheimer's Disease β -Amyloid Peptides A β 42 and A β 40 in Vitro and in Vivo. *Proc. Natl. Acad. Sci.* **2001**, *98*, 5856–5861.
402. Bandaru, V.V.R.; Troncoso, J.; Wheeler, D.; Pletnikova, O.; Wang, J.; Conant, K.; Haughey, N.J. ApoE4 Disrupts Sterol and Sphingolipid Metabolism in Alzheimer's but Not Normal Brain. *Neurobiol. Aging* **2009**, *30*, 591–599.
403. Schönknecht, P.; Lütjohann, D.; Pantel, J.; Bardenheuer, H.; Hartmann, T.; von Bergmann, K.; Beyreuther, K.; Schröder, J. Cerebrospinal Fluid 24S-Hydroxycholesterol Is Increased in Patients with Alzheimer's Disease Compared to Healthy Controls. *Neurosci. Lett.* **2002**, *324*, 83–85.
404. Fernández, A.; Llacuna, L.; Fernández-Checa, J.C.; Colell, A. Mitochondrial Cholesterol Loading Exacerbates Amyloid β Peptide-Induced Inflammation and Neurotoxicity. *J. Neurosci.* **2009**, *29*, 6394–6405.
405. Fernandez-Checa, J.C.; Kaplowitz, N. Hepatic Mitochondrial Glutathione: Transport and Role in Disease and Toxicity. *Toxicol. Appl. Pharmacol.* **2005**, *204*, 263–273.
406. Lluís, J.M.; Buricchi, F.; Chiarugi, P.; Morales, A.; Fernandez-Checa, J.C. Dual Role of

- Mitochondrial Reactive Oxygen Species in Hypoxia Signaling: Activation of Nuclear Factor-KB via c-SRC—and Oxidant-Dependent Cell Death. *Cancer Res.* **2007**, *67*, 7368–7377.
407. Marí, M.; Caballero, F.; Colell, A.; Morales, A.; Caballeria, J.; Fernandez, A.; Enrich, C.; Fernandez-Checa, J.C.; García-Ruiz, C. Mitochondrial Free Cholesterol Loading Sensitizes to TNF-and Fas-Mediated Steatohepatitis. *Cell Metab.* **2006**, *4*, 185–198.
408. Colell, A.; Garcia-Ruiz, C.; Morales, A.; Ballesta, A.; Ookhtens, M.; Rodes, J.; Kaplowitz, N.; Fernandez-Checa, J.C. Transport of Reduced Glutathione in Hepatic Mitochondria and Mitoplasts from Ethanol-treated Rats: Effect of Membrane Physical Properties and S-adenosyl-L-methionine. *Hepatology* **1997**, *26*, 699–708.
409. Puglielli, L.; Tanzi, R.E.; Kovacs, D.M. Alzheimer's Disease: The Cholesterol Connection. *Nat. Neurosci.* **2003**, *6*, 345–351.
410. Dharshini, S.; Taguchi, Y.-H.; Gromiha, M.M. Investigating the Energy Crisis in Alzheimer Disease Using Transcriptome Study. *Sci. Rep.* **2019**, *9*, 1–13.
411. Fagg, G.E.; Foster, A.C.; Ganong, A.H. Excitatory Amino Acid Synaptic Mechanisms and Neurological Function. *Trends Pharmacol. Sci.* **1986**, *7*, 357–363.
412. Danbolt, N.C. Glutamate Uptake. *Prog. Neurobiol.* **2001**, *65*, 1–105.
413. Masliah, E.; Hansen, L.; Alford, M.; Deteresa, R.; Mallory, M. Deficient Glutamate Transport Is Associated with Neurodegeneration in Alzheimer's Disease. *Ann. Neurol. Off. J. Am. Neurol. Assoc. Child Neurol. Soc.* **1996**, *40*, 759–766.
414. Kirvell, S.L.; Esiri, M.; Francis, P.T. Down-regulation of Vesicular Glutamate Transporters Precedes Cell Loss and Pathology in Alzheimer's Disease. *J. Neurochem.* **2006**, *98*, 939–950.
415. Scott, H.A.; Gebhardt, F.M.; Mitrovic, A.D.; Vandenberg, R.J.; Dodd, P.R. Glutamate Transporter Variants Reduce Glutamate Uptake in Alzheimer's Disease. *Neurobiol. Aging* **2011**, *32*, 553-e1.

416. Parsons, C.G.; Stöffler, A.; Danysz, W. Memantine: A NMDA Receptor Antagonist That Improves Memory by Restoration of Homeostasis in the Glutamatergic System-Too Little Activation Is Bad, Too Much Is Even Worse. *Neuropharmacology* **2007**, *53*, 699–723.
417. Milbocker, K.A.; Campbell, T.S.; Collins, N.; Kim, S.; Smith, I.F.; Roth, T.L.; Klintsova, A.Y. Glia-Driven Brain Circuit Refinement Is Altered by Early-Life Adversity: Behavioral Outcomes. *Front. Behav. Neurosci.* **2021**.
418. Lacor, P.N.; Buniel, M.C.; Furlow, P.W.; Clemente, A.S.; Velasco, P.T.; Wood, M.; Viola, K.L.; Klein, W.L. A β Oligomer-Induced Aberrations in Synapse Composition, Shape, and Density Provide a Molecular Basis for Loss of Connectivity in Alzheimer's Disease. *J. Neurosci.* **2007**, *27*, 796–807.
419. Taniguchi, K.; Yamamoto, F.; Amano, A.; Tamaoka, A.; Sanjo, N.; Yokota, T.; Kametani, F.; Araki, W. Amyloid- β Oligomers Interact with NMDA Receptors Containing GluN2B Subunits and Metabotropic Glutamate Receptor 1 in Primary Cortical Neurons: Relevance to the Synapse Pathology of Alzheimer's Disease. *Neurosci. Res.* **2022**, *180*, 90–98.
420. Bagur, R.; Hajnóczky, G. Intracellular Ca²⁺ Sensing: Its Role in Calcium Homeostasis and Signaling. *Mol. Cell* **2017**, *66*, 780–788.
421. Brickley, S.G.; Mody, I. Extrasynaptic GABA_A Receptors: Their Function in the CNS and Implications for Disease. *Neuron* **2012**, *73*, 23–34.
422. Carver, C.M. Role of Delta Subunit-Containing GABA_A Receptors in Hippocampus Tonic Inhibition and Epileptogenesis within Transgenic Mouse Models 2015.
423. Wei, W.; Faria, L.C.; Mody, I. Low Ethanol Concentrations Selectively Augment the Tonic Inhibition Mediated by δ Subunit-Containing GABA_A Receptors in Hippocampal Neurons. *J. Neurosci.* **2004**, *24*, 8379–8382.
424. Parakala, M.L.; Zhang, Y.; Modgil, A.; Chadchankar, J.; Vien, T.N.; Ackley, M.A.; Doherty, J.J.; Davies, P.A.; Moss, S.J. Metabotropic, but Not Allosteric, Effects of Neurosteroids on GABAergic Inhibition Depend on the Phosphorylation of GABA_A Receptors. *J. Biol. Chem.* **2019**, *294*, 12220–12230.

425. Betlazar, C.; Middleton, R.J.; Banati, R.; Liu, G.-J. The Translocator Protein (TSPO) in Mitochondrial Bioenergetics and Immune Processes. *Cells* **2020**, *9*, 512.
426. Lejri, I.; Grimm, A.; Hallé, F.; Abarghaz, M.; Klein, C.; Maitre, M.; Schmitt, M.; Bourguignon, J.-J.; Mensah-Nyagan, A.G.; Bihel, F. TSPO Ligands Boost Mitochondrial Function and Pregnenolone Synthesis. *J. Alzheimer's Dis.* **2019**, *72*, 1045–1058.
427. Yang, J.; Yang, H.; Liu, Y.; Li, X.; Qin, L.; Lou, H.; Duan, S.; Wang, H. Astrocytes Contribute to Synapse Elimination via Type 2 Inositol 1, 4, 5-Trisphosphate Receptor-Dependent Release of ATP. *Elife* **2016**, *5*, e15043.
428. Tournier, B.B.; Tsartsalis, S.; Ceyzeriat, K.; Fraser, B.H.; Grégoire, M.-C.; Kövari, E.; Millet, P. Astrocytic TSPO Upregulation Appears before Microglial TSPO in Alzheimer's Disease. *J. Alzheimer's Dis.* **2020**, *77*, 1043–1056.
429. Liu, X.; Ying, J.; Wang, X.; Zheng, Q.; Zhao, T.; Yoon, S.; Yu, W.; Yang, D.; Fang, Y.; Hua, F. Astrocytes in Neural Circuits: Key Factors in Synaptic Regulation and Potential Targets for Neurodevelopmental Disorders. *Front. Mol. Neurosci.* **2021**, *14*, 729273.
430. Berridge, M.J. The Inositol Trisphosphate/Calcium Signaling Pathway in Health and Disease. *Physiol. Rev.* **2016**, *96*, 1261–1296.
431. Parpura, V.; Grubišić, V.; Verkhratsky, A. Ca²⁺ Sources for the Exocytotic Release of Glutamate from Astrocytes. *Biochim. Biophys. Acta (BBA)-Molecular Cell Res.* **2011**, *1813*, 984–991.
432. Banerjee, A.; Larsen, R.S.; Philpot, B.D.; Paulsen, O. Roles of Presynaptic NMDA Receptors in Neurotransmission and Plasticity. *Trends Neurosci.* **2016**, *39*, 26–39.
433. Chen, C.; Tonegawa, S. Molecular Genetic Analysis of Synaptic Plasticity, Activity-Dependent Neural Development, Learning, and Memory in the Mammalian Brain. *Annu. Rev. Neurosci.* **1997**, *20*, 157–184.
434. Lu, Y.-M.; Jia, Z.; Janus, C.; Henderson, J.T.; Gerlai, R.; Wojtowicz, J.M.; Roder, J.C. Mice Lacking Metabotropic Glutamate Receptor 5 Show Impaired Learning and Reduced CA1 Long-Term Potentiation (LTP) but Normal CA3 LTP. *J. Neurosci.* **1997**, *17*, 5196–5205.

435. Conquet, F.; Bashir, Z.I.; Davies, C.H.; Daniel, H.; Ferraguti, F.; Bordi, F.; Franz-Bacon, K.; Reggiani, A.; Matarese, V.; Condé, F. Motor Deficit and Impairment of Synaptic Plasticity in Mice Lacking MGluR1. *Nature* **1994**, *372*, 237–243.
436. Bashir, Z.I.; Bortolotto, Z.A.; Davies, C.H.; Berretta, N.; Irving, A.J.; Seal, A.J.; Henley, J.M.; Jane, D.E.; Watkins, J.C.; Collingridge, G.L. Induction of LTP in the Hippocampus Needs Synaptic Activation of Glutamate Metabotropic Receptors. *Nature* **1993**, *363*, 347–350.
437. Billard, J.-M. D-Amino Acids in Brain Neurotransmission and Synaptic Plasticity. *Amino Acids* **2012**, *43*, 1851–1860.
438. Zhuang, Z.; Huang, J.; Cepero, M.L.; Liebl, D.J. Eph Signaling Regulates Gliotransmitter Release. *Commun. Integr. Biol.* **2011**, *4*, 223–226.
439. Henneberger, C.; Papouin, T.; Oliet, S.H.R.; Rusakov, D.A. Long-Term Potentiation Depends on Release of D-Serine from Astrocytes. *Nature* **2010**, *463*, 232–236.
440. Masuoka, T.; Ikeda, R.; Konishi, S. Persistent Activation of Histamine H1 Receptors in the Hippocampal CA1 Region Enhances NMDA Receptor-Mediated Synaptic Excitation and Long-Term Potentiation in Astrocyte-and D-Serine-Dependent Manner. *Neuropharmacology* **2019**, *151*, 64–73.
441. Woo, D.H.; Han, K.-S.; Shim, J.W.; Yoon, B.-E.; Kim, E.; Bae, J.Y.; Oh, S.-J.; Hwang, E.M.; Marmorstein, A.D.; Bae, Y.C. TREK-1 and Best1 Channels Mediate Fast and Slow Glutamate Release in Astrocytes upon GPCR Activation. *Cell* **2012**, *151*, 25–40.
442. Hong, S.; Beja-Glasser, V.F.; Nfonoyim, B.M.; Frouin, A.; Li, S.; Ramakrishnan, S.; Merry, K.M.; Shi, Q.; Rosenthal, A.; Barres, B.A. Complement and Microglia Mediate Early Synapse Loss in Alzheimer Mouse Models. *Science (80-.)*. **2016**, *352*, 712–716.
443. Fonseca, M.I.; Zhou, J.; Botto, M.; Tenner, A.J. Absence of C1q Leads to Less Neuropathology in Transgenic Mouse Models of Alzheimer’s Disease. *J. Neurosci.* **2004**, *24*, 6457–6465.
444. McGeer, P.L.; Akiyama, H.; Itagaki, S.; McGeer, E.G. Activation of the Classical

- Complement Pathway in Brain Tissue of Alzheimer Patients. *Neurosci. Lett.* **1989**, *107*, 341–346.
445. Luchena, C.; Zuazo-Ibarra, J.; Valero, J.; Matute, C.; Alberdi, E.; Capetillo-Zarate, E. A Neuron, Microglia, and Astrocyte Triple Co-Culture Model to Study Alzheimer's Disease. *Front. Aging Neurosci.* **2022**, *271*.
446. Carpanini, S.M.; Torvell, M.; Bevan, R.J.; Byrne, R.A.J.; Daskoulidou, N.; Saito, T.; Saido, T.C.; Taylor, P.R.; Hughes, T.R.; Zelek, W.M. Terminal Complement Pathway Activation Drives Synaptic Loss in Alzheimer's Disease Models. *Acta Neuropathol. Commun.* **2022**, *10*, 1–16.
447. Kishore, U.; Gupta, S.K.; Perdikoulis, M. V; Kojouharova, M.S.; Urban, B.C.; Reid, K. Modular Organization of the Carboxyl-Terminal, Globular Head Region of Human C1q A, B, and C Chains. *J. Immunol.* **2003**, *171*, 812–820.
448. Shah, A.; Kishore, U.; Shastri, A. Complement System in Alzheimer's Disease. *Int. J. Mol. Sci.* **2021**, *22*, 13647.
449. Berg, A.; Zelano, J.; Stephan, A.; Thams, S.; Barres, B.A.; Pekny, M.; Pekna, M.; Cullheim, S. Reduced Removal of Synaptic Terminals from Axotomized Spinal Motoneurons in the Absence of Complement C3. *Exp. Neurol.* **2012**, *237*, 8–17.
450. Hickman, S.E.; Allison, E.K.; Coleman, U.; Kingery-Gallagher, N.D.; El Khoury, J. Heterozygous CX3CR1 Deficiency in Microglia Restores Neuronal β -Amyloid Clearance Pathways and Slows Progression of Alzheimer's Like-Disease in PS1-APP Mice. *Front. Immunol.* **2019**, *10*, 2780.
451. Litvinchuk, A.; Wan, Y.-W.; Swartzlander, D.B.; Chen, F.; Cole, A.; Propson, N.E.; Wang, Q.; Zhang, B.; Liu, Z.; Zheng, H. Complement C3aR Inactivation Attenuates Tau Pathology and Reverses an Immune Network Deregulated in Tauopathy Models and Alzheimer's Disease. *Neuron* **2018**, *100*, 1337–1353.
452. Johnson, L. V; Leitner, W.P.; Rivest, A.J.; Staples, M.K.; Radeke, M.J.; Anderson, D.H. The Alzheimer's A β -Peptide Is Deposited at Sites of Complement Activation in Pathologic

- Deposits Associated with Aging and Age-Related Macular Degeneration. *Proc. Natl. Acad. Sci.* **2002**, *99*, 11830–11835.
453. Tenner, A.J. Complement-Mediated Events in Alzheimer's Disease: Mechanisms and Potential Therapeutic Targets. *J. Immunol.* **2020**, *204*, 306–315.
454. Esparza, T.J.; Gangolli, M.; Cairns, N.J.; Brody, D.L. Soluble Amyloid-Beta Buffering by Plaques in Alzheimer Disease Dementia versus High-Pathology Controls. *PLoS One* **2018**, *13*, e0200251.
455. Elgarf, A.A.; Siebert, D.C.B.; Steudle, F.; Draxler, A.; Li, G.; Huang, S.; Cook, J.M.; Ernst, M.; Scholze, P. Different Benzodiazepines Bind with Distinct Binding Modes to GABAA Receptors. *ACS Chem. Biol.* **2018**, *13*, 2033–2039.
456. Shi, Y.; Cui, M.; Ochs, K.; Brendel, M.; Strübing, F.L.; Briel, N.; Eckenweber, F.; Zou, C.; Banati, R.B.; Liu, G.-J. Long-Term Diazepam Treatment Enhances Microglial Spine Engulfment and Impairs Cognitive Performance via the Mitochondrial 18 KDa Translocator Protein (TSPO). *Nat. Neurosci.* **2022**, *25*, 317–329.

Acknowledgment

I would like to extend my heartfelt gratitude to my supervisor Prof. Dr. Gerhard Rammes for his unwavering support and invaluable guidance during this study. His expertise in the field, encouragement, and guidance were instrumental in completing the thesis. I am thankful to him for providing me with this opportunity to work on this interesting project and address an essential question in the field of neurodegeneration. I would take this opportunity to thank my thesis committee members Prof. Dr. Chadi Touma and Prof. Dr. Osborne Almeida for the discussions and suggestions during the course of the project.

I am grateful to all our collaborators PD Dr. Thomas Fenzl, Dr. Martin Schlegel, Dr. Matthias Kreutzer, Prof. Dr. Christian Wetzel, PD Dr. Carsten Wotjak, and Dr. Philippe Liere for sharing their immense knowledge and expertise with us which helped in the completion of the study. I would also like to extend my sincere appreciation to all my labmates for providing me with an environment that fosters intellectual curiosity and creativity. A special thanks to Claudia Klug, Andreas Blaschke, Nina Bayer, and Kristine Kellermann for always helping us out in times of need. I would also like to thank my friend and colleague Qinfang Shi for useful discussions about life and science.

During this journey, I was supported and encouraged by my friends. Their willingness to always lend an ear and provide me with insightful advice has helped me throughout the thesis. Special thanks to Ashwin and Rudra for the useful discussions. Life in Munich was easier because of the amazing group of people I was always surrounded by. I would take this opportunity to extend my heartfelt thanks to Amrit Bhai, Sarwan Bhai, Shalini Di, and Karuna. I am blessed to have had amazing mentors during my undergraduate courses and internships and I would like to thank them for shaping my research career and providing me the right guidance.

Lastly, I would like to extend my gratitude to the two most important pillars of my life my mama and papa for always standing behind me and encouraging me. Thanks for believing in me and showing me the right path.

List of publications

Published

Pradhan, Arpit Kumar, Tatjana Neumueller, Claudia Klug, Severin Fuchs, Martin Schlegel, Markus Ballmann, Katharina Johanna Tartler, Antoine Pianos, Maria Garcia-Sanchez, Philippe Liere, Michael Schumacher, Matthias Kreutzer, Rainer Rupprecht, Gerhard Rammes. Chronic administration of XBD173 ameliorates cognitive deficits and neuropathology via 18 kDa translocator protein (TSPO) in a mouse model of Alzheimer's disease. *Transl Psychiatry* **13**, 332 (2023).

Rupprecht, Rainer, **Arpit Kumar Pradhan**, Marco Kufner, Lisa Marie Brunner, Caroline Nothdurfter, Simon Wein, Jens Schwarzbach, Xenia Puig, Christian Rupprecht, and Gerhard Rammes. "Neurosteroids and translocator protein 18 kDa (TSPO) in depression: implications for synaptic plasticity, cognition, and treatment options." *European Archives of Psychiatry and Clinical Neuroscience* (2022): 1-11.

Pradhan, Arpit Kumar*, Qinfang Shi*, Katharina Johanna Tartler, and Gerhard Rammes. "Quantification of astrocytic synaptic pruning in mouse hippocampal slices in response to ex vivo A β treatment via colocalization analysis with C1q." *STAR protocols* 3, no. 4 (2022): 101687. (* equal contribution)

Wang, Xingxing, Qinfang Shi, **Arpit Kumar Pradhan**, Laura Ziegler, Martin Schlegel, and Gerhard Rammes. "Beta-Site Amyloid Precursor Protein-Cleaving Enzyme Inhibition Partly Restores Sevoflurane-Induced Deficits on Synaptic Plasticity and Spine Loss." *International Journal of Molecular Sciences* **23**, no. 12 (2022): 6637.

Declaration of Author Contributions

1. **Pradhan, Arpit Kumar**, Tatjana Neumueller, Claudia Klug, Severin Fuchs, Martin Schlegel, Markus Ballmann, Katharina Johanna Tartler, Antoine Pianos, Maria Garcia-Sanchez, Philippe Liere, Michael Schumacher, Matthias Kreutzer, Rainer Rupprecht, Gerhard Rammes. Chronic administration of XBD173 ameliorates cognitive deficits and neuropathology via 18 kDa translocator protein (TSPO) in a mouse model of Alzheimer's disease. *Transl Psychiatry* **13**, 332 (2023).

AKP and GR conceptualized the study. AKP contributed to the methodology, data acquisition, investigation, analysis, writing-original draft, and interpretation of the data. TN, MB, CK, SF, KJT, AP, MGS, and PL contributed to the data collection and analysis. GR, MK, MS, MS, and RR supervised the work. GR acquired the funding for the study.

Co-author contribution (in detail)

Tatjana Neumueller performed the LTP experiment with Pregnenolone, Amyloid beta peptides ($A\beta_{1-42}$ and $A\beta_{1-40}$), and XBD173 and imaged in vitro-dendritic spines after treatment with $A\beta_{1-42}$ and XBD173. Severin Fuchs performed the FACS recording of the samples. Markus Ballmann performed the LTP recording with allopregnanolone and $A\beta_{1-40}$, and with $3\beta 5\alpha$ THDOC and $A\beta_{1-42}$. Katharina Johanna Tartler performed the Golgi-Cox staining and analyzed the results. Antoine Pianos, Maria Garcia-Sanchez, and Philippe Liere extracted the neurosteroids and quantified their levels using GC-MS/MS. Claudia Kopp helped in the breeding of transgenic lines.

My contribution

I performed the LTP experiments with Amyloid beta peptides ($A\beta_{1-42}$ and $A\beta_{1-40}$) and XBD173 in wild-type mice slices, TSPOKO mice, and GABA delta KO mice. Additionally, I performed the CA1 LTP recordings for the Allopregnanolone, $3\alpha 5\alpha$ THDOC, and $A\beta_{1-42}$ for wild-type mice and $3\alpha 5\alpha$ THDOC and $A\beta_{1-42}$ for TSPOKO and GABA delta KO mice. I analyzed the dendritic spines by rendering and reconstructing them with IMARIS and categorizing them using a MATLAB plugin. I performed chronic and acute treatments on the mice. I optimized, performed, and analyzed all the behavioral studies with the mice. All the biochemical assays including methoxy staining, and ELISA. In addition to this, I performed all the stainings, recording of confocal images, 3D reconstruction of astrocytes and related proteins as well as the analysis. I prepared the samples for FACS (including single-cell suspension) and also prepared the samples for GC-MS/MS. I analyzed the FACS data and GC-MS/MS study. I wrote the original manuscript.

2. **Pradhan, Arpit Kumar***, Qinfang Shi*, Katharina Johanna Tartler, and Gerhard Rammes. "Quantification of astrocytic synaptic pruning in mouse hippocampal slices in response to ex vivo $A\beta$ treatment via colocalization analysis with C1q." *STAR protocols* **3**, no. 4 (2022): 101687. (* equal contribution)

Conceptualization, A.K.P.; Methodology, A.K.P. and Q.S.; Investigation, A.K.P., K.T., and Q.S.; Writing – Original Draft, A.K.P.; Writing - Review & Editing - A.K.P., K.T., Q.S., and G.R.; Supervision, G.R.

My contribution

I conceptualized the study and developed the methodology of quantification of astrocytic engulfment of C1q eat-me tags. Together with KT and QS, I collected the data. I wrote the original draft and together with QS, KT, and GR contributed to the review and editing of the manuscript.

.....

Arpit Kumar Pradhan

.....

Prof. Dr. Gerhard Rammes

(Supervisor)

Affidavit

Hiermit versichere ich an Eides statt, dass ich die vorliegende Dissertation **Activation of Translocator Protein by XBD173 ameliorates cognitive deficits and neuropathology in an Alzheimer's mouse model** selbstständig angefertigt habe, mich außer der angegebenen keiner weiteren Hilfsmittel bedient und alle Erkenntnisse, die aus dem Schrifttum ganz oder annähernd übernommen sind, als solche kenntlich gemacht und nach ihrer Herkunft unter Bezeichnung der Fundstelle einzeln nachgewiesen habe.

I hereby confirm that the dissertation **Activation of Translocator Protein by XBD173 ameliorates cognitive deficits and neuropathology in an Alzheimer's mouse model** is the result of my own work and that I have only used sources or materials listed and specified in the dissertation.

München, 11.7.2023

Munich, 11.7.2023

.....

Arpit Kumar Pradhan

Unterschrift

Signature